Low-carbon Energy Transition and Planning for Smart Grids

YUECHUAN TAO

Ph.D. (Engineering)

Supervisor: Dr. Jeremy (Jing) Qiu

Associate Supervisor: Dr. Dong Yuan, Professor Zhao Yang Dong

A thesis submitted in fulfillment of
the requirements for the degree of
Doctor of Philosophy

School of Electrical and Information Engineering
Faculty of Engineering
The University of Sydney
Australia

22 December 2022

DECLARATION

This thesis contains no material which has been accepted for the award of any other degree or diploma in any university or other tertiary institution and, to the best of my knowledge and belief, contains no material previously published or written by another person, except where due reference has been made in the text. I give consent to this copy of my thesis, when deposited in the University Library, being made available for loan and photocopying subject to the provisions of the Copyright Act 1968.

I hereby certify that the work embodied in this thesis contains published chapters/scholarly work of which I am a joint author. I have included as part of the thesis a written statement, endorsed by my supervisor, attesting to my contribution to the joint publications/scholarly work. Chapter 3 of this thesis is published as [Y. Tao, J. Qiu, S. Lai, J. Zhao, and Y. Xue, "Carbon-oriented electricity network planning and transformation," *IEEE Transactions on Power Systems,* vol. 36, no. 2, pp. 1034-1048, 2020]. I designed the study, analyzed the data, and wrote the drafts. Chapter 5 of this thesis is published as [Y. Tao, J. Qiu, S. Lai, and J. Zhao, "Renewable energy certificates and electricity trading models: Bi-level game approach," *International Journal of Electrical Power & Energy Systems,* vol. 130, p. 106940, 2021]. I designed the study, analyzed the data, and wrote the drafts. Chapter 6 of this thesis is published as [Y. Tao, J. Qiu, S. Lai, X. Sun, and J. Zhao, "Adaptive Integrated Planning of Electricity Networks and Fast Charging Stations Under Electric Vehicle Diffusion," *IEEE Transactions on Power Systems,* 2022]. I designed the study, analyzed the data, and wrote the drafts. Chapter 7 of this thesis is published as [Y. Tao, J. Qiu, S. Lai, X. Zhang, and G. Wang, "Collaborative planning for electricity distribution network and transportation system considering hydrogen fuel cell vehicles," *IEEE Transactions on Transportation Electrification,* vol. 6, no. 3, pp. 1211 - 1225, 2020]. I designed the study, analyzed the data, and wrote the drafts.

Author:

Yuechuan Tao
December 2022

Approved by Principal Supervisor:

Dr. Jing Qiu
December 2022

ACKNOWLEDGEMENTS

My Ph.D. research experience in Australia was amazing and memorable, during which period I was supported by many kind people, including my supervisors, my wife, my parents, my colleagues, and my two cute bunnies. This thesis has become an important milestone in my life, marking the completion of my Ph.D. studying and the new start of my academic career. I would like to take this precious chance to express my greatest gratitude to those who helped and supported me during my research period.

Firstly, I am truly grateful to my principal supervisor, Dr. Jing Qiu. It is the luckiest thing to work under his supervision. His character, wisdom, leadership, and hard-working have positively influenced other research fellows and me. With continuous and timely support and guidance from Dr. Qiu, I can effectively conduct research and write research papers productively. Meanwhile, I also deeply thank my co-supervisor, Prof. Zhao Yang Dong and Dr. Dong Yuan, who have helped and taught me a lot in my research with their vast experience in both research and engineering practices.

Secondly, I also appreciate my dear wife, Shuying Lai, who takes good care of me a lot in both my studying and living. She has developed a culinary skill, which not only ensures our balanced diet but also provides us with a full range of colors, smells and flavors. She undertook most of the household chores and took care of me and our bunnies in good order with her diligence. She arranged our weekends and holidays in a colorful way so that we could fully relax in the busy. Luckily, she also conducts research under the supervision of Dr. Qiu. During research studying, we often discuss timely-interesting ideas, mathematical models, programming, and even the design of the figures. At other times, we often hang out together to explore the spectacular natural beauty and delicious cuisine of Australia.

Thirdly, I express many thanks to my family, especially my parents. Their love and support are a solid base when I am pursuing my dream. The sacrifice and support of my parents are the strongest motives for me to strive for goals.

Last but not least, I give my gratitude to my two bunnies, i.e., doggy and nature, for their accompanying me during my research period.

LIST OF PUBLICATIONS

The following eight publications are the major Ph.D. research results of this candidate, as well as two manuscripts that are currently under review and are included as part of this thesis.

1. **Y. Tao**, J. Qiu, S. Lai, X. Sun, and J. Zhao, "Adaptive Integrated Planning of Electricity Networks and Fast Charging Stations Under Electric Vehicle Diffusion," *IEEE Transactions on Power Systems,* 2022.
2. **Y. Tao**, J. Qiu, S. Lai, X. Sun, and J. Zhao, "Market-Based Resource Allocation of Distributed Cloud Computing Services: Virtual Energy Storage Systems," *IEEE Internet of Things Journal,* 2022.
3. **Y. Tao**, J. Qiu, S. Lai, X. Sun, Y. Wang, and J. Zhao, "Data-driven Matching Protocol for Vehicle-to-Vehicle Energy Management Considering Privacy Preservation," *IEEE Transactions on Transportation Electrification,* 2022.
4. **Y. Tao**, J. Qiu, S. Lai, X. Sun, J. Zhao, B. Zhou, "Data-driven on-demand energy supplement planning for electric vehicles considering multi-charging/swapping services," *Applied Energy,* vol. 311, p. 118632, 2022.
5. **Y. Tao**, J. Qiu, S. Lai, X. Zhang, Y. Wang, and G. Wang, "A human-machine reinforcement learning method for cooperative energy management," *IEEE Transactions on Industrial Informatics,* vol. 18, no. 5, pp. 2974 - 2985, 2021.
6. **Y. Tao**, J. Qiu, and S. Lai, "Deep Reinforcement Learning Based Bidding Strategy for EVAs in Local Energy Market Considering Information Asymmetry," *IEEE Transactions on Industrial Informatics,* vol. 18, no. 6, pp. 3831 - 3842, 2021.
7. **Y. Tao**, J. Qiu, and S. Lai, "A data-driven management strategy of electric vehicles and thermostatically controlled loads based on modified generative adversarial network," *IEEE Transactions on Transportation Electrification,* vol. 8, no. 1, pp. 1430 - 1444, 2021.
8. **Y. Tao**, J. Qiu, and S. Lai, "A Hybrid Cloud and Edge Control Strategy for Demand Responses Using Deep Reinforcement Learning and Transfer Learning," *IEEE Transactions on Cloud Computing,* vol. 10, no. 1, pp. 56 - 71, 2021.
9. **Y. Tao**, J. Qiu, and S. Lai, "A supervised-learning assisted computation method for power system planning," *IEEE Transactions on Artificial Intelligence,* vol. 1, no. 01, pp. 1-1, 2021.
10. **Y. Tao**, J. Qiu, S. Lai, and J. Zhao, "Integrated electricity and hydrogen energy sharing in coupled energy systems," *IEEE Transactions on Smart Grid,* vol. 12, no. 2, pp. 1149-1162, 2020.
11. **Y. Tao**, J. Qiu, S. Lai, J. Zhao, and Y. Xue, "Carbon-oriented electricity network planning and transformation," *IEEE Transactions on Power Systems,* vol. 36, no. 2, pp. 1034-1048, 2020.
12. **Y. Tao**, J. Qiu, S. Lai, X. Zhang, and G. Wang, "Collaborative planning for electricity distribution network and transportation system considering hydrogen fuel cell vehicles," *IEEE Transactions on Transportation Electrification,* vol. 6, no. 3, pp. 1211 - 1225, 2020
13. **Y. Tao**, J. Qiu, S. Lai, and J. Zhao, "Renewable energy certificates and electricity trading models: Bi-level game approach," *International Journal of Electrical Power & Energy Systems,* vol. 130, p. 106940, 2021.
14. J. Qiu, **Y. Tao***, S. Lai, and J. Zhao, "Pricing Strategy of Cold Ironing Services for All-electric Ships Based on Carbon Integrated Electricity Price," *IEEE Transactions on Sustainable Energy,* vol. 13, no. 3, pp. 1553 - 1565, 2022.
15. X. Zhao, L. Li, **Y. Tao***, S. Lai, X. Zhou, and J. Qiu, "Aggregated operation of heterogeneous small-capacity distributed energy resources in peer-to-peer energy trading," *International Journal of Electrical Power & Energy Systems*, vol. 141, p. 108162, 2022.

16. T. Wan, **Y. Tao***, J. Qiu, and S. Lai, "Data-driven hierarchical optimal allocation of battery energy storage system," *IEEE Transactions on Sustainable Energy,* vol. 12, no. 4, pp. 2097 - 2109, 2021.
17. C. Si, **Y. Tao***, J. Qiu, S. Lai, and J. Zhao, "Deep reinforcement learning based home energy management system with devices operational dependencies," *International Journal of Machine Learning and Cybernetics,* pp. 1-17, 2021.
18. G. Liu, **Y. Tao***, L. Xu, Z. Chen, J. Qiu, and S. Lai, "Coordinated management of aggregated electric vehicles and thermostatically controlled loads in hierarchical energy systems," *International Journal of Electrical Power & Energy Systems,* vol. 131, p. 107090, 2021.
19. X. Sun, J. Qiu, **Y. Tao**, Y. Ma, and J. Zhao, "Coordinated Real-Time Voltage Control in Active Distribution Networks: An Incentive-Based Fairness Approach," *IEEE Transactions on Smart Grid,* vol. 13, no. 4, pp. 2650 - 2663, 2022.
20. S. Lai, J. Qiu, **Y. Tao**, and J. Zhao, "Pricing for Electric Vehicle Charging Stations based on the Responsiveness of Demand," *IEEE Transactions on Smart Grid,* 2022.
21. S. Lai, J. Qiu, **Y. Tao**, and X. Sun, "Demand Response Aggregation with Operating Envelope Based on Data-driven State Estimation and Sensitivity Function Signals," *IEEE Transactions on Smart Grid,* vol. 13, no. 3, pp. 2011 - 2025, 2022.
22. X. Sun, J. Qiu, **Y. Tao**, Y. Yi, and J. Zhao, "Distributed Optimal Voltage Control and Berth Allocation of All-Electric Ships in Seaport Microgrids," *IEEE Transactions on Smart Grid,* vol. 13, no. 4, pp. 2664 - 2674, 2022.
23. X. Sun, J. Qiu, **Y. Tao**, Y. Ma, and J. Zhao, "A Multi-Mode Data-Driven Volt/Var Control Strategy with Conservation Voltage Reduction in Active Distribution Networks," *IEEE Transactions on Sustainable Energy,* vol. 13, no. 2, pp. 1073 - 1085, 2022.
24. S. Lai, J. Qiu, **Y. Tao**, and Y. Liu, "Risk hedging strategies for electricity retailers using insurance and strangle weather derivatives," *International Journal of Electrical Power & Energy Systems,* vol. 134, p. 107372, 2022.
25. Y. Wang, J. Qiu, and **Y. Tao**, "Robust energy systems scheduling considering uncertainties and demand side emission impacts," *Energy,* vol. 239, p. 122317, 2022.
26. **S. Lai**, J. Qiu, Y. Tao, and J. Zhao, "Individualized Pricing of Energy Storage Sharing Based on Discount Sensitivity," *IEEE Transactions on Industrial Informatics,* vol. 18, no. 7, pp. 4642 - 4653, 2022.
27. S. Lai, J. Qiu, and **Y. Tao**, "Credit-based pricing and planning strategies for hydrogen and electricity energy storage sharing," *IEEE Transactions on Sustainable Energy,* vol. 13, no. 1, pp. 67 - 80, 2022.
28. X. Sun, J. Qiu, Y. Yi, and **Y. Tao**, "Cost-effective coordinated voltage control in active distribution networks with photovoltaics and mobile energy storage systems," *IEEE Transactions on Sustainable Energy,* vol. 13, no. 1, pp. 501-513, 2021.
29. Y. Ma, J. Qiu, X. Sun, and **Y. Tao**, "A Multi-stage Information Protection Scheme for CDA-Based Energy Trading Market in Smart Grids," *IEEE Transactions on Smart Grid,* vol. 13, no. 3, pp. 2305 - 2317, 2021.
30. Y. Wang, J. Qiu, and **Y. Tao**, "Optimal Power Scheduling Using Data-Driven Carbon Emission Flow Modelling for Carbon Intensity Control," *IEEE Transactions on Power Systems,* vol. 37, no. 4, pp. 2894 - 2905, 2021.
31. Y. Wang, J. Qiu, **Y. Tao**, and J. Zhao, "Carbon-oriented operational planning in coupled electricity and emission trading markets," *IEEE Transactions on Power Systems,* vol. 35, no. 4, pp. 3145-3157, 2020.
32. S. Lai, J. Qiu, **Y. Tao**, and J. Zhao, "Risk hedging for gas power generation considering power-to-gas energy storage in three different electricity markets," *Applied Energy,* vol. 291, p. 116822, 2021.
33. Y. Wang, J. Qiu, **Y. Tao**, X. Zhang, and G. Wang, "Low-carbon oriented optimal energy dispatch in coupled natural gas and electricity systems," *Applied Energy,* vol. 280, p. 115948, 2020.

34. S. Lai, J. Qiu, and **Y. Tao**, "Option-based portfolio risk hedging strategy for gas generator based on mean-variance utility model," *Energy Conversion and Economics,* vol. 3, no. 1, pp. 20-30, 2022.
35. X. Han, L. Sun, **Y. Tao**, J. Zhao, G. Wang, and D. Yuan, "Distributed energy-sharing strategy for peer-to-peer microgrid system," *Journal of Energy Engineering,* vol. 146, no. 4, p. 04020033, 2020.
36. **Y. Tao**, J. Qiu, S. Lai, Y. Wang, and X. Sun, "Energy management strategy of micro-grids in joint energy, reserve and regulation markets based on non-intrusive load monitoring," in *2021 IEEE International Power and Renewable Energy Conference (IPRECON)*, 2021: IEEE, pp. 1-6.
37. Y. Wang, J. Qiu, H. Zhang, **Y. Tao**, X. Han, and W. Shen, "An optimal scheduling based on carbon-embedded locational marginal price for integrated electricity and gas systems," in *2021 IEEE Power & Energy Society General Meeting (PESGM)*, 2021: IEEE, pp. 1-5.
38. **Y. Tao** *et al.*, "Two-layer scheduling of aggregated electric vehicles and thermostatically controlled loads in micro-grid," in *2019 9th International Conference on Power and Energy Systems (ICPES)*, 2019: IEEE, pp. 1-6.
39. S. Lai, **Y. Tao**, J. Qiu, J. Zhao, and H. Zhao, "Gas generation portfolio management strategy based on financial derivatives: Options," in *2019 9th International Conference on Power and Energy Systems (ICPES)*, 2019: IEEE, pp. 1-6.
40. J. Zhang, **Y. Tao**, J. Qiu, and X. Han, "Design of a smart socket for smart home energy management systems," in *2019 Chinese Control And Decision Conference (CCDC)*, 2019: IEEE, pp. 5543-5548.

ABSTRACT

With the growing concerns of climate change and energy crisis, the energy transition from fossil-based systems to a low-carbon society is an inevitable trend. As one of the major carbon emission contributors, the power sector will face remarkable changes. Power system planning plays an essential role in the energy transition of the power sector to accommodate the integration of renewable energy and meet the goal of decreasing carbon emissions while maintaining the economical, secure, and reliable operations of power systems. The acceleration of distributed energy resources (DERs) and carbon pricing policies have compelled utilities to act and to prioritize carbon-constrained infrastructure augmentation in their capital programs. To implement various carbon emission reduction policies, power system planning has become more challenging. The low-carbon oriented power system planning should comprehensively consider the retirement of traditional coal-fired power plants (CFPPs), construction of renewable energy plants, investment of energy storage systems (ESS), and network expansion.

To achieve a low-carbon society, the transportation sector is under electrification, and electric vehicles (EVs) are encouraged to reduce their reliance on fossil fuels. The increasing charging demand of EVs will cause various problems to the power systems. As emerging electricity demand, the charging load of EVs may jeopardize the electricity network services by increasing circuit loss and voltage violation. Hence, how to accommodate the large scale of EVs becomes a new challenge in power system planning. On the other hand, hydrogen is a promising energy carrier that offers a pathway to sustainable energy utilization in transportation systems. The integration of hydrogen fuel cell electric vehicles (FCEVs) is considered as an alternative to reduce transportation-related emissions and enhance energy flexibility. To this end, the multi-energy systems will bring new opportunities and challenges to future energy system planning.

In this thesis, a low-carbon energy transition framework and strategies are proposed for the future smart grid, which comprehensively consider the planning and operation of the electricity networks, the emission control strategies with the carbon response of the end-users, and the carbon-related trading mechanism. The planning approach considers the collaborative planning of different types of networks (including electricity networks, gas networks, and transportation networks) under the smart grid context. Transportation electrification is considered as a key segment in the energy transition of power systems, so the planning of charging infrastructure for EVs and hydrogen refueling infrastructure for FCEVs is jointly solved with the electricity network expansion. The vulnerability assessment tools are proposed to evaluate the coupled networks towards extreme events. Based on the carbon footprint tracking technologies, emission control can be realized from both the generation side and the demand side. The operation of the low-carbon oriented

power system is modeled in a combined energy and carbon market, which fully considers the carbon emission right (CER) trading and renewable energy certificates (RECs) trading of the market participants. Several benchmark systems have been used to demonstrate the effectiveness of the proposed planning approach. Comparative studies to existing approaches in the literature, where applicable, have also been conducted. The simulation results verify the practical applicability of this method.

TABLE OF CONTENTS

GLOSSARY

Abbreviations

ADN	Active distribution networks
AEMO	Australia Energy Market Operator
BESS	Battery energy storage system
CDF	Cumulative distribution function
CER	Carbon emission right
CFPP	Coal-fired power plants
CPADS	Cyber-physical active distribution system
DEP	Distribution expansion planning
DER	Distributed energy resource
DG	Distributed generator
DPGMM	Dirichlet process Gaussian mixture model
DSO	Distribution system operator
EA	Evolutionary algorithm
ED	Economic dispatch
EMS	Energy management system
ESS	Energy storage system
ETS	Emission trading system
EV	Electric vehicle
FACT	Flexible AC Transmission
FCEV	Fuel cell electric vehicles
FCS	Fast-charging station
FCAS	Frequency control ancillary service
FRTU	Feeder remote terminal unit
GEP	Generation expansion planning
GHG	Greenhouse gas
GMM	Gaussian mixture model
HPS	Hydrogen production station
HPTDF	Hybrid power distribution factor
HRS	Hydrogen refueling station
ICE	Internal-combustion engine
ICT	Information and communication technology
IEHS	Integrated electricity-charging and hydrogen-refueling station
ISO	Independent system operator
MIS	Management information system
MILP	Mixed-integer linear programming
NILM	Non-intrusive load monitoring
PCEF	Probabilistic carbon emission flow model
PH2EV	Plug-in hybrid electric and hydrogen vehicles
PSP	Proportional sharing principle
PTDF	Power transfer distribution factors
P2G	Power-to-gas

P2GS	Power-to-gas station
REC	Renewable energy certificate
SCADA	Supervisory control and data acquisition
SOC	State of charge
TEP	Transmission expansion planning
TSD	Temporal-spatial dynamic
TSO	Transmission system operator
UETEAM	User equilibrium-based traffic assignment model
2PEM	Two-point estimation method

LIST OF FIGURES

LIST OF TABLES

CHAPTER 1

INTRODUCTION

Electric power systems are fundamental infrastructures that supply energy to modern society. These systems can be generally broken down into generation, transmission, and distribution subsystems, each of which has different needs and requirements. With the development of modern Information and communication technologies (ICTs), conventional electrical grids will generation become smart girds, which are more complex. The operation and the planning of modern smart grids play an essential role in maintaining a secure and economical supply of electric energy.

The power energy sector is one of the major emission sources. To reach a low-carbon economy, sustainable energy transition is an inevitable trend. The acceleration of DERs and carbon pricing policies have compelled utilities to act and to prioritize carbon-constrained infrastructure augmentation in their capital programs. To implement various carbon emission reduction policies, power system transmission planning has become more challenging. The existing energy system will face massive retirement of coal-fired power plants (CFPPs), large-scale integration of renewable energy, and network expansion. Therefore, how to solve the trilemma among cost, risk, and emission in future smart grid transition effectively and efficiently needs to be addressed.

This chapter introduces the basic concepts related to power system planning, smart grid components, and other relevant features in a new environment.

1.1 Morden Smart Grids

1.2.1 Smart Grid Characteristics

The smart grid is a modernized electricity grid, which makes conventional grids greener and improves the delivery of power. In the energy transition process, smart grids enable renewable energy resources to be safely plugged into conventional grids. The present revolution in communication systems, particularly stimulated by the internet, offers the possibility of much greater monitoring and control throughout the power system and hence more effective, flexible, and lower-cost operation [1]. The Smart Grid is an opportunity to use new ICTs to revolutionize electrical power systems. Since about 2005, there has been increasing interest in the smart grid. The recognition that ICT offers significant opportunities to modernize the operation of electrical networks has coincided with an understanding that the power

sector can only be de-carbonized at a realistic cost if it is monitored and controlled effectively. In addition, a number of more detailed reasons have now coincided with stimulating interest in the smart grid.

The smart characteristic is revealed through its high-level automation and the integration of varieties of devices and actors. Modern smart grids transform the current grid into one that functions more cooperatively, responsively, and organically. Details can be summarized as follows:

- It realizes demand response (DR) and demand side management (DSM) by integrating smart meters, smart appliances and consumer loads, micro-generation and power storage (electric vehicles), and by providing customers with information related to energy use and price. It is expected to provide customers with information and incentives to modify their consumption patterns to overcome some of the constraints in power systems.
- It accommodates and facilitates all renewable energy, distributed generation, residential micro-generation and storage systems, thereby reducing the environmental impact of the entire power sector and providing a means of aggregation. It will provide simplified interconnection similar to "plug and play".
- It provides optimal solutions to operate assets through the intelligent operation of the delivery system (rerouting power, working autonomously) and the pursuit of efficient asset management. This includes leveraging assets based on what and when they are needed.
- It assures and improves reliability and the security of supply by being resilient to disturbances, attacks, and natural disasters, anticipating and responding to system disturbances (predictive maintenance and self-healing), and strengthening the security of supply through enhanced transfer capabilities.
- It maintains the power quality of the electricity supply to cater to sensitive equipment that increases with the digital economy.
- It opens access to the markets through increased transmission paths, aggregated supply, demand response initiatives, and ancillary service provisions.

Table 1-1 shows the comparison between conventional grids and smart grids.

TABLE 1-1. COMPARISON BETWEEN CONVENTIONAL GRIDS AND SMART GRIDS.

Conventional grids	**Smart grids**
Mechanization	Digitization
One-way communication	Two-way real-time communication
Centralized dispatch	Centralized and distributed dispatch
Less data acquisition	Lage volume of data invovled
Less or no monitoring with a small number of sensors	Great monitoring with many sensors
Manual control	Automatic control
Less security and privacy concerns	Prone to security and privacy issues

Slow response to emergencies	Fast response to emergencies
Less user participation	Frequent demand response
Passive distribution network	Active distribution network
Only wholesale and retail electricity market	More types of electricity markets at different levels

1.2.2 Smart Grid Technologies

The smart grid technologies cover multi-disciplines, main including communication, control, sensing and measurement, simulators and information system, energy management, integration of EVs, integration of renewable energy, demand response, smart home and smart buildings, microgrids, energy storage systems (ESS), design and planning, electricity market and pricing, fault detections, data security, cloud and edge computing, and etc. These technologies can be categorized and summarized as follow:

1) Information and communications technologies: These include:

(a) Two-way communication technologies to provide connectivity between different components in the power system and loads.

(b) Open architectures for plug-and-play home appliances; electric vehicles, and microgeneration;

(c) Communications, and the necessary software and hardware to provide customers with greater information, enable customers to trade in energy markets, and enable customers to provide a demand-side response;

(d) Software to ensure and maintain the security of information and standards to provide scalability and interoperability of information and communication systems.

2) Sensing, measurement, control, and automation technologies: These include:

(a) Intelligent Electronic Devices to provide advanced protective relaying, measurements, fault records, and event records for the power system;

(b) Phasor Measurement Units and Wide Area Monitoring, Protection and Control to ensure the security of the power system;

(c) Integrated sensors, measurements, control, automation systems, and information and communication technologies to provide rapid diagnosis and timely response to any event in different parts of the power system. These will support enhanced asset management and efficient operation of power system components to help relieve congestion in transmission and distribution circuits and prevent or minimize potential outages and enable working autonomously when conditions require quick resolution;

(d) Smart appliances, communication, controls, and monitors to maximize safety, comfort, convenience, and energy savings of homes; home energy management system (HEMS) for energy cost saving through controlling smart appliances.

(e) Smart meters, communication, displays, and associated software to allow customers to have greater choice and control over electricity and gas use. They will provide consumers with accurate bills, along with faster and easier supplier switching, to give consumers accurate real-time information on their electricity and gas use and other related information and to enable demand management and demand side participation.

3) Power electronics and energy storage: These include:

(a) High Voltage DC transmission and back-to-back schemes and Flexible AC Transmission Systems (FACTS) to enable long-distance transport and integration of renewable energy sources;

(b) Different power electronic interfaces and power electronic supporting devices to provide efficient connection of renewable energy sources and energy storage devices;

(c) Series capacitors, Unified Power Flow Controllers, and other FACTS devices to provide greater control over power flows in the AC grid;

(d) HVDC, FACTS, and active filters together with integrated communication and control to ensure greater system flexibility, supply reliability, and power quality;

(e) Power electronic interfaces and integrated communication and control to support system operations by controlling renewable energy sources, energy storage, and consumer loads;

(f) Energy storage to facilitate greater flexibility and reliability of the power system.

These technologies will penetrate through the generation, transmission, distribution, and behind-meter levels of the power systems.

1.2.3 Multi-networks under Smart Grid Context

With the abovementioned smart grid technologies, different types of networks become intensively correlated. The coordination of multi-networks makes the whole system more complex.

1) Coupling between electricity and communication networks

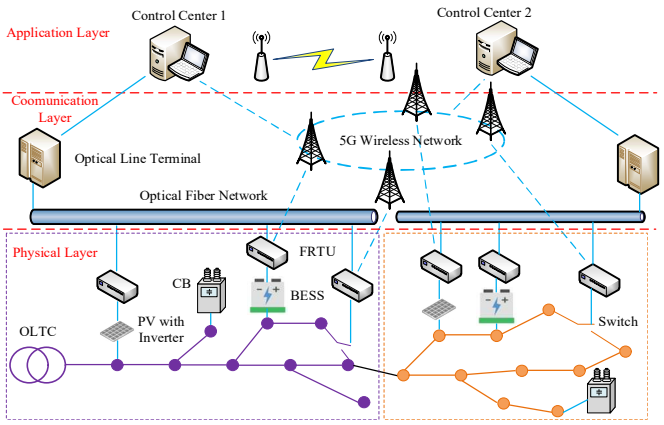

Fig. 1-1. System structure of CPADS.

Fig. 1-1 shows the distributed system structure of the cyber-physical active distribution system (CPADS), which reveals the coupling relationship between electricity and communication networks. CPADS can be divided into a cyber system and a physical system. The cyber system contains an application layer and a communication layer. The application layer is composed of control centers, including supervisory control and data acquisition (SCADA), management information systems (MIS), and energy management systems (EMS), which receive measurements, monitor the network status and formulate the control signals. The communication layer is responsible for the transit of control signals, and it is supported by cyber networks, including optical fiber networks and 5G wireless cellular networks. The physical network contains the electricity networks and the active electric assets. The feeder remote terminal units (FRTUs) are the intelligent interface between the cyber system and the physical system. The FRTUs play a critical role in keeping real-time communication between the controller and active-management devices, including PV inverters, battery energy storage systems (BESS), and switches.

2) Coupling between electricity and gas networks

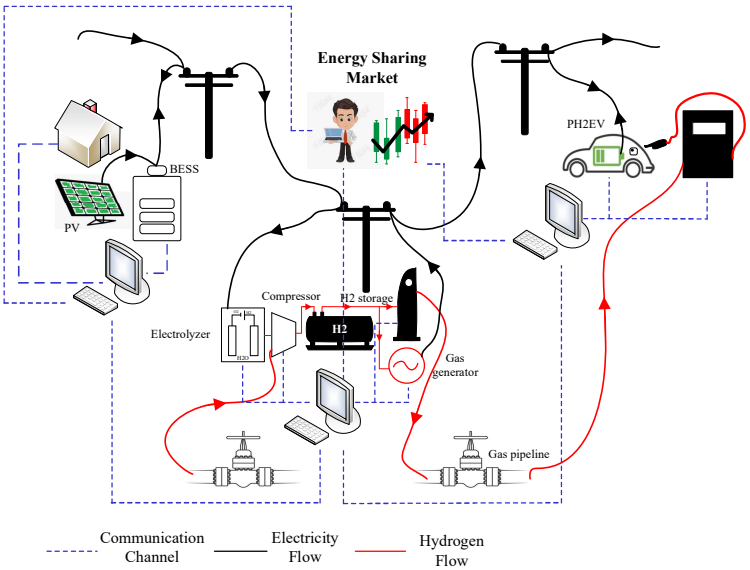

Fig. 1-2. System structure of integrated electricity and gas networks.

Originally, the coupling point between the gas and electricity network was the natural gas generators. With the development of power-to-gas (P2G) technologies and gas-driven vehicles, new coupling points between the gas and electricity network emerge. The coupled gas and electricity network under a smart grid context in a distribution system can be shown in Fig. 1-2. There are two types of coupled points of gas and electricity networks, i.e., P2G devices and plug-in hybrid electric and hydrogen vehicles (PH2EVs). Each player in the system will control the batteries, P2G devices, or PH2EVs and act as buys or sellers in the local energy market. The player can choose to sell surplus energy to or purchase deficient energy from the distribution system operator (DSO). Alternatively, they can also share energy with the other player. The player will communicate with each other through the communication channel to exchange the expected purchase energy and prices. Thus, each player has a processor to solve the local energy management problem rather than a centralized processor that collects all the players' information. The energy market operator collects the trading intentions from the players and supervises the market. Then the energy market informs the trading results to the system operator to realize the energy dispatch.

3) Coupling between electricity and transportation networks

The penetration of EVs makes electricity networks and transportation networks more related. The electricity network and transportation networks are usually coupled at the charging infrastructures of EVs, as shown in Fig. 1-3. This is because the charging of EVs is an important load in electricity networks, and charging infrastructures are located in the transportation networks to capture traffic flows.

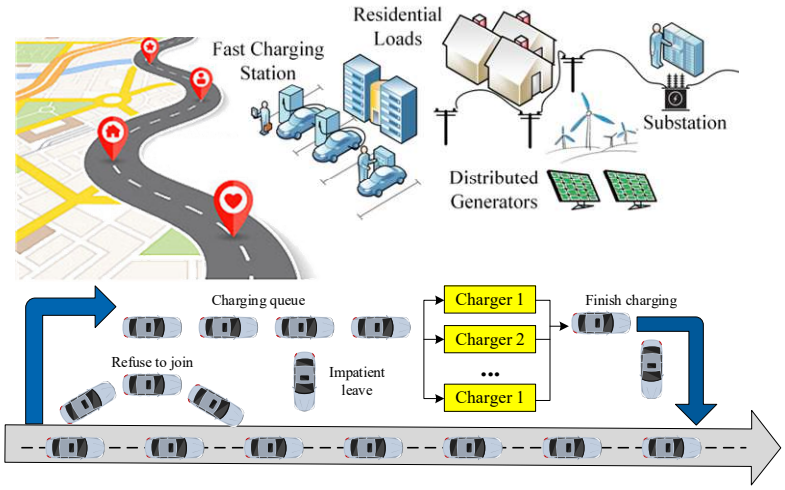

Fig. 1-3. System structure of coupled electricity and transportation networks.

In a modern smart grid, the multi-networks will not only contain the above single coupling relationship but may combine serval of them. For example, when considering the intelligent charging scheduling and management of EVs, the coupling between the information, electricity, and transportation networks should be modeled, as shown in Fig. 1-4. In this framework, both the traffic condition and electricity networks will be monitored. Based on the monitoring, the

charging platform will provide drivers with proper charging scheduling solutions that can meet the charging requirement with less traffic congestion and queuing time, as well as reduce the burden of the electricity networks.

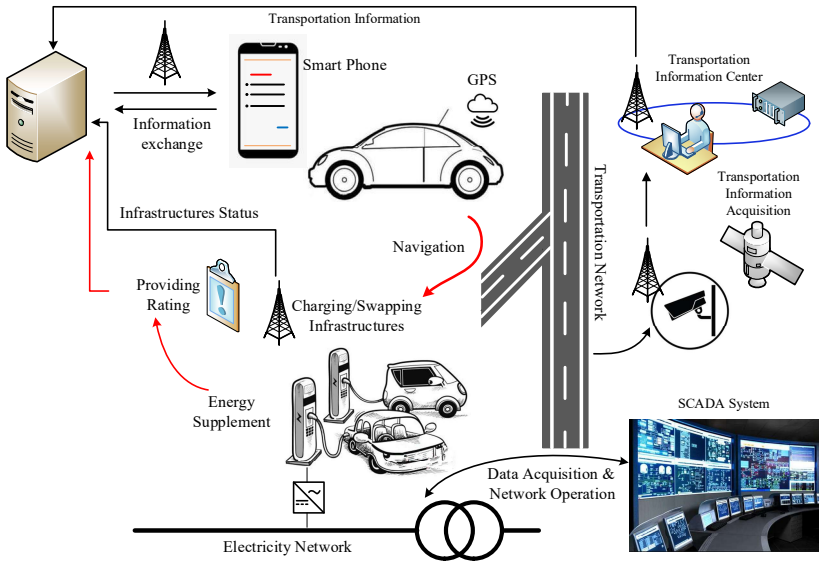

Fig. 1-4. Structure of smart charging scheduling system for EVs.

Furthermore, the integration of hydrogen FCEVs makes the electricity, gas, and transportation networks become coupled, as shown in Fig. 1-5. The coupling point is the hydrogen refueling stations (HRSs) and the hydrogen production stations (HPSs). Although the emergence of FCVs and PH2EVs can enhance energy flexibility and provide transport alternatives, the synergistic effect of electricity, hydrogen, and transportation networks makes the whole coupled network more complicated.

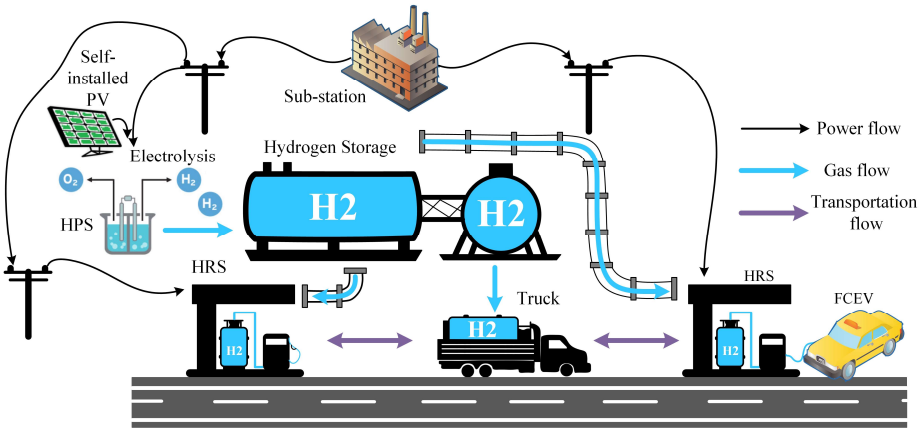

Fig. 1-5. Hydrogen production and delivery system for hydrogen refueling.

To this end, it can be concluded that the transition and planning of future smart grids is a multi-network science. Hence, in this thesis, we aim to model and analyze these coupling relationships and realize the coordination between multi-networks.

1.2 Power System Planning

1.2.1 Electricity Network Planning

Optimal network expansion has always been one of the most important issues in power system planning, referring to a comprehensive analysis to determine the time, location, and type of adding new facilities to facilitate economic, secure and reliable operations of power systems. The power system expansion can be carried out at generation, transmission, and distribution levels [2]. Transmission expansion planning (TEP) has been widely recognized as an essential part of long-term power system planning. The TEP denotes where, when, and how many new lines should be installed in the power transmission systems to support the increasing demand of the network. The generation expansion planning (GEP) will further consider where, when, and how many new generation capacities should be installed in the power systems. Under a low-carbon context, apart from TEP and GEP, the electricity network transition will further consider the retirement of the CFPPs, the construction of renewable energy plants, and the investment in ESS. Electricity network transition is an inevitable trend in the future for the following four reasons. First, the traditional coal-fired power plant is approaching its specific life span, entering the decommissioning stage. Second, to stabilize the global temperature, anthropogenic emissions must be controlled so that the emissions from traditional CFPPs need to be reduced. Third, renewable energy is being invested to take the place of thermal power generators. To smooth the output of intermittent renewable energy output, the ESS should be focused on. Fourth, with the continuously increasing demand in the future, the transmission network, generation capacity, and ESS need to be expanded. These four reasons will lead to great changes in electricity networks. Thus, the strategies that guide the current fossil-fuel dominated system to a low-carbon oriented system need to be researched.

In addition, with the emergence of electricity markets around the world, power systems have undergone reforms from vertical integration and regulatory structure to separation and liberalization of the power industry in the past few decades. These reforms are aimed at promoting competition among market participants and improving market efficiency. For vertically integrated power systems controlled by a single system operator, generation and transmission planning are performed by the same entity. Perform centralized generation and transmission planning to determine how to add new resources to the existing network. Usually, after the power generation plan is given, the advantage of transmission planning is to understand the entry and exit of power generation resources. On the contrary, in the deregulated environment, there are many self-interested market participants, such as brokers, marketers, independent power producers, etc. A remarkable feature of the new power market structure is that many power generation companies (GENCOs) are profit-oriented and focus on strengthening their market competitiveness. The planning and

decommissioning of their personal resources have become part of their market strategy and are no longer controlled by the system operators. Therefore, the market-based power system planning should take into account the self-interest and planning strategies of various market participants and evaluate the relevant risks arising from the current market uncertainty, such as the operation information, bidding strategies, and bilateral contracts of GENCOs.

Conventional distribution expansion planning (DEP) is to ensure that there is adequate substation capacity and feeder capacity to meet the demand [3]. The main decisions include the optimal location of substations, location of feeders, individual feeder design, allocation of load, allocation of substation capacity, and mix of transformers by the substations. In the modern smart grid environment, the DEP problem will further focus on the transition from passive distribution networks to active distribution networks (ADN). One of the major emerging concerns is the planning of distributed generation. The distributed generators (DGs) include PVs, biogas generators, wind generators, capacity banks (CBs), BESS, etc. The rapid onset of the DGs has brought about a paradigm shift in the way conventionally passive distribution networks have been planned and operated, leading to the ADN [4]. ADN is basically driven by advanced ICT and active network management, which helps DG control and optimization, distributed storage utilization, multi-energy integration, coordinated control of various system elements, and demand response planning. At the same time, ADN brings more control problems because the DG interconnections transform the distribution network operator in terms of the bidirectional power flows, intermittent power supplies, voltage rises and fluctuations, aggravated fault levels, lower power losses, and reliability and stability problems [5]. Hence, investigations of DEP planning are required to be focused on reducing power loss, reducing system oscillations, enhancing stability, enhancing loadability, enhancing available power transfer capacity, reducing conjunction, and enhancing operation flexibility.

1.2.2 Multi-energy Network Planning

Integration of different types of energy infrastructure, such as gas, electricity, and heat, provides a large potential to enhance energy efficiency, as well as enable a higher share of renewable energy [6]. Multi-energy networks refer to smart energy systems where various energy vectors interact with each other at various levels. The multi-energy network planning aims to determine the time, location, and type of adding new multi-energy infrastructures. These energy infrastructures include:

- Networks for transmitting and distributing energy. They are natural gas pipelines, power feeders, and district heating and cooling networks that transport natural gas, electricity, and heat (cold).
- Energy conversion devices, such as heat boilers (gas-fired heat exchange), power plants (gas-fired power exchange), cogeneration plants (gas-fired heat and power), heat pumps (power heat exchange), and technologies

for converting electric energy into fuel (such as hydrogen and methane) (power exchange).

- Energy storage devices that are capable of storing gas, electricity, heat, or other chemical substances for a short or long time.

An optimal multi-energy network planning aims to [7]:

- Improve the conversion efficiency and utilization rate of primary energy;
- Promote the optimal allocation of centralized and decentralized resources at the system level by optimizing market interaction, for example, allowing multi-energy systems to cope with fluctuating electricity market prices in renewable energy integrated energy systems;
- Increase the flexibility of the energy system, for example, by providing frequency response and reserve, allowing the thermal load provided by the power (e.g., electric heat pump) with storage characteristics (e.g., through thermal inertia embedded in the building structure) to participate in the power system balance; Or by utilizing flexible storage systems available in electric vehicles to support wind integration while providing clean fuel for transportation

1.2.3 EV Fast-Charging Station (FCS)Planning

The transportation sector, depending on liquid fossil fuel, is also a large emission contributor. To realize energy transition and towards a sustainable society, transportation electrification is an inevitable trend. The main supporting factor for achieving these goals is the popularity of electric vehicles. However, without the infrastructure network (such as FCSs) supporting the launch of full-scale electric vehicles, it is impossible to make any changes to maximize the positive impact [8]. As EVs are an essential load in future electricity networks, collaborative planning of the electricity networks and transportation networks is necessary. The planning of the transportation networks includes the siting and the sizing of the FCSs, as well as the augment of the road capacity (optional). The planning of the electricity network aims to ensure the power supply of the FCSs. In the related work, most co-planning models aim to ensure the energy supply of the charging facilities. But neglected that essence of the government's encouraging EVs, i.e., reducing emissions. It should be noted that EVs should run in a low-carbon electricity network. Hence, the co-planning model should also focus on carbon emissions by comprehensively considering the planning of the charging facilities and renewable energy sources.

Furthermore, access to large-scale EVs will bring a heavy burden to the electricity network, which is another major motivation for the collaborative planning of the electricity network and the transportation network. Hence, in the future planning problem, the construction and expansion of EV FCSs, BESS, and DGs should be integrated to deal with

network risk issues in smart grids. An optimal EV FCS planning strategy will comprehensively consider the economic benefits, the quality of services (measuring waiting time), the electricity network impacts, and the environmental impacts.

1.3 Evaluation Criteria for Power System Planning

1.3.1 Reliability

Reliability is the inherent characteristic and specific measure of any component, device, or system, which describes its ability to perform the intended function [9]. For power systems, reliability refers to the ability of the power systems to transmit power according to the quantity and quality required by energy users.

The definition of reliability by North American Electric Reliability Corporation includes two parts: adequacy and security. Adequacy relates to "*the existence of sufficient facilities in the system to satisfy consumers' electric power and energy demands at all times.*"[10] Security relates to *"the ability of a power system to withstand sudden disturbances in the system*." [10] Adequacy is usually related to static conditions, but security includes static security and dynamic security.

A long-term assessment of the generation and transmission capacity of the required system is critical for system planning and operation. Adequate capacities should be invested considering the future increase in demand based on prediction. The adequacy of power systems means that in the event of unavailability of components, standby or redundant generation and transmission capacity can be used to ensure adequate and acceptable power supply and standby continuity. In the low-carbon oriented planning problem, adequacy should further consider the intermittency of renewable energy. A wide range of indices can be used to measure the adequacy of power systems, including:

- Loss of load indices, e.g., loss of load expectation (LOLE) index, loss of load cost (LOLC), loss of load probability (LOLP);
- Loss of energy indices, e.g., loss of energy expectation (LOEE), expected unserved energy (EUE), and energy index of reliability (EIR);
- Probability or frequency-related indices, e.g., probability of load curtailment (PLC), expected frequency of load curtailment (EFLC), and system average interruption frequency index (SAIFI);
- Duration-related indices, e.g., expected duration of load curtailment (EDLC), the average duration for each load curtailment (ADLC), and system average interruption duration index (SAIDI).

Power system security is an important part of power system reliability analysis [18]. It is a measure of the overall health of the system, including the ability of the power system to maintain the voltage, frequency, current, and other

fields within the specified technical limits, even after disconnecting the main system components. Usually, the “N-1” criterion is utilized to assess the security of the planned networks. The “N-1” criterion is the rule according to which, after an accident, the elements still operating in the control area of the transmission system operator (TSO) can adapt to the new operating conditions without violating the operating limits. The “N-1” criterion can be extended to the “N-K” criterion, which is more strict, considering more occurrences of contingencies. The power system planning considers not only static security but also ensures transient stability by introducing a security-constrained planning model, including steady-state security analysis and transient stability assessment. After the planning is conducted, the system at each planning stage will undertake an AC N-1 security check. The N-1 security check is performed through the time-domain simulation in the PSS@E package. If the network violation happens at any stage, the planning result will be regarded as an infeasible solution, and a new planning decision is enforced to be generated in the next iteration. The iteration will stop, and a final decision is made when there is no security violation.

1.3.2 Resilience

In recent years, the frequency of extreme events, such as hurricanes, earthquakes, and floods, and man-made attacks, like network and physical attacks, have increased dramatically [11]. These events have seriously affected the power system, from long-term power outages to the destruction of major equipment, including substations, transmission lines, and power plants. This requires the development of control and operation methods and planning strategies to improve the grid's ability to respond to such events. The term "resilience" in the power system has many attributes, from the ability of the power system to "resist" and "recover" from interruption events to the ability to actively respond to potential interruption events and emerging threats. The resilience of electric power grids against contingencies, including malicious attacks by adversaries and natural disasters, is emerging as a critical issue in the power sector. Three types of resilience evaluation criteria are summarized in ref. [11], i.e., load curtailment, rate of recovery, and served energy. In some references, the priority of the critical load is considered in the resilience evaluation criteria, where critical load curtailments will degrade system resilience more than non-critical load curtailments. Usually, there are two resilience enhancement strategies, i.e., planning-based methods and operation-based methods. In planning-based methods, redundant transmission lines, backup generators, and BESS are expanded and invested. For operation-based resilience enhancement methods, immediate restoration solutions are formulated to reduce the impact of adverse events on the electricity networks. The possible solutions mainly include network reconfiguration through operating the switches on tie-lines, the formulation of microgrids, and the dispatch of BESS. The load restoration strategies should consider network stability and realize voltage control.

1.3.3 Vulnerability

The failure of the power systems as a key infrastructure will cause considerable damage to society [12]. Therefore, the vulnerability of such facilities should be minimized to cope with multiple interference sources. The vulnerability does not have an explicit definition, and one widely accepted definition is the susceptibility to unusual incidents that can result in considerable reductions in system serviceability. In the power system, vulnerability is a measure of the system's weakness with respect to a sequence of cascading events that may include a line or generator outages. Failure to recognize vulnerable points and critical assets of electricity grids may trigger a sequence of cascading events and eventually result in a large-area blackout when an outage does occur at these critical locations. There are mainly two types of approaches for vulnerability assessment summarized in ref. [12], i.e., topological methods and flow-based methods. The topological methods are also known as complex network analysis by modeling the electricity network as a graph. Based on the concept in graph theory, the node degree, referring to the number of lines connected to a bus, can be utilized as a metric of the structural vulnerability of electricity networks. The line betweenness, referring to the number of shortest paths traversing a given element, was utilized as an index to assess the risk of blackouts. As for the ***flow-based methods***, the power flow is simulated in power system operation and planning. The flow-based methods intrinsically consider the physical feature of power grids, which is neglected in the topological methods.

1.4 Research Significance

Excessive anthropogenic carbon emissions have broken the natural carbon cycle, exacerbating global climate change, which will threaten the sustainable development of human society. According to studies on GHG emissions (mainly carbon dioxide), over 40% of carbon emissions are produced by fossil fuel combustion during the process of power generation. Hence, the power sector is one of the biggest pollutants and emitters, which requires effective methods to consider carbon policies when optimizing power scheduling. Today, climate change, demand-side technologies, available renewable energy, and social/political needs have been driving changes in power generation, transmission, and end-users. These changes will require considerable efforts to construct new infrastructure and capacity-building to strengthen, expand, and retire the existing infrastructure. Under the pressure of change, the transition challenges of energy infrastructure involve major research, combining the engineering, economic, and policy aspects of grid development and investment optimization.

By developing a comprehensive low-carbon oriented planning framework to understand, develop and optimize the future energy network, this paper is of great significance in supporting and guiding investment decisions. The proposed framework will help to ensure that the most efficient and low-emission energy and technologies are used as much as

possible for future power supply. Specifically, this study aims to develop a sustainable multi-energy system, with emphasis on multi-network coordinated planning. The concept of sustainable energy systems will allow the system to investigate the most cost-effective network configuration, enabling the power sector to make cost-effective investment decisions needed to successfully develop and develop the future energy network. Besides, this thesis also provides a guide for the transportation electrification process and considers transportation electrification as a critical section of the energy transition of power systems. Transportation electrification brings a heavy burden to the electricity networks, and the thesis will formulate an effective framework and methodologies to accommodate large-scale EV penetration considering the collaborative planning of electricity and transportation networks. The models and simulation tools developed by the framework will help to identify the lowest cost path for the successful integration of large and small low-emission generators into the grid.

1.5 Research Problems

The core objective of this research is to construct a comprehensive framework of low-carbon oriented smart grid transition. The proposed framework will be completed by focusing on the following six research problems.

1) How to formulate a smooth carbon-oriented transition strategy for power systems considering the emission reduction efficiency? The retirement of CFPPs is an essential factor in developing a low-carbon oriented electricity network because most carbon emissions in the power system come from thermal generators. However, a sudden retirement of CFPPs will cause a supply shortage problem since the traditional CFPPs cover a large power generation share in many countries, such as Australia and China. The retirement of the CFPPs and the construction of renewable energy need to be well coordinated. Besides, in the future, when renewable energy becomes dominant and replaces fossil fuels, the ESS will be crucial for providing frequency regulation services.
2) How to realize emission control considering demand-side obligation through carbon tracking? Although the generation sides are the actual producer of the carbon emissions, the underlying driver of carbon emissions is the demand of consumers. The carbon response of the end-users towards the carbon price should be focused on. A carbon footprint management strategy should be formulated, where emission control is realized from both the generation side and demand side.
3) How to investigate the market interactions in combined CERs, RECs, and the electricity market? The trading modeling of the CERs and RECs should be focused on. Emission trading systems (ETS) and RECs are two methods used to control greenhouse gas (GHG) emissions. However, these two mechanisms are independent. In

the future, the methods to drive the parallel operation of these two mechanisms and how they interact with each other should be comprehensively investigated. Furthermore, under the background of carbon pricing policies, the cooperation of renewable energy plants and emerging storage technology, such as P2G, should be considered.

4) How to consider the integration of EVs in the modern smart grid transition planning problem? With the increasing concerns of environmental issues, the integration of EVs is considered as a promising alternative in order to reduce transportation-related emissions and relieve the dependencies on fossil fuels. However, the proliferation of EVs also causes various problems. First, the lack of energy supplement infrastructure, such as FCSs, will cause dissatisfaction among EV users. Second, the FCSs will attract the neighboring EVs with charging requirements. The construction of FCSs may bring a potential risk of traffic congestion to the transportation network. Third, as emerging electricity demand, the charging load of EVs may jeopardize the electricity network services by increasing circuit loss and voltage violation. Hence, the utility faces challenges in accommodating the increasing number of EVs. Under this context, a proper planning scheme for FCSs should be formulated to cope with the ever-increasing charging demand.
5) How to coordinate the planning of electricity and hydrogen networks with the hydrogen supply chain for FCEVs? Hydrogen serves as the fuel of modern FCEVs, which have the advantages of fast and convenient refueling and exhibit the potential of zero-carbon mobility. Although hydrogen FCEVs have a bright future, one of the main obstacles hindering the commercialization of FCEVs is the insufficient establishment of the hydrogen refueling system. Hence, a multi-network coordinated planning strategy for HRSs and HPSs should be focused on.
6) How to analyze the synergistic effect of multi-energy networks and transportation networks considering the integration of EVs and FCEVs? Due to the increasing coupling between transportation and multi-energy networks, a disruption in any network may directly affect the operation of the other networks as well as the energy supplement of EVs. To this end, a vulnerability assessment of the coupled transportation and multi-energy networks considering different types of EVs has become an emerging topic to be investigated.

1.6 Contribution of This Research

The contribution of this research consists of developing a series of energy transition frameworks, models, and algorithms for the smart grids, which are summarized as follows.

1) Contributions to the electricity network transition planning

First, the early retirement of the CFPPs is optimized in the system expansion. Hence energy transition can be accelerated. Besides, the retirement of CFPPs and the investment of renewable energy are optimized at the same time.

Thus, it can avoid the situation of the sudden retirement of massive CFPPs and the renewable energy investment being unable to keep up. The network can realize energy transition smoothly and reach a real low carbon level in the future. **Second**, the final objective function introduces the concept of the average cost of the emission reduction rather than the total cost presented in other literature. The average cost is the per-unit cost of carbon emission reduction obtained by dividing the total cost ($) by the total emission reduction (ton). It can identify the per-unit cost of emission reduction (i.e., $/ton), thus making electricity network transition more reasonable and effective by investigating the rate of change of cost and emission. It aims at finding out an optimal point where the decision-maker can spend as little cost as possible to reach as large emission reduction as possible. It makes the electricity transition more economical and efficient. **Third**, the power-to-gas stations (P2GSes) construction problem is modeled. The P2GSes can couple the electricity network and gas network while providing ancillary services in the electricity market. The allocation optimization of P2GSes is solved based on a carbon emission flow model. The nodal carbon intensity is utilized in the site selection. Hence, the energy consumed and re-produced by P2GSes is relatively clean. The gas network constraints are modeled to guarantee that P2GSes can work smoothly without energy flow congestion in both electricity and gas networks.

2) Contributions to the emission obligation on the demand side and carbon footprint management

First, a chance-constrained carbon footprint management model is proposed. The direct and indirect carbon emissions are restricted from the supply and demand sides. On the generation side, the network will actively dispatch renewable energy as a priority, and on the demand side, the flexible load will actively respond to carbon-integrated electricity prices. The proposed model aims to address the carbon obligation allocation of the consumers from the perspective of consumption and provide a technical basis for demand-driven stimulation to reduce carbon emissions. **Second**, a probabilistic carbon emission flow model (PCEF) is proposed to track the carbon footprint considering various uncertainties. The two-point estimation method (2PEM) is proposed to evaluate the distribution of the nodal carbon intensity and indirect emissions. **Third**, a solution methodology is proposed to solve the formulated stochastic problem. The Dirichlet process Gaussian mixture model (DPGMM) is applied to model the nonparametric distributions of the uncertainties. The chance constraint is reformulated as a deterministic constraint with parameterized quantiles. A solution algorithm is proposed to solve the optimization problem.

3) Contributions to the CERs and RECs trading

First, a methodology is proposed to investigate the correlation between ETS and RECs, aiming at filling the gap between different mechanisms. The dominant buyers of RECs transfer from electricity consumers to thermal generators. The thermal generators can purchase RECs to increase the carbon emission quotas. The mature ETS drives the development of the RECs market and increases the purchase motivation of RECs. The pricing model of RECs is

proposed for the first time. **Second**, a bi-level optimization model based on a cooperative game approach is proposed. The upper level is to maximize the payoffs from the perspectives of each player, while the lower level is to minimize the total system costs from the perspective of an independent system operator (ISO). A mathematical method is applied to convert the bi-level problem into a single-layer one. Furthermore, in the optimization model, renewable plants can cooperate with P2GSes to compete with thermal generators aiming at earning more payoffs. Hence, the proposed model can investigate how P2GSes smooth the output of renewable energy. **Third**, the proposed model can investigate the interaction between the carbon market and the RECs market. How the carbon price affects the RECs price and total system emissions is studied through sensitivity analysis. The robustness of the proposed model is verified through numeric analysis.

4) Contributions to the EV FCS planning

First, an EV integrated traffic assignment model is formulated based on the conventional path-size logit and stochastic User equilibrium (PSL-SUE) model. The proposed traffic assignment model separates the EV traffic flow from the conventional internal-combustion engine (ICE) vehicle traffic flow and further considers the EV charging behaviors in FCSs. Besides, the randomness of travelers' understanding of the travel cost is taken into consideration. Therefore, the proposed traffic flow assignment model can better simulate the traffic capture of the FCSs in the planning problem under EV diffusion. **Second**, to ensure that the FCSs can provide high-quality fast-charging services to EVs, a QoS assessment method is proposed to help the planned system better adapt to different EV penetration levels at all stages. The QoS assessment is conducted based on the queuing model and two types of queueing dissatisfaction, i.e., reject to join and impatient leave, are modeled. The QoS assessment considers the expected waiting time in FCSs and the number of EVs leaving due to long queues. **Third**, the proposed planning strategy further considers the impact of the distribution system expansion on the transmission level. To cope with the increasing electricity demand of EVs under EV diffusion, several alternatives are available for line expansion as well as fossil-fuel and renewable-based generator expansion at both system levels. Hence, based on [13], an integrated transmission and distribution system planning strategy is further presented to help the planner select an adaptive planning strategy under the EV diffusion to maximize social welfare. The proposed integrated method further enhances the flexibility of the EV charging network and distribution network so that fewer changes are required in the transmission network under different future scenarios.

5) Contributions to multi-network planning for hydrogen refueling system

First, a multi-network planning framework for the hydrogen refueling system is proposed. The proposed framework couples the electricity network, transportation networks, and hydrogen network to enhance the system flexibility. Different from the on-site hydrogen generation, the proposed system structure allows the HPSs and HRSs to be located

at different places, and a flexible hydrogen supply chain is presented. **Second**, collaborative planning enables the cooperation between the electricity network and transportation system to systematically investigate the overall system emissions. The proposed collaborative planning model can investigate the energy trilemma, i.e., the decision-making between system reliability, economics, and environmental sustainability. The planning of the power system helps to equip renewable resources for the EV charging facilities and HRSs. **Third**, the penetration of different vehicles, including internal combustion vehicles, EVs, and FCEVs are discussed. An optimized penetration ratio is solved to realize the complementary role of different types of vehicles. The difference between EV FCSs, charging poles, and HRSs is presented in the proposed model.

6) Contributions to the vulnerability analysis on multi-network system

First, a novel graph representation for the coupled transportation and multi-energy network is proposed. In the traditional topological methods, the graph was utilized to reflect the capacity of energy flow and traffic flow [14]. Different from the traditional representations, the proposed graph representation can further reflect the spatial charging/refueling demand shift between different charging/refueling stations and the energy substitution effect of electricity and hydrogen. **Second**, a critical asset identification tool is applied to find the vulnerability point of the coupled network. Based on the critical asset identification, a new criterion called transfer margin ratio (TMR) is put forward to assess the dynamic vulnerability level under cascade contingencies. **Third**, based on the proposed bi-level optimization model, the lower bound and upper bound of vulnerability, which is the vulnerability envelope while circumventing the need to enumerate all possible disruption scenarios, is investigated. The identification of the vulnerability envelope can be used to assist in the development of possible system improvements in emergency plans.

1.7 Thesis Outline

The thesis is divided into nine chapters. The first chapter is the introduction, which introduces the basic concepts and preliminaries of this research. Chapter 2 is the literature review part. Chapter 3 focuses on carbon-oriented multi-energy network planning. Chapter 4 focuses on emission obligation from the demand side through carbon emission tracing. Chapter 5 focuses on CERs and RECs trading. Chapter 6 focuses on the collaborative planning of the electricity network and transportation networks. Chapter 7 focuses on the integration of FCEVs. Chapter 8 focuses on the evaluation of coupled networks towards extreme events. Chapter 8 outlines concluding remarks and future works.

The outlines of each chapter are briefed as follows.

Chapter 1: This chapter introduces the research background and problem description. Some basic and essential concepts, including modern smart grids and power system planning, are introduced in this chapter.

Chapter 2: This chapter makes a comprehensive review of the power system planning models in both transmission systems and distribution systems. The planning problems also include the planning of FCSs for EVs. Then, the low-carbon oriented operation of the power system is reviewed. Finally, the planning and operation of the power systems in the new environment are reviewed, which includes the new system components and new types of the electricity market.

Chapter 3: In this chapter, a multi-energy network transition and planning roadmap is proposed. First, a retirement model of CFPPs is presented. Second, gas network modeling and P2G technologies are introduced. Then, a two-milestone electricity network transition roadmap that can serve as a guide to assist the current fossil-fuel dominated network to transit into a low-carbon oriented network is proposed. In milestone I, the early retirement of CFPPs and the construction of renewable energy plants are considered in the TEP problem. In milestone II, the planning of P2GSs is focused on. In the model, the P2GSes can realize the energy transition between gas and electricity, and they also can participate in the ancillary market for its fast response.

Chapter 4: In this chapter, a carbon footprint management strategy is proposed, where emission control is realized from both the generation side and the demand side. First, a carbon emission flow (CEF) is introduced to track the carbon footprint, and a PCEF model is proposed to consider the uncertainties. Then, a carbon footprint management strategy from both the generation and demand sides is proposed based on a double carbon taxation mechanism. Third, a price elasticity model to the carbon-integrated electricity price is formulated. Finally, a data-driven solution method is proposed. The feasibility and effectiveness of the proposed method are verified in case studies.

Chapter 5: In this chapter, a bi-level optimization model based on the game approach between thermal generators, renewable energy plants, and P2GSes is proposed to investigate ETS and RECs. First, the market mechanisms of CERs and RECs are introduced. Second, a trading framework of CERs and RECs is presented. Third, the general form of the game-theoretic trading model is presented. Then, based on the kinked demand curve, a pricing model for RECs is proposed. Based on the pricing model, a bi-level optimization model based on the game approach is proposed for a large scale of renewable energy plants and P2GSs, considering the integrated ETS and RECs together. The payoff model of each player is proposed, and three bi-level models are converted to three single-level models through KKT conditions. Nash equilibrium is found via a distributed method. The simulation is conducted on a modified IEEE 30-bus system.

Chapter 6: In this chapter, an adaptive integrated planning of electricity networks and FCSs under EV diffusion is proposed. First, based on the EV diffusion model and the proposed EV-integrated traffic assignment model, the spatial and temporal charging demands are simulated. Second, a multistage stochastic DEP model is presented, where the substations, feeders, DGs, BESS, and FCSs are jointly considered. Third, a QoS assessment is conducted to ensure that the planning solutions can provide high-quality charging services under EV diffusion. Finally, the integrated planning

strategy of transmission and distribution systems is proposed. The cost of the TEP is considered as the adaptive cost arisen from the EV diffusion and the increase of the other normal loads. Based on the presented planning framework and methodologies, we aim to find an adaptive planning strategy that can adapt to a different penetration level of EVs. The proposed strategy is verified in IEEE 24-bus transmission systems encompassing 6 IEEE 33-bus distribution networks.

Chapter 7: In this chapter, a multi-network coordinated HRS and HPS planning strategy for FCEVs is proposed. The proposed mathematical model couples the electricity network, gas network, and transportation network. First, HRS and HPS modeling is presented. Second, the framework of a two-stage coordinated planning of multi-energy networks is proposed. In stage I, the planning of the electricity and gas network is proposed. In stage II, the transportation system planning and optimal penetration ratio of different types of vehicles are optimized. The location selection of the HRSs and HPSs, the electrolysis and refueling operation, and hydrogen delivery through both gas pipelines and logistics systems are modeled. The synergistic effect of the multi-network is investigated to enhance the system flexibility. The proposed methodology is verified in the simulation.

Chapter 8: In this chapter, a vulnerability assessment methodology is proposed for the coupled transportation and multi-energy network, considering the integration of PEVs, FCVs, and PH2EVs. First, a novel graph representation for the coupled transportation and multi-energy network is proposed, where the spatial charging/refueling demand shift between different charging/refueling stations and the energy substitution effect of electricity and hydrogen are reflected. Second, based on the graph theory, the critical assets are identified, and TMR is utilized to assess the vulnerability level. Finally, the lower bound and upper bound of vulnerability, representing the optimistic case and the pessimistic case, are found based on a bi-level optimization problem. The applicability of the proposed method is verified on the IEEE 39-bus power network coupled with a 25-node transportation network and a 50-node hydrogen network.

Chapter 9: The concluding remarks and future works are given in this chapter.

CHAPTER 2

LITERATURE REVIEW

2.1 Power System Planning

2.1.1 Typical Transmission and Distribution Network Planning Model

1) Transmission expansion planning

The TEP has been well studied in the literature. From the aspect of the proposed mathematical model, the present research can be divided into two types: the static model and the dynamic model. For the static model, the planning of the new transmission line and generators are determined based on the new electricity demand at the end of the total planning horizon. Ref. [15, 16] presented a three-level equilibrium model for the static TEP. The pool-based market, generation expansion, and transmission planning were modeled at each level. The three-level model was formulated as a mix-integer linear programming (MILP) problem. Ref. [17] put forward a TRP model with short-circuit level constraints. The mathematical model contained one master problem, namely investment planning, and three subproblems, namely system security, short-circuit level, and the operational optimal. Ref. [18] modeled the TEP considering a probabilistic reliable criterion, which reaches the minimum investment ensuring the reliable criteria of the system are met. All these works focused on the increase in future demand at the end of the year can be met with the advantages of fast convergence.

However, for the dynamic model, the total planning horizon is divided into several intervals. An expansion plan is given in each planning interval. Thus, more factors can be taken into account, such as annual load growth, inflation rate, environmental changes, policy, etc. Ref. [19] put forward the dynamic TEP model and considers the security and the congestion of the system in the environment of a competitive electricity market. Ref. [20] put forward a flexible transmission expansion plan to cope with the increasing risks in the electricity market. The adaptation cost was introduced for the plan selection. The dynamic TEP model is more realistic and can better reflect the dynamic market changes.

In the literature, two uncertainty-associated approaches have been employed: deterministic and probabilistic. The deterministic model only considers a single system operating profile and exams whether the network can remain intact

under normal and N-1 conditions within a variety of technical limits, such as voltage and branch flow [21]. However, the deterministic model neglects the probabilistic features such as intermittent renewable energy and extreme events. Power system expansion planning considering uncertainties has also been well studied. For instance, ref. [22] proposed a two-stage method of expansion that was more robust to handle the uncertainty problems such as demand. Ref. [23] presented stochastic coordination of system expansion by using Monte Carlo simulations. The load duration curve was introduced to simulate the extreme value better. Ref. [24] decomposed the generation expansion and the transmission expansion problem. Refs. [25] and [26] utilized a game-theoretic approach in expansion planning so that transmission expansion and generation expansion could cooperate to earn more profits. Some other papers considered the penetration of renewable energy, such as Refs. [27-29]. But they merely consider renewable energy as an uncertain factor. Ref. [30] proposed a renewable-driven expansion strategy. It set a target for renewable generation capacity in the future. Ref. [31] presented the renewable capacity expansion at the distribution network, and it considers the demand response. Other papers such as refs. [32] and [33] also put forward low carbon development. In the stochastic TEP model, the probabilistic reliability criteria can be integrated into a TEP problem [34]. Refs. [35-37] studied the quantitative risk management in TEP decision-making, which satisfies not only the N-1 criterion but also the risk criterion. Ref. [38] proposed a joint deterministic-probabilities reliability criterion where the planned system should meet both deterministic criterion and acceptable risk criterion under outage. However, one critical drawback of the current risk-based TEP model is that the low-probability but high-impact scenarios, which may cause high economic loss, are discounted when calculating the expected cost of risks. Hence, the risk of extreme events cannot be evaluated properly.

The classification of the present literature is shown in Table 2-1.

TABLE 2-1. SUMMARY OF TEP IN LITERATURE.

No.Ref	Static	Dynamic	Deterministic	Probabilistic				DC	AC
				Renewable energy	load	Market	Other Events		
[1]	☑		☑					☑	
[2]	☑		☑					☑	
[3]	☑		☑					☑	
[4]	☑				☑		☑	☑	
[5]		☑							
[6]		☑			☑	☑			☑
[7]		☑			☑			☑	
[8]	☑				☑		☑	☑	
[9]		☑	☑						☑
[10]		☑	☑					☑	
[11]		☑	☑					☑	

[12]	☑		☑				☑	
[13]	☑		☑	☑			☑	
[14]		☑	☑			☑		☑
[15]	☑		☑	☑			☑	
[16]		☑	☑	☑	☑	☑	☑	
[17]		☑	☑				☑	
[18]		☑	☑	☑			☑	

Some references consider the retirement of CFPPs in the planning problem. Ref. [39] discussed the evolution of the electricity generation mix based on the effect of risk aversion. It pointed out that there would be more closures of thermal power plants when the risk aversion is increased. Ref. [40] considered renewable resources, DR, and energy storage to replace conventional fuels and decrease the average levelized cost of electricity in Ontario. The displacement of fossil fuel generation is considered in the scenarios. However, refs. [39] and [40] have not proposed a detailed dynamic retirement optimization model for CFPPs. Refs. [41, 42] put forward a robust multi-objective model for transmission expansion, considering the retirement of the generators in case studies. However, CFPPs will retire at their designed age, indicating that the retirement problem was not optimized. Ref. [43] proposed a rigorous mathematical model considering generation expansion and retirement planning. The stochastic programming considered the random outage of the generators, and the simulation results found out that the retirement option was beneficial to the power system reliability. Ref. [44] not only modeled the retirement of the aging generators but also the rehabilitation problem. It pointed out that rehabilitation can also be an economical option. Ref. [45] proposed a mathematical model aiming at electricity network expansion and CFPPs retirement targeting low-carbon energy transition. The mathematical model considered carbon tax and carbon trading of thermal generators as environmental factors. These papers considered the retirement of the generators because they are approaching the retirement age and outage becomes more frequent. However, how to model the early retirement of CFPPs in the context of renewable energy transition still need to be discussed. Besides, the method to solve the trilemma of cost, risk, and environment needs to be further considered. All these papers minimize total investment and operation costs. However, whether a minimum cost will result in a good emission reduction is questionable.

2) Distribution expansion planning

DEP planning can also be classified into the static model and dynamic model. The typical objective mainly includes economic cost [46], such as network reinforcement cost and network lifecycle cost, technical indices [47], such as power supply quality, voltage deviation, and performance criteria [48], such as reliability of power supply and renewable energy penetration. In the distribution networks, the emergence of various DERs leads to the advent of active distribution

networks (ADN). The active distribution networks planning (ADNP) problem needs to consider the optimal integration of DERs and new distribution network technologies.

One of the key features of the ADNP problem is the explicit consideration of various uncertain input parameters, e.g., intermittent renewable generation, load demand, and electricity prices. Ref. [5] pointed out that the adequate planning of the ADN necessitates the computationally accurate and efficient modeling of these uncertain input parameters. In the literature, robust optimization [49] and stochastic optimization [50] are widely used to deal with these uncertainties. In stochastic optimization, the representative scenarios that have specific probabilities are utilized to deal with the uncertainties. Although the scenarios improve the planning solution, the computation efficiency is sacrificed, especially when the number of scenarios is large. Hence, advanced scenario generation technologies are required to effectively select and cut down the number of representative scenarios. In robust optimization, the uncertainties are represented by using the parametric bounds. The robust optimization offers planning solutions that retain optimality for the worst-case scenario in uncertainty. However, the plans may be too conservative.

The BESS is an essential new technology that can smooth the output of intermittent renewable energy in the distribution network. The BESS siting and sizing planning have become an important part of ADNP. However, how to effectively incorporate the BESS into the power system needs to be investigated. Ref. [51] focused on the net present value (NPV) of saving and optimizing the capacity of the battery. Ref. [52] not only solved the sizing of the batteries at all the electricity nodes in the distribution system but also considered the voltage regulation and peak load shifting in the cost-benefit function. Besides, the aging of the batteries was considered as a cost that is linear to the discharging circle. Ref. [53] chose the total cost of the system as the objective function to solve the planning of siting, sizing, and rated power of the batteries. Ref. [54] proposed a planning and control strategy for BESS where the maximum profit can be reached by providing the primary frequency regulation service. Ref. [55] utilized game theory to solve the planning of a hybrid power system comprised of wind turbines, PVs, and batteries. With more and more DERs emerging in the distribution system, uncertainties cannot be neglected. In ref. [56], the Monte Carlo method and stochastic scenario method were synthetically applied to realize the stochastic planning of ESS. In ref. [57], an energy storage planning model considering the chance-constrained optimization with non-parametric probability functions has been proposed, which eliminated the dependency of uncertainty factors on statistics and modeled the probability distribution of irregular shapes. Because of the uncertainties in the system, the security and stability of the power grid have been challenged. Ref. [58] focused on the location planning of centralized energy storage and distributed energy storage from the perspective of grid stability. In ref. [59], a two-stage stochastic optimization model was proposed to solve the planning of the BESS, and a load shedding strategy was considered to improve the stability of the system. In ref. [60], a

hierarchical optimal allocation of BESS was proposed, where the sitting of the BESS was solved based on voltage violation risk in the first stage, and the sizing was solved in the second stage.

However, two issues have not been fully addressed in the previous works. First, the distribution network is changing rapidly nowadays. To ensure the long-term effectiveness of the current planning, a planning methodology that considers future uncertainties and a criterion that can evaluate future risks are essential. Some existing references have already considered various types of uncertainties. For example, ref. [53] considered the uncertainties of wind power generation in the planning of BESS. In ref. [56], the stochastic optimal planning for BESS was proposed, where load, PV generation, and wind generation were regarded as important uncertainties. In ref. [57], non-parametric probability functions were used to model the uncertainties in energy storage planning, and a chance-constrained optimization was solved. In fact, one of the critical functions of the BESS is to smooth intermittent renewable energy. However, most references considered the short-term uncertainties in the context of long-term planning of the BESS. The penetration of renewable energy resources will continuously rise in the future, which may introduce new voltage problems in the ADN caused by the inverse power flow. Some references integrated the long-term uncertainties into the planning problem. For example, ref. [20] calculated the adaption cost of flexible planning to deal with long-term uncertainties. However, the current literature lacked proper criteria on nodal voltage risk under large-scale renewable energy. When the penetration of DERs is high in the future, a very high voltage deviation may occasionally happen because of the intermittency of renewable energy but will bring higher risks to the end-users. The currently proposed methods, such as ref. [60], failed to evaluate the nodal voltage risk in such a situation.

Because of the uncertainty of renewable energy, the electricity grid will be faced with stability and security problems. Apart from the cost of the BESS, some researchers focused on the stability of the grid. Ref. [58] modeled the planning of the BESS in the distribution level from the angle of grid security. Ref. [59] put forward a two-stage stochastic model of ESS planning and considered load shedding based on DR.

2.1.2 Market-based Power System Planning

The power system planning problem in the deregulated electricity market environment should be taken into additional consideration, including reliability cost, market signals, congestion surplus, social welfare, market risk, etc., to provide a competitive environment for all participants. The integration of the electricity market can diversify the generation mix, reduce electricity prices by creating a more competitive and transparent market, and provide additional generation capacity in case of a shortage in any country. The liberalization of the energy market requires that power system planning be studied as a decentralized decision-making process based on price. The market signals offer incentives for market

participants' investments. The current literature focused on market-based power system planning is summarized in Table 2-2.

TABLE 2-2. REVIEW OF MARKET-BASED POWER SYSTEM PLANNING IN LITERATURE.

Ref.	Objectives	Techniques	Main Findings
[19]	Presents a multi-year TEP model which considers the transmission congestion	The Benders decomposition approach is utilized, which decomposes TEP into a master problem and two subproblems representing security and optimal operation. The congestion cost is a proper criterion for measuring the degree of competitiveness in an electricity market.	The model evaluates the impact of potential generation investment on TEP in the restructured power system. Regulators can use the proposed model to provide long-term TEP to market participants. Regulators and transmission service providers should consider various factors and the indispensable interdependence between transmission and generation planning to optimize long-term social benefits.
[61]	Presents a mixed-integer linear programming (MILP) formulation for the long-term TEP problem in a competitive pool-based electricity market.	A number of scenarios based on the future demand in the system are defined to achieve optimal expansion planning while modeling market functioning. A set of metrics is proposed to rate the effect of the expansion on the generators, demands, and the system as a whole	The results of different case studies show that the changes in topology, scenarios, and weight factors related to investment and operating costs have appropriate economic explanations for generators, demand, and network planners.
[62]	A Bi-level model of TEP in a market environment is proposed, in which producers and consumers freely trade electric energy through a pool.	Using the duality theory, the proposed bi-level model is recast as a MILP problem, which is solvable using branch-and-cut solvers.	The solution generated by this model has higher social welfare but also higher investment costs than the solution provided by the classical cost minimization method. Simulation results show that the proposed model is workable for real problems and is interested in deriving solutions involving high social welfare.
[63]	A static transmission expansion method is proposed using a multi-objective optimization framework. In optimization, investment cost, reliability (adequacy and security), and congestion cost are regarded as three goals.	In order to overcome the difficulties of solving the nonconvex and mixed integer properties of optimization problems, the NSGA II algorithm based on a genetic algorithm is used, and then fuzzy decision analysis is carried out to obtain the final optimal solution.	The main advantage of this algorithm is that it allows planners to use a cost-effective method rather than a minimum-cost planning process. It defines a model to deal with the preferences of different stakeholders. Finally, it incorporates static security analysis into the first stage of planning, which will produce a more optimized solution than the analysis left for the second stage.
[64]	A methodology for TEP in the deregulated electricity market is presented. The proposed TEP is	Monte Carlo simulation is used to obtain the probability density function of wind turbine output. Then, the uncertainties of WTG and	This method reduces the total investment cost, improves reliability, and realizes the maximization of social welfare.

	associated with Reactive Power Planning (RPP), reliability assessment, and also consideration of wind and load uncertainties.	load are considered in the TEP formula. The particle swarm optimization method is considered to solve the programming problem, which is constrained nonlinear mixed integer optimization programming.	
[65]	To evaluate a critical project in the Ten Year Network Development Plan of the Independent Power TSO, namely the electric interconnection of Crete Island with the mainland electric system.	A general mixed integer linear programming model is proposed, which integrates the medium-term energy planning model with the unit commitment (UC) model. The medium-term energy planning model performs generation and transmission system planning at the annual level, and the unit commitment model performs the simulation of the current electricity market.	This paper proves that the model can provide the best energy roadmap and management, as well as clear price signals of key energy projects under actual operation and design constraints, so as to provide useful insights for investors and/or decision makers to determine strategies and challenging decisions at the national and/or regional levels.
[20]	A flexible planning solution is proposed based on the adaptation cost considering the new uncertainties for market participants introduced by deregulation of the electric power industry	The planning process is modeled as a mixed integer nonlinear programming problem in order to simultaneously optimize conflicting objectives. In order to minimize the planning risk, our method identifies several scenarios based on statistics and expert knowledge; Choose the most flexible expansion plan as the plan with the lowest adaptation cost.	By constructing appropriate scenarios and calculating adaptation costs, the proposed method can generate the most flexible expansion plans in the future. That is, they need less cost and time to adapt to the new environment.
[66]	An ISO model is proposed to coordinate TEP and competitive generation capacity planning in the power market. The purpose of this model is to simulate the generation and transmission capacity expansion in the market environment as a whole.	The model adopts the joint energy and transmission auction market and capacity mechanism. The joint auction market enables competition between power generation and transmission resources. The capacity mechanism provides incentives for the investment of market participants and reflects the location value of additional capacity. The decision of transmission capacity expansion is made by commercial transmission lines, and their capacity investment is recovered through transmission marginal pricing and capacity payment.	Transmission network security is reflected in the proposed competitive resource planning model. An example is given to illustrate the coordinated planning of generation and transmission in a restructured power system.

2.1.3 Multi-energy Network Planning

The multi-energy network (as known as an integrated energy network) is an approach to finding environmentally friendly and cost-effective solutions for the best mix of energy supply and demand options [67]. It is believed that the multi-energy network will dedicate to long-term sustainable development considering the emerging advanced energy conversion technologies, such as P2G. In the discipline of power engineering, multi-energy networks mainly include electricity networks, gas networks (natural gas or hydrogen), and heat networks. In the multi-energy system, the purpose

of energy infrastructure is to produce, transform and transport energy. The energy infrastructure includes the network facilities (electricity feeders, gas pipelines, and heat network), the energy conversion units (boiler, gas power plant, P2Gs, heat pump, cogeneration plants, etc.), and energy storage (battery, gas tank, heat tank, chemical storages, etc.). From the view of network modeling, different types of networks show some similarities and discrepancies [6]. First, the driving force of the modeling is different. The driving force of the electricity network is the voltage gap, while that of the thermal and gas network is the pressure gap. The difference in the driving force will result in discrepancies in modeling. The electricity network is modeled based on the nonlinear power flow. Linearized technologies are provided to simplify the modeling [68]. The thermal and gas network modeling has some similarities in driving force, but the dynamic process is different since gas is a compressible fluid while water is incompressible. Therefore, gas network modeling is based on nonlinear compressible flow, while the thermal network is based on conservation equations. In ref. [69], a linearization approximation method is proposed to simplify the gas flow modeling. Table 2-3 summarizes the modeling structure, conversion mode and storage devices in the literature.

TABLE 2-3. SUMMARY OF MODELING STRUCTURE, CONVERSION, AND STORAGE DEVICES IN MULTI-ENERGY SYSTEM.

Ref.	Structure			Energy conversion mode			Storage			
	CHP	CCHP	P2G	to electricity	to heat	to gas	BESS	TES	HES	NGS
[70]	☑			☑	☑		☑	☑		
[71]	☑			☑				☑		
[72]	☑			☑	☑		☑			
[73]	☑			☑	☑		☑	☑		
[74]	☑			☑	☑					
[75]		☑		☑	☑		☑	☑		
[76]		☑			☑					
[77]		☑	☑	☑	☑					☑
[7]		☑		☑	☑		☑	☑		
[78]		☑		☑	☑			☑		
[79]			☑	☑		☑		☑	☑	☑
[80]			☑	☑	☑	☑	☑		☑	
[81]	☑			☑	☑	☑	☑	☑	☑	

The energy conversion units and energy storage modeling are usually modeled as an energy hub system in the literature. The integrated energy under the framework of the energy hub system can contribute to increasing the reliability of the system and energy efficiency. The research works on hybrid energy systems can be divided into two types. The first one focuses on the expansion planning model of the energy hub, such as [82]. The second type focuses on the management and trading of hybrid energy. Ref. [83] proposed energy management models based on DR under the framework of the energy hub system to reduce the operation cost of the energy hubs. Ref. [84] proposed a cooperative trading mode for the community to realize risk management by considering the conditional value at risk

(CVaR). Ref. [85] proposed a distributed auction mechanism for the energy hubs that serve to build energy users. To earn more profit and save energy costs, game theories, such as a noncooperative game [86], exact potential game [87], monotone generalized Nash game [88], and bargaining game [89], are widely used in the energy trading strategies for the energy hub. All these references show that a multi-energy system can increase the flexibility of the energy system, provide the customer with reliable services, and reduce the burden of the utility grid. However, these papers are based on the existence of energy hubs. Besides, the system scale is relatively small, such as the community-level. Compare with the framework of the energy hub system, the framework of the proposed integrated energy sharing system does not rely on the energy hub but can aggregate the prosumers who are widely spread in the distribution system. Through control of the distributed energy storage devices, the utilization rate of the ESS can be increased.

2.1.4 Renewable Energy Integrated Planning

Considering the combat climate change, renewable energy is carrying a great expectation in the energy transition process. Power system planning requires to facilitate the integration of renewable energy sources. In the previous part, it is mentioned that the uncertainties of renewable energy are a critical concern in power system planning, especially in ADNP. In this part, a comprehensive and detailed review of renewable energy integrated planning will be provided.

The large penetration of renewable energy will impose more complexity on the power system. Its inherent variability leads to the overall deviation between power generation forecasts and excessive or insufficient energy, which makes it difficult to balance supply and demand at high time resolution with limited storage and backup capacity [90]. Due to the limited dispatchability of renewable energy, it is becoming more and more important to integrate flexible energy and technology to enhance system flexibility. Converting the traditional planning problem to renewable energy integrated planning, the changes are embodied in objective functions, constraints, and uncertainty analysis [91].

In the objective function, not only should investment cost be considered, but the environmental cost should also be taken into consideration [92]. Renewable energy needs to undertake more power generation tasks, and the corresponding objective function is also generated. The most commonly used method is to maximize the share of renewable energy in the power generation portfolio, such as the maximum share of renewable energy power generation [93] and the maximum contribution of renewable energy to peak load [94]. Some references also focused on minimizing the excess wind and solar power [95], minimizing the backup generation and transmission capacity, and minimizing the additional reliability requirement of variable renewable energy. To this end, the single objective function may be expanded to a multi-objective function, which concerns the investment cost, environmental impact, and system reliability.

For the condition constraints, apart from the power balance constraints, capacity expansion constraints, generation

and transmission constraints, and fuel supply constraints, which also exist in conventional planning problems, the renewable energy integrated planning problem may further consider the policy constraints, especially for carbon policy [96]. The carbon emissions of thermal generators are limited by the emission reduction target from the government. Besides, the integration goal of renewable energy as a renewable power rate constraint is presented in some countries' energy strategy planning to mitigate climate change and energy [97].

The uncertainty analysis has been discussed in the ADNP problem. Two widely used methods, i.e., stochastic optimization and robust optimization, are presented. In recent years, with the development of machine learning and deep learning technologies, more advanced tools have been utilized to model the uncertainties of renewable energy. For example, the ref. [98] proposed a two-step approach to solar power generation prediction based on machine learning. Ref. [99] provided an accurate estimation of community-level behind-the-meter PV generation based on a Bayesian neural network. In ref. [100], a nonparametric Bayesian method based on the Dirichlet process mixture model was presented to estimate the distribution of wind farm generation. These data-driven methods will be utilized to assist in building a more refined and accurate uncertainty model in integrated renewable energy planning.

2.1.5 EV FCS Planning

In the literature, the collaborative planning models of EV FCSs, transportation systems, and distribution systems were well studied. The EV FCSs are expected to capture the largest traffic flows in the transportation network [101]. The electricity network is planned to support the physical connection between the FCSs and the electricity network [102]. Thus, FCSs become coupling points between the electricity and transportation networks, and the two types of networks become intensely correlated [103]. In this context, Quevedo *et al.* [29] proposed a joint planning strategy for FCSs, BESS, DGs, substations, and network expansion. From the view of the transportation network, Zhang *et al.* [104] proposed a charging facility planning model considering the congestion based on Yen's algorithm. Gan *et al.* [105] further considered the expansion of the road sections in the FCS planning to avoid traffic congestion. Ref. [106] proposes an optimal allocation model for EV charging stations to maximize the total social welfare. Refs. [107, 108] propose a heuristic planning method for EV charging stations for the freeway, and the charging demand of EVs is estimated according to the Shared Nearest Neighbor Clustering algorithm. Refs. [109-111] figure out both location and sizing problems of charging stations by a sequential planning method. In ref. [17], a scenario-based stochastic model has also been proposed with the objective function of minimizing the system cost. The stochastic co-planning model is utilized to address future uncertainties, namely the penetration ratio of EVs and the charging method. However, these co-planning models only aim at helping the system avoid redundant expansion of feeders and sub-stations, but neglect the

essence of the government's encouraging EVs, i.e. reducing emissions. It should be noticed that the collaborative planning of the electricity distribution network and transportation network can also reduce total system emissions.

The planning of FCSs will face various uncertainties [112]. To deal with the uncertainties, such as the mobility of EVs and renewable energy generations, Hajebrahimi *et al.* [113] proposed a distributionally robust optimization for electricity networks and electrified transportation network planning. The increasing penetration of EVs will cause uncertain charging demand in the future. Therefore, Li *et al.* [114] proposed a data-driven planning framework, where the EV charging demand was first predicted, and then a market-based competitive planning strategy for FCSs was formulated. To cope with the uncertain charging behaviors, such as the choice of fast charging and slow charging, Yao *et al.* [115] proposed a scenario-based planning strategy considering the integration of plug-in EVs. Apart from the choice of the charging mode, the choice of the charging stations is also a stochastic factor. Hence, as demonstrated in [116, 117], an agent-based traffic assignment model was proposed to simulate the behaviors of EVs. Luo *et al.* [118] further considered the real-time charging navigation of EVs when planning the FCS. Some references also considered the queueing in the FCSs in the planning problem based on stochastic analysis [119-121]. Yang *et al.* [122] integrated the EV dynamics in the FCSs into the planning problems, and EV dynamics were modeled by a Markov chain and queueing theory. Wang *et al.* [123] proposed a stochastic model to minimize the weighted sum of network investment cost, energy losses, and queue waiting time to address the stochastic feature of EVs' driving behaviors.

Some reference also considers the charging strategies of the EVs in the planning problem of FCS [115]. The studies of EV charging behaviors can help the planner better estimate the charging demand in FCSs. In the literature, the smart charging strategies of EVs have been widely studied, where EVs obtain energy via grid-to-vehicle (G2V) transfer [124]. For instance, ref. [125] proposed a real-time EV charging scheduling via ordinal optimization, which could search for good enough charging policies within seconds while still providing a probabilistic performance guarantee. Ref. [126] presented a decentralized failure-tolerant algorithm for optimizing EV charging, which handled capacity, peak demand, and ancillary services coupling constraints. To estimate the expenses inherent with smart charging, e.g., battery aging costs, ref. [127] integrated battery aging in the optimization for smart charging of EVs. In recent years, big data and machine learning technologies developed rapidly and are gradually utilized in EV charging strategies. In ref. [128], a deep reinforcement learning (DRL) based method was proposed to learn the optimal charging control strategy by interacting with the dynamic environment. The proposed method could crack the individual EV charging scheduling considering the dynamic user behaviors and the electricity price. To mitigate the complexity of the dimensionality of unknown states, ref. [129] established the nodal multi-target characterization of the optimal scheduling policy, and the charging scheduling was solved by the model-free soft-actor-critic-based method.

With the advancement of bidirectional chargers, the energy can be delivered from EVs to the grid through vehicle-to-grid (V2G) technology [130-132]. EVs not only serve as transportation tools but also act as energy storage units. With the V2G technology, EV owners become prosumers and can participate in the energy market actively [133]. However, individual EV power capacity is too small to affect the entire system operation. Therefore, EV aggregators (EVAs) aggregate the EVs to make them compatible as a concise collection of power ramping controls [134]. Then, the aggregated EVs can be utilized in frequency and voltage regulation [135-137]. Ref. [138] focused on the day-ahead optimal reserve management problem of EVA, which was solved by a discrete bilevel optimization model and exact algorithm. EVA aggregated the reserve capacity provided by the EV owners and then bid in the reserve market. Ref. [139] proposed a hierarchical voltage control strategy for distribution networks considering the customized charging of EVs.

The arbitraging behaviors and DR of EVs in certain periods will result in a large-scale simultaneous charging and discharging of participating EVs [140]. It will lead to overloading problems in the distribution network, which can also affect the quality of services provided to EV owners. Therefore, a local energy transaction, where generation and consumption coexist in a region, is preferred to reduce the reliance on network transmission. On the other hand, the updated technologies of the internet-of-things (IoT) facilitate point-to-point transactions. Although the IoT devices will increase the local load, it is widely accepted that various parties, including network operators and prosumers, can obtain more benefits from the updated technologies. Under these contexts, the concept of vehicle-to-vehicle (V2V) was proposed, which can offer more flexible charging plans for EVs [141]. When a number of EVs are allotted to a region, such as communities or parking lots, this region will become a suitable power grid for the V2V operation [142]. There are various benefits of V2V summarized in ref. [143]. The advantages can be concluded from two aspects. First, from the grid side, V2V encourages local transactions, which mitigates the power transmission burden of electricity networks. By using V2V operation, the power reserve can be kept within the community of EVs, which can greatly reduce the power loss and the trading loss between the local region and the power grid. Besides, V2V has uncomplicated infrastructure requirements. Second, from the customers' side, V2V offers more flexible charging plans so that customers can earn extra revenue and save on charging costs by participating in V2V. Besides, ref. [144] also pointed out that V2V is helpful in mitigating the range anxiety of EV users. In the work of Zhang *et al*. [145], a smart V2V charging strategy was proposed to realize a cooperative charging strategy allowing communication between end-users. A max-weight V2V matching algorithm was proposed in order to optimize the network's social welfare. In the work of Zeng *et al*. [140], a hierarchical bipartite graph matching method was proposed to promote transactive V2V power exchanges in a distribution system. Through the proposed methods, individual EV's electricity trading price could track

that of the subsystem by adjusting respective power exchange objectives adaptively. In the works of Wang *et al*. [146], a smart grid architecture with enhanced communication capabilities for mobile EVs via a heterogeneous wireless network-enhanced smart grid was presented. In the formulated grid architecture, an online spatial-temporal coordinated V2V energy swapping strategy was presented based on price control.

However, two problems have not been fully addressed in the current literature. First, although some references considered the queuing model in the FCSs planning [119-123], they failed to assess the quality-of-service (QoS) of the charging services from the perspectives of the whole system. Therefore, the diffusion of EVs will result in the currently planned charging infrastructure cannot provide sufficient charging services. Second, the usage growth of EVs, which brings in an increase in local electricity demand, will result in a system expansion. However, in most of the references, the transmission and distribution networks were planned independently for each other, thereby leading to lacking effective coordination between different system levels. In [13, 147], an integrated transmission and distribution system expansion planning strategy was proposed. The proposed method identified the best alternative for the candidate assets under the uncertainties associated with demand and renewable energy generation. In [148], a coordinated decision-making framework was proposed to determine the planning scheme and scenario-based generation schedule for integrated transmission and distribution networks based on decentralized and hierarchical optimization. A stochastic bi-level hierarchy was presented to decompose the centralized optimal planning. Baughman [149] proposed an expanded planning framework that integrated the transmission and distribution into an integrated resource planning framework to evaluate the demand-side options. Based on these previous works, integrated planning of EV charging infrastructure, distribution network, and transmission network under the context of EV diffusion, needs to be further investigated.

2.2 Low Carbon Oriented Operation of Power System

2.2.1 Emission Control from Generation Side

In the literature, the low carbon-oriented operation of the power system has been focused on. The emission control strategies can be classified into two aspects. The first aspect is renewable energy plant investment. For example, ref. [150] proposed a method based on a numerical Genetic Algorithm (GA) for wind farming optimization to determine both the siting of wind turbines and the LCOE. The planning model considered the complex terrain while analyzing the energy offset in terms of demand and supply of the area to encourage decentralized and more stable energy networks. Ref. [151] proposed a multi-stage interval-stochastic integer programming model to plan power systems under uncertainty while managing GHG emissions. Refs. [152] and [153] also considered the aging and retirement of coal-fired generators in the energy transition planning problem.

The coal-fired generators were substituted by the renewable energy plants, and the renewable energy penetration level was increased based on the multi-stage planning model. Besides, ref. [154] considered the emission control devices, which were utilized to capture CO_2 from the power plant and deposit it in a place where it is not able to enter the atmosphere. The second aspect is from the low-carbon operation constrained modeling. The environmentally constrained optimal dispatch method has been thoroughly studied in recent years. In ref. [155], a conventional low-carbon dispatch model based on wind generators was developed and analyzed. It was pointed out that although wind generation did not itself produce any harmful emissions, its effect on power system operation could actually cause an increase in the emissions of conventional plants if the wind generation could not be forecasted accurately. Wind power generation running in the system that includes wind power generation prediction in the scheduling decision has higher emission reduction benefits than the system that only accommodates wind power generation when wind power generation is available. With the increase of installed capacity, CO_2 decreases significantly; however, in order to significantly reduce SO_2 and NO_2 emissions, wind power generation must be combined with alternative emission reduction measures such as emission taxes. In ref. [156], the optimal dispatch of the CO_2 capture power plant was taken into consideration. In the proposed model, the energy flow and operation characteristics of carbon capture plants (CCPs) were modeled, and the mutual constraints between the total power generation of CCPs and the operating power consumption of the carbon capture system were analyzed. Then, the generation output model and the optimal scheduling principle of CCPs were established, which can determine how much carbon captured can represent the premium payment to offset the cost increase caused by the reduction of power output caused by carbon capture and storage (CCS). On this basis, considering the factors of a low-carbon economy, a power dispatching model considering CCPs was proposed. To limit the emissions of thermal generators, their carbon emission rights (CERs), also known as quotas, are restricted. The emission trading scheme (ETS) is introduced to allow the thermal generators to trade the CERs. Ref. [157] pointed out emission trading was the most effective policy to minimize the overall costs of carbon abatement, and it investigated the allocation problem of free carbon permits for generation companies. Ref. [158] developed a full-infinite interval-stochastic mixed-integer programming (FIMP) method for planning carbon emission trading (CET) under dual uncertainties. FIMP showed advantages in uncertainty reflection and policy analysis. Ref. [159] proposed a multi-objective regional carbon emission management model based on probabilistic power flow. The three objective functions to be minimized were the cost of electricity generated, the total carbon emissions, and the carbon emission difference among regions which reflects the regional carbon emission imbalance from the supply side.

2.2.2 Emission Obligation from Demand Side

In most of the references, the emission control strategies were imposed on the generation side. However, it should be noted that the demands are the underlying driver of emissions. Therefore, some references began to focus on the emission obligation on the demand side. The demand side management (DSM) can reduce the emission level by improving energy efficiency. The frequent demand response (DR) requires higher payouts than generation scheduling from the supply side. To this end, proper carbon-oriented DSM strategies should be focused on. The DR program is classified into *price-based programs* and *incentive-based programs* in the literature [160]. In the *price-based program*, the end-users save the electricity bills through actively responding to the tariff price programs [161], such as time-of-use (TOU) price [162], real-time price (RTP) [163], and critical peak price (CPP) [164]. These DR electricity prices vary during the off-peak and on-peak periods, indicating the ability of the utility to provide electricity. Ref. [165] proposed a two-stage approach of price-based DR to enhance operational reliability and reduce operational costs using interval optimization. An *incentive-based program* provides financial incentives to the end-users who participate in the DR program. Therefore, the participants are obliged to reduce or shift their energy consumption according to the contract. The *incentive-based program* can be further categorized into direct load control, load curtailment, and demand bidding program [166]. The direct load control program allows the system operator to control end-users' appliances remotely. Ref. [167] proposed a direct load control strategy for HVAC units that cooperated with the shared BESS. In ref. [168], the author extended the conventional incentive-based DR to the integrated energy system where energy substitution effects among different energy carriers exist. In the load interruption/curtailment program, the system operator is authorized to cut down the end-users' energy supply during an emergency [169]. In the demand bidding program, the consumers bid for the load reduction day-ahead [170]. Ref. [171] proposed a demand bidding model to facilitate DR trading in load curtailment formed between the aggregator and customers.

Ref. [172] analyzed the relationship between the DSM and emission reduction. It was pointed out that carbon tax reduces capacity factors of base load serving units while DR reduces the capacity factors of peak load serving units. Then, it quantified the relationship between emission reductions and the capacity factor of the peaking units. Ref. [173] proposed a two-stage scheduling model to comprehensively investigate the environmental benefits of consumers participating in both electricity and carbon emission trading markets through active demand-side management. Ref. [174] further extended the carbon response of the end-users into a multi-energy network. A two-stage low-carbon operation planning model considering P2G technologies was proposed based on a bilateral trading mechanism with active demand side management, aiming to mitigate carbon emissions. Ref. [175] developed an n analysis tool to address

the carbon obligation allocation issue from a consumption-based perspective and provide technique grounds for demand-driven stimulus to reduce carbon emissions.

Ref. [173] pointed out that the underlying driver of carbon emissions was the demand of consumers. Hence, methodologies were proposed in the literature to track the carbon footprints of the electricity load. Marginal carbon intensity was proposed to determine how a change at the generation side/demand side influences the system's carbon emissions [176]. In ref. [177], the carbon emission flow (CEF) model was proposed to track the carbon footprint. Virtual carbon flow is supposed within electricity flow from the generation side to the consumer side across the electricity network. The basic assumptions are the same as the well-known electricity flow tracing: proportional-sharing rule and the priority of generators to supply loads at the same node. In ref. [178] an analytical model for CEF in the multi-energy system was proposed to quantify the carbon emissions associated with the energy delivery and conversion process. The explicit CEF models for different energy networks, including the power network, gas network, and heating network, were established. Based on the CEF model, the indirect carbon emissions on the demand side can be estimated. Ref. [103] estimated the indirect emissions of electric vehicles (EVs) and fuel cell vehicles (FCVs), which tracked the emissions from the generation side to the demand side.

2.2.3 Participation in Carbon Market and Green Certificate Market

In the literature, carbon emission trading is well studied. At the transmission level, Refs. [179-181] consider the carbon emission trading in the unit commitment model (UC) to investigate how the ETS and demand-side resources lead to low carbon emissions in the power system. Ref. [182] investigates the influence of the carbon price and output-based quota allocation mechanism on emission reduction under the background of emission abatement policy. Ref. [183] considers ETS in a storage planning model to assist China in fulfilling the emission reduction target. In ref. [157], different methods to allocate the free initial quotas are discussed. Refs. [184, 185] have studied the emission trading behavior from the perspectives of a power generation company. Ref. [186] studies the spinning reserve capacity of the power system under the background of carbon trading. Refs. [187, 188] have modeled the interactions between the carbon market and the electricity market. At the distribution level, ref.[189] puts forward a bidding strategy for virtual power plants when considering the carbon-electricity trading ancillary market. In refs. [190, 191], a bi-level model is proposed to solve the planning problem of a multi-energy hub considering the carbon constraints. Ref. [192] proposes a model based on carbon emission flow to find out how the carbon trading cost at transmission-level shifts to the downstream distribution level through carbon integrated local marginal electricity price. Ref. [193] proposes a demand management approach aiming at carbon footprint control. Ref. [173] considers the carbon DR of the consumers to

investigate how the response of the consumers affects the total emissions of the system.

However, the research regarding RECs is limited. In ref. [194], it is mentioned that the RECs mechanism is a kind of renewable energy support policy. In ref. [195], as a government incentive, RECs can contribute to the rapid development of renewable energy. Ref. [196] reveals the evolution of the RECs supporting scheme for promoting renewable energy in Romania. But there is no quantitative model and analysis on how RECs benefit the renewable energy plants and the overall emissions. Ref. [197] points out that REC trading can relieve the government's financial burden by reducing the expenditure on the subsidization of renewable energy. To verify the effectiveness of the RECs, the development of renewable energy and economic benefits under different carbon policies are investigated. Ref. [198] analyzes the tradable RECs market, where renewable energy investors receive certificates based on their production and sell RECs to retailers. The retailers require to purchase in an amount proportional to their total sales. Ref. [199] proposes a multi-objective dynamic economic emission dispatch model for wind-solar-hydro power under tradable RECs. However, no research focuses on how to improve the motivation to purchase RECs. Apart from carbon trading, ref. [200] also introduced REC trading. The REC is another tool to motivate the end-users to consume renewable energy.

2.3 Energy Transition in New Environment

2.3.1 Planning and Operations in Consideration of New Network Elements

1) Sustainable seaport microgrid for all-electric ships

The maritime sector currently accounts for the logistics of 90% of the world's trade. Meanwhile, the shipping industry is responsible for an increasing amount of global carbon emissions. The worldwide shipping emitted 930 million CO_2 in 2020, which accounts for 2.73% of the total carbon emissions [201]. Therefore, the environmental impact of vessels cannot be neglected. To establish an environmental-friendly maritime transportation system, the deployment of all-electric ships (AESs) becomes an effective measure. The AESs are equipped with hybrid energy systems, including photovoltaic (PV), battery, diesel generators, etc. Onshore power, also known as cold ironing, conventionally refers to the electricity from the shore to provide shoreside electrical power to a ship at the berth that will replace the auxiliary diesel generators in the ship. The auxiliary diesel generators that power cargo handling equipment and other ship services while in port are the primary source of air emissions from ships in ports today because the auxiliaries run on heavy fuel oil or bunkers. For AESs, cold ironing cannot only permit emergency equipment, refrigeration, cooling, heating, lighting, and other equipment to receive continuous electrical power while the shiploads or unloads its cargo but can also charge the battery of the AESs.

In the literature, the energy management strategy of electric ships is widely studied. The references can be categorized into cruising speed control and onboard energy management. For the cruising speed control, ref. [202] established a cruising speed scheduling model to evaluate the impact of speed scheduling on emission reduction. Ref. [203] proposed an adaptive model predictive control to solve the large propulsion-load fluctuations due to waves. Ref. [204] proposed an optimal route planning strategy for AESs with hybrid ESS, where the navigation and the cruising speed of the AESs fully considered the sea states and Beaufort scale. Some references further focused on onboard energy management. The AESs can be regarded as shipboard microgrids [205], consisting of both an energy network and a communication network. The generators and battery deliver power via the energy network to meet the propulsion and service loads. As for the communication network, the shipboard EMS can optimally calculate the power generators and battery outputs and send the control signals to each component by the communication network. Ref. [206] proposed a coordinated method for energy dispatch and voyage scheduling based on a risk-averse adaptively stochastic optimization. The proposed method minimized the total voyage cost and conditional value-at-risk (CVaR). Ref. [207] proposed a data-driven robust optimization of energy dispatch of AESs where diverse uncertainties from solar irradiation and ship swinging angle were comprehensively considered during cruising. Ref. [208] proposed an EMS based on bond graph system models where the configuration of the ship's onboard machinery system was optimized based on the current operating condition. In ref. [209], an optimal power-flow dispatch of the hybrid energy systems with PVs, batteries, diesel generators, and cold ironing was proposed to obtain operational safety and efficiency of the AESs.

Seaport microgrid is a newly proposed concept for seaport management, which is depicted by ref. [210]. With the advancement of cold-ironing technologies, seaport microgrids can supply energy to the AESs in berths. Seaport microgrids have similar structures and components compared with land-based microgrids. However, the typology of the seaport microgrid change frequently due to AESs' berthing in and out. To this end, some references focused on the operation and planning strategy of seaport microgrids. In ref. [211], two practical projects of seaport microgrids in Hamburg (German) and Genoa (Italy) were manifested in detail, and the operating data proved the validity of seaport microgrids.

Since the extensive electrification of maritime transportation, the logistic-side and electric-side of seaport and ship are both connected [212]. Thereby, in future maritime transportation management, the coordination *management of seaport microgrids and shipboard microgrids* will be focused on. The coordination can be divided into short-term (seconds to minutes) and long-term (hours and above). Short-term management refers to the AC/DC control problems [213], which is out of the scope of this paper and will not be further discussed. This paper mainly discusses the long-term operation, which focuses on the energy management strategy. In the literature, two operation patterns are

summarized: berthed-in mode and berthed-out mode [214]. In the berthed-in mode, the AESs are berthed in the seaports and receive the cold-ironing power supply. The seaports will allocate a berth position which refers as the berth allocation problems [215]. In this time period, the seaport microgrids schedule the berth schemes to facilitate the operation of the seaport microgrids to meet both the onboard power demand and the loading power demand of the port cranes. In the berthed-out mode, the AESs navigate on the sea and coordinate with the seaports under the punctuality requirement and navigation route selections. In this process, the AESs become physically independent from the seaports, and the seaports use the updated arrival time to arrange energy plans [204].

In recent years, the public has been increasingly concerned about climate issues, and the environmental impact of the AESs aroused attention. Hence, the onboard and seaport renewable energy and ESS integration were focused on [214]. From the shipside, ref. [216] proposed an interval optimization method to determine the optimal size of the ESS in the power system on AESs to reduce the fuel cost, capital cost of the ESS, and GHG emissions. Ref. [217] proposed an optimal control on the ship to dispatch the power flow when the ship is in the seaport based on the model predictive control method, and it was verified that a green ship with onboard PV/battery/diesel/cold-ironing hybrid energy system could reduce the electricity cost of a ship to a large extent. From the shoreside, ref. [218] proposed an energy management strategy for the seaports, which comprised a large number of flexible electric loads like refrigerated containers, electric vehicles, and electric shore power supplies to ships at berth, etc. To establish a link between shoreside and shipside, ref. [219] designed a renewable energy-based cold ironing system from the seaport side, which contributed to the achievement of zero-emission from berthed ships. Ref. [220] pointed out that the cold ironing technology could eliminate the emissions of auxiliary engines at berth if the grid powering the ships was from renewable energy. Ref. [221] evaluated the cold ironing and speed reduction policies to reduce ship emissions near and at seaports and concluded that the evaluation and prioritization of various policies should be made according to the unique characteristics of each seaport. Ref. [222] investigated the electrical characteristics of the shoreside electrical network and discussed how the cold ironing system influenced important electrical network characteristics such as bus voltages and power quality.

2) Internet data center considering green computation

In recent years, the development of information and communication technologies in smart grids has brought a new type of electricity load, i.e., Internet data center (IDC) load. Internet-service companies (ISCs) build IDCs distributed across different geographical zones to provide Internet-scale services. According to ref. [223], the data centers consumed roughly 3% of the social electricity consumption in 2016. With the implementation of the smart grid, more computing

tasks of energy management strategy are brought to the cloud servers [224]. This indicates that the electricity consumption of IDCs will continuously increase in the future, and it is estimated that the value will double every four years. Therefore, the IDC load becomes a non-ignorable factor in the process of the low-carbon transition.

In the literature, the computing resource allocation of IDCs has become an emerging research topic [225, 226]. Computing resource allocation refers to the approach to allocating computing workloads to different computing resources. The game theoretic-based method was proposed to allocate cloud resources (CRs) under a market context [227]. With the increasing number of IDCs, the energy consumption of IDCs will become an essential load component in power systems. It is estimated that the global electricity usage of IDCs and data transmission networks accounted for 1% of the total electricity consumption in 2019 [228], and this consumption is expected to double every four years. Under this context, researchers began to focus on the energy management of the IDCs to relieve the burden of the power systems [229]. There are three main types of demand response (DR) of IDCs summarized in the literature [230], namely, the geographical workload balancing (GWB) method [231], batch workload scheduling (BWS) method [232], and the thermal storage operation utilizing thermal inertia of buildings (TSTI) method [233]. For the GWB method, the interactive workloads are distributed from the front-end servers (FSs) and can be transferred between various IDCs [234]. For the BWS method, the batch workloads can be scheduled within tolerant delay to realize the electricity load shifting [235]. For the TSTI method, the load regulation potentials of each IDC can be revealed by controlling the cooling systems [236]. Therefore, the flexibility of IDCs can be regarded as an important DR resource in smart grids. Based on these three DR methods, ref. [237] proposed a coordination of multiple coupled regulation methods of IDCs, and the simulation result showed that the DR capability was increased by 6.32%. Ref. [238] further proposed an incentive-compatible DR strategy in the electricity market by deriving the IDC-based locational marginal electricity price (ILMP). Refs. [239, 240] considered the DR capacity of the IDCs in a TEP problem, and the importance of IDC-based DR under contingency was verified.

3) Mobile power sources

Apart from the stationary energy storage systems (SESS), EVs are considered as mobile power sources in the distribution network, running errands to "transport" energy from other places [241]. Ref. [242] proposed a mobility-aware vehicle-to-grid (V2G) control algorithm where EVs can act as energy transporters among different regions. Through aggregating these dispersed energy storage devices, EVs can also provide various services in smart grids. For example, the coordinated charging and discharging of EVs can realize peak shaving by responding to the real-time electricity price [133]. As a manner of DR, the dispatch of aggregated EVs can be utilized in frequency and voltage

regulation [135]. In ref. [136], the state-space model was proposed to realize the real-time frequency control by EVs with high efficiency. However, controlling a large scale of distributed energy storage may face challenges such as strong randomness.

Unlike EVs, the mobile energy storage system (MESS), a utility-scale storage bank carried by trucks [243], is more controllable. The MESS can provide various services in distribution systems, including ancillary services, grid congestion relief, renewable energy integration, and transmission deferral [244]. Compared with SESS, the mobility of MPS enhances its capability to tap into multiple value streams that have spatial-temporal variability, which in turn improves its asset utilization and potentially its value proposition. Therefore, MESS is a promising technology. Ref. [243] proposed a MESS scheduling model based on a transit delay model where MESS can provide both active and reactive energy. A particle swarm optimization-based algorithm was developed to tune the commuting time of the MESS according to a transit delay model. Ref. [245] proposed an energy management scheme to coordinate the MESS, hybrid AC/DC microgrids, and coupled distribution and transportation network. To achieve coordination among different coordinators while considering the system uncertainties of renewable energy and traffic demands, a two-stage stochastic management scheme was proposed to minimize the expected system operational cost. To relieve the transmission congestion and lower the system operation costs, ref. [246] proposed a battery-based energy storage transportation model through railways. A time-space network model was adopted to represent transportation constraints, and the hourly security-constrained unit commitment was integrated with vehicle routing problems. Despite of normal operation [247], MESS could also function in emergency events [248]. To reduce the load shedding brought by the disasters, MESS was transported to the blackout region to form a dynamic microgrid [249]. The spatial flexibility is utilized to bridge the gap between the economically optimal locations during normal operations and the locations where extra backup capacity is necessary during disasters. To enhance the resilience of the network, ref. [250] proposed a restoration scheme based on MESS. It is verified that a distribution system with MESS is more resilient compared with SESS. Ref. [251] proposed an integrated service restoration strategy based on rolling optimization to minimize the total system cost through operating the MPS, dispatching micro-grids, and network reconfiguration. Ref. [252] further proposed a proactive pre-positioning of MPS based on robust optimization to enhance the survivability of the distribution systems.

2.3.2 Planning and Operations under Emerging Energy Markets

On the one hand, some studies focused on the bidding strategies for prosumers with DERs under the current electricity market mechanism. Ref. [253] proposed a conditional value-at-risk (CVaR)- constrained optimal bidding strategy for prosumers in both day-ahead and real-time markets. Ref. [254] proposed a game-theoretic bidding approach for

prosumers with EVs considering variable wind energy resources. To cope with the uncertainties of DERs, ref. [255] proposed a new distributional robust optimization via scenario-wise ambiguity set to establish a bidding strategy. To earn more profits and enhance the reliability of the power systems, other references also considered the bidding strategies in the ancillary market for prosumers [256-259].

On the other hand, with the increasing penetration of DERs, DGs generation and electricity consumption will coexist in a region. Therefore, the emergence of the local energy market (LEM) allows the DERs to be traded locally within the distribution level. The LEM is also known as a decentralized market or community market in the other references. In the U.S., a green energy market, where distributed renewable energy and uncertain energy can be traded, is established [260]. In the Netherlands, a trading platform is established where customers can trade self-generated energy with peers [261]. Therefore, the development of LEM is a promising trend. Ref. [262] proposed a bidding strategy for an autonomous smart transactive agent in LEM and introduced metrics and criteria for evaluating the bidding strategies. Ref. [263] proposed a systematic approach to derive the optimal bidding strategy for prosumers in a distribution-level energy market. In LEM, more data are generated from the prosumer side, like load profiles of EVs and BESS and energy transactions data. But most of the data of the prosumers are not transparent, and the information is asymmetric.

In recent years, digitalization and communication technologies developed rapidly, and the concept of Internet-of-Things (IoT) has emerged. Under this context, peer-to-peer (P2P) trading and energy sharing have become a new transaction mode in LEM that arouses more and more attention. Ref. [264] summarized three types of P2P market structures, including a fully decentralized market, community-based market, and composite market. In a fully decentralized market, the customers can independently and directly negotiate with one another to decide on transaction results without any centralized supervision [265]. In a community-based market, each member generally trades their energy within the community through a community manager [266]. The members have the same interests and goals, and the overall electricity procurement for the community reflects prosumers' preferences by introducing the concept of energy collectives [267]. The community manager can also trade with the other community representing its members. A composite market is essentially a combination of fully decentralized and community-based markets [268].

The current literature focuses on solving the P2P trading problems in the virtual layer and physical layer under these different market structures. At the virtual layer, the most important problem is to help the customer reduce energy costs and earn financial benefits [269-271]. Proper pricing mechanisms are designed to incentive extensive individual customers to participate in local transactions [272]. Besides, P2P trading is expected to contribute to the achievement of balancing local supply and demand [273]. With P2P trading, the local energy is expected to be traded locally, so that peak shaving of the local demand can be realized [274]. Recently, data security has attracted more social attention. To

ensure securing trading, a trustless P2P energy sharing market is established based on black-chain and encryption technologies [275, 276]. From the physical layer, the research focused on whether P2P trading will bring negative effects on network assets and affect power quality. If the decision-making process in the virtual layer fails to consider the potential impact of P2P trading of energy on the physical layer, the energy transition may violate physical constraints in the electricity network. Under this context, the literature investigated three types of network challenges that might be brought to the grids, including violation of voltage and capacity constraints [277], network power loss [278], and loss of system strength [279].

Different P2P trading and sharing strategies are modeled to help prosumers earn more profits. The existing approaches can be divided into three categories: game-theoretic model, auction-based model, and negotiation-based model. In a game-theoretic model, the decision-makers will consider other players' potential strategies and search for the Nash equilibrium, which is the best solution for all players [269]. For example, in refs. [270, 271], a non-cooperative energy-sharing game for the buildings was presented. The sharing strategies considered the sustainable and profitable energy sharing profile of building clusters by maximizing the total social welfare. Ref. [280] proposed a P2P energy trading scheme where a cooperative Stackelberg game is formulated. The prosumers, acting as followers, will form suitable coalitions with neighbors. Ref. [281] investigated the energy cooperation between PV prosumers and community energy storage, considering cheating behaviors. Ref. [282] proposed an incorporated clustering technique to allocate the financial incentives of the prosumers, and the prosumers' willingness to participate in the sharing scheme is also guaranteed.

As for the auction-based model, the double-auction-based local community energy market is designed, and the market is cleared in a centralized manner [283]. In ref. [284], a combinatorial auction approach was presented for the multi-resource allocation of an energy-sharing system in a residential community. In refs. [285, 286], a continuous double-auction market was designed for P2P energy sharing.

In a negotiation-based model, the prosumers negotiate with each other in peers in a distributed manner. Distributed algorithms, such as the sub-gradient algorithm [287, 288], and the Alternating Direction Method of Multipliers (ADMM) [276, 289], were introduced to solve the problem. By applying these distributed algorithms, the prosumers can solve their local sub-problem in parallel and do not have to share their private information [290, 291]. Ref. [292] proposed an optimal solution in different distributed P2P mechanisms. In ref. [293], a distributed bilateral energy trading system was designed to incentivize players to participate in the local market. To encourage prosumers to participate in a trustless P2P energy sharing market. The blockchain-based platform is developed, where prosumers can learn the energy usage pattern of the other participants [275, 276]. In some works, secured transactions were modeled through designing the

block-chain based smart contract [294].

Also, there are also some overlapping between these three categories of modeling. For example, in ref. [295], a non-cooperative game is formulated between storage units where each owner can decide on the maximum amount of energy to sell in a local market so as to maximize a utility that reflects the tradeoff between the revenues from energy trading and the accompanying costs. The price at which energy is traded is determined via an auction mechanism. Similarly, to determine the double-side auction market spot price, a non-cooperative game was formulated among all participants involved in the community sharing in refs. [296, 297].

CHAPTER 3

CARBON ORIENTED MULTI-ENERGY NETWORK PLANNING

Electricity network transition is an inevitable trend in the future for the following four reasons. First, the traditional CFPPs are approaching their specific life span, entering the decommissioning stage. Second, to stabilize the global temperature, anthropogenic emissions must be controlled so that the emissions from traditional CFPPs needs to be reduced. Third, renewable energy is being invested to take the place of thermal power generators. To smooth the output of intermittent renewable energy output, the ESS should be focused on. Fourth, with the continuously increasing demand in the future, the transmission network, generation capacity, and ESS need to be expanded. These four reasons will lead to great changes in electricity networks. In this chapter, a planning roadmap is proposed, which is a guidance that can direct the current electricity network to be transited into a low-carbon and multi-carrier energy network. In this chapter, a multi-energy network transition and planning roadmap is proposed.

3.1 Retirement Model of Coal-fired Power Plant

The retirement cost model of each CFPP consists of three parts: the retirement cost, the maintenance cost, and the outage rate, which can be described as:

$$C_{i,y}^{Coal} = C^{rt} + C^{mt} + C^{ot} = \frac{(\eta_{i,y-1}^{rt} - \eta_{i,y}^{rt})}{(1+\varepsilon)^{y-1}} \times \left[C_i^u - \underbrace{C_i^s + \sum_{n=1}^{y}\left(\sum_{m=1}^{n}\left(C_i^s \times r_i^s \times (-1)^{m+1}\right)\right)}_{\text{accelerating depreciation of scrap value}} \right] P_i^{cap}$$
$$+ \frac{\eta_{i,y}^{rt} C_i^m (1+r^m)^{A_i^{ref}+y-1}}{(1+\varepsilon)^{y-1}} \times P_i^{cap} + \frac{\eta_{i,y}^{rt} f_i (1+r^f)^{A_i^{ref}+y-1}}{(1+\varepsilon)^{y-1}} \times P_i^{cap} \times \chi \quad , \ \forall i \in \Omega^{CG}, \forall y \in [1,Y] \ (3.1)$$

$$r_i^s = 1 - \sqrt[L_i^s]{\frac{SV_i}{C_i^s}}, \forall i \in \Omega^{CG}, \ \forall i \in \Omega^{CG} \quad (3.2)$$

where Y is the total planning year; Ω_{CG} is the set of the buses which have CFPP; $C_{i,y}^{Coal}$ is the cost model of the retirement of the i^{th} CFPP at the y^{th} year from reference year; C^{rt} is the retirement cost; C^{mt} is the maintenance cost; C^{ot} is the outage rate; $\eta_{i,y}^{rt}$ is the online percentage of the i^{th} CFPP at the y^{th} year; ε is the discount rate; C_i^u is the disposal cost per MW; C_i^s is the scrap value per MW; r^s is the depreciation rate; P_i^{cap} is the capacity of the CFPP;

C_i^m is the maintenance cost per MW; r^m is the annual increasing rate of maintenance cost; A_i^{ref} is the age of the CFPP at the reference year; f_i is the outage rate at normal operation stage; r^f is the annual increasing rate of outage rate; SV_i is the salvage value per MW; L_i^s is the life span of CFPPs; χ is the unit price of the value of customer reliability.

There are two components in retirement cost: disposal cost and scrap value of the CFPPs [298]. The disposal cost is a constant value for per unit capacity, including the removal of the turbine, boilers, exciter, transformer, control devices, and structural demolition, etc. The scape value of the CFPPs is the income that can be obtained through recycling the equipment. It will depreciate with the increase in the age of the CFPPs. The reducing balance method, which is an accelerating depreciation, is assumed so that the asset loses book value at a faster rate than the traditional straight-line method [299]. The asset faces greater deductions in its value in the earlier years than in the later years. As for maintenance costs, they will increase annually because the performance of the plants will become worse. As for the outage rate, it is constant during the normal stage [300]. However, the CFPPs to be retired are at the wear-out stage. So, the outage rate is also assumed as an annually increasing function.

3.2 Gas Network Modeling

3.2.1 Gas Network Constraints

1) Flow equation

It is assumed that only the steady-state characteristics of the gas system are considered to describe the gas network behaviors [301]. The flow rate of the pipeline can be expressed by the Weymouth flow equation as follows.

$$f_{pq,t}^g = \mathrm{sgn}(\pi_{p,t}^{PRESS}, \pi_{q,t}^{PRESS}) \times \mu_{pq} \times \sqrt{\left| \left(\pi_{p,t}^{PRESS}\right)^2 - \left(\pi_{q,t}^{PRESS}\right)^2 \right|}, \quad \forall p,q \in \Omega^{Gas} \tag{3.3}$$

$$\mathrm{sgn}(\pi_{p,t}^{PRESS}, \pi_{q,t}^{PRESS}) = \begin{cases} 1 & \pi_{p,t}^{PRESS} \geq \pi_{q,t}^{PRESS} \\ -1 & \pi_{p,t}^{PRESS} < \pi_{q,t}^{PRESS} \end{cases}, \quad \forall p,q \in \Omega^{Gas} \tag{3.4}$$

where Ω^{Gas} is the set of the gas nodes; $f_{pq,t}^g$ is the gas flow; $\pi_{p,t}^{PRESS}$ is the gas pressure at buses p; μ_{pq} is the pipeline constant; $\mathrm{sgn}(\pi_{p,t}^{PRESS}, \pi_{q,t}^{PRESS})$ donates to the flow direction.

Equation (3.3) describes the gas flow from bus p to q. The parameter μ_{pq} donates to the pipeline constant. The function $\mathrm{sgn}(\bullet)$ describes the gas flow direction, which depends on the pressure difference at buses p and q.

Equation (3.5) enforces the pressure bounds for the gas buses.

$$\underline{\pi_{p/q}^{PRESS}} \le \pi_{p/q,t}^{PRESS} \le \overline{\pi_{p/q}^{PRESS}}, \quad \forall p,q \in \Omega^{Gas} \tag{3.5}$$

where $\underline{\pi_{p/q}^{PRESS}}$ and $\overline{\pi_{p/q}^{PRESS}}$ are the lower and upper bound of the nodal gas pressure.

Equation (3.6) enforces the flow bounds of the gas pipelines. The parameter $\eta_{pq}^{GL,EX}$ is the binary parameter indicating whether the pipeline exists between bus *p* and *q* during the current gas system, while the variable $\eta_{pq}^{GL,NB}$ is the binary decision variable indicating whether the new pipeline will be built in the future.

$$\left| f_{pq,t}^{g} \right| \le f_{pq}^{g,\max} \times \left(\eta_{pq}^{GL,EX} + \eta_{pq}^{GL,NB} \right), \quad \forall p,q \in \Omega^{Gas} \tag{3.6}$$

where $f_{pq,t}^{g}$ is the gas flow; $f_{pq}^{g,\max}$ is the maximum gas flow.

2) Compressor model

The compressor station is a facility to help the gas move from one bus to another, and it can offset the pressure loss. When a compressor station locates at the pipeline between bus *p* and *q*, the horsepower consumption of the compressor station can be expressed as:

$$H_{pq,t} = \kappa_{pq} \times f_{pq,t}^{g} \times \left[\left(\frac{\pi_{p,t}^{PRESS}}{\pi_{q,t}^{PRESS}} \right)^{\psi_{pq}} - 1 \right], \quad \forall p,q \in \Omega^{Gas} \tag{3.7}$$

The horsepower consumption $H_{pq,t}$ is a crucial factor that depends on the gas flow through the station and the pressure of the nodes. The parameter κ_{pq} is a constant associated with compressor suction temperature and efficiency. The parameter ψ_{pq} is a constant regarding the specific heat ratio and gas compressibility factor at the compressor inlet.

The gas withdrawn of the compressor can be expressed in equation (3.8). The withdrawn gas will be utilized to generate electricity by a micro-gas turbine to power the compressor.

$$\phi_{pq,t} = \alpha_{pq} + \beta_{pq} \times H_{pq,t} + \gamma_{pq} \times {H_{pq,t}}^{2}, \quad \forall p,q \in \Omega^{Gas} \tag{3.8}$$

where $\phi_{pq,t}$ is the gas withdrawn by the station compressor; $\alpha_{pq}, \beta_{pq}, \gamma_{pq}$ is the conversion factor between $H_{pq,t}$ and $\phi_{pq,t}$.

3) Gas flow balance model

The conservation of the gas flow is expressed through the mass-flow balance equation, indicating that the overall gas flowing into the bus *q* equals to the overall gas flowing out of that bus.

$$\sum_{a \in \Omega_q^{GW}} G_{a,t}^{Well} + \sum_{p \ne q} f_{pq,t}^{g} - \sum_{p \in \Omega^{GAS}} \eta_{pq}^{CP} \phi_{pq,t} + \sum_{i \in \Omega} P_{i,t,y}^{P2G,SG} = G_{q,t}^{GFD} + G_{q,t}^{GLD} \tag{3.9}$$

In equation (3.9), on the left of the equal sign, the first term regards to the gas production from the gas well, the second term regards to the gas flow flowing into bus q through the other buses (negative value means gas flowing out), the third term presents the gas consumption of the compressor, and the fourth term presents the gas output of P2GSes. The right of the equal sign and the gas demand of the gas-fired generators and the gas load.

However, because of the congestion constraint of the pipeline, the dispatch of the natural gas network may not converge. If it happens, $G_{q,t}^{GFD}$ needs to be reduced. The upper bound of the output of the gas-fired generator needs to be updated according to:

$$P_{i,b,y}^{G,gas} \le G_{q,t}^{GFD} \times HR\,, \quad \forall q \in \Omega^{Gas} \quad \forall i \in \Omega \tag{3.10}$$

where $P_{i,b,y}^{G,gas}$ is the output of the gas-fired generators; HR is the heat rate.

3.2.2 Power-to-gas (P2G) Technology

The P2G technology introduces a flexible solution for electricity storage through methane production by converting electricity into natural gas. The two-step process for the internal chemical reaction procedure of P2G is shown in (3.11) and (3.12). The first step is water electrolysis, in which hydrogen (H2) and oxygen (O2) are produced. The second step is catalysis, in which CO2 is absorbed and consumed to be converted into methane (CH4).

$$2H_2O \xrightarrow{electrolysis} 2H_2 \uparrow + O_2 \uparrow \tag{3.11}$$

$$4H_2 + CO_2 \xrightarrow{catalysis} CH_4 \uparrow + 2H_2O \tag{3.12}$$

P2GSes are the coupling point of the electricity network and the natural gas network, as shown in Fig. 3-1. The gas network model needs to be established to ensure that P2GSes can work properly to meet the gas system requirement and guarantee that P2GSes are connected to gas buses physically. It means that a new pipeline will be built if the P2GSes located at the electricity buses are not coupled with the gas network. Besides, if the construction of P2GSes causes congestion in the gas network, the gas network will be expanded.

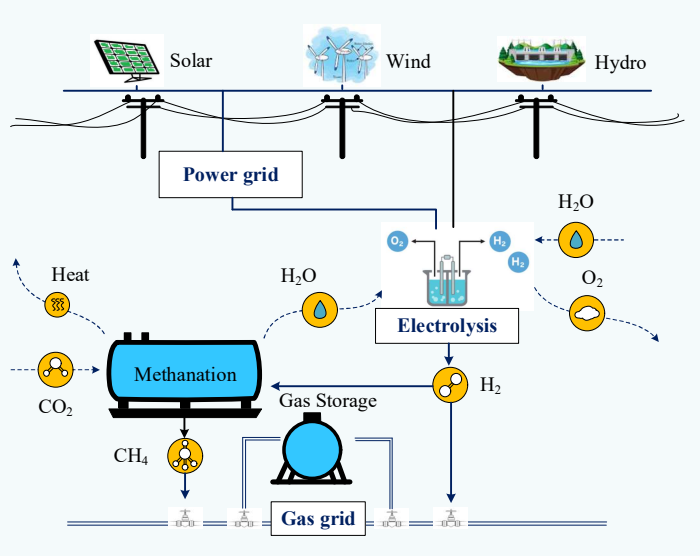

Fig. 3-1. P2G and multi-energy System.

3.3 Multi-energy Network Planning Strategy

3.3.1 Energy Transition and Planning Roadmap

The electricity network transition roadmap can be divided into two milestones. The first stage is the planning problem of the CFPPs retirement, renewable energy investment, and network expansion. According to ref. [302], the carbon neutrality goal should be achieved by 2050, which means that the net anthropogenic emissions of carbon dioxide (CO2) should approach zero by mid-century. CFPPs, as a major carbon dioxide emission source, will inevitably face retirement. How to make the CFPPs retire economically is essential, and it is the main research object in the first stage. Besides, the investment of renewable energy is normally emphasized in the government's report, as stated in [303], "*The transformed electricity system is positioned to efficiently maintain system reliability, support renewable energy growth and achieve zero net carbon emissions by 2050*." Hence, in the future, the capacity of renewable energy will increase, and the network will be expanded to cope with the continuing growth of load demand.

In the second milestone, the P2GSes planning problem will be focused on. P2G technology can be utilized as an ESS to smooth the fluctuating renewable energy and participate in frequency control ancillary service (FCAS). Also, in the future, when the hydrogen fuel battery is popularized in vehicles, P2GSes can contribute to the emission reduction in traffic networks. The P2GSes are the coupling points of the electricity network and gas network. Hence, a multi-energy network planning strategy should be formulated. The construction location of P2GSes is specified at the buses whose carbon intensity is relatively low. The nodal carbon intensity is calculated based on the carbon emission flow model, which will be introduced in the next chapter. Thus, it can be guaranteed that the electricity used by P2GSes is relatively clean. The overall transition roadmap is shown in Fig. 3-2.

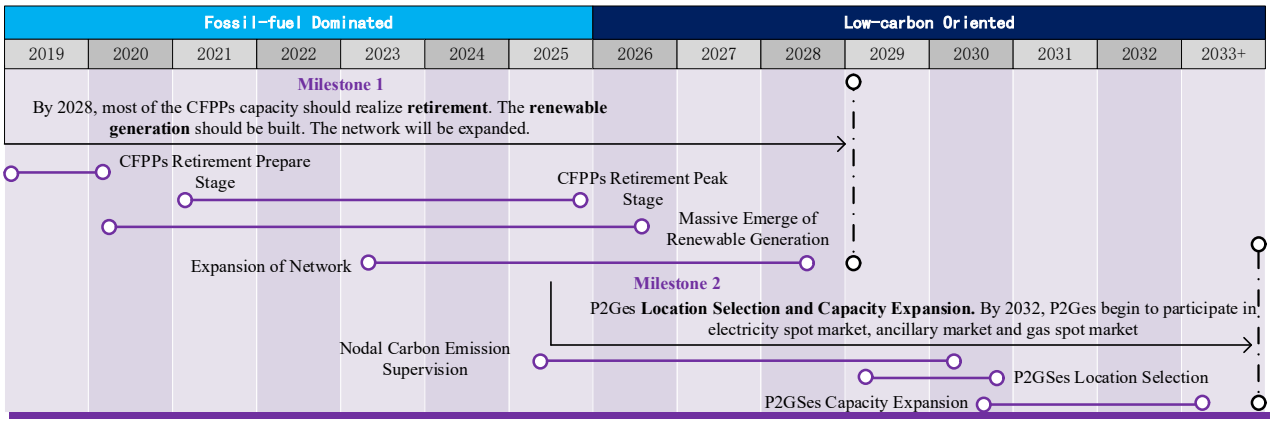

Fig. 3-2. Proposed electricity network roadmap.

3.3.2 Milestone I: CFPP Retirement and Electricity Network Expansion

In the first milestone, the CFPPs will realize retirement, and the new renewable power generation and network will be augmented. The average cost of carbon emission reduction is defined as *the proportion of the total cost and reduced carbon emissions,* based on economics theory. We proposed a new TEP model based on the average cost of carbon emission reduction. The objective function is to minimize the average cost of carbon emission reduction as (3.13).

$$Min\frac{C^{E}}{\Delta E} \tag{3.13}$$

The cost function has four parts, which can be described as:

$$C^{E}=C^{Coal}+C^{Renew}+C^{Net}+C^{Opr} \tag{3.14}$$

where C^{Coal} is the cost concerned with the retirement of the coal-fired power plant; C^{Renew} is the investment cost of renewable energy plants; C^{Net} is the cost of network expansion; C^{Opr} is the operation cost of the whole system.

Even if the retirement of CFPPs is considered in some literature, the CFPPs are retired at their designed technical age [26]. But in our proposed model, the early retirement of CFPPs is optimized. The total retirement cost of CFPPs in the system is equal to the sum of the retirement cost of each CFPP shown in (3.15). The retirement cost of each CFPP is modeled in (3.1).

$$C^{Coal}=\sum_{y=1}^{Y}\sum_{i\in\Omega_{CG}}C_{i,y}^{Coal} \tag{3.15}$$

To simulate the influence of extreme load conditions, the annual load duration curve will be utilized. In the load duration curve, there are several blocks with different amounts of load. For different blocks, their duration time is different.

The operation cost comes from all the thermal generators (including gas generators and CFPPs) and the load curtailment:

$$C^{Opr}=\sum_{y=1}^{Y}\sum_{b=1}^{B}\sum_{i\in\Omega_G}\frac{\left[a_i\left(P_{i,b,y}^{G}\right)^2+b_i\left(P_{i,b,y}^{G}\right)+c_i\right]\times D_{b,y}}{(1+\varepsilon)^{y-1}}+\sum_{y=1}^{Y}\sum_{b=1}^{B}\sum_{i\in\Omega}\frac{\left(\chi L_{i,b,y}^{r}\right)\times D_{b,y}}{(1+\varepsilon)^{y-1}} \tag{3.16}$$

Where B is the total number of the blocks; Ω_G is the set of the buses which have thermal generators; $P_{i,b,y}^{G}$ is the energy generated by the thermal generator at the b^{th} block at the y^{th} year at bus i; $L_{i,b,y}^{r}$ is the unserved load; χ is the unit price of value of customer reliability; a_i, b_i, c_i and are the fuel cost co-efficiency of the thermal generators; $D_{b,y}$ is the duration time of the b^{th} block of the y^{th} year.

The net expansion cost can be described as:

$$C^{Net}=\sum_{y=1}^{Y}\sum_{i,j\in\Omega}\frac{\left(\eta_{ij,y}^{TL}-\eta_{ij,y-1}^{TL}\right)C_{ij}^{TL}}{(1+\varepsilon)^{y-1}} \tag{3.17}$$

where $\eta_{i,t,y}^{TL}$ is the number of the transmission lines between bus i and j; C_{ij}^{TL} is the investment cost of one transmission line.

The reduced carbon emissions are modeled as equation (3.18). The first and second terms represent the carbon emissions when the CFPPs do not retire and after retirement, respectively.

$$\Delta E=E'-E=\sum_{i\in\Omega_G}\sum_{b=1}^{B}\sum_{t=1}^{T}\left(P_{i,b,y}^{G'}\times E_i^{G}\right)\times D_{b,y}-\sum_{i\in\Omega_G}\sum_{b=1}^{B}\sum_{t=1}^{T}\left(P_{i,b,y}^{G}\times E_i^{G}\right)\times D_{b,y} \tag{3.18}$$

where E' and E are the total carbon emissions if the CFPPs are not retired and retired respectively; $P_{i,b,y}^{G'}$ and $P_{i,b,y}^{G}$ are the output of thermal generators before and after the retirement of CFPPs is considered; E_i^{G} is the carbon intensity of generators.

s.t.

$$P_{i,b,y}^{G}+\sum_{k\in R}P_{k,i,b,y}^{R}+\sum_{j\neq i}P_{ij,b,y}^{B}=L_{i,b,y}^{d}\text{-}L_{i,b,y}^{r},\quad \forall i\in\Omega,\forall b\in[1,B],\forall y\in[1,Y] \tag{3.19}$$

$$B_{ij}^{AD}\theta_{ij,b,y}=S_{ij,b,y},\quad \forall i,j\in\Omega,\forall b\in[1,B],\forall y\in[1,Y] \tag{3.20}$$

$$P_i^{G,\min}\cdot\eta_{i,y}^{rt}\le P_{i,b,y}^{G}\le P_i^{cap}\cdot\eta_{i,y}^{rt},\quad \forall i\in\Omega,\forall b\in[1,B],\forall y\in[1,Y] \tag{3.21}$$

$$P_{k,i,b,y}^{R}=g_k(P_{k,i,y}^{R,\max}),\quad \forall i\in\Omega,\forall b\in[1,B],\forall y\in[1,Y],\forall k\in R \tag{3.22}$$

$$S_t^{total}=\sum_{i\in\Omega_G}S_{i,t}=\sum_{i\in\Omega_G}(P_i^{cap}\cdot\eta_{i,y}^{rt}-P_{i,b,y}^{G})\ge L_{i,b,y}^{d}\times\mathfrak{L}\%+\sum_{k\in R}P_{k,i,b,y}^{R}\times\Re\%,\forall b\in[1,B],\forall y\in[1,Y] \tag{3.23}$$

$$P_{k,i,y}^{R,\max}=P_{k,i,y-1}^{R,\max}+Cap_{k,i,y}^{R},\quad \forall i\in\Omega,\forall b\in[1,B],\forall y\in[1,Y],\forall k\in R \tag{3.24}$$

$$\left|P_{ij,b,y}^{B}\right|\le P_{ij}^{B,\max}\times\eta_{ij,y}^{TL},\quad \forall i,j\in\Omega,\forall b\in[1,B],\forall y\in[1,Y] \tag{3.25}$$

$$\eta_{i,y}^{rt} \le \eta_{i,y-1}^{rt}, \quad \forall i \in \Omega, \forall y \in [1,Y] \tag{3.26}$$

$$0 \le \eta_{i,y}^{rt} \le 1, \quad \forall i \in \Omega, \forall y \in [1,Y] \tag{3.27}$$

$$\eta_{i,y}^{TL} \ge \eta_{i,y-1}^{TL}, \quad \forall i \in \Omega, \forall y \in [1,Y] \tag{3.28}$$

$$\eta_{i,y}^{TL} \in \{Z^{+} \cup \{0\}\}, \quad \forall i \in \Omega, \forall y \in [1,Y] \tag{3.29}$$

where $P_{k,i,b,y}^{R}$ is the energy output of the renewable energy; $L_{i,b,y}^{r}$ is the unserved load; $P_{ij,b,y}^{B}$ is the power flow from bus *i* to *j*; $L_{i,b,y}^{d}$ is the load demand; B_{ij}^{AD} is the admittance between bus *i* and *j*; $\theta_{ij,b,y}$ is the phase angle between bus *i* and *j*; $P_{i}^{G,\min}$ is the minimum power output of the i^{th} generators; $g_k(\bullet)$ is the energy output function of the k^{th} renewable energy; $P_{k,i,y}^{R,\max}$ is the current capacity of the renewable energy; S_{t}^{total} is the system total spinning reserve capacity; $S_{i,t}$ is the spinning reserve capacity that can be provided by the i^{th} generator at time t; $\mathfrak{L}\%$ is the load upward spinning reserve index; $\Re\%$ is the requirement of the upward spinning reserve index caused by the reduction of renewable energy output; $P_{ij}^{B,\max}$ is the maximum power flow of one transmission line.

Equations (3.19) and (3.20) model the system power constraints using the DC power flow model. Equation (3.21) ensures that the output of the CFPPs should be lower than its current capacity. Equation (3.22) shows the output of renewable energy. Equation (3.23) is the constraint of system spinning reserve capacity. Equation (3.24) means that the current capacity of renewable energy equals the last-year capacity plus this year's newly built capacity. Equation (3.25) limits the power flow on the transmission lines. Equations (3.26) and (3.27) are the constraints for the retirement condition of the CFPPS. A retirement condition is a natural number between 0 and 1, representing how much percentage of the CFPPs capacity is still online. And this figure should become smaller and smaller with the increase in the planning year. Equations (3.28) and (3.29) are the constraints of the number of the transmission line expanded.

3.3.3 Milestone II: Multi-energy Network and P2Ges Planning

In this section, we proposed a low-carbon oriented model for site selection and planning of P2GSes. To optimize the planning of P2GSes, the profit needs to be maximized. The time-series load curve is used because P2GSes is a kind of ESS, and there is a strong correlation between two sequential time slots. The P2GSes in this chapter are combined with gas-fired power generation units. It means that the P2GSes can convert the surplus electricity from renewable energy to gas, and the stored gas can also be converted to electricity when needed.

The objective function can be described as:

$$MAX.Pro^{P2G} = Rev^{P2G} - \left(C^{P2G,IN} + C^{P2G,OP} + C^{P2G,CAR}\right) \tag{3.30}$$

where Pro^{P2G} is the total profits of P2GSes; Rev^{P2G} is the revenue of the P2GSes; $C^{P2G,IN}$, $C^{P2G,OP}$ and $C^{P2G,CAR}$ are the investment cost, the operation cost, and the carbon environment cost of the P2GSes, respectively.

The revenue has two parts. The first part is selling gas to the gas network. The second part is providing ancillary service.

$$Rev^{P2G} = Rev^{P2G,SG} + Rev^{P2G,AS} \tag{3.31}$$

where $Rev^{P2G,SG}$ is the revenue from selling gas; $Rev^{P2G,AS}$ is the revenue from the ancillary service market.

The revenue of selling gas to gas network can be shown as:

$$Rev^{P2G,SG} = \frac{\sum_{y=1}^{Y}\sum_{t=1}^{T}\sum_{i\in\Omega}\lambda_{i,t,y}^{P2G,SG} \times P_{i,t,y}^{P2G,SG}}{(1+\varepsilon)^{y-1}} \tag{3.32}$$

where $\lambda_{i,t,y}^{P2G,SG}$ is the price of the gas; $P_{i,t,y}^{P2G,SG}$ is the quantity of the gas that is sold.

The revenue from the ancillary service market is divided into two parts: the income from providing secondary reserve capacity and the income from providing secondary reserve energy as (3.33).

$$\begin{aligned} &Rev^{P2G,AS} = Rev^{P2G,EN} + Rev^{P2G,CAP} \\ &= \frac{\sum_{y=1}^{Y}\sum_{t=1}^{T}\sum_{i\in\Omega}\left(\lambda_{i,t,y}^{EN,UP} \times P_{i,t,y}^{EN,UP} - \lambda_{i,t,y}^{EN,DW} \times P_{i,t,y}^{EN,DW}\right)}{(1+\varepsilon)^{y-1}} + \frac{\sum_{y=1}^{Y}\sum_{t=1}^{T}\sum_{i\in\Omega}\left(\lambda_{i,t,y}^{CAP,UP} \times P_{i,t,y}^{CAP,UP} + \lambda_{i,t,y}^{CAP,DW} \times P_{i,t,y}^{CAP,DW}\right)}{(1+\varepsilon)^{y-1}} \end{aligned} \tag{3.33}$$

where $Rev^{P2G,EN}$ is the revenue from providing secondary reserve energy; $Rev^{P2G,CAP}$ is the revenue from providing secondary reserve capacity; $\lambda_{i,t,y}^{EN,UP}$ and $\lambda_{i,t,y}^{EN,DW}$ are the prices of providing upward secondary reserve energy and the price of purchasing downward secondary reserve energy; $P_{i,t,y}^{EN,UP}$ and $P_{i,t,y}^{EN,DW}$ are the actual energy of providing upward and downward secondary reserve energy; $\lambda_{i,t,y}^{CAP,UP}$ and $\lambda_{i,t,y}^{CAP,DW}$ are the prices of providing upward and downward secondary reserve capacity; $P_{i,t,y}^{CAP,UP}$ and $P_{i,t,y}^{CAP,DW}$ are the upward and downward secondary reserve capacity provided by P2GSes.

In equation (3.33), the P2GSes can earn profit from providing both upward and downward secondary reserve capacity. During the real-time market dispatch, an upward reserve bid indicates offering energy, and P2Ges will get income. However, a downward reserve indicates absorbing energy, and P2Ges should pay the cost of the energy.

The investment cost and operation cost of P2GSes are shown in (3.34) and (3.35).

$$C^{P2G,IN}=\frac{\left(\sum_{i\in\Omega}\left(C^{P2G}\cdot Cap_{i,y}^{P2G}\right)+\sum_{p,q\in\Omega^{GAS}}\left(\eta_{pq}^{GL,NB}\cdot C_{pq}^{GL}\right)\right)}{(1+\varepsilon)^{y-1}} \tag{3.34}$$

where C^{P2G} is the investment cost of P2GSes per MW; $Cap_{i,y}^{P2G}$ is the newly built P2GSes at bus i at the y^{th} year; the variable $\eta_{pq}^{GL,NB}$ is the binary decision variable indicating whether the new pipeline will be built in the future; C_{pq}^{GL} is the cost of building a pipeline between gas bus p and q.

$$C^{P2G,OP}=\sum_{y=1}^{Y}\sum_{t=1}^{T}\sum_{i\in\Omega}\left(\lambda_{i,t,y}^{P2G,ELE}\cdot P_{i,t,y}^{pur}\right)\Big/(1+\varepsilon)^{y-1}+\sum_{y=1}^{Y}\sum_{i\in\Omega}\left(C^{P2G}\cdot S_{i,y-1}^{P2G,\max}\cdot\zeta\%\right)\Big/(1+\varepsilon)^{y-1} \tag{3.35}$$

where $\lambda_{i,t,y}^{P2G,ELE}$ is the price of purchasing energy from the electricity market; $P_{i,t,y}^{pur}$ is the quantity of the electricity that P2GSes purchase; $S_{i,y}^{P2G.\max}$ is the current P2GSes capacity at the y^{th} year.

The operation cost in (3.35) mainly includes the cost of purchasing electricity from the spot market and maintenance cost, which is $\zeta\%$ of the investment cost.

The carbon environment cost depends on the average carbon potential of the place where P2GSes are built, and it is modeled as:

$$C^{P2G,CAR}=\sum_{y=1}^{Y}\sum_{i\in\Omega}\left(\left(P_{i,t,y}^{EN,DW}+P_{i,t,y}^{pur}\right)\cdot\overline{E_{i,y}^{N}}\cdot\lambda_{i,t,y}^{CAR}\right)\Big/(1+\varepsilon)^{y-1} \tag{3.36}$$

where $\overline{E_{i,y}^{N}}$ is the average nodal carbon intensity at bus i at the y^{th} year; $\lambda_{i,t,y}^{CAR}$ is the price of the carbon environment cost.

The annual average nodal carbon intensity is calculated as:

$$\overline{E_{i,y}^{N}}=\sum_{b=1}^{B}\left(E_{i,b,y}^{N}\times D_{b,y}\right)\Big/\sum_{b=1}^{B}\left(D_{b,y}\right),\quad\forall i\in\Omega,\forall y\in[1,Y] \tag{3.37}$$

where $E_{i,b,y}^{N}$ is the nodal carbon intensity at bus i at the b^{th} block of the y^{th} year.

s.t.

Equations (3.3)-(3.10)

$$S_{i,y}^{P2G,\max}=S_{i,y-1}^{P2G,\max}+Cap_{i,y}^{P2G},\quad\forall i\in\Omega,\forall y\in[1,Y] \tag{3.38}$$

$$0\le P_{i,t,y}^{EN,UP}\le P_{i,t,y}^{CAP,UP},\quad\forall i\in\Omega,\forall t\in[1,T],\forall y\in[1,Y] \tag{3.39}$$

$$0\le P_{i,t,y}^{EN,DW}\le P_{i,t,y}^{CAP,DW},\quad\forall i\in\Omega,\forall t\in[1,T],\forall y\in[1,Y] \tag{3.40}$$

$$0\le P_{i,t,y}^{CAP,UP}\le S_{i,t,y}^{P2G}\times\eta^{D},\quad\forall i\in\Omega,\forall t\in[1,T],\forall y\in[1,Y] \tag{3.41}$$

$$0 \le P_{i,t,y}^{CAP,DW} \le \left(S_{i,y}^{P2G,\max} - S_{i,t,y}^{P2G}\right)/\eta^{D}, \quad \forall i \in \Omega, \forall t \in [1,T], \forall y \in [1,Y] \tag{3.42}$$

$$0 \le S_{i,t,y}^{P2G} \le S_{i,y}^{P2G,\max}, \quad \forall i \in \Omega, \forall t \in [1,T], \forall y \in [1,Y] \tag{3.43}$$

$$S_{i,t,y}^{P2G} = S_{i,t-1,y}^{P2G} - \frac{P_{i,t,y}^{P2G,SG}}{\eta^{D}} - \frac{P_{i,t,y}^{EN,UP}}{\eta^{D}} + P_{i,t,y}^{EN,DW} \times \eta^{D} + P_{i,t,y}^{pur} \times \eta^{C}, \quad \forall i \in \Omega, \forall t \in [1,T], \forall y \in [1,Y] \tag{3.44}$$

where $S_{i,y}^{P2G.\max}$ is the current P2GSes capacity at the y^{th} year; $S_{i,t,y}^{P2G}$ is the current energy storage state of P2GSes; η^{D} and η^{C} are the discharging and charging rate of P2GSes.

Equation (3.38) represents that the current year capacity of P2GSes equals the capacity of last year plus this year's newly built capacity. Equations (3.39) and (3.40) ensure that upward and downward secondary reserve energy should be lower than upward and downward secondary reserve capacity. Equation (3.41) indicates that the upward secondary reserve capacity should be lower than the current energy storage in P2GSes. Equation (3.42) indicates that the downward secondary reserve capacity should be lower than the remaining energy capacity of P2GSes. Equation (3.44) is the energy balance constraint.

3.4 Case Study

The proposed electricity network transition roadmap is verified on a modified IEEE 24-bus system. The objective function in section 3.3.2 is non-linear and non-convex with mixed-integer. To solve the problem, we integrate PSO with the interior point method (IPPSO) according to [304]. The interior point is efficient for finding local optimal, and PSO can prevent being trapped in local optimal. The objective function in section 3.3.3 is non-linear and non-convex because of the gas flow equation (26), but it can be converted into mixed-integer linear programming (MILP)by using the first-order Taylor series according to Ref. [69]. The solver is SCIP of OPTI toolbox in MATLAB. The simulations were completed by a PC with an Intel Core (TM) i7-9750 CPU @ 2.60 GHZ with 16.00 GB RAM.

In the simulation, the electricity price, gas price, electricity demand, and gas demand are obtained through Australia Energy Market Operator (AEMO) [305] [306]. The wind speed, solar radiation, and temperature are obtained from the Australia Government Bureau of Meteorology[307]. The carbon price is obtained through Ref. [308].

3.4.1 The First Milestone

The first milestone of the roadmap concerns the retirement of the CFPPs. The overall transition horizon is 10 years. Five cases are established for comparison.

Base case: The CFPPs will not retire until they reach their designed life span. The CFPPs will be expanded to cope with the increasing demand in the future.

Case 1: The CFPPs will not retire. Renewable energy will be utilized to cope with the increasing demand in the future.

Case 2: The CFPPs will retire at a certain rate every year to reach full retirement in the future. The renewable device will be built by minimizing cost.

Case 3: The CFPPs will retire according to the minimum cost. The carbon emissions will be a penalty term to the cost (treated as a carbon tax), which is the objective function in other literature.

Case 4: The CFPPs will retire according to the minimum average cost of carbon emission reduction (proposed).

The main parameters regarding the retirement of CFPPs are shown in Table 3-1, which is obtained from AEMO (2019 Inputs and Assumptions Workbook v1.2). [309]

TABLE 3-1. CFPPS RETIREMENT REGARDING PARAMETERS

Parameter	Value	Parameter	Value
C_i^u	\$140000~ \$170000/MW	r^m	0.04~0.06
C_i^s	\$15000~ \$16000/MW	r^f	0.045~0.05
C_i^m	\$54000~ \$113000/MW/year	SV_i	\$200000~ \$300000/MW
f_i	0.02	ε	0.06
r^s	0.03~0.04	L^s	50 years
A^{ref}	15~30 years		

The network topology diagram is shown in Fig. 3-3. The simulation is conducted on the IEEE-24 benchmark test system. Before the simulation, we have chosen some candidate buses where PV farms and wind farms can be installed, which are shown in Fig. 3-3. At these candidate buses, we assume that certain resource is abundant, and the installed requirement is met (such as enough spare area). For example, we assume that buses 4,5,6 and 8 have plenty of wind energy, and all the requirements are met to build centralized wind farms on these buses. The hydro plant also has a candidate bus. The installed requirement of the hydro plant is met. In the test system, there is only one candidate bus for the hydro plant. There are 6 candidate PV farms, 4 candidate wind farms, and 10 candidate transmission lines to be planned. The hydro plant is planned to be built on bus 21 in the future.

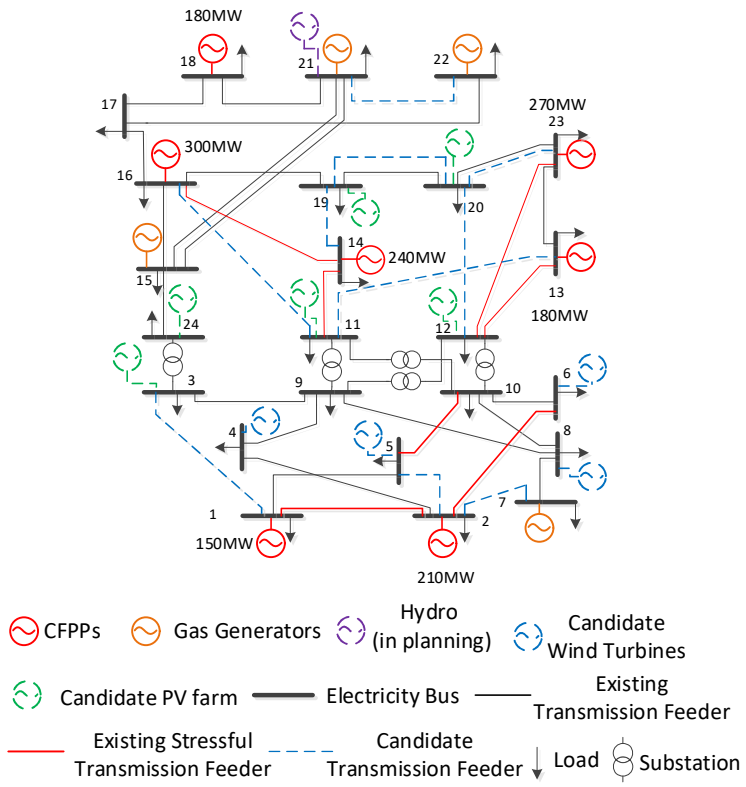

Fig. 3-3. Modified IEEE-24 bus system.

The final optimizing result for Case 4 is shown in Fig. 3-4. It can be found that two wind farms and three PV farms will be built. To realize the system transition and planning, 5 transmission lines will be built. The capacity of CFPPs on all buses reduce greatly. The total capacity of CFPPs of the system is reduced from 1530 MW to 236 MW. The largest planned PV farm has a capacity of 326MW.

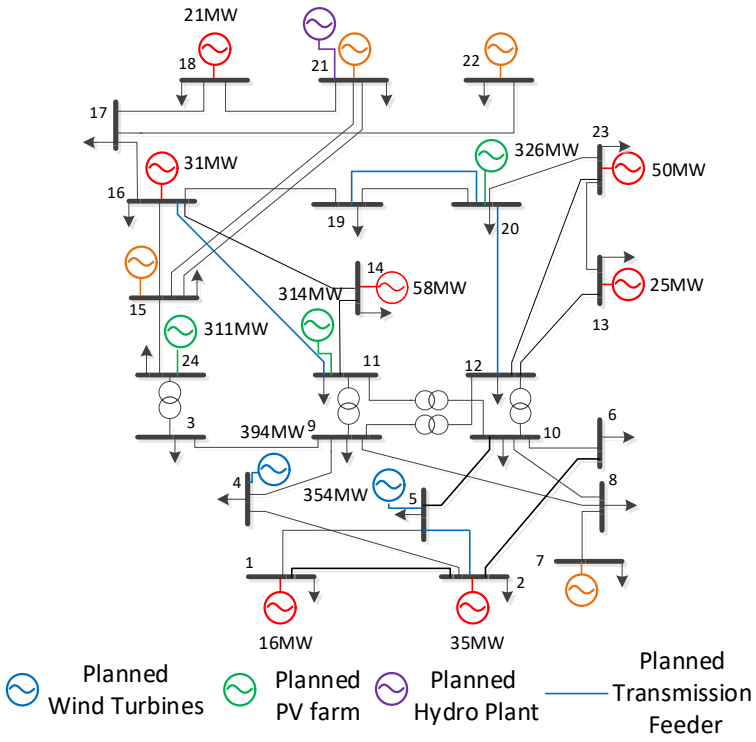

Fig. 3-4. The final planning scheme for the first milestone.

To show the advantages of the proposed method, Case 4 is compared with the other cases. First, the retirement conditions of the CFPPs for different cases are shown in Fig. 3-5. Apart from Case 1 (no retirement is considered), Cases 2, 3, and 4 will finally reach a retirement percentage of more than 80%. For Cases 3 and 4, different plants will retire at different rates.

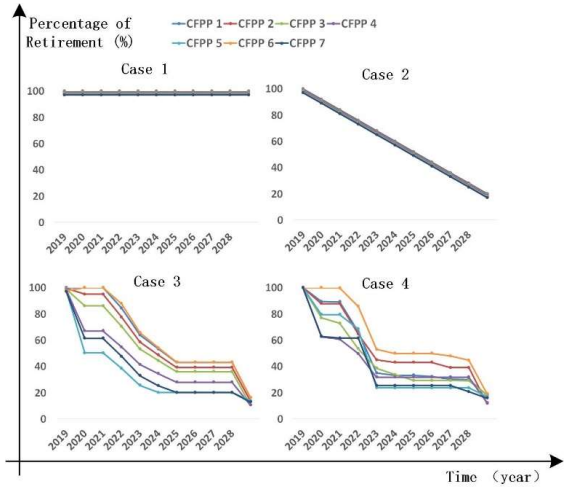

Fig. 3-5. The retirement condition of CFPPs.

Fig. 3-6 shows the capacity changes of different types of energy. For Case 1, CFPPs do not retire, so the capacity remains constant, but renewable energy will be applied from 2023 because of the increasing demand. For the other cases, the capacity of CFPPs will decrease, and massive renewable energy devices will be constructed.

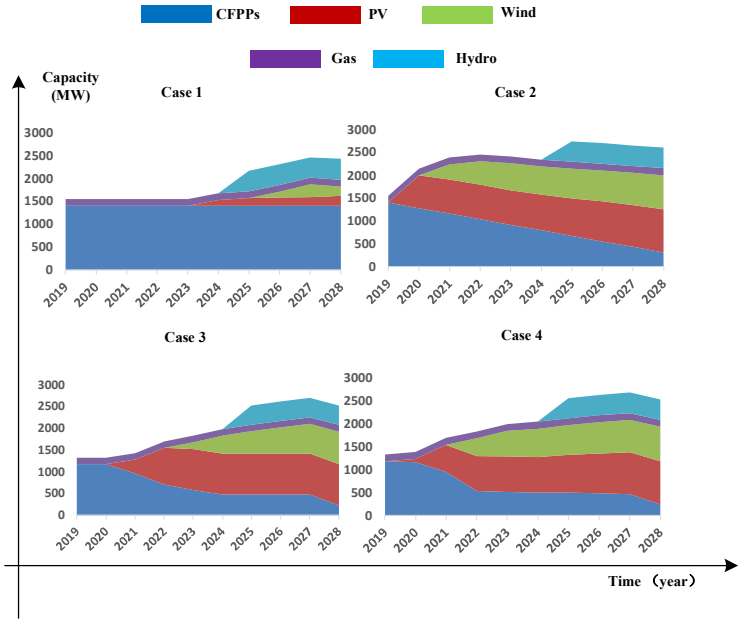

Fig. 3-6. The capacity composition of different energy.

The emission conditions of 4 cases are shown in Fig. 3-7(a)-(d). Obviously, Case 1 is the poorest because its emission reduction is unapparent. Case 2 has the best emission reduction result because the CFPPs began to retire very early. However, this incoordinate retirement strategy is not the best choice. From Fig. 3-6, the total installed capacity of Case 2 firstly increases and then decreases (2019 to 2024). That is because the retirement of CFPPs becomes too fast at an early stage, and massive renewable energy devices need to be built in a short time to meet the demand. So, Case 2 is certainly not an economical method. Cases 3 and 4 both have a smooth retirement process. But, Case 4 is better in emission reduction because the retirement time of CFPPs of Case 3 is the latest.

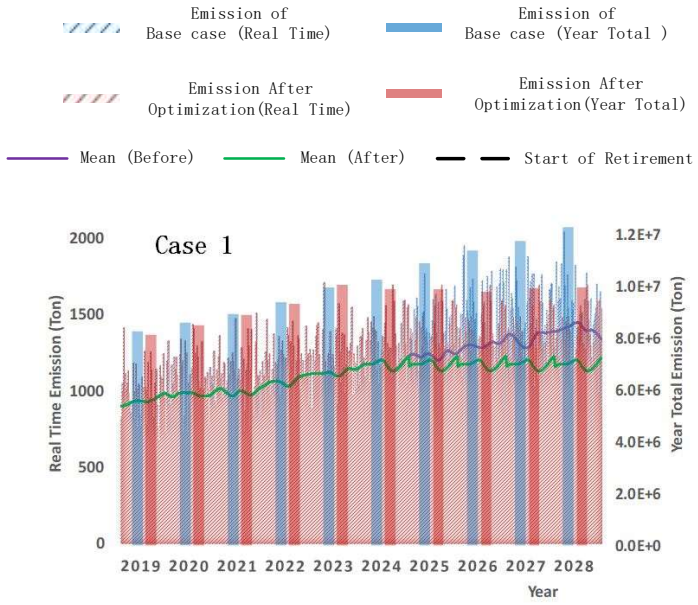

Fig. 3-7(a). The carbon emissions of Case 1 compared with the base case.

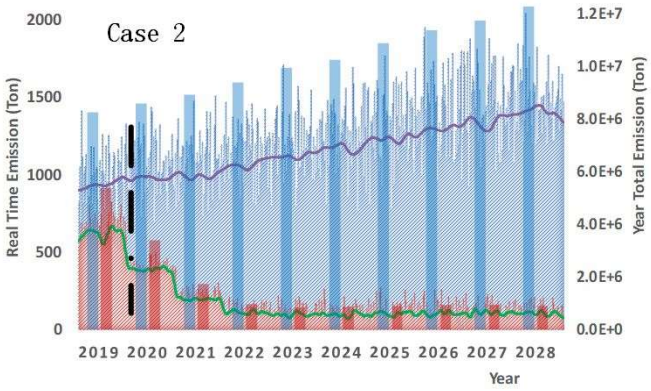

Fig. 3-7(b). The carbon emissions of Case 2 compared with the base case.

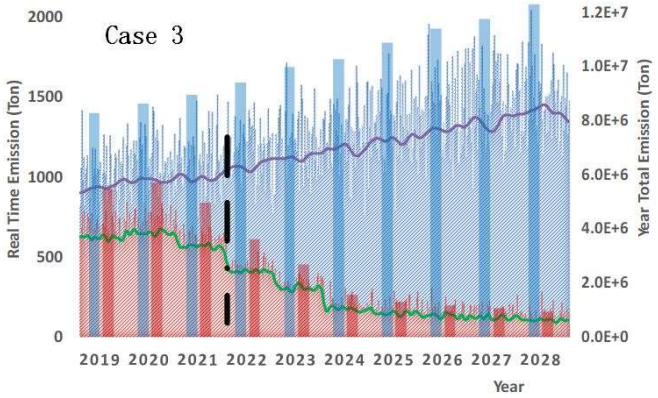

Fig. 3-7(c). The carbon emissions of Case 3 compared with the base case.

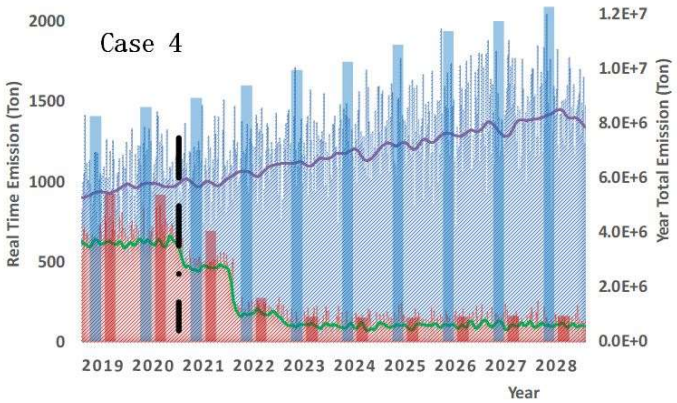

Fig. 3-7(d) The carbon emissions of Case 4 compared with the base case.

Fig. 3-8 shows the real-time power output of different kinds of energy. The colored gradient under the figure represents the capacitor factor of the generators. The capacitor factor is defined as the expected output against total capacity over a certain period. The gradient of the color represents the occurrence frequency of the expected output against total capacity. In other words, the deepest color represents that the generators are working at this capacitor factor most of the time, i.e., more frequently. For example, for CFPPs, they normally work at the capacitor factor of around 0.5, while for wind generators, they work at the capacitor factor of around 0.3 most of the time. In all cases, PVs will

be developed earlier than wind. However, the output of PVs fluctuates and becomes 0 at night. During the early stage (2020 to 2023), the CFPPs can fill in the shortage. In the later stage, the majority of CFPPs are retired, and wind farms are constructed to realize the complementary of PVs and wind. The wind energy is also intermittent. The remaining CFPPs, gas and hydro take response together to realize the frequency regulation. The marked rectangle area is to show the output of the gas generation (in purple). Since the total capacity of gas generation is small in the system, we enlarge the rectangle area to show that the gas generation will play a more important role during the early stage (CFPPs start to retire) and later stage (renewable energy covers most of the capacity in the system).

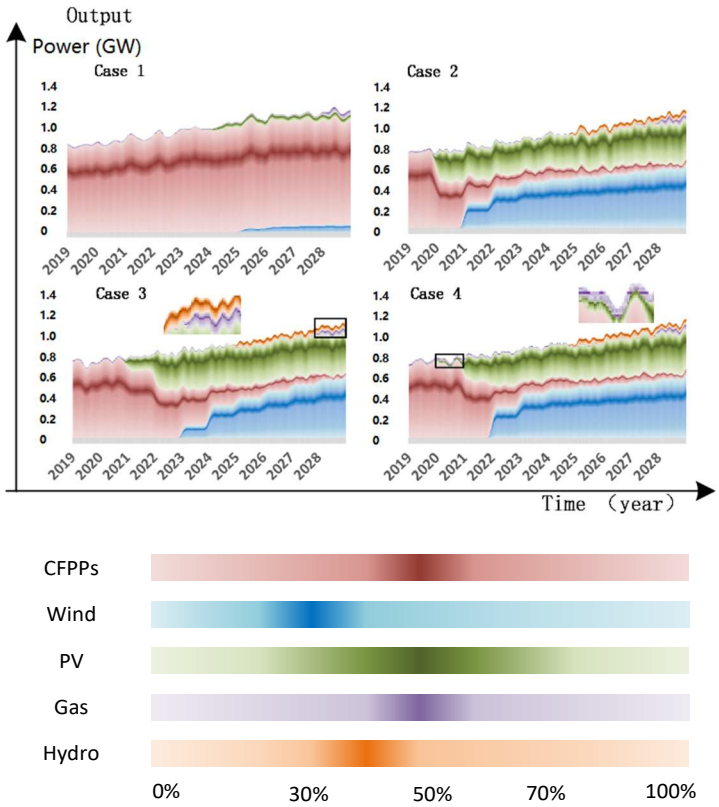

Fig. 3-8. Real-time output of different kinds of generations.

Five cases are compared according to the total cost, total emission reduction, and average cost of carbon emission reduction in Table 3-2. Case 1 has the lowest cost because it almost remains the current system, and its carbon emission reduction is very low. Compared with our proposed method (Case 4), Case 3 has a lower cost, and Case 2 has a higher emission reduction. However, the average cost of carbon emissions is higher than in Case 4. The average cost of carbon emissions in Case 4 is very close to the current carbon tax ($27.15/ton, New Zealand Carbon Market, 01.22.2020, Spot).

TABLE 3-2. THE COST AND EMISSION RESULTS OF ALL CASES

	Cost ($)	Emission Reduction (Ton)	Average Cost of Emission Reduction ($ / Ton)
Base Case	5.442*10^8	0	/

Case 1	5.806*10^8	7.278*10^6	80
Case 2	2.852*10^9	8.471*10^7	33.67
Case 3	2.088*10^9	7.328*10^7	28.49
Case 4	2.130*10^9	7.969*10^7	26.74

3.4.2 The Second Milestone

The gas network coupled with the electricity network is shown in Fig. 3-9, and the parameters of the gas network are shown in Table 3-3, according to Refs. [310, 311] The final planning result is shown in Fig. 3-10. The result of the expansion of the gas network is shown in Table 3-4. Three P2GSes are built and become the new coupled points by building new pipelines to connect the P2GSes to the gas network. From Fig. 3-10, it can be concluded that the nodal carbon intensity of all buses decreases dramatically. For example, the nodal carbon intensity of bus 5 drops from 0.9 to 0.0099 ton/MWh, which means that before planning, most of its energy consumption comes from non-renewable energy, but it consumes renewable energy most of the time after planning. It can be concluded that the system can realize the transition from fossil-fuel dominated to low-carbon oriented. Also, according to Fig. 3-10, the P2GSes are likely to be built at a place where carbon intensity is low (0, 0.0099, 0.025, respectively). The largest capacity of P2GS (120MW) is built at bus 4, where carbon intensity is 0.

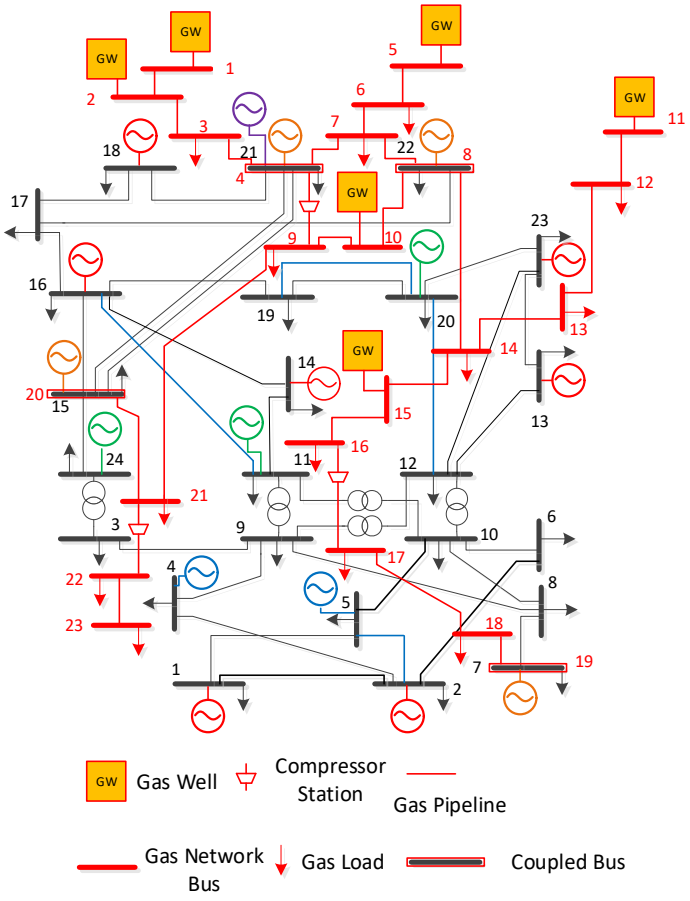

Fig. 3-9. The coupled electricity and gas network.

TABLE 3-3. GAS NETWORK PARAMETERS

Capacity: 1p.u.= 100m^3/hour

Line	Length (km)	Capacity (p.u.)	Line	Length (km)	Capacity (p.u.)
1-2	40	10	11-12	50	10
2-3	60	10	12-13	60	10
3-4	60	10	13-14	80	10
4-7	60	10	14-15	60	10
4-9	100	10	15-16	60	10
5-6	50	10	16-17	100	10
6-7	50	10	17-18	120	10
7-8	50	10	18-19	40	10
8-10	120	5	20-21	80	10
8-14	180	10	21-22	50	10
9-10	50	5	22-23	40	10
9-21	200	10			

TABLE 3-4. GAS NETWORK EXPANSION RESULT

(·) represents the electricity buses

No.	Bus	Investment Cost (M $)	Capacity (1p.u.=100m^3/hour)
1	22-(4)	72	10p.u.
2	17-(5)	75	10p.u.
3	11-(16)	60	5p.u.
4	17-18	53	5p.u.

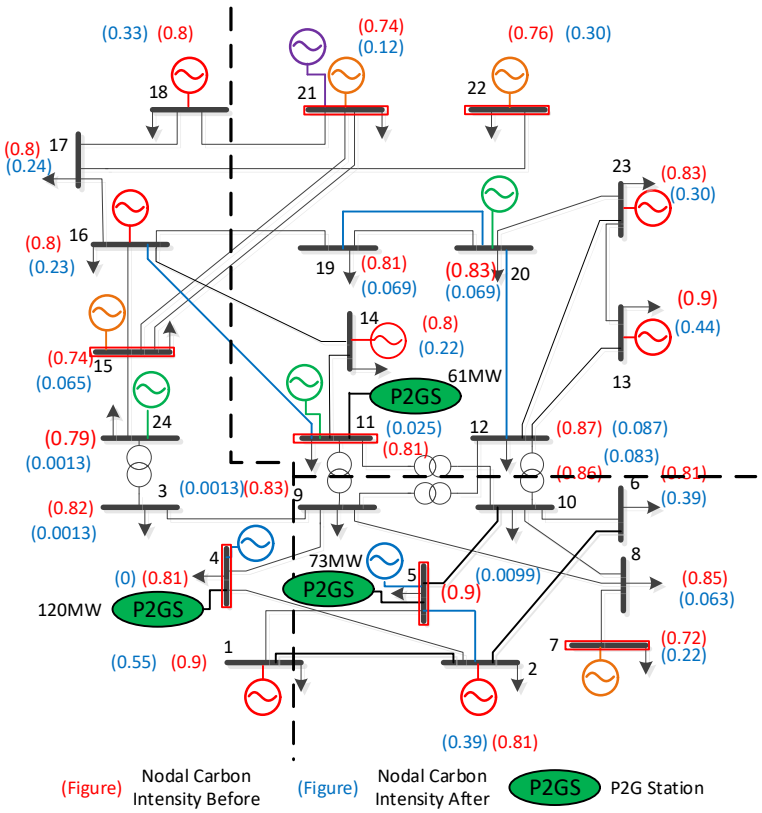

Fig. 3-10. The final planning scheme for the second milestone.

The operation results of one of the P2GSes are shown in Fig. 3-11. The P2GSes can finish the frequency regulation task well. The upward and downward enable energy is always within the secondary reserve capacity. The energy storage of P2GSes is changed with the behaviors of selling gas, purchasing electricity, and providing secondary reserve energy. When P2GSes are providing upward secondary reserve energy, the energy storage will decrease. Likewise, when P2GSes are providing downward secondary reserve energy, the energy storage will increase.

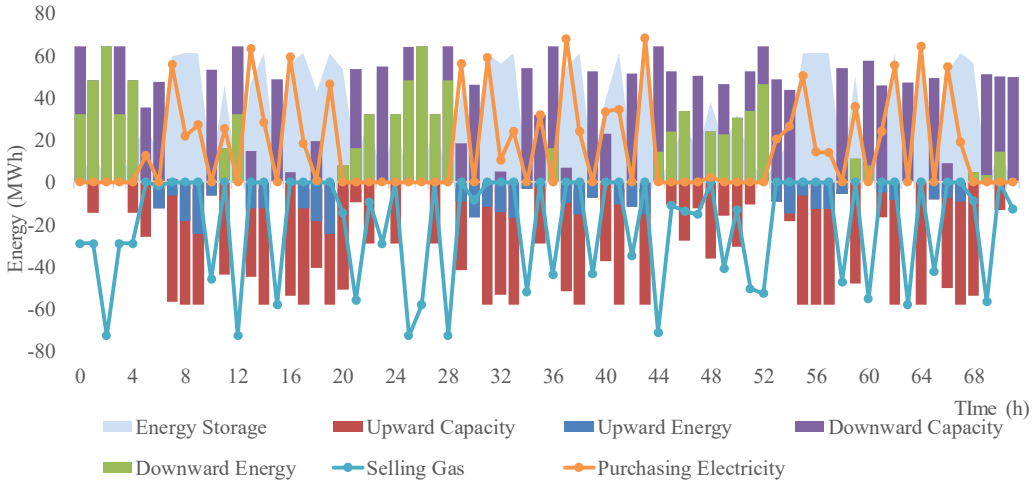

Fig. 3-11. The operation of P2GSes.

TABLE 3-5. DIFFERENCES BETWEEN CASES WITH AND WITHOUT P2GSES

(At the end of the planning horizon)	With P2GSeS		Without P2GSes
Unserved energy in the electricity network	Amount (GWh/year)	12.856	87.712
	Percentage of total energy	0.11%	0.75%
Curtailed renewable energy (GWh/year)	16.233		71.241
Savings in gas network M$/year	20.98		N/A
Carbon emission factor of the gas network tons/GJ	0.1189		0.1245

Table 3-5 shows the differences between cases with P2GSes and the case without P2GSes from four aspects. First, with P2GSes, the unserved energy in the electricity network is reduced by 74.856 GWh/year because P2GSes can provide upward regulation in the electricity system. As shown in Fig. 3-11, when providing upward regulation in the ancillary market, the energy storage of P2GSes will decrease. This part of the energy is converted back to electricity to support the previous unserved load so that the power system reliability can be improved. Second, the curtailed renewable energy is reduced by 77.2% because P2GSes can provide downward regulation to smooth intermittent renewable energy. From Fig. 3-10, it can be found that the P2GSes are built at the places where the nodal carbon intensity is low (0, 0.0099,

and 0.025 ton/MWh, respectively), indicating that P2GSes absorb the electricity mainly from renewable energy. Thus, when there is surplus renewable energy, P2GSes can act as ESS to absorb that part of electricity by providing downward ancillary service or directly purchasing electricity, as shown in Fig. 3-11. Third, in the natural gas network, there will be a saving of 20.98 million per year because the energy absorbed by P2GSes is mainly from surplus renewable energy. P2GSes can convert them into natural gas and sell gas to the gas network at a proper time, as shown in Fig. 3-11. Last but not least, the carbon emission factor of the gas network is reduced from 0.1245 ton/GJ to 0.1189 ton/GJ because the injected natural gas from P2GSes is mainly from renewable energy. It means that the carbon emissions can be reduced by 1.6 million tons per year merely in the gas network in the benchmark test system. Hence, P2GSes can help the integration of renewable energy and help the emission reduction in the gas network. In conclusion, the planning of the P2GSes can benefit both the electricity network and the gas network, especially when running in a low-carbon context.

To summarize, the details of the network changes are shown in Fig. 3-12.

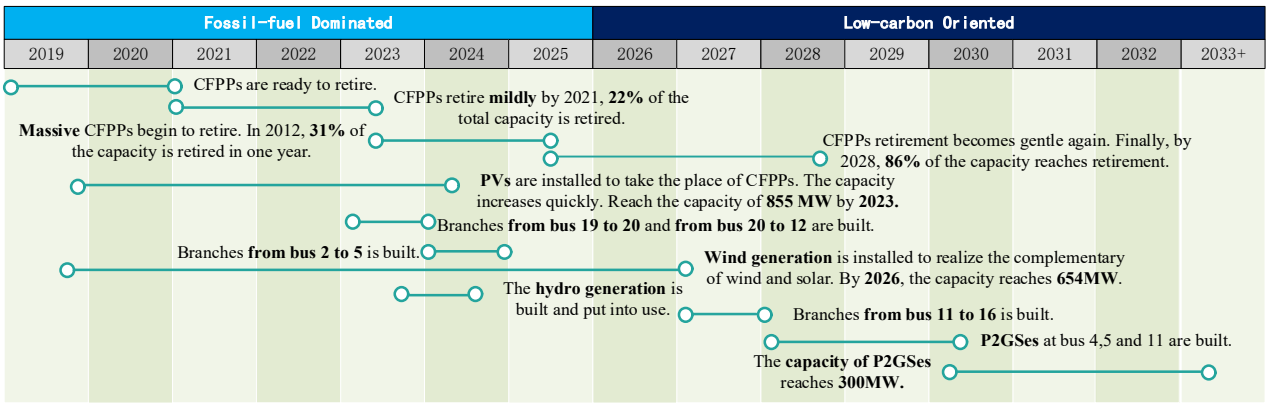

Fig. 3-12. The final planning of the electricity network transition roadmap.

3.5 Chapter Summary

Under the pressure of climate change, this chapter has proposed a two-milestone electricity network transition roadmap that can serve as a guide to assist the current fossil-fuel dominated network to transit into a low-carbon oriented network. First, it makes the best scheme for CFPP retirement and renewable generation investment. It avoids the sudden retirement of CFPPs and enables a smooth retirement. Moreover, our proposed model introduces the average cost of carbon emission reduction. According to the simulation results, our model (Case 4) will reduce carbon emissions by 79.7 million tons. This number is higher than that of Case 1 (no early retirement of CFPPs) and Case 3 (considering minimum system cost), 7.3 million tons and 73.3 million tons, respectively. Even though the emission reduction of Case 4 is slightly lower than Case 2 (CFPPs will retire at a certain rate every year, 84.7 million tons), the average cost of the emission reduction of Case 4 is reduced by 7 Ton/$, compared with that of Case 2. Also, the average cost of emission reduction in Case 4 is the lowest in all cases. Therefore, our proposed model can identify the most economical transition

plans in terms of carbon emission mitigation. Second, P2GSes construction is planned. P2GSes are believed to become one of the critical elements in the future energy network. In the model, the P2GSes can realize the energy transition between gas and electricity, and they also can participate in FCAS for its fast response. Besides, our planning model of P2GSes is based on the carbon emission flow model. From the simulation result, three P2GSes are built at the buses where the average nodal carbon intensity is low (0, 0.025 and 0.0099). Hence, the energy absorbed and produced by P2GSes is cleaner.

CHAPTER 4

EMISSION OBLIGATION FROM DEMAND SIDE THROUGH CARBON EMISSION TRACING

Most of the current carbon financing policies (e.g., carbon tax, carbon trading market) aim to utilize financial incentives to motivate emission reduction. However, most of the existing research works focus on the "observed" emissions, i.e., the interaction between power systems and carbon policies is considered from the generation perspective. It has been criticized by many carbon pricing opponents that power generators would simply fully (or almost fully) pass-through carbon cost to energy end-users. It should be noted that end-users are the underlying driver of emissions [312]. How the demand side and the generation side cooperate with each other to achieve a higher emission reduction efficiency needs to be further studied. Therefore, carbon emissions produced from the generation side should be identified from the perspective of the demand side. The concept of "virtual" carbon flow accompanying power flows has been introduced. In this chapter, a carbon footprint management strategy is proposed, where emission control is realized from both the generation side and the demand side.

4.1 Carbon Emission Flow Model

4.1.1 Deterministic Carbon Emission Flow (DCEF) Model

In order to trace carbon emissions from the generation side to the customer side, a carbon emission flow (CEF) model based on the proportional sharing principle has been proposed in [177]. In this case, a "virtual" emission flow accompanying power flow is introduced to clarify the footprint of carbon emissions, as shown in Fig. 4-1.

According to [313], for a given node, its nodal carbon intensity e^N, only depends on the total inflow branch carbon emission flow and the ejected carbon emission flow from any generators at this node; all the outflow branches from this node share the same branch carbon flow intensity e^B, the value equals to the nodal carbon intensity of node which they traveled out. It should be noted that the proportional sharing principle (PSP) is the basic assumption for the CEF model, which can linearize the relationship between power flow P^B and accompanying virtual emission flow C^B. Moreover, in this chapter, power loss in the transmission line is not considered.

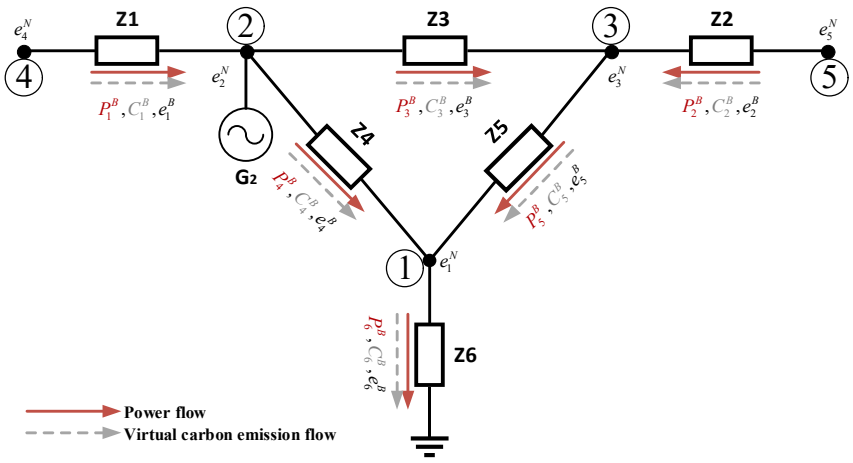

Fig. 4-1. CEF accompanying with power flow in power system.

In power systems, the power flow model can be expressed as:

$$P_{i,t}^{G}+\sum_{z\in\Omega^{R}}P_{i,z,t}^{R}=P_{i,t}^{D}-P_{i,t}^{ESS,CH}+P_{i,t}^{ESS,DS}+\sum_{j\in\Omega_{i}^{+}}P_{ij,t}^{B},\quad \forall i\in\Omega,\forall t\in[1,T] \tag{4.1}$$

$$Q_{i,t}^{G}=Q_{i,t}^{D}+\sum_{j\in\Omega_{i}^{+}}Q_{ij,t}^{B},\quad \forall i\in\Omega,\forall t\in[1,T] \tag{4.2}$$

$$P_{ij,t}^{B}=U_{i,t}U_{j,t}\left(G_{ij}\cos\theta_{ij,t}+B_{ij}\sin\theta_{ij,t}\right)-U_{i,t}^{2}G_{ij},\quad \forall i,j\in\Omega,\forall t\in[1,T] \tag{4.3}$$

$$Q_{ij,t}^{B}=-U_{i,t}U_{j,t}\left(B_{ij}\cos\theta_{ij,t}-G_{ij}\sin\theta_{ij,t}\right)+U_{i,t}^{2}G_{ij},\quad \forall i,j\in\Omega,\forall t\in[1,T] \tag{4.4}$$

where $P_{i,t}^{G}$ and $Q_{i,t}^{G}$ are the active power and reactive power generation of thermal generators at bus i time t; $P_{i,z,t}^{R}$ is the output of the z^{th} type of renewable energy; $P_{i,t}^{D}$ is the electricity demand; $P_{i,t}^{ESS,CH}$ and $P_{i,t}^{ESS,DS}$ are the charging and discharging power of ESS; $U_{i,t}$ is the nodal voltage; $\theta_{ij,t}$ is the phase angle; G_{ij} and B_{ij} are conductance and susceptance; Ω^{R} is the set of renewable energy types; Ω_{i}^{+} is the set of buses adjacent to bus i.

According to the PSP in [314] and [315], take node 2 as an example, the nodal carbon intensity in a typical time can be calculated as:

$$e_{2}^{N}=e_{3}^{B}=\frac{P_{1}^{B}\cdot e_{1}^{B}+P_{2}^{G}\cdot e_{2}^{G}}{P_{1}^{B}+P_{2}^{G}} \tag{4.5}$$

Extending node 2 to a general node, the nodal intensity in the conventional CEF model can be calculated as:

$$e_{i,t}^{N}=\left(P_{i,t}^{G}e_{i}^{G}+\sum\nolimits_{b\in L_{i}^{+}}\left|P_{b,t}^{B}\right|e_{b,t}^{B}\right)\Big/\left(P_{i,t}^{G}+\sum\nolimits_{z\in\Omega^{R}}P_{i,z,t}^{R}+\sum\nolimits_{b\in L_{i}^{+}}\left|P_{b,t}^{B}\right|\right),\quad \forall i\in\Omega,\forall t\in[1,T] \tag{4.6}$$

where $e_{i,t}^{N}$ is the nodal intensity; $P_{b,t}^{B}$ is the power flow on the b^{th} branch; $e_{b,t}^{B}$ is the branch intensity; L_{i}^{+} is the set of the transmission lines that inject active power into bus i.

Equation (4.6) can be rewritten into a matrix form by defining several matrixes.

The branch power flow distribution matrix is defined as $\mathbf{P}^B = \left(P_{ij}^B\right)_{N\times N}$. If there is positive power flow P from bus i to j, we have $P_{ij}^B = P$ and $P_{ji}^B = 0$; if there is negative power flow P from bus j to i, we have $P_{ij}^B = 0$ and $P_{ji}^B = P$.

The power injection distribution matrix is defined as $\mathbf{P}^G = \left(P_{kj}^G\right)_{K\times N}$. If the k^{th} generator is connected to the j^{th} bus and its injecting power is P, we have $P_{kj}^G = P$.

The nodal active power flux matrix is defined as $\mathbf{P}^N = \left(P_{ij}^N\right)_{N\times N}$. It is calculated by:

$$P_{ij}^N = \sum_{s\in S_i^+} P_s^B + P_i^G, \quad \forall i, j \in \Omega, \forall t \in [1,T] \tag{4.7}$$

The unit carbon emission intensity vector is defined as:

$$\mathbf{E}^G = \left[e_1^G, e_2^G, e_3^G ... e_K^G\right]^T \tag{4.8}$$

The nodal carbon intensity vector can be defined as:

$$\mathbf{E}^N = \left[e_1^N, e_2^N, e_3^N ... e_N^N\right]^T \tag{4.9}$$

Then, equation (4.6) can be transformed into equation (4.10).

$$\mathbf{E}^N = \left(\mathbf{P}^N - \left(\mathbf{P}^B\right)^T\right)^{-1} \left(\mathbf{P}^G\right)^T \mathbf{E}^G \tag{4.10}$$

4.1.2 Energy Storage Integrated CEF Model

However, the conventional CEF model does not consider the ESS in power systems. To further integrate the ESS into the system, we made an adjustment to the conventional CEF model. The ESS has three working states, i.e., charging, discharging, and idle. When the ESS is idle, the carbon intensity of ESS will not be changed. When the ESS is charging, it can be regarded as a load to absorb the energy from the grid. During this process, the carbon intensity of the ESS will be affected by the carbon intensity of the absorbed energy. When the ESS is discharging, it can be regarded as a generator, and the carbon intensity will not change. Therefore, a nodal carbon intensity evolution equation for ESS is proposed, shown as equation (4.11).

$$e_{i,t+1}^{ESS} = \left(e_{i,t}^{ESS} \cdot E_{i,t}^{ESS} + e_{i,t}^N P_{i,t}^{ESS,CH} \Delta t\right) \Big/ \left(E_{i,t}^{ESS} + P_{i,t}^{ESS,CH} \Delta t\right), \quad \forall i \in \Omega, \forall t \in [1,T] \tag{4.11}$$

Then, the CEF model can be reformulated as (4.12)-(4.13).

$$e_{i,t}^N = \frac{P_{i,t}^G e_i^G + P_{i,t}^{ESS,DS} e_{i,t}^{ESS} + \sum_{b\in L_i^+} \left|P_{b,t}^B\right| e_{b,t}^B}{P_{i,t}^G + \sum_{z\in\Omega^R} P_{i,z,t}^R + P_{i,t}^{ESS,DS} + \sum_{b\in L_i^+} \left|P_{b,t}^B\right|}, \quad \forall i \in \Omega, \forall t \in [1,T] \tag{4.12}$$

$$e_{b,t}^B = e_{i,t}^N, \quad \forall i \in \Omega, \forall b \in L_i^+, \forall t \in [1,T] \tag{4.13}$$

where Γ_b is the power injection bus.

4.1.3 Probabilistic CEF (PCEF)Model

Based on the formulated equations, it can be found that both power flow and carbon flow are affected by the uncertainties of renewable energy output and electricity demand. Hence, in this chapter, we further extend the DCEF model to a PCEF model. Considering there are *m* uncertain input parameters, the output variables (nodal carbon intensity in PCEF model) can be expressed through a nonlinear function shown as:

$$y = f\left(x_1, x_2, ..., x_k, ..., x_m\right) \tag{4.14}$$

In this chapter, the 2m+1 estimate scheme is employed to model the PCEF. In $L \times M$ scheme, the uncertainties provided by the first moment are concentrated on *L* points for each input parameter x_k, called *concentration* [35]. The l^{th} concentration is represented by a location $x_{k,l}$ and a weight $w_{k,l}$. The location $x_{k,l}$ is determined by:

$$x_{k.l} = \mu_{x_k} + \xi_{k.l} \cdot \sigma_{x_k}, \quad \forall k, \forall l, \forall x_k \tag{4.15}$$

where $\xi_{l,k}$ is the standard location; μ_{x_l} and σ_{x_l} are the mean and standard deviation of the stochastic input parameter x_k.

The standard location $\xi_{k.l}$ can be formulated as:

$$\xi_{k.l} = \frac{\lambda_{x_{k,3}}}{2} + (-1)^{3-l}\sqrt{\lambda_{x_{k,4}} - \frac{3}{4}\left(\lambda_{x_{k,3}}\right)^2}, \quad \forall k, \forall l, \forall x_k \tag{4.16}$$

where $\lambda_{x_{l,3}}$ and $\lambda_{x_{l,4}}$ are the coefficients of skewness and kurtosis of x_k, and they can be computed as:

$$\lambda_{x_{k,n}} = \int_{-\infty}^{+\infty} \frac{\left(x_k - \mu_{x_k}\right)^n f_{x_k} dx_k}{\left(\sigma_{x_k}\right)^n}, \quad \forall k, \forall x_k \tag{4.17}$$

For each $x_{k,l}$, the weight can be expressed as:

$$w_{k,l} = \frac{(-1)^{3-l}}{\xi_{k,l}\left(\xi_{k,1} - \xi_{k,2}\right)}, \quad \forall k, \forall l \tag{4.18}$$

$$w_{k,3} = \frac{1}{m} - \frac{1}{\lambda_{k,4} - \left(\lambda_{k,3}\right)^2}, \quad \forall k \tag{4.19}$$

For each pair ($x_{k,l}$, $w_{k,l}$), the output variables can be calculated as:

$$y(k,l) = F\left(\mu_{x_1}, \mu_{x_2}, ..., \mu_{x_m}\right), \quad \forall k, \forall l \tag{4.20}$$

Then, the n^{th} raw moment of the variable y^n can be estimated as:

$$\mathbb{E}\left[y^n\right] \cong \sum_{k=1}^{m}\sum_{l=1}^{3}\left(w_{k,l}\cdot y^n\left(l,k\right)\right) \tag{4.21}$$

In the proposed PCEF model, the estimated value of the probabilistic nodal carbon intensity can be expressed as:

$$\mathbb{E}\left[e_{i,t}^{N(n)}\right] \cong \sum_{k=1}^{m}\sum_{l=1}^{3}\left(w_{k,l}\cdot e_{i,t}^{N(n)}\left(l,k\right)\right),\quad \forall i\in\Omega,\forall t\in\left[1,T\right] \tag{4.22}$$

4.2 Low-carbon Oriented Operation of Electricity Network

4.2.1 Double Carbon Taxation Mechanism

Double carbon taxation refers to a taxation principle that carbon emissions are taxed at both the supply level and the consumption level. Like the existing double taxation in economic theory, double carbon taxation definitely demonstrates the responsibility of emissions. For example, there are many light industrial products (e.g., cloths) made in developing countries (e.g., China), but the majority of them are exported and consumed in developed countries (e.g., USA). It is always a big debate on which country should actually pay for the carbon cost. The "observed" emissions occur in developing countries, while the demand of developed countries is the original cause of emissions, and the "virtual" emissions should not be ignored. Overall, this philosophy holds the same for the power sector. Although emissions are physically produced by fossil fuel combustion at power generators, end-users are the underlying driver of emissions. End-users should pay extra carbon costs for electricity consumption. However, it is unreasonable to simply pass through the carbon cost to end-users, as this would make generators' responsibility in emission control vague. As an example, the double carbon taxation mechanism will be under trial in Shenzhen in China. In reality, end users are responsible for underwriting a certain fraction of the carbon cost, as the costs of power generation, transmission, distribution, and carbon tax are already reflected in the retail electricity price that consumers pay. This fraction depends on the carbon cost pass-through rate.

4.2.2 Carbon Footprint Management Strategy

In this chapter, carbon footprint management is realized by flexibly dispatching the ESS and generators while restricting the direct emissions of thermal generators and the indirect emissions of the consumers. Although the electricity consumers do not produce direct carbon emissions, the consumption results in indirect emissions if the electricity is generated by fossil fuel. The objective function minimizes the total cost of the system of a year, shown as:

$$\min F = \sum_{t=1}^{8760}\left(\sum_{i\in\Omega^G} C_i\left(P_{i,t}^G\right) + \sum_{i\in\Omega^{ESS}}\left(\tau P_{i,t}^{ESS,DS}\Delta t + \tau\varsigma E_{i,t}^{ESS}\right)\right) \tag{4.23}$$

where $C_i\left(\cdot\right)$ is the cost function of the thermal generators; τ is the cost coefficient of the lifetime degradation of the battery; ς is the leakage loss factor of the battery; Ω^G is the set of thermal generators; Ω^{ESS} is the set of ESSs.

The following constraints should be satisfied:

Eqs. (4.1)-(4.4), (4.11)-(4.13)

$$0 \le P_{i,t}^{G} \le P_{i}^{G,\max},\ \ 0 \le Q_{i,t}^{G} \le Q_{i}^{G,\max},\ \ \forall i \in \Omega, \forall t \in [1,T] \tag{4.24}$$

$$P_{i,t}^{G} - P_{i,t-1}^{G} \le Ramp_{i}^{Up}, P_{i,t-1}^{G} - P_{i,t}^{G} \le Ramp_{i}^{Dw},\ \ \forall i \in \Omega, \forall t \in [1,T] \tag{4.25}$$

$$U_{i}^{\min} \le U_{i,t} \le U_{i}^{\max},\ \ \forall i \in \Omega, \forall t \in [1,T] \tag{4.26}$$

$$-P_{ij}^{B,\max} \le P_{ij,t}^{B} \le P_{ij}^{B,\max}, -Q_{ij}^{B,\max} \le Q_{ij,t}^{B} \le Q_{ij}^{B,\max},\ \ \forall i,j \in \Omega, \forall t \in [1,T] \tag{4.27}$$

$$E_{i,t+1}^{ESS} = E_{i,t}^{ESS} + P_{i,t}^{ESS,CH}\Delta t\eta^{CH} - P_{i,t}^{ESS,DS}\Delta t / \eta^{DS},\ \ \forall i \in \Omega, \forall t \in [1,T] \tag{4.28}$$

$$E_{i}^{ESS,\min} \le E_{i,t}^{ESS} \le E_{i}^{ESS,\max}, 0 \le P_{i,t}^{ESS,CH/DS} \le \overline{P_{i}^{CH/DS}},\ \ \forall i \in \Omega, \forall t \in [1,T] \tag{4.29}$$

$$\sum_{t} e_{i}^{G} P_{i,t}^{G} \le Cap_{i},\ \ \forall i \in \Omega \tag{4.30}$$

$$-\Theta \le \sum_{t}\sum_{i \in \Omega_{m}^{reg}} e_{i}^{G} P_{i,t}^{G} - \sum_{t}\sum_{j \in \Omega_{n}^{reg}} e_{j}^{G} P_{j,t}^{G} \le \Theta \tag{4.31}$$

$$\widetilde{P_{i,t}^{FL}} = \varepsilon\left(P_{i,t}^{FL}, \lambda_{i,t}^{LMP,CB}\right),\ \ \forall i \in \Omega, \forall t \in [1,T] \tag{4.32}$$

$$\mathbb{E}\left[e_{i,t}^{N(n)}\right] \cong \sum_{k=1}^{m}\sum_{l=1}^{3}\left(w_{k,l} \cdot e_{i,t}^{N(n)}(l,k)\right),\ \ \forall i \in \Omega, \forall t \in [1,T] \tag{4.33}$$

$$\sum_{t} \mathbb{E}\left[e_{i,t}^{N(n)}\right]\left(P_{i,t}^{L} + \widetilde{P_{i,t}^{FL}}\right)\Delta t \le M_{1},\ \ \forall i \in \Omega \tag{4.34}$$

$$\Pr\left\{\sum_{t} e_{i,t}^{N}\left(P_{i,t}^{L} + \widetilde{P_{i,t}^{FL}}\right)\Delta t \le M_{2}\right\} \ge \kappa,\ \ \forall i \in \Omega \tag{4.35}$$

where $P_{i}^{G,\max}$ and $Q_{i}^{G,\max}$ are the active and reactive power generation of the thermal generators; $Ramp_{i}^{Up}$ and $Ramp_{i}^{Dw}$ are the ramp-up and ramp-down limits of the thermal generators; $U_{i}^{\min}$ and $U_{i}^{\max}$ are the minimum and maximum nodal voltage; $P_{ij}^{B,\max}$ and $Q_{ij}^{B,\max}$ are the maximum active and reactive power flow; η^{CH} and η^{DS} are the charging and discharging efficiencies; $E_{i}^{ESS,\min}$ and $E_{i}^{ESS,\max}$ are the minimum and maximum energy storage states of ESS; $\overline{P_{i}^{CH/DS}}$ is the maximum charging/discharging power of ESS; Cap_{i} is the allocated carbon emission quotas of thermal generators; Θ is the cap of the carbon emission difference among regions; $P_{i,t}^{FL}$ is the flexible load; $\widetilde{P}_{i,t}^{FL}$ is the adjusted power consumption of the flexible load; $\lambda_{i,t}^{LMP,CB}$ is the carbon-integrated electricity price; $\varepsilon(\cdot)$ is the elasticity function.

Equation (4.24) is the output power limits of the thermal generators. Equation (4.25) is the ramping limits of the thermal generators. Equation (4.26) is the limit of nodal voltage. Equation (4.27) is the limit of power flow. Equation

(4.28) is the power balance equation of the ESS. Equation (4.29) is the limits of energy storage state and charging/discharging power of ESS. Equation (4.30) is the limits of direct carbon emissions of thermal generators. If the emissions of the thermal generators exceed the quotas, they need to purchase extra quotas in the emissions from the ETS and pay the carbon tax. Carbon trading is further discussed in the next chapter. Equation (4.31) manages the regional direct carbon emissions by limiting the carbon emission difference among regions. Equation (4.32) describes the elasticity of flexible load representing the responsiveness of flexible load to the carbon integrated electricity prices [192]. In a double carbon taxation mechanism, the prosumers are faced with carbon-integrated electricity prices. The elasticity function will be further modeled in the next section. Equation (4.34) restricts the expected indirect emissions of the prosumers. Equation (4.35) is a chance constraint for the indirect emissions.

4.3 Price Elasticity to the Carbon Integrated Electricity Price

The carbon integrated electricity price can be expressed as:

$$\lambda_{i,t}^{LMP,CB}=\lambda_{i,t}^{LMP}+\lambda_{t}^{CB}{}_{t}e_{i,t}^{N},\quad \forall i\in\Omega,\forall t\in[1,T] \tag{4.36}$$

The carbon integrated electricity has two components, i.e., the locational marginal electricity price $\lambda_{i,t}^{LMP}$ and the carbon price λ_{t}^{CB}.

Normally, consumers' demand would increase following the decrease in electricity prices. In economic theory, the elasticity coefficient, ε, is defined to describe the rate of this changing relationship, expressed as ref. [316]:

$$\varepsilon=\frac{\frac{\Delta Q}{Q}}{\frac{\Delta\lambda}{\lambda}}=\frac{\lambda}{Q}\frac{\Delta Q}{\Delta\lambda} \tag{4.37}$$

where λ, $\Delta\lambda$ denote commodity price and changing price, respectively; Q, ΔQ denote purchase amount of commodity associated with price λ and changing purchase amount, respectively.

Based on equation (4.36), it can be seen that the consumers will undertake the carbon tax through carbon integrated locational marginal electricity price. Hence, the flexible loads of consumers will respond to both electricity prices and carbon prices. Hence, cross-elasticity ε^{E} is also considered, shown in (4.38).

$$\varepsilon^{E}=\frac{\partial P^{FL}/P^{FL}}{\partial\lambda^{LMP}/\lambda^{LMP}},\varepsilon^{C}=\frac{\partial P^{FL}/P^{FL}}{\partial\lambda^{CB}/\lambda^{CB}} \tag{4.38}$$

where ε^{E} is the self-elasticity; ε^{C} is the cross-elasticity.

Market Share Model (MSD) and Discrete Attraction Model (DAM) are usually used to analyze the relationship

between the demand of customers and the attraction of commodities at different times mathematically. These two models can provide a methodology to investigate the calculation of the elasticity matrix. MSD describes the sharing proportion for one commodity among similar commodities in a trading market:

$$S_{it} = D_{it} \big/ D_t , \quad \forall i \in \Omega , \forall t \in [I,T] \tag{4.39}$$

$$D_t = \sum_{i=1}^{I} D_{it} , \quad \forall t \in [I,T] \tag{4.40}$$

where S_{it} denotes the sharing proportion of commodity *i* at time *t*; D_{it} denotes the demand amount of commodity *i* at time *t*; D_t denotes the overall demand amount of similar commodities including *i*.

Following MSD, DAM reveals that the attraction of commodities to customers is the key influence for its sharing proportion in the trading market. If one commodity has a high attraction, it means this commodity would share more market proportion. In other words, the demand amount for this commodity is massive. Therefore, according to the logic consistency principle, the problem of changing demand corresponding to various prices can be carried out by switching the problems of attraction to price under combination models of MSD and DAM [317]. Note that price and attraction are also a negative correlation. Further, in electricity markets, low electricity prices would lead to high attraction, and then the demand for electricity under this price would increase. This would share more market proportion for electricity under this price in the overall demand amount.

According to the DAM, the attraction of carbon price and electricity price can be expressed as:

$$D_{it} = e^{\varsigma_t} \varpi_t \prod_{h=1}^{H} \left(\lambda_h^{CB} e_{i,h}^{N} \right)^{\chi_h^{CAR}} \cdot \left(\lambda_h^{LMP} \right)^{\chi_h^{ELE}} , \quad \forall i \in \Omega , \forall t \in [I,T] \tag{4.41}$$

where ς_t is the fixed influence coefficient of carbon price; ϖ_t is the carbon price deviation; χ_h^{CAR} and χ_h^{ELE} are the influence coefficient of the carbon price and electricity price at time *h*.

Combining equations (4.39)-(4.41) the market sharing proposition can be calculated as:

$$S_{it} = \frac{e^{\varsigma_t} \varpi_t \prod_{h=1}^{H} \left(\lambda_h^{CB} e_{i,h}^{N} \right)^{\chi_h^{CAR}} \cdot \left(\lambda_h^{LMP} \right)^{\chi_h^{ELE}}}{\sum_{p=1}^{H} \left(e^{\varsigma_p} \varpi_p \prod_{h=1}^{H} \left(\lambda_h^{CB} e_{i,h}^{N} \right)^{\chi_h^{CAR}} \cdot \left(\lambda_h^{LMP} \right)^{\chi_h^{ELE}} \right)} , \quad \forall i \in \Omega , \forall t \in [I,T] \tag{4.42}$$

Since electricity consumption and carbon emissions occur concurrently, electricity and CERs are complementary goods. Therefore, the self-elasticity and cross-elasticity can be finally formulated as:

$$\varepsilon_{it}^{E} = \chi_t^{ELE} \left(1 - S_{it} \right), \quad \forall i \in \Omega , \forall t \in [I,T] \tag{4.43}$$

$$\varepsilon_{it}^{C} = \chi_t^{CAR} S_{it} , \quad \forall i \in \Omega , \forall t \in [I,T] \tag{4.44}$$

After obtaining the estimated elasticity coefficient, as a result of changing prices, the amount of changing demand can be obtained. Normally, a quadratic function is used to describe this relationship [318]. According to ref. [319], a more accurate exponential function is illustrated as:

$$\widetilde{P_{i,t}^{FL}} = P_{i,t}^{FL} \times e^{-\sum_{h=-0.5T}^{0.5T}\left(\lambda_{t+h}^{CB} e_{i,t+h}^{N} + \varepsilon_{i,t+h}^{E} \lambda_{i,t+h}^{ELE}\right)}, \quad \forall i \in \Omega, \forall t \in [1,T] \tag{4.45}$$

4.4 Data-driven Solution Method

In section 4.3, a chance-constrained carbon footprint management model based on PCEF is established. To solve the optimization model, serval aspects need to be further addressed, as shown in Fig. 4-2. First, the power consumption of the flexible load is disaggregated from the smart meter readings through non-intrusive load monitoring (NILM) technologies [320]. Then, to complete the PCEF model, the distribution of the uncertainties should be constructed. The uncertainties include the renewable energy output, the fixed load, and the flexible load. Second, the chance constraints should be reformulated for the convenience of computation. Third, a solution algorithm should be designed to solve the PCEF-based chance-constrained carbon footprint management model.

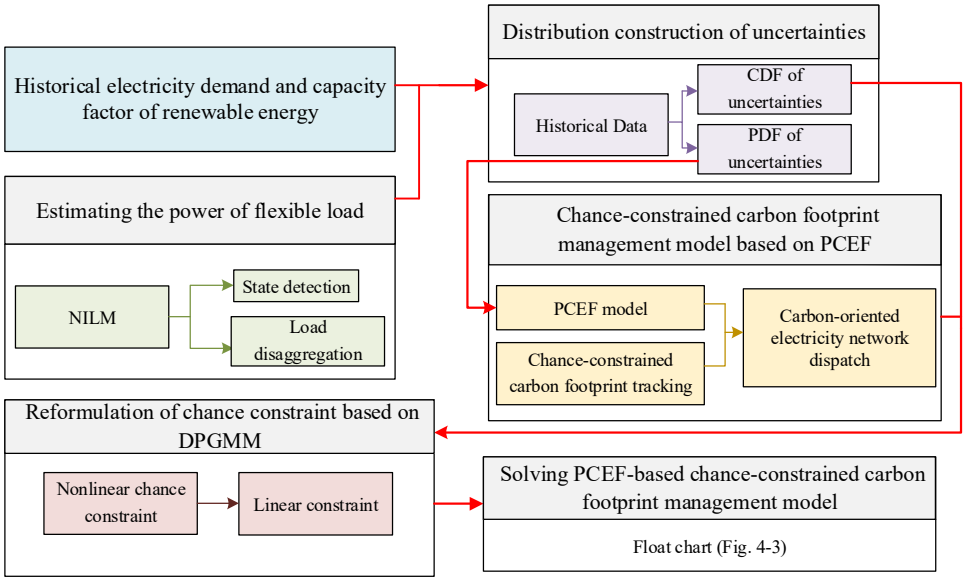

Fig. 4-2. Solution methodology of the formulated problem.

4.4.1 Distribution Construction for Uncertainties

The gaussian mixture model (GMM) is utilized to construct the probability density function (PDF) of the uncertainties. GMM is a probability model that can be used to represent the probability model with C sub-distributions in the overall distribution. The general expression of GMM for multivariate vector $\mathbf{x}$ is presented as follows:

$$GMM = \sum_{c=1}^{C} \pi_c \phi\left(\mathbf{x} \mid \vartheta_c\right), \quad \sum_{c=1}^{C} \pi_c = 1 \tag{4.46}$$

where C is the component number; π_c is the corresponding weight; $\phi(\cdot)$ is the multivariate Gaussian distribution;

ϑ_c is the parameter of the distribution, including mean μ and covariance φ.

However, the number of the components is unknown. To this end, the Dirichlet process (DP) is a random process for the Bayesian nonparametric model, which is commonly used for the prior of the Dirichlet process Gaussian mixture model (DPGMM)[321]. In DP, the limit for the number of clusters C goes to infinity. The conditional for the indicators can be expressed as (4.47). The values of indicator variables encode the mixture component to which observation belongs.

$$\Pr\left(\varepsilon_q = c \mid \varepsilon_{q-}, \alpha\right) = \frac{N_{-q,c} + \alpha / C}{N - 1 + \alpha} \tag{4.47}$$

where ε_q is the indicator of the q^{th} observation; $q-$ indicates all indices except q; α is the concentration parameter; N is the total number of observations; $N_{-q,c}$ is the number of observations in component c for all data points except point q.

Defining a joint prior distribution $\mathcal{G}$ on the component parameters and indicators, the model can be written as:

$$\mathbf{x} \mid \varepsilon_q, \vartheta \sim \phi\left(\mu, \varphi\right) \tag{4.48}$$

$$\mathcal{G} \sim DP\left(\alpha, \mathcal{G}_0\right) \tag{4.49}$$

$$\vartheta_q \sim \mathcal{G} \tag{4.50}$$

where $DP\left(\alpha, \mathcal{G}_0\right)$ is the DP with base distribution $\mathcal{G}_0$ (distribution of the component parameters in an infinite mixture model) and concentration parameter α; $\mathcal{G}$ is a random discrete distribution drawn from $DP\left(\alpha, \mathcal{G}_0\right)$.

Given π, the distribution of the number of observations assigned to each component is multinomial, shown as:

$$\Pr\left(N_1, .., N_C \mid \pi\right) = \frac{N!}{N_1! N_2! ... N_C!} \prod_{c=1}^{C} \pi_c^{N_c} \tag{4.51}$$

The distribution of the indicators can be expressed as follows:

$$\Pr\left(c \mid \pi\right) = \prod_{c=1}^{C} \pi_c^{N_c} \tag{4.52}$$

By performing DPGMM, the number, mean vectors, and covariance matrices of the multivariate Gaussian distributions can be obtained so that the PDF of the uncertainties can be constructed.

4.4.2 Reformulation of Chance Constraints

The chance constraint (4.12) is required to be linearized for further processing. Equation (4.12) can be first reformulated as (4.53) by introducing $P_{ji,t}^{B,inj}$.

$$e_{i,t}^{N}=\frac{P_{i,t}^{G}e_{i}^{G}+P_{i,t}^{ESS,DS}e_{i,t}^{ESS}+\sum_{j\in\Omega_i^{+}}P_{ji,t}^{B,inj}e_{b,t}^{B}}{P_{i,t}^{G}+\sum_{z\in\Omega^{R}}P_{z,t}^{R}+P_{i,t}^{ESS,DS}+\sum_{j\in\Omega_i^{+}}P_{ji,t}^{B,inj}},\quad \forall i,j\in\Omega,\forall t\in[1,T] \tag{4.53}$$

where $P_{ji,t}^{B,inj}$ is the positive power flow injection from bus *j* to *i*.

The positive power flow injection can be expressed as:

$$P_{ji,t}^{B,inj}=\max\left\{P_{ji,t}^{B},0\right\},\quad \forall i,j\in\Omega,\forall t\in[1,T] \tag{4.54}$$

The maximization function can be linearized according to:

$$P_{ji,t}^{B,inj}\geq P_{ji,t}^{B},\quad P_{ji,t}^{B,inj}\geq 0,\quad \forall i,j\in\Omega,\forall t\in[1,T] \tag{4.55}$$

$$P_{ji,t}^{B,inj}\leq P_{ji,t}^{B}+\mathcal{M}(1-\chi_1),\quad P_{ji,t}^{B,inj}\leq 0+M(1-\chi_2),\quad \forall i,j\in\Omega,\forall t\in[1,T] \tag{4.56}$$

$$\chi_1+\chi_2\geq 1,\quad \chi_1,\chi_2\in\{0,1\} \tag{4.57}$$

where $\mathcal{M}$ is a large number; χ_1 and χ_2 are auxiliary binary variables.

After the absolute sign in (4.12) is eliminated, equation (4.53) can be further linearized based on the first-order Taylor series approximation at the point $\left(\hat{x}_k^1,\hat{x}_k^2,...,\hat{x}_k^6\right)$, shown as:

$$\chi_1+\chi_2\geq 1,\quad e_{i,t}^{N}\widetilde{P}_{i,t}^{EV}\approx e_{i,t}^{N(n)}\widetilde{P}_{i,t}^{EV}\Big|_{\left(\hat{x}_k^1,\hat{x}_k^2,...,\hat{x}_k^8\right)}+\sum_{n=1}^{8}\left(\hat{x}^n-\hat{x}_k^n\right)f_{\hat{x}^n}^{'}\left(\hat{x}_k^1,\hat{x}_k^2,...,\hat{x}_k^8\right),\quad \forall i\in\Omega,\forall t\in[1,T] \tag{4.58}$$

where $\hat{\mathbf{x}}=\left\{P_{i,t}^{G},P_{i,t}^{ESS,DS},P_{ji,t}^{B,inj},\widetilde{P}_{i,t}^{EV},e_{i,t}^{ESS},e_{b,t}^{B},P_{z,t}^{R}\right\}$

Then, the chance constraint (4.58) can be reformulated as the compact form as (4.59).

$$\Pr\left\{\mathbf{a}^T\hat{\mathbf{x}}+\mathbf{b}^T\varpi\leq M\right\}\geq\kappa \tag{4.59}$$

where $\mathbf{a}$ and $\mathbf{b}$ are the coefficients; $\hat{\mathbf{x}}$ is the decision variables; ϖ is the random variables. The random variables include $P_{z,t}^{R}$ and $P_{i,t}^{EV}$.

According to ref. [322], equation (4.59) is equivalent to:

$$M-\mathbf{a}^T\hat{\mathbf{x}}\geq\mathcal{Q}_{\mathbf{b}^T\varpi}^{-1}(\kappa) \tag{4.60}$$

where $\mathcal{Q}_{\mathbf{b}^T\varpi}^{-1}$ is the quantile of $\mathbf{b}^T\varpi$ with the violation probability 1-κ.

The cumulative distribution function (CDF) of $\mathbf{b}^T\varpi$ equals to a weighted sum of the CDFs of standard Gaussian distributions, shown as

$$\mathcal{Q}_{\mathbf{b}^T\varpi}(y)=\sum_{c=1}^{C}\pi_c\mathcal{Q}_{\phi}\left(\frac{y-\mathbf{b}^T\mu_c}{\sqrt{\mathbf{b}^T\varphi_c\mathbf{b}}}\right) \tag{4.61}$$

where $\mathcal{Q}_{\phi}$ is the CDF of standard Gaussian distribution. Based on DPGMM, a quantile $\mathcal{Q}_{\mathbf{b}^T\varpi}^{-1}$ can be obtained.

4.4.3 Solution Algorithm

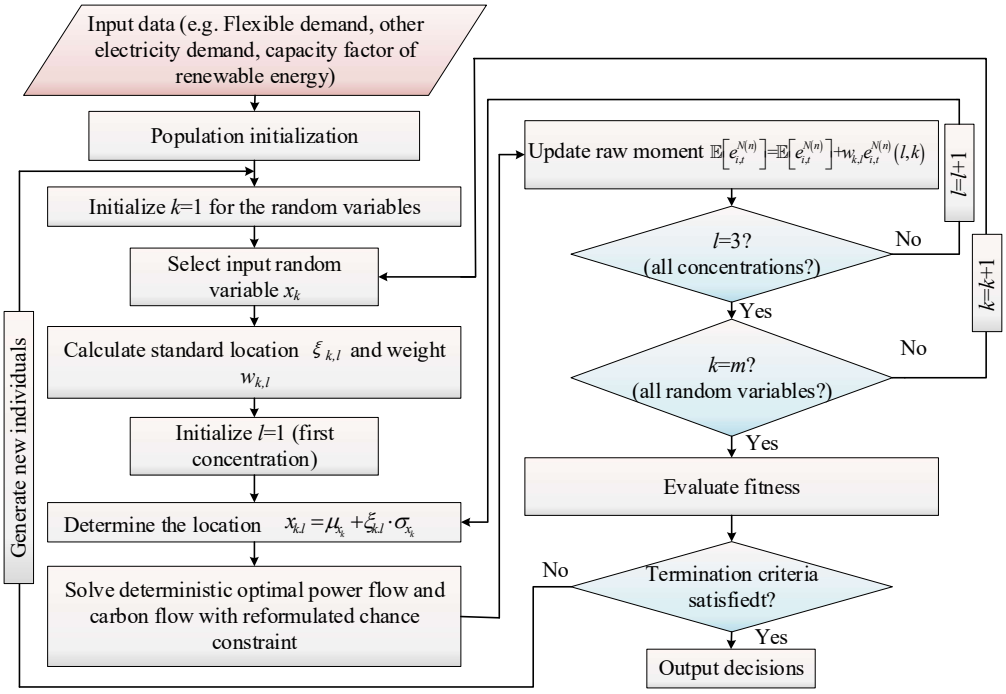

Fig. 4-3. Flowchart of the algorithm to solve the optimization problem.

The difficulty in solving the proposed mathematical model (4.23)-(4.35) is that it has two special constraints, i.e., and. The expectation in (4.34) can be solved by the point estimation method based on PCEF introduced in (4.14)-(4.22). The chance constraint (4.35) is reformulated as an ordinary constraint according to (4.53)-(4.61). Then, a hybrid mathematical and heuristic algorithm is developed to solve the formulated problem, as shown in Fig. 4-3. First, the initial population for the planning decision is generated. Then, the values of the random variables are determined based on the point estimation method. After fixing the values of the random variables, the probabilistic optimal model is converted to a deterministic model. The deterministic model will be solved for 3 times for each random variable. The solving of the deterministic model (power flow is linearized) is realized based on MILP. After the operation of the network is solved at the given population, the fitness of the population will be evaluated. Finally, the population will be updated according to the evolutionary algorithm (EA) until the termination criteria are satisfied.

4.5 Case Study

The proposed carbon footprint management strategy is verified on the IEEE 39-bus benchmark system. The network typology, generation capacity, and the candidate buses for the renewable energy plants are provided in Fig. 4-4. The time-series network information, such as renewable energy output and load, is obtained from [323].

The simulations were completed by a PC with an Intel Core (TM) i7-9750 CPU @ 2.60 GHz with 16.00 GB RAM.

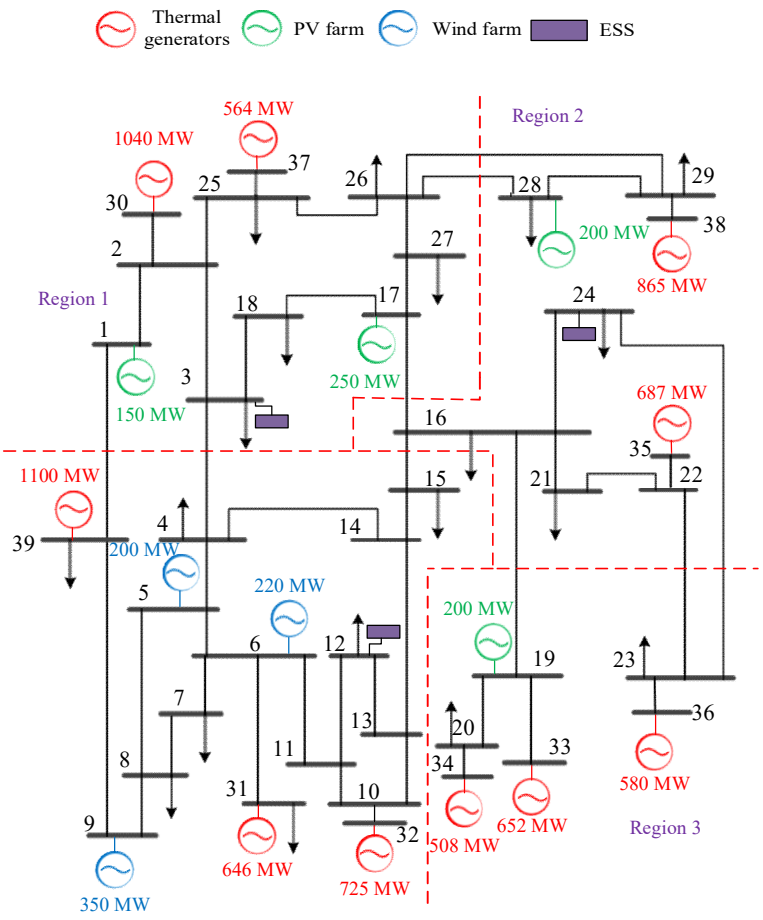

Fig. 4-4. IEEE 39-bus tested system.

4.5.1 Distribution Construction of Uncertainties and PCEF Model

The PDF construction performance of different fitting models for different uncertainties at 12:00, including wind generation on bus 5, solar generation on bus 19, load (apart from flexible load) on bus 18, and flexible load on bus 18, are demonstrated in Figs. 4-5 to 4-8, respectively.

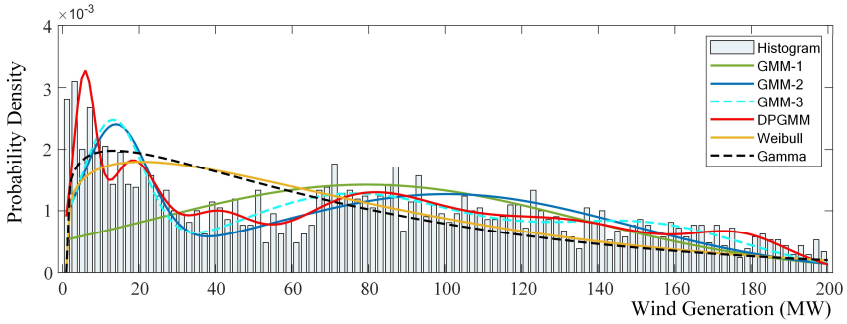

Fig. 4-5. PDF of the wind generation on bus 5 based on different probabilistic models.

For wind generation, usually, the wind speed is usually modeled by Weibull distribution. However, from Fig. 4-5, it can be concluded that the stochastic characteristics of wind generation are too complicated to be captured by Weibull as well as Gamma and Gaussian model (GMM-1) distributions. The Gaussian mixture model with 2 and 3 components

(GMM-2 and GMM-3) can fit the distribution relatively well. However, compared with DPGMM, which does not require the predetermination of the number of components, the fitting of GMM-2 and GMM-3 is still not detailed enough.

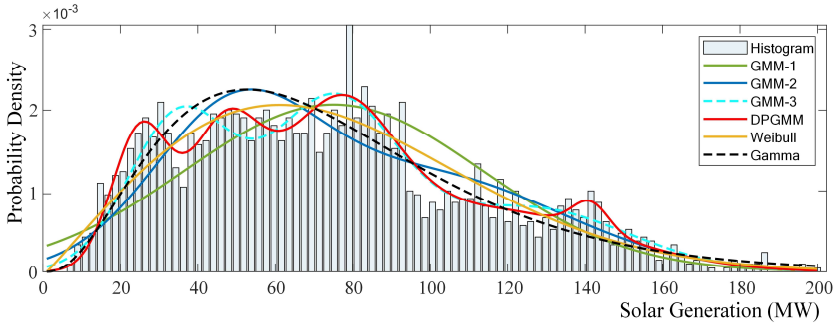

Fig. 4-6. PDF of the solar generation on bus 19 based on different probabilistic models.

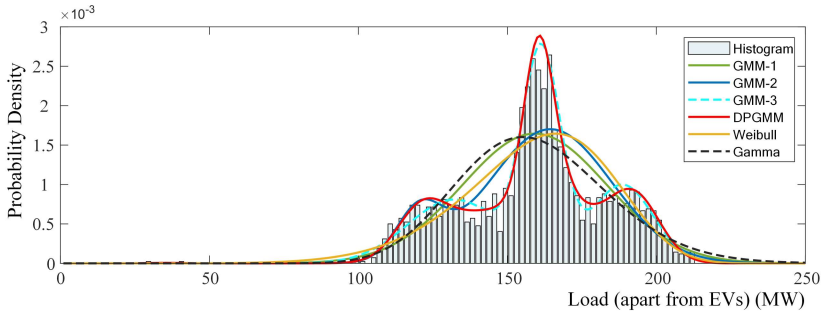

Fig. 4-7. PDF of the load on bus 18 based on different probabilistic models.

For the solar generation and load (apart from flexible load), it can be seen that both GMM-3 and DPGMM have relatively good performance. However, for solar generation, GMM-3 misses some peaks.

The histograms of flexible loads are created partially based on the NILM result, which are used as references for PDF construction. A similar conclusion can be obtained that DPGMM shows superior performance to the other models.

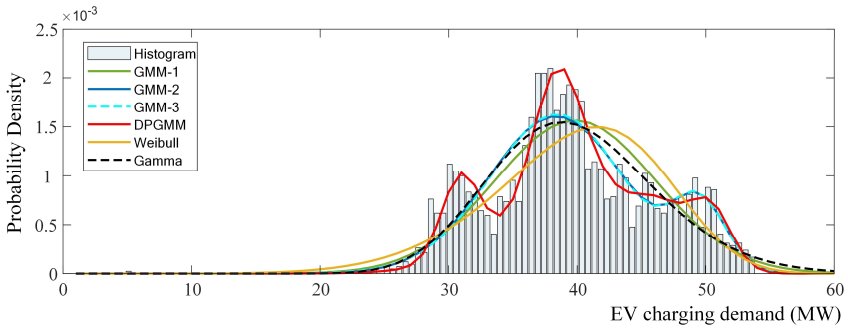

Fig. 4-8. PDF of the flexible load on bus 18 based on different probabilistic models.

The PCEF model based on the two-point estimate method (2PEM) is compared with the Monte Carlo simulation (MCS). The PDF of the carbon intensity at bus 18 is depicted in Fig. 4-9. Over 20000 MCS samples are needed for the result convergence, which is a significant computation burden. However, from Fig. 4-9, it can be seen that the PCEF model based on 2PEM can provide satisfactory estimation (acceptable accuracy) with more computational efficiency.

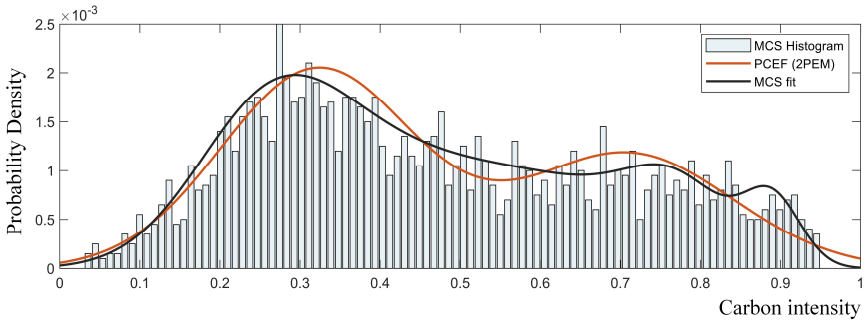

Fig. 4-9. PDF of the carbon intensity at bus 18 based on MCS and 2PEM.

The PDF of the total indirect emissions is depicted in Fig. 4-10. Also, it can be seen that the 2PEM can achieve a close result to MCS. The expected indirect emissions based on 2PEM can be calculated as 22.088 million tons, while the indirect emissions based on MCS can be calculated as 22.091 million tons. From Table 4-1, the errors of the carbon intensity for the mean and deviation between MCS and 2PEM are only 2.25% and 1.19%, respectively. The errors of the total emissions for the mean and deviation between MCS and 2PEM are only 0.0135% and 0.0239%, respectively. However, the computation efficiency of 2PEM is improved to a large extent.

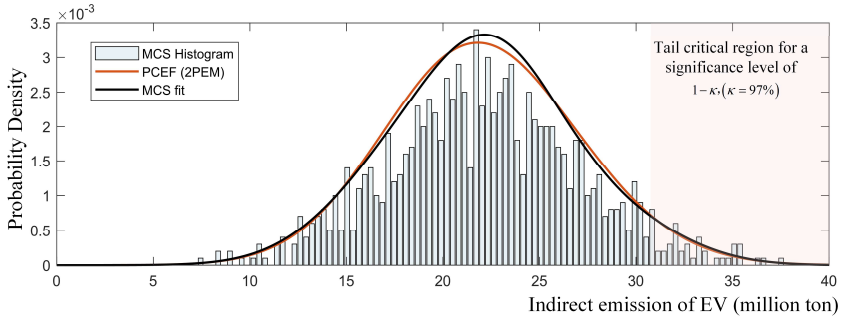

Fig. 4-10. PDF of the indirect emissions of flexible load based on MCS and 2PEM.

TABLE 4-1. PERFORMANCE COMPARISON BETWEEN MCS AND 2PEM

		Computation time	Mean	Standard deviation
MCS	Carbon intensity	1341.3 second	0.267	0.0505
	Total emissions		22.091	25.143
2PEM	Carbon intensity	3456.8 second	0.273	0.0511
	Total emissions		22.088	25.137

4.5.2 Comparision of Different Emission Control Strategies

To further display the superiority of the proposed method, five cases are established.

Case 0: Without carbon emission obligation.

Case 1: The emission quota mechanism is applied to thermal generators, but no demand-side carbon emission obligation is considered.

Case 2: The emission quota mechanism is applied to thermal generators. The carbon-integrated electricity price is formulated.

Case 3: The carbon footprint management strategy based on the DCEF model is applied.

Case 4: The proposed carbon footprint management strategy based on the PCEF model is applied.

The indirect emissions from the loads in different cases are displayed in Fig. 4-11. In Case 0, the emission control is not considered, which obviously has the largest emissions. In Case 1, the emissions of the thermal generators are limited by quotas, and more renewable energy is integrated. Therefore, it can be verified that running on low-carbon electricity is very necessary. In Case 2, the carbon-integrated electricity price is applied, which means flexible loads will respond to the carbon signals. Therefore, consumers tend to consume electricity from renewable energy to achieve lower indirect carbon emissions. In Cases 3 and 4, the carbon footprint management strategy is applied. Comparing the DCEF with the PCEF model, the result is very close, but the PCEF model can realize a precise emission control to achieve the lowest indirect emissions through uncertainty modeling.

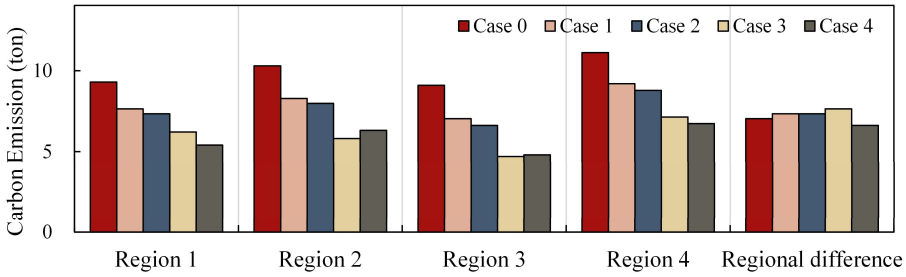

Fig. 4-11. Indirect carbon emissions of flexible load in different cases.

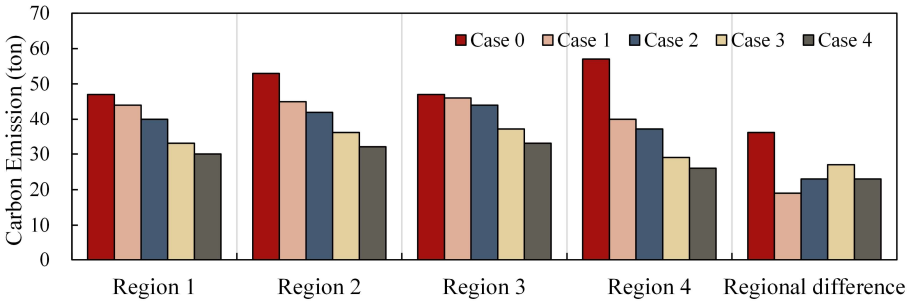

Fig. 4-12. Direct carbon emissions of the generators in different cases.

The direct emissions from the supply side in different cases are displayed in Fig. 4-12. It can be concluded that the proposed method that realizes the indirect emission control from the demand side can also significantly promote the direct emission reduction from the supply side.

The carbon intensity of bus 18 of a day is provided in Fig. 4-13. It can be found that the proposed method remarkably reduces the nodal carbon intensity of the selected bus. During noon, solar generation is sufficient, which results in lower carbon intensity. Hence, the carbon intensity implies the renewable energy penetration level, and the energy system configuration and the power generation mix can facilitate emission reduction. Fig. 4-14 shows the carbon intensity of the ESS located on bus 3. It can be found that the carbon intensity of the ESS in Cases 3 and 4 are lower than that in the

other cases. It indicates that ESS absorbs more renewable energy. In other words, ESS can better function in smoothing the fluctuation of renewable energy output.

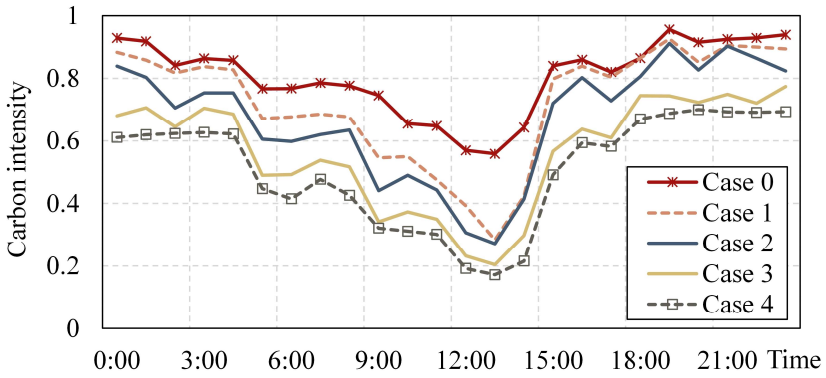

Fig. 4-13. Nodal carbon intensity of bus 18 within a day.

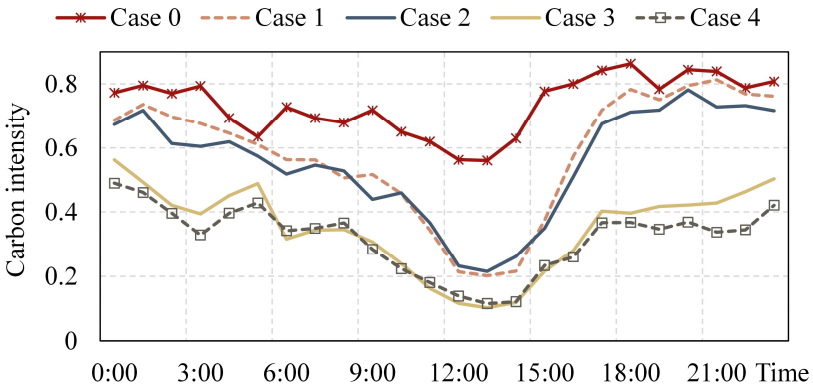

Fig. 4-14. Carbon intensity of the ESS on bus 3 within a day.

Apart from the operation strategy of electricity networks, we further combine the transmission planning strategy formulated in chapter 3 with the proposed emission control strategy. The quantitative results of the five cases are provided in Table 4-2. It can be concluded that Case 4 has the highest annual cost due to the investment in renewable energy plants. However, the proposed method brings huge environmental benefits measured by direct and indirect emissions. Besides, Case 4 achieves the highest emission reduction rate measured in ton/$. In other words, less cost is paid to achieve per ton of emission reduction through tracking the carbon footprint of consumers.

TABLE 4-2. COMPARISON BETWEEN DIFFERENT EMISSION CONTROL STRATEGIES

	Case 0	Case 1	Case 2	Case 3	Case 4
Wind capacity (MW)	770	1123	1255	2031	2335
Solar capacity (MW)	600	851	983	1100	1324
Cost (billion $)	1.33	2.33	2.51	3.01	3.13
Direct emissions (million tons)	204.12	175.34	163.65	135.11	121.25
Indirect emissions of flexible load (million tons)	39.83	32.14	26.78	15.83	15.29
Emission reduction rate (ton/$)	-	0.029	0.034	0.041	0.046

4.6 Chapter Summary

Carbon financing policies such as emission trading have been used to assist in emission mitigation worldwide. As energy end-users are the underlying driver of emissions, it would be difficult to effectively mitigate carbon emissions without active end-users' involvement. In this chapter, a carbon footprint management strategy is proposed. First, a PCEF is proposed to track the carbon footprint based on 2PEM, considering various uncertainties, including wind generation, solar generation, normal load, and flexible load. The probability distribution of the uncertainties is solved based on DPGMM. Based on these models, a stochastic chance-constrained carbon footprint management model is proposed to address the carbon obligation allocation of consumers from the perspective of consumption and provide a technical basis for demand-driven stimulation to reduce carbon emissions. Finally, a solution methodology is proposed to solve the formulated problem. The feasibility and effectiveness of the proposed method are verified in case studies. Compared with MCS, the proposed PCEF model is accurate and efficient. Compared with the other emission control strategies, the proposed method achieves the highest emission reduction rate indicating that less cost is paid to achieve per ton of emission reduction through tracking the carbon footprint.

CHAPTER 5

CARBON EMISSION RIGHT AND RENEWABLE ENERGY CERTIFICATES TRADING

Carbon emission is one of the major reasons that cause global warming. To control carbon emissions, the allowance of GHG emissions of conventional thermal generators is restricted. The emission trading system (ETS) has been operated in many countries, such as the United States, Japan, Canada, and the EU. As a result, renewable power plants have seen a marked increase over the past decades. To support the prior dispatch of renewable energy, renewable energy certificates (RECs) are designed. Currently, the main buyers of RECs are electricity consumers. The buyers cannot obtain direct economic income from the RECs. Hence, how to increase the purchase incentive of RECs needs to be investigated. ETS and RECs are two methods used to control GHG emissions. However, these two mechanisms are independent. In the future, the methods to drive the parallel operation of these two mechanisms and how they interact with each other should be comprehensively investigated. Furthermore, under the background of carbon pricing policies, the cooperation of renewable energy plants and emerging storage technology, such as P2G, should be considered. In this chapter, a bi-level optimization model based on the game approach between thermal generators, renewable energy plants, and P2GSes is proposed to investigate ETS and RECs.

5.1 Market Mechanism and Trading Framework

5.1.1 Carbon Emission Quota

To control the emissions produced by the primary energy consumption, such as coal, quotas are allocated to each thermal generator to restrict its annual carbon emissions. Some generators can finish the task, and they can sell surplus quotas, while other generators cannot fulfill the mission, and they must buy extra quotas. Thus, carbon trading emerges. The carbon market is a pool, and everyone can sell or buy quotas to or from the pool. In most of the previous works, there is a default assumption that the pool is infinitely large so that the thermal generators can buy as many quotas as they want. However, the marginal cost of coal-fired generators is very low, and they tend not to care about the carbon emission tax, so they buy massive quotas to ensure the output. This phenomenon betrays the original establish intention of ETS. In the current application, an empty carbon pool is difficult to reach, and that is the reason why an infinitely large carbon pool is assumed to default in the literature. However, according to the experience of the Europe Union's

Emissions Trading Scheme (EU ETS), *the relative scarcity of emission permits in a cap and trade system must be maintained* [324]. In other words, the amount of free quota allocated to the firms should be restricted in the future. Therefore, the demand for the quota will exceed the supply, which may result in an empty carbon pool. In this chapter, we specify that the thermal generators cannot purchase quota from an empty carbon pool in order to prevent them from purchasing quota aggressively.

5.1.2 Renewable Energy Certificates

Other than the restriction on the outputs of non-renewable plants, encouraging the output of renewable energy is another perspective to reduce the system emissions. RECs, also known as green certificates and green tags, are predominantly used in Europe first but now becoming more widespread globally. It is used to prove that certain electricity is generated using renewable energy sources. One certificate indicates one Megawatt hour of electricity from renewable energy. It is a tradable commodity whose sellers are renewable generators. Originally, its buyers were electricity consumers. In fact, after the electricity on-grid, it is impossible to separate renewable energy from conventionally generated energy. It means that buyers cannot decide to consume what kinds of energy but pay extra money to support the output of renewable energy and take social responsibility. Then the buyer does not obtain any direct profits from purchasing RECs. Lack of purchasing motivation is the reason why the subscription rate of RECs is not high in some countries, such as Australia.

Currently, there is no close relationship between RECs and carbon trading. Although the two mechanisms seem to have different policy backgrounds at present, they are actually inextricably linked. In this chapter, we study the correlation between RECs and carbon emission quotas. When thermal generators purchase the RECs, it indicates that the specific amount of electricity from renewable energy is dispatched in priority. When the total demand of the electricity market is fixed, every increase of renewable energy to the grid means reducing the emission of per unit primary energy consumption. In other words, the total output from the thermal generators will be decreased when the thermal generators purchase RECs. Therefore, the thermal generators can purchase the RECs and convert them to quotas. The purchasing motivation for RECs is increased. In many countries, the RECs mechanism is still in the test stage, and the market is not fully open. However, in the future, when the REC market is well-developed, the price of RECs will be fully dependent on market trading rather than government formulation. In this chapter, the price of the RECs is modeled according to the market supply and demand. Different from carbon trading, which has a carbon pool, in RECs trading, the producers and consumers must match.

5.1.3 Proposed framework

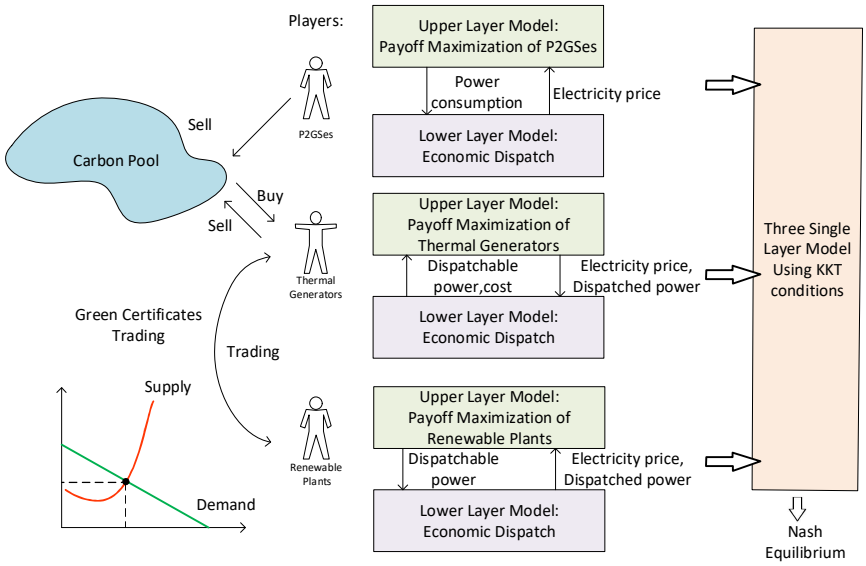

Fig. 5-1. Proposed framework of CER and REC trading.

In the proposed model, game theory is utilized to help each player in making decisions. There are three kinds of players, i.e., P2GSes, renewable energy plants, and thermal generators. Each player will maximize their payoffs, which can be solved by a bi-level model, as shown in Fig. 5-1. For all the players, the upper-level objective is to maximize their payoffs, while the lower level is the economic dispatch (ED) of the system. For the payoff model, P2GSes will sell carbon quotas, and thermal generators will either sell or buy quotas. The RECs trading will happen between each pair of thermal generators and renewable plants. These three bi-level models will be transformed into three single-layer models by using KKT conditions. Nash equilibrium will be found in which the optimal strategy is for all players.

5.2 Game-theoretic Trading Model

In many references, such as ref. [173], the market is assumed to be perfectly competitive. However, in real life, most markets are oligopoly markets. In this chapter, the number of PV farms, wind farms, P2GSes, and large-scale thermal generators is limited, and they are owned by several big firms. Each firm expects its maximum profits by considering its rivals' strategies. Thus, the game theory model is built to help decision making.

5.2.1 Noncooperative Game model

In this chapter, there are three kinds of players: P2GSes, renewable generators, and thermal generators. They have strategies marked as ：

- Players: $\mathcal{P}$, $\mathcal{R}$, $\mathcal{T}$;
- Strategies: $\mathcal{S}_{\mathcal{P}}$, $\mathcal{S}_{\mathcal{R}}$, $\mathcal{S}_{\mathcal{T}}$;

In the game theory model, the players expect to find a Nash equilibrium (if it exists). It is the optimal outcome of the

game. According to ref. [325], the Nash equilibrium must satisfy:

$$\mathcal{S}_{\mathcal{P}}^{*}=\arg\max_{\mathcal{S}_{\mathcal{P}}} F^{P2G}\left(\mathcal{S}_{\mathcal{P}},\mathcal{S}_{\mathcal{R}}^{*},\mathcal{S}_{\mathcal{T}}^{*}\right) \tag{5.1}$$

$$\mathcal{S}_{\mathcal{R}}^{*}=\arg\max_{\mathcal{S}_{\mathcal{R}}} F^{R}\left(\mathcal{S}_{\mathcal{P}}^{*},\mathcal{S}_{\mathcal{R}},\mathcal{S}_{\mathcal{T}}^{*}\right) \tag{5.2}$$

$$\mathcal{S}_{\mathcal{T}}^{*}=\arg\max_{\mathcal{S}_{\mathcal{T}}} F^{G}\left(\mathcal{S}_{\mathcal{P}}^{*},\mathcal{S}_{\mathcal{R}}^{*},\mathcal{S}_{\mathcal{T}}\right) \tag{5.3}$$

where $\mathcal{S}_{\mathcal{P}}^{*},\mathcal{S}_{\mathcal{R}}^{*}$ and $\mathcal{S}_{\mathcal{T}}^{*}$ are the strategies at Nash equilibrium for each player. F^{P2G}, F^{R} and F^{G} are the payoffs for them.

In the Nash equilibrium, each player believes that regardless of how the other players change the strategy, his/her strategy is the best choice indicating that *no player can do better by unilaterally changing his or her strategy*.

5.2.2 Cooperative Game model

In most situations, the profits gained by a noncooperative game will be less than a cooperative game. One player may cooperate with the other players to maximize their total coalition value and then allocate their profits. In this chapter, renewable power plants and P2GSes are assumed to cooperate.

- Coalition: $\{\mathcal{P},\mathcal{R}\}$, $\{\mathcal{T}\}$;
- Strategy: $\{\mathcal{S}_{\mathcal{P}},\mathcal{S}_{\mathcal{R}}\},\{\mathcal{S}_{\mathcal{T}}\}$;

Thus, the first coalition contains renewable power plants and P2GSes, while the second coalition contains thermal power plants. Whether this coalitional game is cohesive will be verified in the case studies. A coalitional game is cohesive if $\nu(\Gamma)\geq\sum_{\kappa=1}^{K}\nu(\tau_{\kappa})$ for every partition $\{\tau_1,...,\tau_K\}$ of Γ, where Γ is a finite set of players; ν is the worth function of Γ, i.e., payoff function; τ is the sub-set of Γ.

Currently, in some countries, such as China and Australia, the energy transition is still developing, and conventional coal-fired generators are still in a dominant position. If renewable energy firms and P2GSes compete independently, they may lose their advantages. Therefore, it is assumed that such a coalition $\{\mathcal{P},\mathcal{R}\}$ is the core, indicating that *the coalition outcome is stable because no deviation is preferable* [326]. Then, Nash Equilibrium can be searched according to (5.4)-(5.5).

$$\left(\mathcal{S}_{\mathcal{P}}^{*},\mathcal{S}_{\mathcal{R}}^{*}\right)=\arg\max_{\mathcal{S}_{\mathcal{P}},\mathcal{S}_{\mathcal{R}}} F^{P2G,R}\left(\mathcal{S}_{\mathcal{P}},\mathcal{S}_{\mathcal{R}},\mathcal{S}_{\mathcal{T}}^{*}\right) \tag{5.4}$$

$$\mathcal{S}_{\mathcal{T}}^{*}=\arg\max_{\mathcal{S}_{\mathcal{T}}} F^{G}\left(\mathcal{S}_{\mathcal{P}}^{*},\mathcal{S}_{\mathcal{R}}^{*},\mathcal{S}_{\mathcal{T}}\right) \tag{5.5}$$

The joint payoff of P2GSes and renewable energy plants is derived in section V, which is the sum of (5.22) and

(5.27). As for the division of payoff among the members of the group, there are no specific restrictions. In this chapter, the payoffs are divided in a bargaining way: $\max \prod_{\kappa=1}^{K}\left(\nu(\tau_\kappa)^* - \nu(\tau_\kappa)\right)$, where $\nu(\tau_\kappa)^*$ is the allocated payoff with cooperation; $\nu(\tau_\kappa)$ is the payoff without cooperation.

5.2.3 Nash equilibrium Solving Process

In the game model, the problem is not a single optimization problem but a multi-distribution optimization problem. An iterative search procedure is utilized to find out the Nash equilibrium in this chapter.

Step 1: Initialize the Nash equilibrium, which is the initial strategies of the players choosing from the strategies set randomly $\left(\mathcal{S}_\mathcal{P}^0, \mathcal{S}_\mathcal{R}^0, \mathcal{S}_\mathcal{T}^0\right)$.

Step 2: Each player or coalition makes decisions in turns based on the rivals' strategies in the previous turn, shown as:

$$\left(\mathcal{S}_\mathcal{P}^i, \mathcal{S}_\mathcal{R}^i\right) = \arg\max_{\mathcal{S}_\mathcal{P}, \mathcal{S}_\mathcal{R}} F^{P2G,R}\left(\mathcal{S}_\mathcal{P}, \mathcal{S}_\mathcal{R}, \mathcal{S}_\mathcal{T}^{i-1}\right) \tag{5.6}$$

$$\mathcal{S}_\mathcal{T}^i = \arg\max_{\mathcal{S}_\mathcal{T}} F^G\left(\mathcal{S}_\mathcal{P}^{i-1}, \mathcal{S}_\mathcal{R}^{i-1}, \mathcal{S}_\mathcal{T}\right) \tag{5.7}$$

where i indicating the sequence of turns.

Step 3: Check whether the strategy is the Nash equilibrium. Nash equilibrium is found when no players change their strategy, shown as:

$$\left(\mathcal{S}_\mathcal{P}^i, \mathcal{S}_\mathcal{R}^i, \mathcal{S}_\mathcal{T}^i\right) = \left(\mathcal{S}_\mathcal{P}^{i-1}, \mathcal{S}_\mathcal{R}^{i-1}, \mathcal{S}_\mathcal{T}^{i-1}\right) = \left(\mathcal{S}_\mathcal{P}^*, \mathcal{S}_\mathcal{R}^*, \mathcal{S}_\mathcal{T}^*\right) \tag{5.8}$$

Step 4： Repeat step 2 and step 3. Stop iteration when Nash equilibrium is found. The Nash equilibrium is the final strategy for all players.

5.3 Renewable Energy Certificate Pricing Model

5.3.1 Kinked Demand Curve

The price modeling of RECs can be solved through the demand-supply curve. The producers of the RECs are the renewable energy plants, while the consumers are the thermal generators. According to ref. [327], in the oligopoly market, the demand curve (D/AR) is a kinked curve shown in Fig. 5-2. Along the kinked curve, the elasticity of the demand is different. When the firm raises its price above P_o, the other rivals will not follow, so the firm will lose the market share, and a large substitution effect is expected. As a result, the demand curve above P_o will be relatively elastic. When the firm reduces its price, demand will be inelastic because its rivals will follow. In the oligopoly price model,

there is no price competition. The firm aims at reaching the maximum total profits, which can be gained when the first-order derivative of the total profits equals zero, expressed as:

$$\pi' = TR' - TC' = MR - MC = 0 \tag{5.9}$$

where π is total profit; TR is total revenue; TC is total costs; MR is marginal revenue; MC is marginal cost.

When marginal cost equals marginal revenue, the profits can be maximized. The marginal cost curve (MC) is the supply curve (S) shown in Fig. 5-2. Total revenues can be expressed as:

$$TR = P \cdot Q \tag{5.10}$$

where P is the selling price; Q is the quantity.

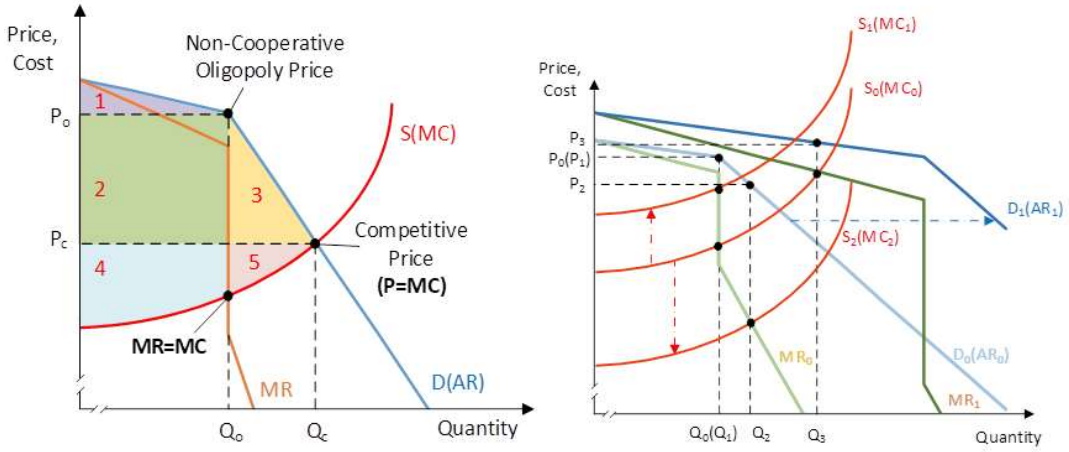

Fig. 5-2. Kinked demand curve.

We assume the demand curve (average revenue curve) is:

$$P = aQ + b \tag{5.11}$$

So, we can get:

$$TR = P \cdot Q = aQ^2 + bQ \tag{5.12}$$

$$MR = TR' = 2aQ + b \tag{5.13}$$

Hence, the marginal revenue curve (MR) always has the same intercept and twice the slope as the demand curve (D), as shown in Fig. 5-2. Then the intersection of the marginal revenue curve and marginal cost curve can specify the quantity Q_o. When quantity equals Q_o, the price can be figured out as P_o through the demand curve. In this situation, the consumer surplus is area 1, while the producer surplus is area 2 plus 4. However, in the competitive market, the price can be found out at the intersection of the demand curve and supply curve at P_c. In this situation, the consumer surplus is areas 1, 2, and 3, while the producer surplus is areas 4 and 5. Compared with oligopoly and competitive markets, the producer surplus is larger in the oligopoly market. However, from the social welfare, the oligopoly market loses areas 3 and 5, known as the deadweight loss.

5.3.2 The shift of the Supply and Demand Curve

At present, the REC price is formulated by the government, and the price of the RECs of PVs is higher than that of wind because they have different investment costs. This causes the market tilting to wind RECs. However, when the REC market opens in the future, the RECs price can be unified. As seen in Fig. 5-2, when the demand curve is fixed as D_0, and the supply curve is S_0, the market price is P_0. When the cost increases or decreases in a small range, the market price will not change. For example, when the cost increases, the supply curve will shift up vertically to S_1. At this time, the market price can be modeled as P_1, which is the same as P_0. Quantitatively, the demand curve and marginal revenue curve can be expressed as:

$$P=\begin{cases} aQ+b, Q<Q_0 \\ cQ+d, Q\geq Q_0 \end{cases} \qquad MR=\begin{cases} 2aQ+b, Q<Q_0 \\ 2cQ+d, Q\geq Q_0 \end{cases} \tag{5.14}$$

The supply curve can be expressed as: $P=\alpha Q^2+\beta Q+\gamma$.

When $\alpha Q_o^{\,2}+\beta Q_o+\gamma<2aQ_o+b$ and $\alpha Q_o^{\,2}+\beta Q_o+\gamma>2cQ_o+d$, the price can be modeled as follows:

$$P_o=aQ_o+b=cQ_o+d \tag{5.15}$$

Only when the cost change greatly, for example, decreasing to S_2, the market price will change. To be quantitative, when $\alpha Q_o^{\,2}+\beta Q_o+\gamma<2cQ_o+d$, the intersection of the supply curve and marginal revenue curve can be solved as follows:

$$\alpha Q^2+\beta Q+\gamma=2cQ+d \tag{5.16}$$

$$Q=\frac{2c-\beta+\sqrt{(2c-\beta)^2-4\alpha(\gamma-d)}}{2\alpha} \tag{5.17}$$

Price can be modeled as：

$$c\times\frac{2c-\beta+\sqrt{(2c-\beta)^2-4\alpha(\gamma-d)}}{2\alpha}+d \tag{5.18}$$

In the same way, when $\alpha Q_o^{\,2}+\beta Q_o+\gamma>2aQ_o+b$, the price can be modeled as $a\times\frac{2a-\beta+\sqrt{(2a-\beta)^2-4\alpha(\gamma-b)}}{2\alpha}+b$.

There is a problem when we combine the emission quota mechanism with the REC mechanism. When the RECs price is lower than the carbon price, some speculative market participants may purchase massive RECs and then sell them as emission quotas. This is not the objective of our design. But if the RECs are marketized, the problem can be

avoided in our model. This time we fix the supply curve as S_0, and when the demand increases dramatically, the demand curve will shift right from D_0 to D_1. The market price will increase from P_0 to P_3. When the market price exceeds the carbon price, there are no benefits for this speculation. The demand and price will reduce to a normal value finally. To be quantitative, the demand curve and marginal revenue curve are shifted to:

$$P=\begin{cases} a(Q+m)+b=aQ+am+b, Q<Q_0 \\ c(Q+m)+d=cQ+cm+d\ , Q\geq Q_0 \end{cases} \tag{5.19}$$

$$MR=\begin{cases} 2aQ+am+b, Q<Q_0 \\ 2cQ+cm+d\ , Q\geq Q_0 \end{cases} \tag{5.20}$$

The price can be modeled as:

$$a\times\frac{2a-\beta+\sqrt{(2a-\beta)^2-4\alpha(\gamma-b)}}{2\alpha}-am+b \tag{5.21}$$

5.4 Carbon Quotas and Renewable Energy Certificate Trading Formulation

In this section, the methodology that is utilized to find out the optimal strategies for three different players is proposed. For each player, the profits are maximized through a bi-level model considering the rivals' strategies. Because of the large penetration of renewable energy, a stochastic model is considered. The probabilistic optimal power flow (POPF) is established to capture the uncertainties involved with renewable energy resources (i.e., wind speed and solar irradiation) and load[100].

5.4.1 Upper-Level Model for Payoffs of Each Player

1) P2GSes

The payoffs of P2GSes include the revenues of selling gas and carbon environment profits minus the costs of purchasing electricity shown as:

$$MAX.F^{P2G}=\sum_{t}^{T}\sum_{p\in\Omega^P}\left(\lambda_{p,t}^{gas}P_{p,t}^{P2G,sg}-\pi^C P_{p,t}^{P2G,pur}+\lambda_t^{CAR}\left(\alpha^{P2G}P_{p,t}^{P2G,pur}\right)\right) \tag{5.22}$$

where Ω^P is the set of P2GSes; $\lambda_{p,t}^{gas}$ is the local marginal price of natural gas; $P_{p,t}^{P2G,sg}$ is the amount of gas sold by P2GSes; π^C is the electricity market clearing price; $P_{p,t}^{P2G,pur}$ is the amount of electricity purchased by P2GSes; λ_t^{CAR} is the carbon price; α^{P2G} is the carbon emission reduction factor of P2GSes.

s.t.

$$E_{p,t+1}^{P2G}=E_{p,t}^{P2G}+P_{p,t}^{P2G,pur}\eta^{c}-P_{p,t}^{P2G,sg},\forall p\in\Omega^{P} \tag{5.23}$$

$$0\le P_{p,t}^{P2G,pur}\le\overline{P_{p}^{P2G,rate}},\forall p\in\Omega^{P} \tag{5.24}$$

$$0\le P_{p,t}^{P2G,sg}\le\overline{P_{p}^{P2G,SG}},\forall p\in\Omega^{P} \tag{5.25}$$

$$0\le E_{p,t}^{P2G}\le\overline{E_{p}},\forall p\in\Omega^{P} \tag{5.26}$$

where $E_{p,t}^{P2G}$ is the storage state of P2GSes; η^{c} is the charging efficiency of P2GSes; $\overline{P_{p}^{P2G,rate}}$ is the rated working power of P2GSes; $\overline{E_{p}}$ is the maximum energy storage of P2GSes.

Equation (5.23) is the energy balance of the storage of P2GSes. Equations (5.24) and (5.25) are the boundary limits of the amount of purchased electricity and sold gas within a unit of time. Equation (5.26) is the storage limitation.

2) Renewable Plants

The payoffs of the renewable plants have two parts: revenues from selling electricity and revenues from RECs, as shown in (5.27). The energy sold by renewable plants can be classified into three parts: being subscribed by consumers, being subscribed by thermal generators, and having not been subscribed.

$$MAX.F^{R}=\sum_{t}^{T}\sum_{i\in\Omega^{I}}\left(\underbrace{\lambda_{i,t}^{LMP}\left(P_{i,t}^{R,NGC}+\sum_{g\in\Omega^{G}}P_{ig,t}^{R,GC}+\sum_{j\in\Omega^{J}}P_{ij,t}^{R,GC-}\right)}_{Revenue\ \ from\ \ Selling\ \ Electricity}+\underbrace{\lambda_{t}^{GC}\left(\sum_{g\in\Omega^{G}}P_{ig,t}^{R,GC}+\sum_{j\in\Omega^{J}}P_{ij,t}^{R,GC-}\right)}_{Revenue\ \ from\ \ Renewable\ \ Energy\ \ Certificates}\right) \tag{5.27}$$

where Ω^{I} is the set of renewable plants; $\lambda_{i,t}^{LMP}$ is the local marginal price of electricity; $P_{i,t}^{R,NGC}$ is the output of renewable plants which is not subscribed as RECs; $P_{ig,t}^{R,GC}$ is the energy with RECs that is sold; $P_{ij,t}^{R,GC-}$ is the output of renewable plants which is subscribed by consumers; λ_{t}^{GC} is the RECs price.

s.t.

$$P_{i,t}^{R,NGC}+\sum_{g\in\Omega^{G}}P_{ig,t}^{R,GC}+\sum_{j\in\Omega^{J}}P_{ij,t}^{R,GC-}=P_{i,t}^{PV}+P_{i,t}^{W},\forall i\in\Omega^{I} \tag{5.28}$$

$$P_{i,t}^{R,NGC}+\sum_{g\in\Omega^{G}}P_{ig,t}^{R,GC}+\sum_{j\in\Omega^{J}}P_{ij,t}^{R,GC-}\le\overline{P_{i,t}^{PV}}+\overline{P_{i,t}^{W}},\forall i\in\Omega^{I} \tag{5.29}$$

$$P_{ig,t}^{R,GC}\le P_{gi,t}^{G,GC},\ \ \forall i\in\Omega^{I}\ \ \forall g\in\Omega^{G} \tag{5.30}$$

where $P_{i,t}^{PV}$ and $P_{i,t}^{W}$ are the actual output of PVs and wind generators; $\overline{P_{i,t}^{PV}}$ and $\overline{P_{i,t}^{W}}$ are the maximum dispatchable energy of PVs and wind generators; $P_{ig,t}^{R,GC}$ is the output of renewable plants which is subscribed by thermal generators.

Equation (5.28) means that renewable plants consist of PVs and wind generations. Equation (5.29) means that the

on-grid energy of PVs and wind generation cannot exceed the total dispatchable energy. So, it means that solar and wind discards may exist. Equation (5.30) means that the RECs sold by renewable plants will not be larger than the number of RECs that thermal generators need.

3) Thermal Generators

The payoffs of the thermal generators equal the revenue of selling electricity minus the costs of purchasing RECs and then minus the costs of purchasing carbon emission quotas.

$$MAX.F^{G} = \sum_{t=1}^{T}\sum_{g\in\Omega^{G}}\left(\lambda_{i,t}^{LMP}P_{g,t}^{G}\right) - \lambda_{t}^{GC}\left(\sum_{g\in\Omega^{G}}\sum_{t=1}^{T}\sum_{i\in\Omega^{I}}P_{gi,t}^{G,GC}\right) - \lambda_{t}^{CAR}\left(\sum_{g\in\Omega^{G}}P_{g}^{QT,pur}\right) \tag{5.31}$$

where Ω^{G} is the set of thermal generators; $P_{g,t}^{G}$ is the output of thermal generators; $P_{gi,t}^{G,GC}$ is the amount of RECs offered by i^{th} renewable plants; $P_{g}^{QT,pur}$ is the carbon quotas brought by thermal generators.

s.t.

$$P_{g}^{QT,pur} = \sum_{t=1}^{T}\left(P_{gt}^{G}e_{g}^{G}\right) - \sum_{t=1}^{T}\sum_{i\in\Omega^{I}}\left(P_{gi,t}^{G,GC}\alpha^{GC}\right) - e^{g} : \chi_{g}, \forall g\in\Omega^{G} \tag{5.32}$$

$$\sum_{g\in\Omega^{G}}P_{g}^{QT,pur} \le \sum_{t}^{T}\sum_{p\in\Omega^{P}}\left(\alpha^{P2G}P_{p,t}^{P2G,pur}\right) + Q^{pool} : \kappa_{g}, \forall g\in\Omega^{G} \tag{5.33}$$

$$\underline{P_{g}^{G}} \le P_{g,t}^{G} \le \overline{P_{g}^{G}} : \phi_{g,t}^{min,G}, \phi_{g,t}^{max,G}, \forall g\in\Omega^{G} \tag{5.34}$$

$$\sum_{t=1}^{T}\sum_{i\in\Omega^{I}}P_{gi,t}^{G,GC} \ge \sum_{t=1}^{T}P_{g,t}^{G}\times ERO R\% : \xi_{g}, \forall g\in\Omega^{G} \tag{5.35}$$

$$P_{gi,t}^{G,GC} \le P_{ig,t}^{R,GC}, \quad \forall i\in\Omega^{I}\ \forall g\in\Omega^{G} \tag{5.36}$$

where e_{g}^{G} is the carbon emission coefficient of thermal generators; α^{GC} is the shift factor from RECs to carbon quotas; CAP_{g} is the carbon quotas of thermal generators; Q^{pool} is the number of quotas in the pool; $\underline{P_{g}^{G}}$ and $\overline{P_{g}^{G}}$ are the minimum and maximum output of thermal generators; $ERO R\%$ is the enforced renewable output rate of thermal generators.

Equation (5.32) expresses the method to calculate the number of quotas that the generators need to purchase (or sell). It equals the total emissions minus the quotas converted from purchased RECs and then minus the allocated quotas. If the value is negative, it means that the generator can sell quotas. Equation (5.33) means that the generators cannot buy quotas anymore when there is no carbon emission quota in the pool. Equation (5.34) is the output limitation of thermal

generators within a unit of time. Equation (5.35) means that according to government policy, the renewable output of thermal generators should be larger than a certain rate of their total output. Equation (5.36) means that the RECs bought by thermal generators will not be larger than the number of RECs that renewable energy plants provide.

5.4.2 Lower Level Model for Economic Dispatch

Economic dispatch (ED) is carried out by the ISO. Through the ED model, market-clearing and optimal dispatch are realized. The bidding of the thermal generators will include the costs of purchasing RECs and carbon emission quotas, which means the emission reduction cost is transferred to the consumers. The ED model can be expressed as:

$$min\sum_{t=1}^{T}\left(\sum_{g\in\Omega^G}(a_g^G P_{g,t}^G)+\lambda_t^{GC}\left(\sum_{g\in\Omega^G}\sum_{t=1}^{T}\sum_{i\in\Omega^I}P_{gi,t}^{G,GC}\right)+\lambda_t^{CAR}\left(\sum_{g\in\Omega^G}P_g^{QT,pur}\right)+\sum_{i\in\Omega^I}(a_i^{PV}P_{i,t}^{PV})+\sum_{i\in\Omega^I}(a_i^W P_{i,t}^W)\right) \quad (5.37)$$

where a_g^G, a_i^{PV} and a_i^W are the bidding price of thermal generators, PVs, and wind generators.

s.t. Equations (5.32) (5.33) (5.34) (5.35)

$$\sum_{g\in\Omega^G}P_{g,t}^G+\sum_{i\in\Omega^I}\left(P_{i,t}^{PV}+P_{i,t}^W\right)-\sum_{p\in\Omega^P}P_{p,t}^{P2G,pur}-\sum_{j\in\Omega^J}P_{j,t}^L=0:\mu_t,\forall t\in(1,T) \quad (5.38)$$

$$\underline{P_l^B}\le\sum_{m\in\Omega}GSF_{l,m}\left(P_{m,t}^G+P_{m,t}^{PV}+P_{m,t}^W-P_{m,t}^{P2G,pur}-P_{m,t}^L\right)\le\overline{P_l^B}:\omega_{l,t}^{min},\omega_{l,t}^{max},\forall t\in(1,T) \quad (5.39)$$

where $P_{j,t}^L$ is the load demand; $GSF_{l,m}$ is the generation shift factor; $\underline{P_l^B}$ and $\overline{P_l^B}$ are the upward and downward limitations of line capacity.

The objective function is to minimize the total system costs. Equation (5.38) is the energy balance of the system. Equation (5.39) is the power flow limitation. The power flow in this chapter is calculated through DC models using *power transfer distribution factors (PTDF).*

To convert the bi-level optimization problem into a single level, the Lagrange function of the problem above needs to be obtained, shown below:

$$
\begin{aligned}
&\sum_{t=1}^{T}\left(\sum_{g\in\Omega^G}(a_g^G P_{g,t}^G)+\sum_{i\in\Omega^I}(a_i^{PV} P_{i,t}^{PV})+\sum_{i\in\Omega^I}(a_i^W P_{i,t}^W)\right)\\
&+\lambda_t^{GC}\left(\sum_{g\in\Omega^G}\sum_{t=1}^{T}\sum_{i\in\Omega^I}P_{gi,t}^{G,GC}\right)+\lambda_t^{CAR}\left(\sum_{g\in\Omega^G}P_g^{QT,pur}\right)\\
&+\sum_{g\in\Omega^G}\begin{pmatrix}
-\chi_g\left(P_g^{QT,pur}-\sum_{t=1}^{T}\left(P_{g,t}^G e_g^G\right)+\sum_{t=1}^{T}\sum_{i\in\Omega^I}\left(P_{gi,t}^{G,GC}\alpha^{GC}\right)+CAP_g\right)\\
-\kappa_g\left(\sum_{t}^{T}\sum_{p\in\Omega^P}\left(\alpha^{P2G}P_{p,t}^{P2G,pur}\right)-P_g^{QT,pur}+Q^{pool}\right)\\
-\xi_g\left(\sum_{t=1}^{T}\sum_{i\in\Omega^I}P_{gi,t}^{G,GC}-\sum_{t=1}^{T}P_{g,t}^G\times EROR\%\right)
\end{pmatrix}\\
&+\sum_{t=1}^{T}\begin{pmatrix}
-\mu_t\left(\sum_{g\in\Omega^G}P_{g,t}^G+\sum_{i\in\Omega^I}\left(P_{i,t}^{PV}+P_{i,t}^W\right)-\sum_{p\in\Omega^P}P_{p,t}^{P2G,pur}-\sum_{j\in\Omega^J}P_{j,t}^L\right)\\
-\sum_{l\in L}\omega_{l,t}^{min}\left(\sum_{m\in\Omega}GSF_{l,m}\left(P_{m,t}^G+P_{m,t}^{PV}+P_{m,t}^W-P_{m,t}^{P2G,pur}-P_{m,t}^L\right)-\underline{P_l^B}\right)\\
-\sum_{l\in L}\omega_{l,t}^{\max}\left(\overline{P_l^B}-\sum_{m\in\Omega}GSF_{l,m}\left(P_{m,t}^G+P_{m,t}^{PV}+P_{m,t}^W-P_{m,t}^{P2G,pur}-P_{m,t}^L\right)\right)\\
-\sum_{g\in\Omega^G}\phi_{g,t}^{min,G}\left(P_{g,t}^G-\underline{P_g^G}\right)-\sum_{g\in\Omega^G}\phi_{g,t}^{max,G}\left(\overline{P_g^G}-P_{g,t}^G\right)\\
-\sum_{i\in\Omega^I}\phi_{i,t}^{min,PV}\left(P_{i,t}^{PV}-0\right)-\sum_{i\in\Omega^I}\phi_{i,t}^{max,PV}\left(\overline{P_{i,t}^{PV}}-P_{i,t}^{PV}\right)\\
-\sum_{i\in\Omega^I}\phi_{i,t}^{min,W}\left(P_{i,t}^W-0\right)-\sum_{i\in\Omega^I}\phi_{i,t}^{max,W}\left(\overline{P_{i,t}^W}-P_{i,t}^W\right)
\end{pmatrix}
\end{aligned}
\tag{5.40}
$$

where χ_g, κ_g, ξ_g, μ_t, $\omega_{l,t}^{min}$, $\omega_{l,t}^{\max}$, $\phi_{g,t}^{min,G}$, $\phi_{g,t}^{max,G}$, $\phi_{i,t}^{min,PV}$, $\phi_{i,t}^{max,PV}$, $\phi_{i,t}^{min,W}$ and $\phi_{i,t}^{max,W}$ are the Lagrange multiplier.

For the lower model, the optimal solution should satisfy the KKT conditions written as Equations (5.41)-(5.55).

$$a_g^G+\chi_g e_g^G+\xi_g EROR\%-\mu_t-\sum_{l\in L}GSF_{l,g}\left(\omega_{l,t}^{min}-\omega_{l,t}^{max}\right)-\phi_{g,t}^{min,G}+\phi_{g,t}^{max,G}=0,\forall g\in\Omega^G \tag{5.41}$$

$$a_i^{PV}-\mu_t-\sum_{l\in L}GSF_{l,i}\left(\omega_{l,t}^{min}-\omega_{l,t}^{max}\right)-\phi_{i,t}^{min,PV}+\phi_{i,t}^{max,PV}=0,\forall i\in\Omega^I \tag{5.42}$$

$$a_i^{W}-\mu_t-\sum_{l\in L}GSF_{l,i}\left(\omega_{l,t}^{min}-\omega_{l,t}^{max}\right)-\phi_{i,t}^{min,W}+\phi_{i,t}^{max,W}=0,\forall i\in\Omega^I \tag{5.43}$$

$$\lambda_t^{GC}-\chi_g\alpha^{GC}-\xi_g=0,\forall g\in\Omega^G \tag{5.44}$$

$$\lambda_t^{CAR}-\chi_g-\kappa_g=0,\forall g\in\Omega^G \tag{5.45}$$

$$0\le\kappa_g\perp\left(\sum_{t}^{T}\sum_{p\in\Omega^P}\left(\alpha^{P2G}P_{p,t}^{P2G,pur}\right)-P_g^{QT,pur}\right)\ge 0,\forall g\in\Omega^G \tag{5.46}$$

$$0\le\xi_g\perp\left(\sum_{t=1}^{T}\sum_{i\in\Omega^I}P_{gi,t}^{G,GC}-\sum_{t=1}^{T}P_{g,t}^G\times EROR\%\right)\ge 0,\forall g\in\Omega^G \tag{5.47}$$

$$0 \le \omega_{l,t}^{min} \perp \left(\sum_{m \in \Omega} GSF_{l,m} \left(P_{m,t}^{G} + P_{m,t}^{PV} + P_{m,t}^{W} - P_{m,t}^{P2G,pur} - P_{m,t}^{L} \right) - \underline{P_{l}^{B}} \right) \ge 0 \,, \forall l \in L \;\; \forall t \in (1,T) \tag{5.48}$$

$$0 \le \omega_{l,t}^{\max} \perp \left(\overline{P_{l}^{B}} - \sum_{m \in \Omega} GSF_{l,m} \left(P_{m,t}^{G} + P_{m,t}^{PV} + P_{m,t}^{W} - P_{m,t}^{P2G,pur} - P_{m,t}^{L} \right) \right) \ge 0 \,, \forall l \in L \;\; \forall t \in (1,T) \tag{5.49}$$

$$0 \le \phi_{g,t}^{min,G} \perp \left(P_{g,t}^{G} - \underline{P_{g}^{G}} \right) \ge 0 \,, \forall g \in \Omega^{G} \;\; \forall t \in (1,T) \tag{5.50}$$

$$0 \le \phi_{g,t}^{max,G} \perp \left(\overline{P_{g}^{G}} - P_{g,t}^{G} \right) \ge 0 \,, \forall g \in \Omega^{G} \;\; \forall t \in (1,T) \tag{5.51}$$

$$0 \le \phi_{i,t}^{min,PV} \perp \left(P_{i,t}^{PV} - 0 \right) \ge 0 \,, \forall i \in \Omega^{I} \;\; \forall t \in (1,T) \tag{5.52}$$

$$0 \le \phi_{i,t}^{max,PV} \perp \left(\overline{P_{i,t}^{PV}} - P_{i,t}^{PV} \right) \ge 0 \,, \forall i \in \Omega^{I} \;\; \forall t \in (1,T) \tag{5.53}$$

$$0 \le \phi_{i,t}^{min,W} \perp \left(P_{i,t}^{W} - 0 \right) \ge 0 \,, \forall i \in \Omega^{I} \;\; \forall t \in (1,T) \tag{5.54}$$

$$0 \le \phi_{i,t}^{max,W} \perp \left(\overline{P_{i,t}^{W}} - P_{i,t}^{W} \right) \ge 0 \,, \forall i \in \Omega^{I} \;\; \forall t \in (1,T) \tag{5.55}$$

The lower model can be inserted into the upper-level model as complementary constraints [328]. For example, the bi-level problem for renewable plants can be reformulated as:

Objective function: Equation (5.27)

Constraints: (5.28)- (5.30), (5.41)-(5.55)

In the same way, the bi-level problem of the other two players can also be reformulated. After obtaining the reformulated single-layer mathematical model of three players, the cooperative payoffs of P2GSes and renewable energy plants can be modeled by summing up the individual payoffs, and the maximum total payoffs are expected, shown as:

$$\arg\max_{\mathcal{S}_{\mathcal{P}}, \mathcal{S}_{\mathcal{R}}} F^{P2G,R} \left(\mathcal{S}_{\mathcal{P}}, \mathcal{S}_{\mathcal{R}}, \mathcal{S}_{\mathcal{T}}^{*} \right) \tag{5.56}$$

Then, an iteration process, which is stated in section III, part C, is conducted to find a Nash equilibrium $\left(\mathcal{S}_{\mathcal{P}}^{*}, \mathcal{S}_{\mathcal{R}}^{*}, \mathcal{S}_{\mathcal{T}}^{*} \right)$. The detailed iteration process of searching the Nash equilibrium is shown in Fig. 5-3. First, the cooperation of renewable energy plants and P2GSes make the decision by solving the sum of equations (5.22) and (5.27), subject to (5.23)-(5.26), (5.28)-(5.30), (5.41)-(5.53), based on the initial strategy of the thermal generators. The decision variables include $P_{p,t}^{P2G,sg}$, $P_{p,t}^{P2G,pur}$, $P_{i,t}^{R,NGC}$, $P_{ig,t}^{R,GC}$, $P_{i,t}^{PV}$, $P_{i,t}^{W}$. Among them, $P_{p,t}^{P2G,pur}$, $P_{i,t}^{R,NGC}$, $P_{ig,t}^{R,GC}$, $P_{i,t}^{PV}$, $P_{i,t}^{W}$ will be transited to the problem of thermal generators. The strategy of the cooperation of renewable energy plants and P2GSes has become known variables in the problem of thermal generators. Then, the thermal generator solves objective function

(5.31), subject to (5.32)-(5.36), (5.41)-(5.53) based on the strategy of the cooperation of renewable energy plants and P2GSes. The decision variables, including $P_{g,t}^{G}$, $P_{gi,t}^{G,GC}$, $P_{g}^{QT,pur}$, are transited to the problem of the cooperation of renewable energy plants and P2GSes as input. The iteration process continues until the Nash equilibrium is found.

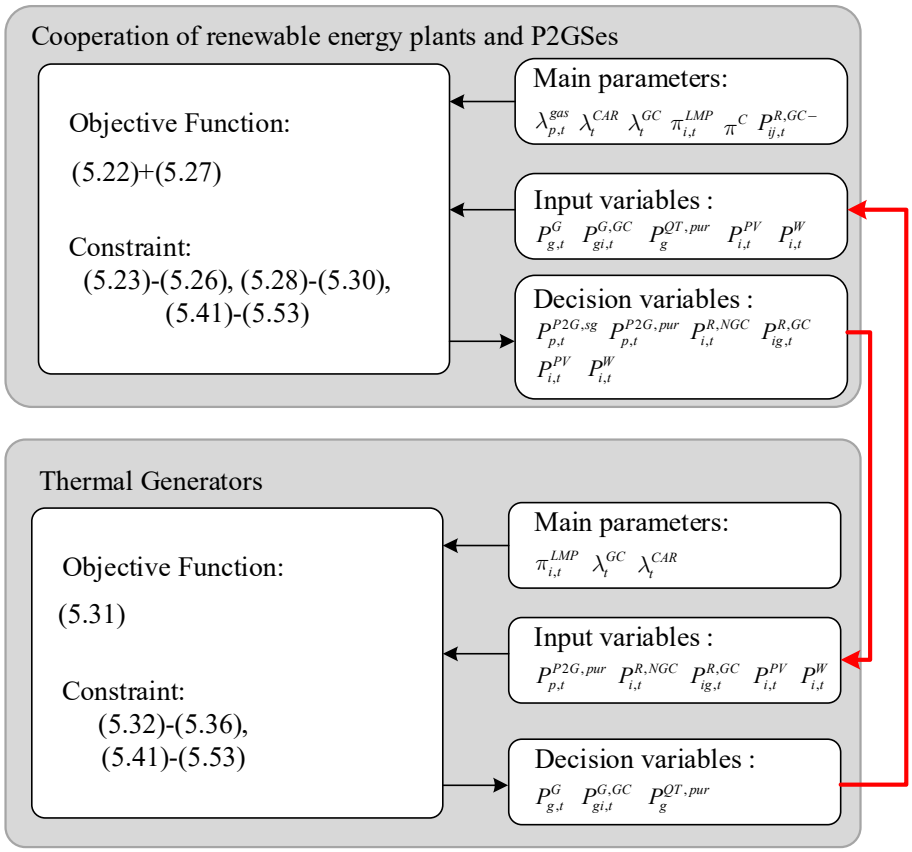

Fig. 5-3. The process of searching the Nash equilibrium.

5.4.3 Existence and Uniqueness of the Nash Equilibrium

The Nash Equilibrium is searched based on (5.1)-(5.3). This searching method can only find out one Nash Equilibrium point. Thus, the existence and uniqueness of the Nash Equilibrium of the proposed method need to be further proved. First, for all players $i \in \{\mathcal{P}, \mathcal{R}, \mathcal{T}\}$, the strategy set $\mathcal{S}_i$ is nonempty, compact, and convex because the decision variables in (5.22), (5.27), and (5.31) are nonempty, compact, and convex. For each player, the payoff function is a bi-level problem and is converted to a single-level problem through KKT conditions, such as (5.40). The reformulated problem for each player is continuously differentiable. Based on the features of the proposed model, it can be concluded that the proposed model is a convex game, and according to ref. [88, 329], the Nash Equilibrium of the convex game exists and is unique.

5.5 Case Study

The proposed model is tested on the modified IEEE 30-bus system, shown in Fig. 5-4. The simulations were completed by a PC with an Intel Core (TM) i7-9750 CPU @ 2.60 GHz with 16.00 GB RAM. The solver is SCIP of OPTI toolbox in MATLAB. The details of the thermal generators, renewable energy plants, and P2GSes are shown in Table 5-1. The other main parameters are given in Table 5-2.

Three cases are set to compare the proposed model with the conventional optimal power dispatch model.

Case 1: no RECs are considered, and a perfectly competitive market is assumed.

Case 2: RECs are considered; an oligopoly market is assumed, and non-cooperated game theory is applied.

Case 3: RECs are considered, the oligopoly market is assumed, and the cooperated game model between P2GSes and renewable plants is applied.

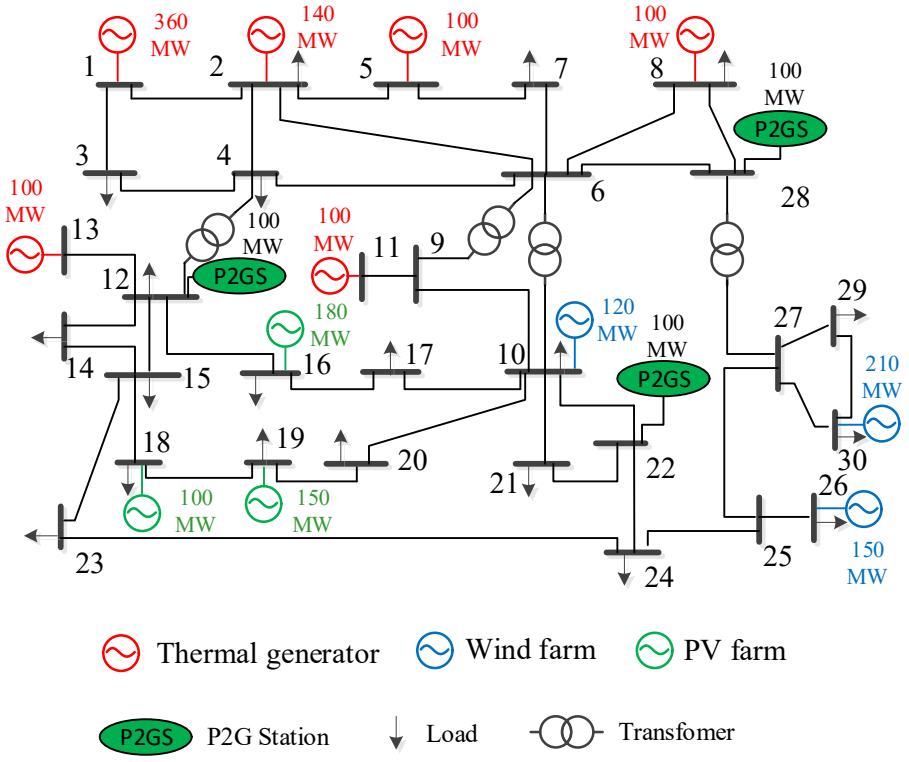

Fig. 5-4. IEEE 30-bus system.

TABLE 5-1. PARAMETER SETTINGS OF THERMAL GENERATORS, RENEWABLE ENERGY PLANTS, AND P2GSES

Bus	Type	Capacity (MWh)	Bus	Type	Capacity (MWh)
1	Thermal	360	16	PV	180
2	Thermal	140	10	Wind	120
5	Thermal	100	26	Wind	150
8	Thermal	100	30	WInd	210
11	Thermal	100	12	P2G	100

13	Thermal	100	22	P2G	100
18	PV	100	28	P2G	100
19	PV	150			

TABLE 5-2. PARAMETER SETTINGS

Parameter	Value	Parameter	Value
a^g	\$7/MW	Quotas	12000k ton/year
a^{pv}	\$25/MW	*EROR%*	15%
a^w	\$14/year	α^{P2G}	0.75
e^g	0.875~0.985	α^{GC}	0.8

5.5.1 Simulation Results

In the simulation, the electricity price and gas price are obtained through the Australian Energy Market Operator [330, 331]. The carbon price is obtained through Ref. [332]. The 7-day electricity price, gas price, and carbon price profile are shown in Fig. 5-5. From the figure, obviously, if P2GSes only rely on the arbitrage mechanism of buying electricity at a low price and selling the gas at a relatively high price, the profits are very limited because the electricity price is higher than the gas price most of the time. For the RECs price, it is unchanged according to the simulation result based on the pricing model. However, when the carbon price continuously increases, the RECs price may increase because of the change in demand.

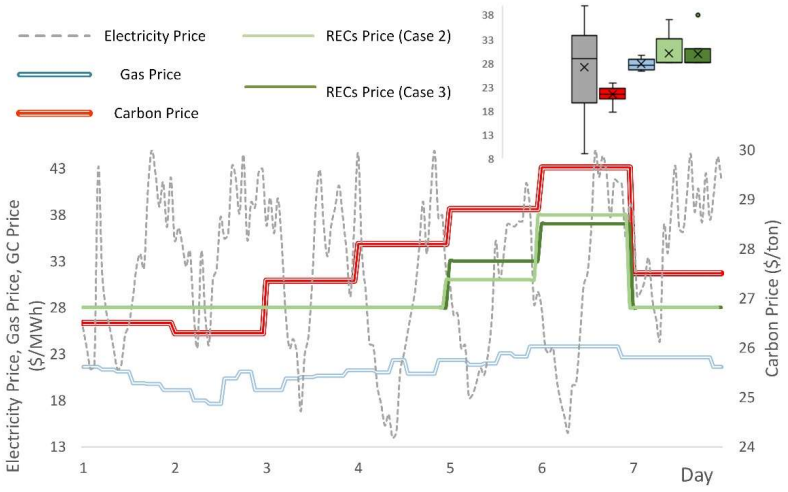

Fig. 5-5. Electricity, gas, carbon, and RECs price.

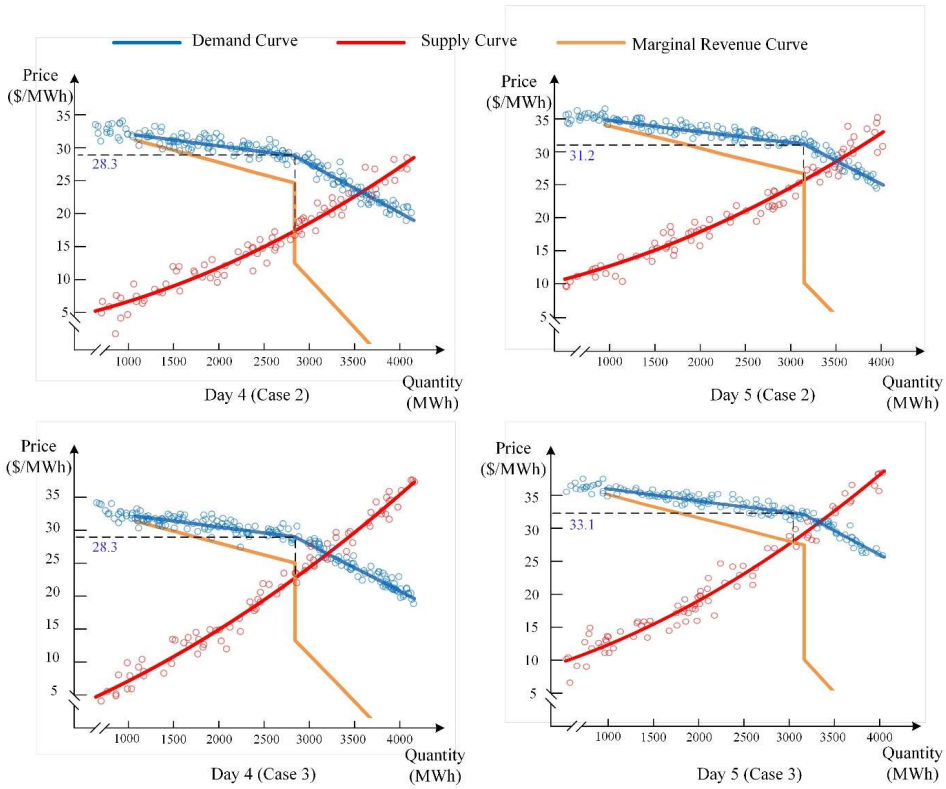

Fig. 5-6. Demand curves and supply curves of RECs on day 4 and day 5 of Cases 2 and 3.

The RECs price is figured out according to the kinked demand curve in the proposed pricing model. The demand and supply curves are dynamic, and hence, two specific days are selected in the case study to illustrate the process of the RECs pricing. In Fig. 5-6. the demand curve and supply curve on day 4 and day 5 of Cases 2 and 3 are provided. In Case 2, the RECs price is settled at 28.3 $/MWh on day 4, and it is increased to 31.2 $/MWh on day 5 because of the shift of the demand curve. In Case 3, the RECs price is 28.3 $/MWh and 33.1 $/MWh on day 4 and day 5, respectively.

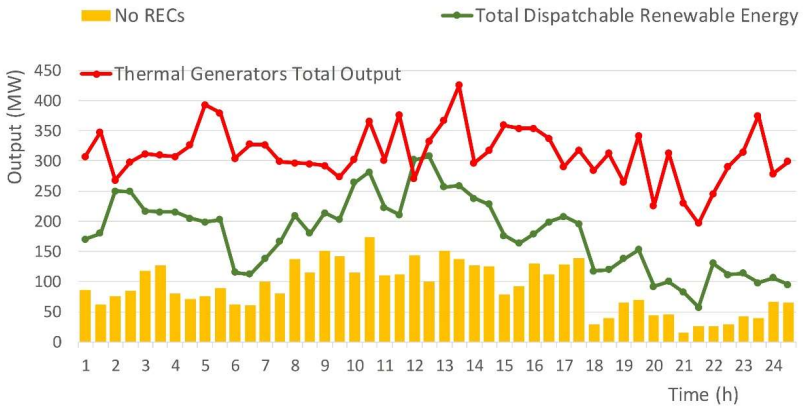

Fig. 5-7. The output of thermal generators and renewable plants (Case 1).

Figs. 5-7 to 5-9 show the ED results and RECs trading results of thermal generators and renewable plants in Cases 1 to 3. The green line is the dispatchable energy of renewable plants, while the bars represent the actual dispatched energy of renewable plants. The spare area between the green line and the bars represents the discarded renewable energy.

More renewable energy is absorbed by the system in Cases 2 and 3 compared with Case 1 because of the RECs (green and blue bars). Compared with Cases 2 and 3, the output of renewable energy in Case 3 is slightly higher than that in Case 2. Besides, because of the cooperation of P2GSes and renewable plants, more RECs are sold, which will certainly increase the total income of the collision. From the perspective of the thermal generators, it is smoother in Case 3 than Cases 1 and 2. That is because when the renewable plants cooperate with P2GSes, P2GSes began to play the role of frequency regulation. However, in Cases 1 and 2, this job is done by thermal generators indicating that the output of thermal generators fluctuates with intermittent renewable energy.

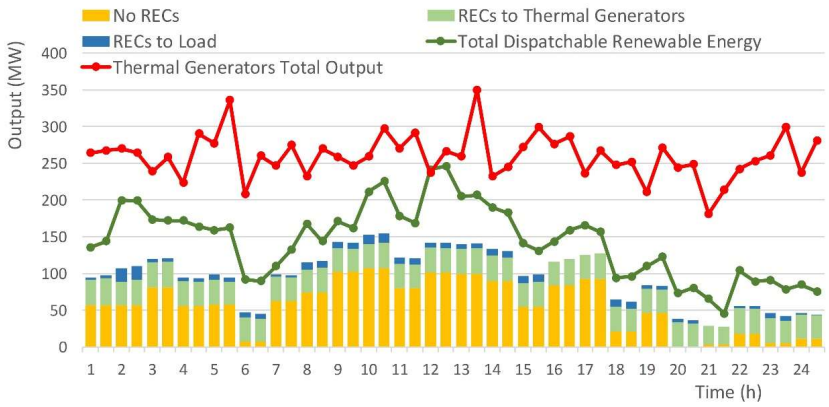

Fig. 5-8. The output of thermal generators and renewable plants (Case 2).

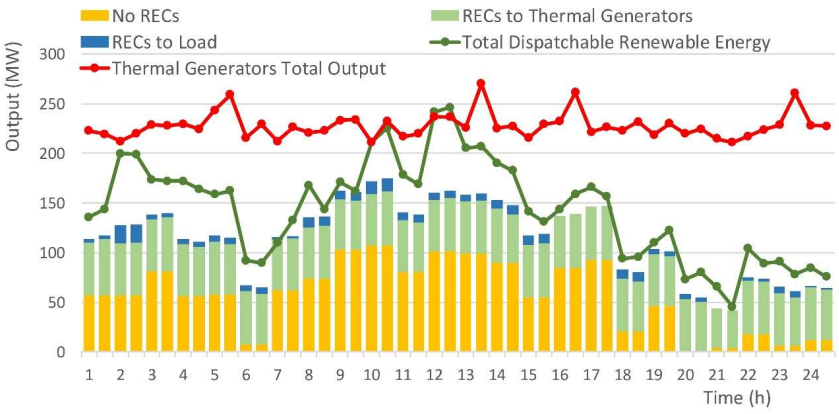

Fig. 5-9. The output of thermal generators and renewable plants (Case 3).

TABLE 5-3. PAYOFF AND NET PROFITS

Case	The payoff of each player or coalition (1*10^8$)			Total payoff	Net Profits
	Total Payoffs of each player	Selling gas/electricity	Carbon/GC Trading		
1	F^{P2G}=0.17	0.14	0.03	5.05	4.43
	F^{R}=2.22	2.22	N/A		
	F^{G}=2.66	2.66	N/A		
2	F^{P2G}*=0.15	0.13	0.02	5.28	4.88
	F^{R}*=2.65	2.34	0.31		

	F^{G}*=2.48	2.48	N/A		
3	$F^{P2G,R}$*=3.31	2.56	0.75	5.34	4.93
	F^{G*}=2.03	2.03	N/A		

The final payoffs and net profits of each player in different cases are shown in Table 5-3. In Case 1, the total payoffs and net profits of all the players are less than Cases 2 and 3. That is because in Case 1, no RECs are considered, and renewable plants lose the profits from RECs. If the profits of RECs are removed in each case, the total payoff in Case 1 is the largest because, in Case 1, a perfectly competitive market is assumed. The deadweight loss will exist in an oligopoly market. When the RECs are applied in Case 2, the payoffs of renewable plants increase from 2.22 to 2.66*10^8$ since they can get extra profits. However, the payoffs of P2GSes are still very low at the Nash equilibrium (0.15*10^8$). To earn more market share, a cooperative game model of P2GSes and renewable plants is considered in Case 3, and at the Nash equilibrium, the total payoffs of the collision are increased to 3.31*10^8$. The payoffs of thermal generators decrease from 2.48 to 2.03*10^8$, indicating that the competition is successful and the collision is cohesive.

5.5.2 Parameter Sensitivity Analysis

The simulation result in part B is based on the selected parameters. The sensitivity of different parameters on the Nash equilibrium is studied in this section. We are interested in how the carbon market will affect the RECs market when two mechanisms are operated paralleled.

1) Influence of Carbon Price

The carbon price is an external parameter that is decided by many factors apart from the power system. The strategy of each player cannot largely affect the price, and each player can only be a price-taker. Table 5-4 shows when the carbon price is changed, how the Nash equilibrium, price of RECs, and system emissions will change.

It can be concluded that for renewable plants, when the carbon price decreases, the payoffs will decrease, and when the price increases, the payoffs will increase. For thermal generators, the situation is different. But for renewable plants and P2GSes, the payoffs are more sensitive when the carbon price increases (5.7, 6.1 compared with -0.61, -0.42). For carbon emissions, it will decrease when the carbon price increases, and it is sensitive when the carbon price increases by 10%. Furthermore, through sensitivity analysis, the interaction between the carbon market and the REC market is investigated. When the changes in the carbon price within ±5%, the REC prices remain unchanged due to the kinked demand curve. When the changes in the carbon price reach ±10%, the increase or decrease of the RECs price will follow the change in the carbon price. When the carbon price is decreased by 10%, the REC price will be decreased by 12.3%. When the carbon price is increased by 10%, the REC price will be increased by 10.7%.

TABLE 5-4. SENSITIVE ANALYSIS: CARBON PRICE

Carbon Price	$\Delta F^{P2G,R}$ * (%)	ΔF^{G} * (%)	$\Delta \lambda^{GC}$	Δ Emission
-10%	-0.61	1.2	-12.3	0.13
-5%	-0.42	0.43	0	0.07
5%	5.7	-1.3	0	-0.13
10%	6.1	-2.5	10.7	-3.4

2) Influence of Allocated quotas

Table 5-5 shows when the allocated quotas are changed, how the simulation result will change. When the number of quotas decreases, the payoff of renewable plants and P2GSes increases while that of thermal generators decreases. However, thermal generators are more sensitive to changes in quotas. As for emissions, it is also sensitive when the quotas are reduced largely. Then, we investigate how the carbon quota can affect the REC price. The slight decrease (within 15%) in quotas will not affect the RECs price. But if it is reduced by 20%, the RECs price will increase by 14.5% because of the change in market demand.

TABLE 5-5. SENSITIVE ANALYSIS: QUOTAS

Quota	$\Delta F^{P2G,R}$ * (%)	ΔF^{G} * (%)	$\Delta \lambda^{GC}$	Δ Emission
90%	0.61	-1.7	0	-0.24
85%	0.88	-5.4	0	-1.34
80%	1.2	-6.4	14.5	-4.56

5.6 Chapter Summary

In this chapter, a bi-level optimization model based on the game approach is proposed for a large scale of renewable energy plants and P2GSs, considering the integrated ETS and REC together. The payoff model of each player is proposed, and three bi-level models are converted to three single-level models through KKT conditions. Nash equilibrium is found via a distributed method. The simulation is conducted on a modified IEEE 30-bus system. From the numeric results, the cooperation of renewable energy plants and P2GSs considering REC trading can preferably contribute to the penetration of large-scale renewable energy. From the perspective of payoff, RECs help renewable energy plants increase income by 19.4% without considering cooperation. Renewable energy plants earn an extra profit of 36 million Australian (AU) dollars through selling RECs. The cooperation of P2GSs and renewable energy plants can successfully compete with the thermal generators and compress the payoff of thermal generators by 63 million AU dollars per year in the tested system. According to sensitivity analysis, the relationship between the carbon market and the REC market is revealed. When the changes in the carbon price are within ±5%, the REC prices remain unchanged due to the kinked demand curve. When the carbon price is decreased by 10%, the REC price will be decreased by 12.3%. When the carbon price is increased by 10%, the REC price will be increased by 10.7%. When the quota of the thermal

generators is decreased within 15%, the REC price remains unchanged, but when the quota is decreased by 20%, the REC price will be increased by 14.5%. Furthermore, through sensitive analysis, it is also revealed that the payoff of cooperation of renewable energy plants and P2GSs is more sensitive to the rise of the carbon price. The payoff of thermal generators is more sensitive to the decrease of the allocated quota.

CHAPTER 6

TRANSPORTATION ELECTRIFICATION: COLLABORATIVE PLANNING OF ELECTRICITY NETWORK AND TRANSPORTATION NETWORK

Electric vehicles (EVs) are drawing attention for their environmental benefits to society. The proliferation of EVs is an inevitable trend to realize transportation electrification and has become an essential part in the energy transition. Meanwhile, utilities face various challenges in accommodating the increasing number of EVs. The diffusion of the EVs increases charging demands, circuit losses, and the risks of voltage violation, which brings new problems to future smart grids. The diffusion of EVs not only refers to the growth of EVs but also describes the spatial popularization from the high-penetration region to the neighboring area, just like urbanization and people migration between cities and villages. Hence, in the future distribution expansion planning (DEP) problem, the construction and expansion of EV fast-charging stations (FCSs), BESS, and distributed generators (DGs) should be integrated to deal with network risk issues in smart grids [333].

6.1 Transportation Network Modeling

6.1.1 Conventional User equilibrium (UE) model

In most of the references regarding the FCS planning, such as ref. [101], the conventional UE model is utilized to assign the traffic flow, shown as (6.1). It described that each traveler wants to minimize his own travel time and the congestion effects. Therefore, the traffic flow distribution would reach a stable state, which is referred to the UE.

$$\min Z = \sum_t \sum_{a\in\mathcal{A}} \int_0^{c_{a,t}} t_{a,t}(\omega)\, d\omega, \quad \forall t \in [1,T] \tag{6.1}$$

where $\mathcal{A}$ is the set of road sections; $c_{a,t}$ is the traffic flow on the a^{th} road section at time t; $t_{a,t}$ is the road impedance measured in traveling time.

Equation (6.2) is a commonly used road impedance function, i.e., the Bureau of Public Roads (BPR) function [334], proposed by the U.S. Bureau of Public Roads.

$$t_{a,t}(c_{a,t}) = t_a^0\left(1+\xi\left(c_a/\mathcal{C}_a\right)^{\tau}\right), \quad \forall a \in \mathcal{A}, \forall t \in [1,T] \tag{6.2}$$

where t_a^0 is the free travel time of the a^{th} road; ξ and τ are the pre-determined parameters (usually choose 0.15 and 4), which can be changed according to different cities; $\mathcal{C}_a$ is the maximum capacity of the a^{th} road.

However, two essential aspects are ignored in the conventional UE. First, travelers can not accurately estimate travel impedance and have an understanding error for actual travel impedance. Second, the conventional UE fails to consider the impact of EV penetration.

6.1.2 Cost function of different types of vehicles

To further consider the EV penetration into the transportation model, it should be noted that the EVs and internal-combustion engine (ICE) vehicles have different traveling costs, shown as equations (6.3) and (6.4).

$$J_{p,t}^{od,E} = \sum\nolimits_{a\in\mathcal{A}}\left[\alpha t_{a,t}\left(c_{a,t}\right)+\beta^{E}\left(H^{E}l_a\right)\right]\sigma_{a,p}^{od}+\alpha\left(T_p^{CH}+T^{W}\right),\ \ \forall p\in\mathcal{P},\forall t\in\left[1,T\right] \tag{6.3}$$

$$J_{p,t}^{od,G} = \sum\nolimits_{a\in\mathcal{A}}\left[\alpha t_{a,t}\left(c_{a,t}\right)+\beta^{G}\left(H^{G}l_a\right)\right]\sigma_{a,p}^{od},\ \ \forall p\in\mathcal{P},\forall t\in\left[1,T\right] \tag{6.4}$$

where $J_{p,t}^{od,E}$ and $J_{p,t}^{od,G}$ are the traveling cost of EVs and ICE vehicles on the p^{th} path from origin o to destination d; α is the time cost coefficient; β^E and β^G are energy cost of EVs and ICE vehicles; H^E and H^G are the energy consumption of EVs and ICE vehicles per km; l_a is the length of the road; $\sigma_{a,p}^{od}$ is binary variables indicating whether the p^{th} path from o to d passes through the a^{th} road section; T_p^{CH} and T^W are the charging time and the waiting time of the EVs.

6.1.3 Proposed EV integrated path-size logit and stochastic User equilibrium (PSL-SUE)model

When the randomness of travelers' understanding of the travel cost obeys independent identically distributed Gumbel distribution, we can get a polynomial logit model [335]. The stochastic of the UE can be modeled based on the path-size logit. According to the PSL-SUE model and Fisk model [336], we further propose an EV-integrated PSL-SUE model, which can be expressed as (6.5)-(6.10).

$$\begin{aligned}\min Z = &\sum_t\left\{\sum_{(o,d)\in o}\sum_{p\in\mathcal{P}}\left[\frac{1}{\vartheta}f_{p,t}^{od,E}\left(\ln f_{p,t}^{od,E}-\ln q_t^{od,E}\right)+J_{p,t}^{od,E}f_{p,t}^{od,E}\right]\right\}+\\ &\sum_t\left\{\sum_{(o,d)\in o}\sum_{p\in\mathcal{P}}\left[\frac{1}{\vartheta}f_{p,t}^{od,G}\left(\ln f_{p,t}^{od,G}-\ln q_t^{od,G}\right)+J_{p,t}^{od,G}f_{p,t}^{od,G}\right]\right\}\end{aligned} \tag{6.5}$$

where $\mathcal{P}$ is the set of the paths; o is the set of origin-destination (OD) sections; $f_{p,t}^{od,E}$ and $f_{p,t}^{od,G}$ are traffic flow

of EVs and ICE vehicles on the p^{th} path of the OD section from o to d; $q_t^{od,E}$ and $q_t^{od,G}$ are the traffic demand of EVs and ICE vehicles from o to d; ϑ is the non-negative correction parameters indicating the aggregated measure of the travelers' understanding on traffic impedance.

s.t. $$\sum_{p\in\mathcal{P}} f_{p,t}^{od,E} = q_t^{od,E}, \sum_{p\in\mathcal{P}} f_{p,t}^{od,G} = q_t^{od,G}, \quad \forall t \in [1,T] \tag{6.6}$$

$$f_{p,t}^{od,E} \geq 0, f_{p,t}^{od,G} \geq 0, \quad \forall p \in \mathcal{P}, \forall t \in [1,T] \tag{6.7}$$

$$c_{a,t} = \sum_{(o,d)\in O} \sum_{p\in\mathcal{P}} \left(f_{p,t}^{od,E} + f_{p,t}^{od,G}\right) \sigma_{a,p}^{od}, \quad \forall a \in \mathcal{A}, \forall t \in [1,T] \tag{6.8}$$

$$\left[S_0 - \sum_{a\in\mathcal{A}_p} \left(H^E l_a / \Psi\right)\right] f_{p,t}^{od,E} \geq 0, \quad \forall p \in \Theta^{NCP}, \forall t \in [1,T] \tag{6.9}$$

$$\left[S_0 - H^{FCS} / \Psi\right] f_{p,t}^{od,E} \geq 0, \quad \forall p \in \Theta^{CP}, \forall t \in [1,T] \tag{6.10}$$

where Ψ is the maximum capacity of the EVs; S_0 is the initial state of charge (SOC) of the EVs; H^{FCS} is the energy consumption from the origin to the FCS; Θ^{NCP} and Θ^{CP} are the sets of the noncharging paths and the charging paths.

Equation (6.6) describes the relationship between traffic demand and traffic flows. Equation (6.7) is the non-negative constraints of traffic flows. Equation (6.8) describes traffic flow on each road section. Equations (6.9) and (6.10) indicate that if the mileage of the EVs cannot support the trip to the destination or FCSs, the traffic flow on the path should be assigned as 0.

The traffic capture of the i^{th} FCSs can be calculated as:

$$f_{i,t}^{cap} = \sum_{(o,d)\in O} \sum_{p\in\mathcal{P}} f_{p,t}^{od,E} \hat{\sigma}_{i,p}^{od}, \quad \forall i \in \Omega^{FCS}, \forall t \in [1,T] \tag{6.11}$$

where $f_{i,t}^{cap}$ is the traffic flow capture of the FCS on the i^{th} node; $\hat{\sigma}_{i,p}^{od}$ is the binary parameters indicating whether the p^{th} path from o to d passes the i^{th} FCS; Ω^{FCS} is the set of FCSs.

Then, the arrival rate of the FCSs can be estimated as (6.12) according to ref. [101].

$$\lambda_{i,t} = D^{CH} \kappa \frac{f_t^{trip}}{\sum_t f_t^{trip}} \frac{f_{i,t}^{cap}}{\sum_{i\in\Omega^{FCS}} f_{i,t}^{cap}}, \quad \forall i \in \Omega^{FCS}, \forall t \in [1,T] \tag{6.12}$$

where $\lambda_{i,t}$ is the arrival rate of the EVs at the FCS; D^{CH} is the total charging demand of EVs in the system; κ is the choosing ratio of fast charging; f_t^{trip} is the travel ratio; Ω^{FCS} is the set of FCSs.

6.2 Adaptive Planning Framework of Electricity Networks and Fast Charging Stations

6.2.1 Proposed Framework

In this chapter, we propose an adaptive planning framework for EV FCSs and electricity networks to cope with the future diffusion of EVs, as shown in Fig. 6-1.

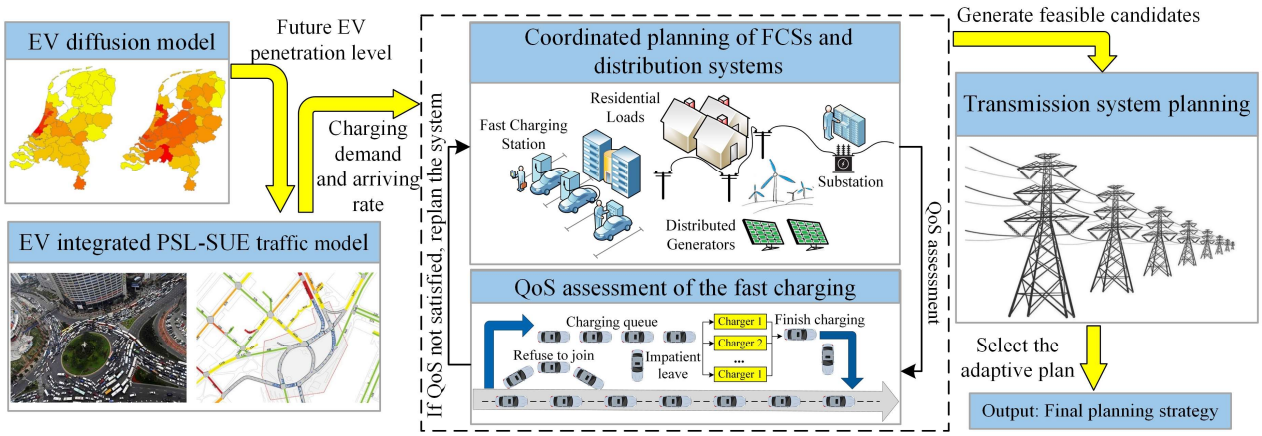

Fig. 6-1. Proposed adaptive planning of the integrated networks and FCSs.

First, based on the EV diffusion model, the future penetration level of EVs and the charging demand can be estimated. The EV charging demand is an input of the proposed EV integrated traffic flow assignment model (section 6.1). Based on the traffic flow assignment model, the traffic flow capture and the arriving rate at the candidate FCSs can be calculated. Then, in the next stage, the coordinated planning of the FCSs and the distribution networks is realized (section 6.3). In this section, the charging demand constraints should be satisfied through FCS investment, which is formulated based on the traffic flow capture calculated from the traffic flow assignment model. To ensure that sufficient fast-charging infrastructure is planned to provide the increasing number of EVs with high-quality services at each planning stage, a QoS assessment is conducted (section 6.4). The QoS assessment is based on the queueing model, and the calculated arrival rate from the traffic flow assignment model is the input. Several feasible planning candidates, which pass the QoS assessment, are generated at this stage.

It should be noted that the increase of the EV loads will result in not only distribution expansion but also augmentation in the transmission system. In most of the references, the transmission and distribution networks were planned independently for each other, thereby leading to suboptimal solutions. Therefore, in this chapter, we further consider the adaptive cost of the transmission system arising from the EV diffusion and the increase of the other electrical loads. Thus, several alternatives are available for the line expansion as well as fossil-fuel and renewable-based generator expansion at both system levels. For example, if more DGs are planned at the distribution level to satisfy the increasing

charging demand, less adaptive cost may occur in the transmission system. Hence, we aim to find an adaptive solution for the integrated planning of network systems (section 6.5). At this stage, the feasible planning candidates from section IV are the input, and the final output is the selected adaptive planning solution.

It should be claimed that the proposed planning is a collaborative planning of the electricity distribution network, the transmission network, and the EV charging network. Although ownership of the distribution network, the transmission network, and the FCSs belong to different parties/entities, the centralized planning can maximize total social welfare. The collaborative planning is a common strategy in the planning problem of EV charging infrastructure since there is a strong correlation between the electricity network and the EV charging network [101].

6.2.2 EV Diffusion Modeling

In this chapter, the EV diffusion is modeled based on a customer-based method proposed in ref. [337]. It generally models the purchase behaviors of the customers from four aspects: car age, attractiveness, neighbor influence, and customer economics. Then, purchase scores and defer scores are evaluated based on these four criteria. The detailed scoring model can be referred to ref. [337]. Then, the probability of purchase, deferral, choosing EVs, and choosing ICE vehicles can be formulated based on the weighted score, shown as (6.13) and (6.14).

$$\Pr^{Buy} = \sum_{k=1}^{4} w_k^{B/D} S_k^{Buy}, \Pr^{Def} = \sum_{k=1}^{4} w_k^{B/D} S_k^{Def} \tag{6.13}$$

$$\Pr^{EV} = \Pr^{Buy} \sum_{k=2}^{4} w_k^{E/G} S_k^{EV}, \Pr^{IC} = \Pr^{Buy} \sum_{k=2}^{4} w_k^{E/G} S_k^{IC} \tag{6.14}$$

where $\Pr^{Buy}$, $\Pr^{Def}$, $\Pr^{EV}$, and $\Pr^{IC}$ are the probability of purchasing a vehicle, deferring purchase, purchasing EV, and purchasing ICE vehicle; S is the scores of the behavior; w is the corresponding weight.

Through Monte Carlo simulation, we can predict the future penetration level of EVs and evaluate the charging demand.

6.3 Coordinated Planning of FCS and Distribution Network

6.3.1 Objective Function

In the multistage expansion planning model, scenario-based stochastic programming is proposed to minimize the expected total cost of the distribution network, shown as (6.15). The total system cost includes the investment cost of the network assets, the maintenance cost, energy production cost, system loss cost, and unserved load cost.

$$\begin{aligned}\min .F^{DEP}=&\sum_{y}\left(1+\gamma\right)^{-y}C_{y}^{INV,D}/\gamma\\&+\left[\sum_{y}\left(1+\gamma\right)^{-y}\left(C_{y}^{MT,D}+C_{y}^{EN,D}+C_{y}^{LS,D}+C_{y}^{US,D}\right)\right]\\&+\left[\left(1+\gamma\right)^{Y}\left(C_{Y}^{MT,D}+C_{Y}^{EN,D}+C_{Y}^{LS,D}+C_{Y}^{US,D}\right)/\gamma\right]\end{aligned}\tag{6.15}$$

where $C_{y}^{INV,D}$, $C_{y}^{MT,D}$, $C_{y}^{EN,D}$, $C_{y}^{LS,D}$, $C_{y}^{US,D}$ are the investment cost, maintenance cost, energy purchase cost, energy loss cost, unserved load cost in the y^{th} planning stage in the distribution systems; γ is the discount rate; Y is the total planning stage.

The investment cost of the assets includes the expansion of the feeders, substations, DGs, BESS, and FCSs, as shown in (6.16).

$$\begin{aligned}C_{y}^{INV,D}=&CRF^{L,D}\sum_{(i,j)\in\Omega^{L,D}}\lambda^{INV,L,D}l_{ij}\delta_{ij,y}^{L,D}+CRF^{SS}\sum_{i\in\Omega^{SS}}\lambda^{INV,SS}\delta_{i,y}^{SS}\\&+\sum_{r\in\mathcal{R}}CRF_{r}^{DG}\sum_{i\in\Omega_{r}^{DG}}\lambda_{r}^{INV,DG}\delta_{i,r,y}^{DG}+CRF^{BESS}\sum_{i\in\Omega^{BESS}}\lambda^{INV,BESS}\delta_{i,y}^{BESS}+CRF^{FCS}\sum_{i\in\Omega^{FCS}}\lambda^{INV,FCS}\delta_{i,y}^{FCS},\quad\forall y\in\left[1,Y\right]\end{aligned}\tag{6.16}$$

where $\Omega^{L,D}$, Ω^{SS}, Ω_{r}^{DG}, Ω^{BESS}, and Ω^{FCS} are the candidate sets of the feeders, substations, the r^{th} type of DGs, BESS, and FCSs; $\mathcal{R}$ is the set of types of DGs; $\lambda^{INV,L,D}$, $\lambda^{INV,SS}$, $\lambda_{r}^{INV,DG}$, $\lambda^{INV,BESS}$, and $\lambda^{INV,FCS}$ are the per-unit investment cost of the corresponding assets; $\delta_{ij,y}^{L,D}$, $\delta_{i,y}^{SS}$, $\delta_{i,r,y}^{DG}$, $\delta_{i,y}^{BESS}$, and $\delta_{i,y}^{FCS}$ are the decision variables indicating whether the corresponding assets are expanded or constructed at the y^{th} stage; l_{ij} is the distance between buses i and j; CRF is the capital recovery factor for the corresponding asset.

Since we assume that the utility companies and the FCS company cooperate with each other to maximize the total social welfare, the investment of FCSs is considered in the total cost in (6.16).

The maintenance cost can be expressed as (6.17).

$$\begin{aligned}C_{y}^{MT,D}=&\sum_{(i,j)\in\Omega^{L}}\lambda^{MT,L,D}x_{ij,y}^{L,D}+\sum_{r\in\mathcal{R}}\sum_{i\in\Omega_{r}^{DG}}\lambda_{r}^{MT,DG}x_{i,r,y}^{DG}\\&+\sum_{i\in\Omega^{SS}}\lambda^{MT,SS}x_{i,y}^{SS}+\sum_{i\in\Omega^{BESS}}\lambda^{MT,BESS}x_{i,y}^{BESS}+\sum_{i\in\Omega^{FCS}}\lambda^{MT,FCS}x_{i,y}^{FCS},\quad\forall y\in\left[1,Y\right]\end{aligned}\tag{6.17}$$

where $\lambda^{MT,L,D}$, $\lambda_{r}^{MT,DG}$, $\lambda^{MT,SS}$, $\lambda^{MT,BESS}$, and $\lambda^{MT,FCS}$ are the per-unit investment cost of the corresponding assets; $x_{ij,y}^{L,D}$, $x_{i,r,y}^{DG}$, $x_{i,y}^{SS}$, $x_{i,y}^{BESS}$, and $x_{i,y}^{FCS}$ are the utilization states of the corresponding assets, indicating the current capacity of the assets.

The energy production cost can be expressed as (6.18).

$$C_y^{EN,D} = \sum_{q\in\mathcal{Q}}\sum_{b\in\mathcal{B}}\sum_{s\in\mathcal{S}}\pi_{qbs}\Delta_{qb}\left(\begin{array}{l}\sum_{i\in\Omega^{SS}}\lambda_{i,yqbs}^{EN,SS}P_{i,yqbs}^{SS}+\sum_{r\in\mathcal{R}}\sum_{i\in\Omega_r^{DG}}\lambda_r^{EN,DG}P_{i,r,yqbs}^{DG}\\+\sum_{i\in\Omega^{BESS}}\lambda^{EN,BESS}P_{i,yqbs}^{BESS,DS}\end{array}\right),\ \forall y\in[1,Y] \quad (6.18)$$

where $\mathcal{Q}$, $\mathcal{B}$, and $\mathcal{S}$ are sets of quarters, duration blocks, and scenarios; π_{qbs} is the weight of the scenarios; Δ_{qb} is the duration time; $\lambda_{i,yqbs}^{EN,SS}$ is the per-unit energy purchase cost from the utility grid at substations; $\lambda_r^{EN,DG}$ and $\lambda^{EN,BESS}$ are the per-unit energy production cost from the DGs and BESS; $P_{i,yqbs}^{SS}$ is the output power from the substations; $P_{i,r,yqbs}^{DG}$ is the output power from the DGs; $P_{i,yqbs}^{BESS,DS}$ is the discharging power from the BESS.

The energy loss cost can be expressed as (6.19).

$$C_y^{LS,D} = \sum_{q\in\mathcal{Q}}\sum_{b\in\mathcal{B}}\sum_{s\in\mathcal{S}}\pi_{qbs}\Delta_{qb}\lambda_{i,yqbs}^{EN,SS}\left(\sum_{i\in\Omega^{SS}}Z_i^{SS}\left(\sum_{i\in\mathbf{N}_i}I_{ij,yqbs}\right)^2+\sum_{(ij)\in\Omega^{L,D}}Z_{ij}^{LD}\left(I_{ij,yqbs}\right)^2\right),\ \forall y\in[1,Y] \quad (6.19)$$

where Z_i^{SS} is the impedance of the substations; Z_{ij}^{LD} is the impedance of the feeders; $I_{ij,yqbs}$ is the branch current; $\mathbf{N}_i$ is the set of buses connected to bus *i*.

The unserved load cost can be expressed as (6.20).

$$C_y^{US,D} = \sum_{q\in\mathcal{Q}}\sum_{b\in\mathcal{B}}\sum_{s\in\mathcal{S}}\pi_{qbs}\Delta_{qb}\sum_{i\in\Omega}\left(P_{i,yqbs}^{LC,D}\lambda^{US}\right),\ \forall y\in[1,Y] \quad (6.20)$$

where λ^{US} is the value of customer reliability; $P_{i,yqbs}^{LC,D}$ is the load curtailment.

The impact of economic development and government policy should be taken into consideration since these factors may affect the planning results. Government policies such as carbon policy will accelerate the transition to zero-emission networks, and economic development will affect the yearly budget. These factors can be considered as uncertainties that can be solved through the utilized stochastic optimization method. To deal with uncertainties, a scenario set $\mathcal{S}$ is established, and a weight π_{qbs} is given to each scenario.

6.3.2 Constraints

To solve the optimization, the following constraints should be considered:

1) Electricity network constraints

The electricity network constraints include power balance constraints, voltage constraints, current calculation, thermal stability constraints, and power source constraints.

Equations (6.21) and (6.22) describe the DistFlow in the distribution system.

$$P_{ij,yqbs}^{B,D} - \sum_{k\in\mathbf{N}_j\setminus\{i\}}P_{jk,yqbs}^{B,D} = -P_{j,yqbs}^{inj,D},\ \forall i,j\in\Omega,\forall y\in[1,Y],\forall q\in\mathcal{Q},\forall b\in\mathcal{B},\forall s\in\mathcal{S} \quad (6.21)$$

$$Q_{ij,yqbs}^{B,D} - \sum_{k \in \mathbf{N}_j \setminus \{i\}} Q_{jk,yqbs}^{B,D} = -Q_{j,yqbs}^{inj,D}, \quad \forall i, j \in \Omega, \forall y \in [1,Y], \forall q \in \mathcal{Q}, \forall b \in \mathcal{B}, \forall s \in \mathcal{S} \tag{6.22}$$

where $P_{ij,yqbs}^{B,D}$ and $Q_{ij,yqbs}^{B,D}$ are the active and reactive power flows on each branch; $P_{j,yqbs}^{inj,D}$ and $Q_{j,yqbs}^{inj,D}$ are the active and reactive power injection at each bus.

The active and reactive power injection at each bus can be expressed as (6.23) and (6.24).

$$P_{i,yqbs}^{inj,D} = P_{i,yqbs}^{SS} + \sum_{r \in \mathcal{R}} P_{i,r,yqbs}^{DG} + P_{i,yqbs}^{BESS,DS} - P_{i,yqbs}^{LD,D} - P_{i,yqbs}^{BESS,CH} - P_{i,yqbs}^{FCS} + P_{i,yqbs}^{LC,D}$$

$$, \quad \forall i \in \Omega, \forall y \in [1,Y], \forall q \in \mathcal{Q}, \forall b \in \mathcal{B}, \forall s \in \mathcal{S} \tag{6.23}$$

$$Q_{i,yqbs}^{inj,D} = Q_{i,yqbs}^{SS} + \sum_{r \in \mathcal{R}} Q_{i,r,yqbs}^{DG} - Q_{i,yqbs}^{LD,D} + Q_{i,yqbs}^{LC,D}, \quad \forall i \in \Omega, \forall y \in [1,Y], \forall q \in \mathcal{Q}, \forall b \in \mathcal{B}, \forall s \in \mathcal{S} \tag{6.24}$$

where $P_{i,yqbs}^{SS}$ and $Q_{i,yqbs}^{SS}$ are the active and reactive power from the substations; $P_{i,r,yqbs}^{DG}$ is the output of the r^{th} type of DG; $P_{i,yqbs}^{BESS,DS}$ and $P_{i,yqbs}^{BESS,CH}$ are the discharging and charging power of the BESS; $P_{i,yqbs}^{LD,D}$ and $Q_{i,yqbs}^{LD,D}$ are the active and reactive load; $P_{i,yqbs}^{FCS}$ is the load of the FCSs; $P_{i,yqbs}^{LC,D}$ and $Q_{i,yqbs}^{LC,D}$ are the active and reactive load curtailment.

In this chapter, the linearized DistFlow is utilized to enhance computation efficiency. It is verified in the literature that the result of the linearized DistFlow is approximate to the nonlinear DistFlow, and the error is acceptable, according to [60].

The nodal voltage can be calculated as (6.25), and the voltage magnitude of each node should be within the limit of (6.26).

$$V_{i,yqbs} - V_{j,yqbs} = \left(r_{ij} P_{ij,yqbs}^{B,D} + x_{ij} Q_{ij,yqbs}^{B,D}\right) / V_0, \quad \forall i, j \in \Omega, \forall y \in [1,Y], \forall q \in \mathcal{Q}, \forall b \in \mathcal{B}, \forall s \in \mathcal{S} \tag{6.25}$$

$$V^{\min} \le V_{i,yqbs} \le V^{\max}, \quad \forall i \in \Omega, \forall y \in [1,Y], \forall q \in \mathcal{Q}, \forall b \in \mathcal{B}, \forall s \in \mathcal{S} \tag{6.26}$$

where $V^{\min}$ and $V^{\max}$ are the minimum and maximum nodal voltage; V_0 is the reference voltage.

The branch current can be calculated as:

$$\left(I_{ij,yqbs}\right)^2 = \frac{\left(P_{ij,yqbs}^{B,D}\right)^2 + \left(Q_{ij,yqbs}^{B,D}\right)^2}{V_{j,yqbs}}, \quad \forall i, j \in \Omega, \forall y \in [1,Y], \forall q \in \mathcal{Q}, \forall b \in \mathcal{B}, \forall s \in \mathcal{S} \tag{6.27}$$

However, equation (6.27) is nonconvex. To convexify (6.27), it is relaxed into inequality as (6.28) and then reformulated into a second-order cone constraint as (6.29).

$$\left(I_{ij,yqbs}\right)^2 \ge \frac{\left(P_{ij,yqbs}^{B,D}\right)^2 + \left(Q_{ij,yqbs}^{B,D}\right)^2}{V_{j,yqbs}}, \quad \forall i, j \in \Omega, \forall y \in [1,Y], \forall q \in \mathcal{Q}, \forall b \in \mathcal{B}, \forall s \in \mathcal{S} \tag{6.28}$$

$$\left\| \left(2P_{ij,yqbs}^{B,D}, 2Q_{ij,yqbs}^{B,D}, V_{j,yqbs} - I_{ij,yqbs}\right) \right\|_2 \le V_{j,yqbs} + I_{ij,yqbs}, \quad \forall i, j \in \Omega, \forall y \in [1,Y], \forall q \in \mathcal{Q}, \forall b \in \mathcal{B}, \forall s \in \mathcal{S} \tag{6.29}$$

To ensure the cable thermal stability, the branch power flow should be limited as equations (6.30) and (6.31).

$$-x_{ij,y}^{L,D} P^{B,D,\max} \le P_{ij,yqbs}^{B,D} \le x_{ij,y}^{L,D} P^{B,D,\max}, \quad \forall i, j \in \Omega, \forall y \in [1,Y], \forall q \in \mathcal{Q}, \forall b \in \mathcal{B}, \forall s \in \mathcal{S} \tag{6.30}$$

$$-x_{ij,y}^{L,D} Q^{B,D,\max} \le Q_{ij,yqbs}^{B,D} \le x_{ij,y}^{L,D} Q^{B,D,\max}, \quad \forall i, j \in \Omega, \forall y \in [1,Y], \forall q \in \mathcal{Q}, \forall b \in \mathcal{B}, \forall s \in \mathcal{S} \tag{6.31}$$

where $P^{B,D,\max}$ and $Q^{B,D,\max}$ are the maximum active and reactive power capacity of the feeders.

With these constraints, the branch power flow is limited. Therefore, if the congestion happens, the power flow needs to be rerouted to ensure that the thermal overloading constraints can be satisfied.

In a medium and long-term planning model, the data are arranged based on the duration blocks and scenarios, where chronological information is missing. Hence, according to ref. [29], the representation of the energy balance equation of the BESS can be expressed as (6.32). The charging and discharging power of each BESS should be limited according to the current utilization state of the assets, shown as (6.33).

$$\sum_{b \in \mathcal{B}} \left[\Delta_{qb} \left(\eta^{CH} P_{i,yqbs}^{BESS,CH} - \frac{1}{\eta^{DS}} P_{i,yqbs}^{BESS,DS} \right) \right] = 0, \quad \forall i \in \Omega, \forall y \in [1,Y], \forall q \in \mathcal{Q}, \forall s \in \mathcal{S} \tag{6.32}$$

$$0 \le P_{i,yqbs}^{BESS,CH/DS} \le P^{BESS,\max} x_{i,y}^{BESS}, \quad \forall i \in \Omega, \forall y \in [1,Y], \forall q \in \mathcal{Q}, \forall b \in \mathcal{B}, \forall s \in \mathcal{S} \tag{6.33}$$

where η^{CH} and η^{DS} are the charging and discharging efficiency of the BESS; $P^{BESS,\max}$ is the maximum power of the BESS.

The power output of the substations is limited by their capacity, shown as (6.34).

$$0 \le P_{i,yqbs}^{SS} \le P^{SS,\max} x_{i,y}^{SS}, \quad \forall i \in \Omega, \forall y \in [1,Y], \forall q \in \mathcal{Q}, \forall b \in \mathcal{B}, \forall s \in \mathcal{S} \tag{6.34}$$

where $P^{SS,\max}$ is the maximum active power of the substations.

The power output of the DGs can be expressed as (6.35).

$$P_{i,r,yqbs}^{DG} = CF_{i,r,yqbs}^{DG} \cdot P_r^{DG,CAP} x_{i,r,y}^{DG}, \quad \forall i \in \Omega, \forall y \in [1,Y], \forall q \in \mathcal{Q}, \forall b \in \mathcal{B}, \forall s \in \mathcal{S}, \forall r \in \mathcal{R} \tag{6.35}$$

where $CF_{i,r,yqbs}^{DG}$ is the capacity factor of the r^{th} type of DGs; $P_r^{DG,CAP}$ is the maximum capacity of DGs.

1) Budget constraints

To ensure that the planning strategy is financially feasible, the budget at each planning stage can be constrained as (6.36).

$$C_y^{INV,D} \le BG_{y,s}, \quad \forall y \in [1,Y], \forall s \in \mathcal{S} \tag{6.36}$$

where $BG_{y,s}$ is the budget of the y^{th} planning stage.

2) FCS charging demand constraints

The charging demand at the FCSs can be estimated based on the traffic capture of the FCSs, shown as (6.37). The traffic capture of the FCSs is derived in section II, part (C).

$$P_{i,yqbs}^{FCS} = D_{yq}^{CH}\kappa \frac{f_{yqbs}^{trip}}{\sum_{b\in\mathcal{B}}\sum_{s\in\mathcal{S}} f_{yqbs}^{trip}} \frac{f_{i,t}^{cap}}{\sum_{i\in\Omega^{FCS}} f_{i,t}^{cap}} \mathbb{I}\left(x_{i,y}^{FCS}\right), \forall i\in\Omega, \forall y\in[1,Y], \forall q\in\mathcal{Q}, \forall b\in\mathcal{B}, \forall s\in\mathcal{S} \quad (6.37)$$

where $P_{i,yqbs}^{FCS}$ is the charging demand of FCSs; D_{yq}^{CH} is the system total charging demand; $\mathbb{I}\left(x_{i,y}^{FCS}\right)$ is the indicator function, which equals one if $x_{i,y}^{FCS} > 0$ and zero otherwise.

To ensure that the planning result can provide sufficient fast charging services, the charging provided by FCSs should be higher than a certain percentage of the total charging demand.

$$\sum_{i\in\Omega^{FCS}}\sum_{b\in\mathcal{B}}\sum_{s\in\mathcal{S}} \pi_{qbs}\Delta_{qb}P_{i,yqbs}^{FCS} \geq \ell D_{yq}^{CH}\kappa, \quad \forall y\in[1,Y], \forall q\in\mathcal{Q} \quad (6.38)$$

where ℓ is the minimum EV charging demand ratio at FCS.

3) Planning variable constraints

The utilization states of different assets evolve according to planning decisions at each stage shown as (6.39). The initial utilization states of the assets can be expressed as (6.40).

$$x_{i,y}^{(\cdot)} = x_{i,y-1}^{(\cdot)} + \delta_{i,y}^{(\cdot)}, \quad x_{ij,y}^{L,D} = x_{ij,y-1}^{L,D} + \delta_{ij,y}^{L,D}, \quad \forall i,j\in\Omega, \forall y\in[1,Y] \quad (6.39)$$

$$x_{i,y}^{(\cdot)} = \hat{x}_{i}^{(\cdot)}, \quad x_{ij,y}^{L,D} = \hat{x}_{ij}^{L,D}, \quad \forall i,j\in\Omega, \forall y\in[1,Y] \quad (6.40)$$

where $\hat{x}_{i}^{(\cdot)}$ and $\hat{x}_{ij}^{L,D}$ are the initial utilization state.

$$\sum_{i\in\Omega^{FCS}} x_{i,y}^{FCS} \geq \chi_{y}^{FCS}, \quad \forall y\in[1,Y] \quad (6.41)$$

where χ_{y}^{FCS} is the least capacity of the FCSs to be planned.

To ensure network radiality, the following constraints should be considered according to [338]:

$$\sum_{(i,j)\in\Omega^{L}} \varpi_{ij,y} = N^{B} - 1, \quad \forall y\in[1,Y] \quad (6.42)$$

$$\varpi_{ij,y} \leq \varpi_{ij,y+1}, \varpi_{ij,y} \leq x_{ij,y}^{L}, \quad \forall i,j\in\Omega, \forall y\in[1,Y] \quad (6.43)$$

$$\varpi_{ij,y} \in \{0,1\}, \quad \forall i,j\in\Omega, \forall y\in[1,Y] \quad (6.44)$$

$$-\varpi_{ij,y}\Upsilon \leq P_{ij,yqbs}^{B,D} \leq \varpi_{ij,y}\Upsilon, \quad \forall i,j\in\Omega, \forall y\in[1,Y], \forall q\in\mathcal{Q}, \forall b\in\mathcal{B}, \forall s\in\mathcal{S} \quad (6.45)$$

$$-\varpi_{ij,y}\Upsilon \leq Q_{ij,yqbs}^{B,D} \leq \varpi_{ij,y}\Upsilon, \quad \forall i,j\in\Omega, \forall y\in[1,Y], \forall q\in\mathcal{Q}, \forall b\in\mathcal{B}, \forall s\in\mathcal{S} \quad (6.46)$$

where $P_{ij,yqbs}^{B,D}$ and $Q_{ij,yqbs}^{B,D}$ are the active and reactive power flow; N^{B} is the number of the buses; Υ is a large

positive number; $\varpi_{ij,y}$ is the connection status between buses *i* and *j*. If there is a feeder between buses *i* and *j*, $\varpi_{ij,y}$ =1; otherwise, $\varpi_{ij,y}$=0.

The uncertainties in the planning model mainly include renewable energy generation and EV usage growth. The model calibration is conducted based on the Monte Carlo simulation. Monte Carlo analysis is deployed for Y-year simulation repeatedly with random seeds to obtain the most likely results from the stochastic simulation as well as the prediction model. Since the prediction model is not the main contribution of this chapter, the detailed model calibration is not provided in the manuscript. The model calibration for renewable energy generation and EV diffusion can be referred to refs. [337, 339].

6.4 Quality-of-service Assessment

6.4.1 Queueing Model

The QoS assessment of the FCSs is analyzed based on the queueing model. In this chapter, we utilize the $M_1/M_2/N$ queuing model, where M_1 denotes the arrival rate, which follows a non-homogenous Poisson process; *M2* denotes the service time that follows a negative exponential distribution; *N* denotes the number of servers. The number of servers equals the utilization state of the FCSs $x_{i,y}^{FCS}$. According to ref. [340], the probability of the number of EVs charging simultaneously can be expressed as:

$$P_t(n)=\frac{(N\rho)^n}{n!}P_t(0),\quad \forall t\in[1,T], \tag{6.47}$$

where ρ is the occupation rate.

The probability that no EV is in the FCS $P_t(0)$ is:

$$P_t(0)=\left[\sum_{m=0}^{N-1}\frac{(N\rho)^m}{m!}+\frac{(N\rho)^N}{N!}\frac{1}{1-\rho}\right]^{-1},\quad \forall t\in[1,T], \tag{6.48}$$

The occupation rate of the FCS can be expressed as:

$$\rho=\lambda_t/(N\mu_t),\quad \forall t\in[1,T] \tag{6.49}$$

where A_t is the arriving rate; μ_t is the service rate.

The expected number of EVs waiting at the FCS can be estimated by the Little's Law in queuing theory, shown as (6.50).

$$\mathbb{E}\left[N_t^W\right]=P_t(0)\left[\frac{1}{(N-1)!}\left(\frac{A_t}{\mu_t}\right)^N\frac{A_t\mu_t}{\left(N\mu_t-A_t\right)^2}\right],\ \ \forall t\in[1,T] \tag{6.50}$$

Consequently, the expected waiting time of the EVs is:

$$T_t^W=\mathbb{E}\left[N_t^W\right]/A_t,\ \ \forall t\in[1,T] \tag{6.51}$$

6.4.2 QoS Assessment Considering Leaving Behaviors

In fact, a long queue will also result in leaving behaviors, which brings disutility to the customers. In this chapter, the leaving behaviors are categorized into *refusing to join* and *impatient leave*. The leaving behaviors are considered in the QoS metric.

When arriving at the FCS, the EV finds the waiting line is too long and thus refuses to join the queue, even if the total vehicle number is less than the maximum queueing length *H*. The probability that an EV will choose to queue is relevant to the vehicle number in the FCS and is assumed to be

$$\mathrm{Pr}_t^{CJ}(n)=\begin{cases}1 & n<N\\ e^{-(n-N)\xi} & N\le n\le H\\ 0 & n>H\end{cases},\ \ \forall t\in[1,T] \tag{6.52}$$

where ξ is the probability decrease rate; N is the number of charging infrastructure, which equals the utilization variables u^{HRS}; H is the maximum queuing length.

Even if the waiting line is not too long, the queuing EVs may still choose to leave the FCS when they get too impatient. The number of EVs left in the queue during each time interval is assumed to be:

$$IL_t(n)=\begin{cases}0 & n\le N\\ \ell\ln(n-N+1) & N\le n\le H\end{cases},\ \ \forall t\in[1,T] \tag{6.53}$$

where ℓ is the probability of leaving the FCS.

Considering the two leaving conditions above, the arriving rate A and leaving rate Γ can be updated as:

$$\mathrm{A}_t(n)=\mathrm{Pr}_t^{CJ}(n)\cdot\mathrm{A},\Gamma_t(n)=\Gamma-IL_t(n),\ \ \forall t\in[1,T] \tag{6.54}$$

According to Markov chain analysis and stochastic process theory, $\mathrm{Tr}(\cdot)$, the steady-state probability of the Markov chain being in at state *k*, should satisfy the balance equation:

$$\sum_{n\in\Pi}\mathrm{Pr}_t(n)=1,\mathrm{Pr}_t(n)\sum_{h\in\Pi}\mathrm{Tr}_t(n,h)=\sum_{n\in\Pi}\mathrm{Pr}_t(h)\mathrm{Tr}_t(h,n),\ \ \forall t\in[1,T] \tag{6.55}$$

where $\mathrm{Tr}_t(n,h)$ is the transition rate from state *n* to *h*; Π is the state space.

Equation (6.55) means that the sum of all state probabilities should be 1. Also, the probability in and out of each

state should be equal.

In our problem, the state transitions in the FCS only have *arriving* and *leaving*. Therefore, the FCS balance equation can be expressed as:

$$\left(\mathrm{A}_t(n)+\Gamma_t(n)\right)\mathrm{Pr}_t(n)=\mathrm{A}_t(n-1)\mathrm{Pr}_t(n-1)+\Gamma_t(n+1)\mathrm{Pr}_t(n+1),\quad \forall t\in[1,T] \tag{6.56}$$

Then, combining equations (6.47)-(6.56), the probability that *k* EVs are simultaneously in FCS can be updated as:

$$\mathrm{Pr}_t(n)=\begin{cases}\left(\left(\mathrm{A}_t(n)/\Gamma_t(n)\right)^n/n!\right)\mathrm{Pr}_t(0) & 0<n\le N\\ \dfrac{e^{\frac{-(n-N)(n-N-1)}{2}\sigma}\left(\mathrm{A}_t(n)/\Gamma_t(n)\right)^n}{N!\prod_{\chi=1}^{n-N}[N+(\ell/\Gamma_t(n))\ln(\chi+1)]}\mathrm{Pr}_t(0) & N<n\le H\end{cases},\quad \forall t\in[1,T] \tag{6.57}$$

The probability that no EV is in the FCS $\mathrm{Pr}_t(0)$ is:

$$\mathrm{Pr}_t(0)=\left\{\sum_{n=0}^{N}\frac{\left(\mathrm{A}_t(n)/\Gamma_t(n)\right)^n}{n!}+\sum_{n=N+1}^{H}\frac{e^{\frac{-(n-N)(n-N-1)}{2}\xi}\left(\mathrm{A}_t(n)/\Gamma_t(n)\right)^n}{N!\prod_{\chi=1}^{n-N}\left[K+(\ell/\Gamma_t(n))\ln(\chi+1)\right]}\right\}^{-1},\quad \forall t\in[1,T] \tag{6.58}$$

The expected number of EVs in FCS can be expressed as:

$$\mathbb{E}\left[N_t^W\right]=\sum_{n=0}^{N}n\,\mathrm{Pr}_t(n)+N\sum_{w=N+1}^{H}\mathrm{Pr}_t(n),\quad \forall t\in[1,T] \tag{6.59}$$

To ensure the QoS, we designed a chance-constrained QoS assessment. First, the probability that the expected waiting time at the FCS is less than c_1 should be larger than β_1.

$$\mathrm{Pr}\left\{\lim_{t\to\infty}\frac{1}{t}\sum_{t}\mathbb{E}\left[N_t^W\right]/\mathrm{A}_t\le c_1\right\}\ge\beta_1 \tag{6.60}$$

Besides, the probability that the expected number of EVs that leave the queue is less than c_2 should be larger than β_2.

$$\mathrm{Pr}\left\{\lim_{t\to\infty}\frac{1}{t}\sum_{t}\begin{bmatrix}\int_{k=0}^{H}\left[\mathrm{A}_t\,\mathrm{Pr}_t(n)\cdot\left(1-\mathrm{Pr}_t^{CJ}(n)\right)\right]dn\\ \int_{k=0}^{H}\left[\mathrm{Pr}_t(n)\,IL_t(k)\,dn\right]\end{bmatrix}\le c_2\right\}\ge\beta_2 \tag{6.61}$$

To ensure that the planning of the FCSs can adapt to the EV diffusion, the QoS assessment is conducted to ensure the charging infrastructures can provide high-quality services. Before QoS assessment, the traffic flow needs to be reassigned according to (6.5)-(6.12), since the locations of FCSs will change the driving patterns of vehicles and thus influence the traffic flow. The proposed traffic assignment model separates the EV traffic flow from the conventional

ICE vehicle traffic flow. Besides, it further considers the charging behaviors of EVs and the distance from FCSs. Therefore, the influence of FCSs on the traffic flow can be reflected. Then, we propose a QoS-based planning strategy for FCSs and distribution systems. If the current solution fails to pass the QoS assessment at a specific planning stage, the system at this stage needs to be re-planed by increasing the value of χ_y^{FCS} in (6.41) manually. The process is shown as follows:

Proposed QoS-based planning strategy:

Initialization: Obtain the system parameters and scenarios
Solve the initial DEP (6.15)-(6.46)
Flag=false
while (*Flag=false***) do:**
  Metric=true
  for (*y*=1:*Y*)**:** // Traverse all the planning stages
    Reassign the traffic flow (6.5)-(6.12)
    Simulate the queue model based on Monte Carlo simulation.
    if either QoS metric 1 or QoS metric 2 is not satisfied
      then Re-plan the FCS and the distribution system at the y^{th} planning stage (6.15)-(6.46)
      Metric=false
      break
  end
  if *Metric=true*
    then *Flag=true*
end
Output: final planning solution

6.5 Adaptive Planning Strategy Considering the TEP

Due to the diffusion of EVs, the charging demand will gradually increase. Hence, the increase of the total load in the distribution system may lead to an expansion in the transmission system. Usually, the distribution network and transmission network belong to different companies or entities. The distribution company and the transmission company have little information exchange in reality. Also, in most references, the transmission and distribution networks were planned independently of each other. This may lead to the potential waste of redundant assets and the lack of effective coordination between different system levels. To eliminate these problems, cooperation between the distribution networks and the transmission networks is necessary. For example, the AEMO does not own any energy network assets. However, it acts as a coordinator to provide planning guidance and facilitate the cooperation between distribution networks and transmission networks. It should be noted that the proposed integrated planning through cooperation will

bring incentives to both the transmission and distribution companies so that all the participants have the motivation to join the coalition. When independent planning strategies are applied, an entity is required to assume the expansion plans of the other entities due to lacking communication. Under this situation, a potential increase in the investment cost of redundant assets or the reduced reliability may occur to both the transmission and distribution companies due to underestimating or overestimating the expanded capacity of the other entities. The use of the integrated planning strategy can overcome the weaknesses associated with the functional decoupling of transmission and distribution network planning. Through cooperation, social welfare is increased, and the total cost can be reduced. Hence, reasonable cost/profit allocation methods, such as Sharply value (the more contributions, the more gains) and Nucleolus (ensure everyone is willing to stay in the coalition), can be applied to compensate for the compromise/economic sacrifice of participants so that every participant can gain interest through cooperation [341]. It should be noted that this chapter is from an engineering perspective to investigate a planning strategy for FCSs and electricity networks and the commercial mode, negotiation protocol, as well as the design of profit allocation methods and incentive mechanisms, are beyond the scope of this chapter.

Hence, in this chapter, we assume that the distribution network and transmission network can cooperate with each other to cope with the increasing EV charging demand and other future uncertainties. In this chapter, the TEP cost is considered as a kind of adaptive cost arising from the EV diffusion and normal load growth. Therefore, we propose an adaptive integrated network expansion strategy where the impact of the EV diffusion on the DEP and TEP can be comprehensively considered, shown as (6.62).

$$Min\left\{\sum\nolimits_{\varsigma} F_{\varsigma}^{DEP} + F^{TEP}\right\} \tag{6.62}$$

where F_{ς}^{DEP} is the planning cost of the ς^{th} distribution system; F^{TEP} is the adaptive planning cost of the transmission system.

The TEP problem can be formulated as (6.63)-(6.67). Due to the page limit, the TEP problem is written in a compact form [342]. The detailed mathematical model can be referred to [35].

$$Min.F^{TEP} = \mathbf{a}^{T}\,\mathrm{x} + \mathbf{b}^{T}\,\mathrm{y} \tag{6.63}$$

s.t.

$$\mathbf{A}\,\mathrm{x} \le \mathbf{c} \tag{6.64}$$

$$\mathbf{B}\,\mathrm{x} + \mathbf{C}(\mathrm{x})\,\mathrm{y} = \mathbf{d} \tag{6.65}$$

$$\mathbf{D}\,\mathrm{x} + \mathbf{E}\,\mathrm{y} + \mathbf{F}\,\mathrm{z} \le \mathbf{e} \tag{6.66}$$

$$\mathrm{x}, \mathrm{z} \in \{0,1\} \tag{6.67}$$

where x is vector of the expansion variables; y is the continuous operation variables; z is the binary operation

variables; $\mathbf{A}$, $\mathbf{B}$, $\mathbf{C}$, $\mathbf{D}$, $\mathbf{E}$, and $\mathbf{F}$ are the coefficient matrices; $\mathbf{a}$, $\mathbf{b}$, $\mathbf{c}$, $\mathbf{d}$ and $\mathbf{e}$ are the coefficient vectors.

The objective function (6.63) minimizes the total cost in TEP, composing both the investment and operating costs. Constraint (6.64) imposes an investment budget. Constraints (6.65) and (6.66) model the operating feasibility set, including the power balance, power flow limits through existing and candidate transmission lines, the capacity limits of the power sources, etc.

When considering the integrated planning of the distribution system and the transmission system, the interface nodes are modeled as (6.68), which is the power balance equation of the nodes connecting the transmission and distribution levels.

$$P_{i,yqbs}^{LD,T} = P_{i,yqbs}^{SS}, \quad \forall i \in \Omega, \forall y \in [I, Y], \forall q \in \mathcal{Q}, \forall b \in \mathcal{B}, \forall s \in \mathcal{S} \tag{6.68}$$

Based on the DEP strategy in sections III and IV, the distribution companies first generate several candidate planning plans for the distribution networks. The candidates are the optimal and several sub-optimal solutions of the optimization problem that have passed the QoS assessment. Then we further solve the stochastic TEP planning for each candidate solution and obtain the adaptive cost. A lower adaptive cost means that the DEP planning strategy is more flexible because fewer changes happen at the transmission level. The final plan, which is decided by the distribution companies and the transmission company together, is selected based on the minimum total cost. The transmission company is responsible for the optimization, and the distribution companies take the role of supervision to make sure that the transmission company fulfills the cooperation agreement. After the optimal solution is obtained, the distribution companies have to accept the final plan because the changes in the planning solution of any entity will affect the other entities' interests. Through the proposed adaptive planning strategy, the solution that maximizes the total social welfare can be selected from several available alternatives for the line expansion as well as fossil-fuel and renewable-based generator expansion at both system levels. The procedure of the adaptive integration network planning is shown as follows:

Proposed adaptive integrated network planning:

Initialization: Obtain all the DEP candidate**s** (6.15)-(6.61)
for *Plan*=1:*Tot_plan***:** // Traverse all the DEP strategies
  for *Scn*=1:*Tot_scn***:** // Traverse all the future scenarios
    Generate future scenarios randomly
    Solve TEP planning problem (6.63)-(6.68)
  end
    Calculate the weighted average *adaptive cost* of TEP
    total cost=DEP cost+adaptive cost
end

Select the plan with the lowest total cost (6.62)

There are mainly two main methods to find the candidate solution for distribution companies. The first method is to tune the value of customer reliability λ^{US}. This parameter turns the unserved load into the monetary unit, and its value determines how the planner is concerned about the system's reliability. The planner can solve various candidate plans by tuning this parameter, and these plans do not have distinguishment between optimal and sub-optimal. The second method is to utilize the heuristic optimization algorithm to obtain the sub-optimal value. In heuristic algorithms, including the genetic algorithm, particle swarm optimization, etc., the feasible individuals with a lower fitness value than the optimal individual are considered as the sub-optimal solutions. In this chapter, we apply the second method.

6.6 Case Study

The proposed planning framework and methodology are verified in the IEEE 24-bus system, which encompasses 6 IEEE 33-bus distribution networks connected to buses 4, 5, 6, 14, 19, and 20, shown in Fig. 6-2. For each distribution system, the electric grid is coupled with the transportation network, as shown in Fig. 6-3. In the simulation, the total planning horizon is divided into five stages, and each stage consists of five years.

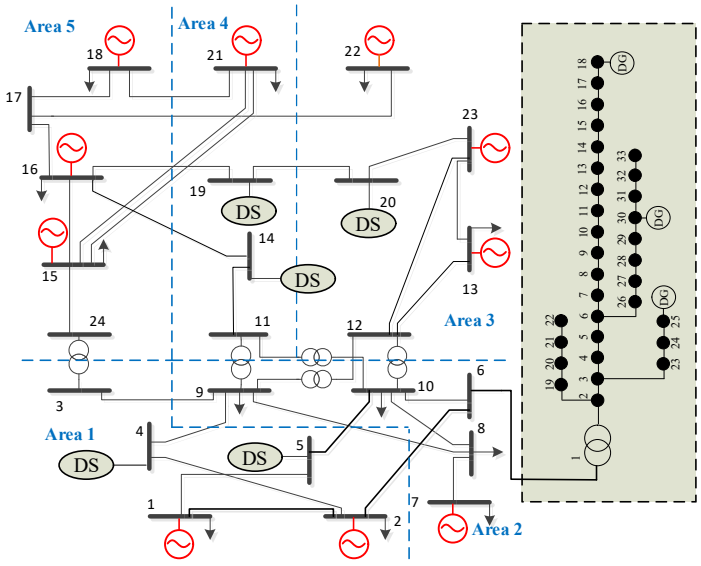

Fig. 6-2. IEEE 24-bus system encompassing 6 IEEE 33-bus distribution networks.

To verify the advantages of the proposed planning model, four cases are established.

Case 1: A FCS planning strategy proposed in [101] without considering the QoS assessment and adaptive cost of TEP.

Case 2: The FCSs are planned without conducting a QoS assessment. The integrated distribution system and transmission system planning is realized according to [13].

Case 3: The QoS assessment is conducted to ensure that the FCS planning strategy can provide high-quality services

under EV diffusion. However, the distribution and transmission systems are planned independently and sequentially.

Case 4: The proposed planning strategy considers the QoS assessment and adaptive cost of TEP under EV diffusion.

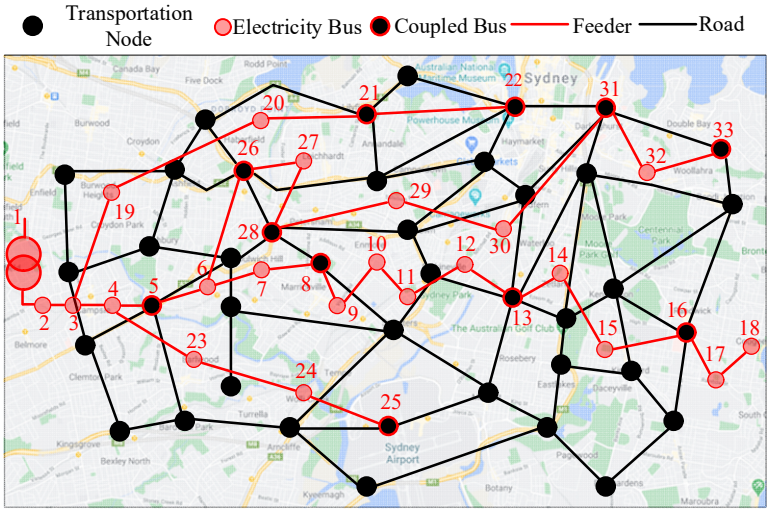

Fig. 6-3. Coupling electricity and transportation network at transmission bus 6.

The simulations were completed by a PC with an Intel Core (TM) i7-9750 CPU @ 2.60 GHz with 16.00 GB RAM.

6.6.1 Simulation Result

In the simulation, we first predict the penetration level of the EVs based on the EV diffusion model proposed in [337]. Fig 6-4. displays the EV penetration level of the first and last planning stages for the distribution system located at bus 6. It can be found that at the start of the planning horizon, the penetration level of EVs is relatively low, which indicates a low charging demand. At the end of the planning horizon, the penetration level of EVs is increased to a large extent in different regions, and it indicates that the total charging demand brings challenges to the planning of the charging infrastructures. It is also found that the EV adopters are showing up in clusters and are radial toward neighboring regions with prosperous areas as centers due to the neighboring influence.

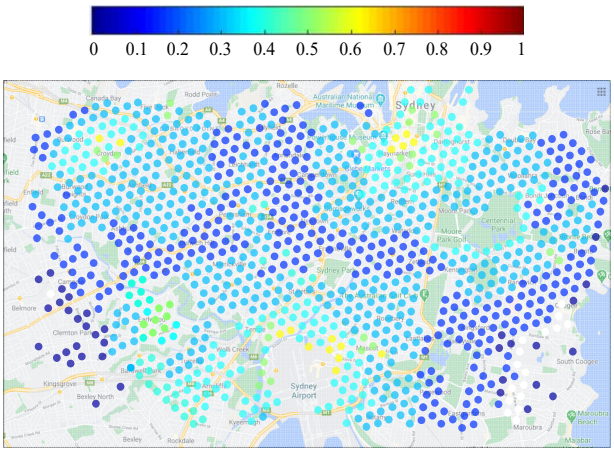

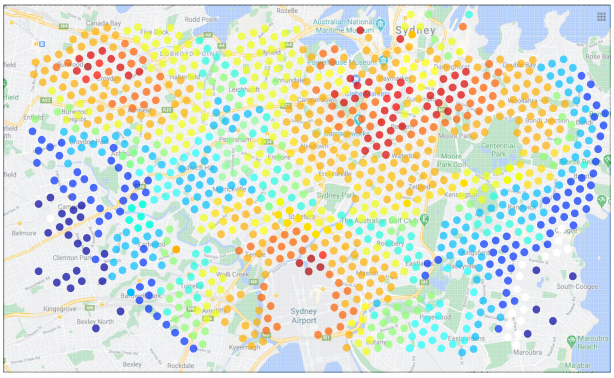

Fig. 6-4. The simulation result of EV diffusion at the start (top) and the end (bottom) of the planning horizon.

Fig. 6-5 shows the planning result of this distribution network at the end of the planning horizon. There are five FCSs planned in total. The FCSs are located at the transportation nodes. If the location of the FCS is not a transportation and electricity coupling node, a new feeder is required to construct to ensure the electric supply of the FCS. To ensure that the distribution system can work under the operation constraints, some feeders are expanded, and the DGs and BESSs are planned to provide supplies to charging infrastructures and the other loads.

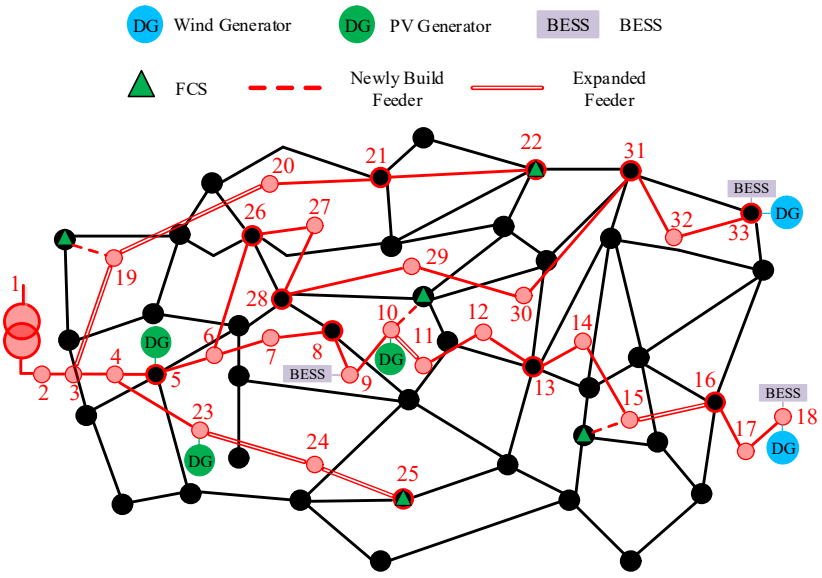

Fig. 6-5. The planning result of the proposed strategy at the end of the planning horizon.

Candidate transmission line New built transmission line

To further intuitively display the planning result of Cases 3 and 4 in the transmission system, we further provide the changes in the typology in Fig. 6-6. It can be found that without cooperation between transmission networks and distribution networks, four additional transmission lines are selected from the candidate lines. If the proposed adaptive planning is applied, two new transmission lines from buses 11 to 16 and from buses 2 to 5 are built.

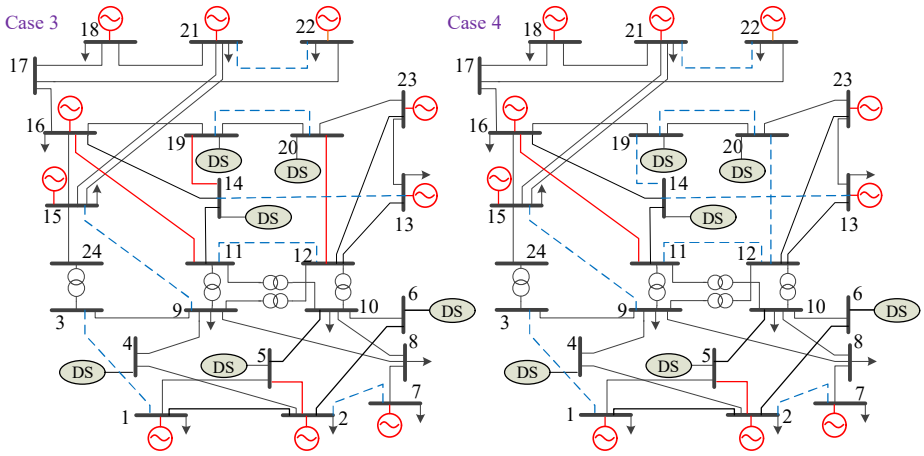

Fig. 6-6. The planning result of the transmission system in Cases 3 and 4.

6.6.2 Case Comparison

In this section, the proposed planning strategy (Case 4) is compared with the other three cases. Tables 6-1 to 6-4 show the investment decisions at different stages in different cases. In general, more FCSs are planned in Cases 3 and 4 to ensure the QoS, and more DGs and BESS are planned in Cases 2 and 4 because they consider the adaptive cost in TEP.

TABLE 6-1. INVESTMENT DECISION-CASE 1

Investment		Stage 1	Stage 2	Stage 3	Stage 4	Stage 5
DG	PV	10				
	Wind		33			
BESS			18			
Feeder	New	10-FCS			29-FCS	
	Expand	1-2		3-19	20-21	
		2-3		19-20	21-22	
FCS		10		22	29	

TABLE 6-2. INVESTMENT DECISION-CASE 2

Investment		Stage 1	Stage 2	Stage 3	Stage 4	Stage 5
DG	PV				10	23
	Wind		33		18	
BESS			33		18	
Feeder	New			29-FCS	10-FCS	
	Expand		1-2		10-11	23-24
			2-3		11-12	24-25
FCS		22		29	10	25

TABLE 6-3. INVESTMENT DECISION-CASE 3

Investment		Stage 1	Stage 2	Stage 3	Stage 4	Stage 5
DG	PV	10				
	Wind					18
BESS		9				
Feeder	New	10-FCS				15-FCS
	Expand	1-2	4-23	23-24	3-19	15-16

		2-3		24-25	19-20	
FCS		10	25	22	26	15

TABLE 6-4. INVESTMENT DECISION-CASE 4

Investment		Stage 1	Stage 2	Stage 3	Stage 4	Stage 5
DG	PV			5, 10	23	
	Wind				18	33
BESS		9		18		33
Feeder	New	10-FCS			19-FCS	15-FCS
	Expand	3-19	19-20	23-24		15-16
		10-11	20-21	24-25		
FCS		10		25, 22	19	15

Fig. 6-7 compares four different cases in terms of the average queue at FCS, average leaving rate, average waiting time, and the average number of services. First, from the perspective of the number of services that FCSs provide, it increases with the diffusion of the EVs, and different cases do not show a large difference in this aspect. It indicates that the charging demand for EVs can be satisfied in all cases. Second, the queue length and the waiting time of Cases 1 and 2 are higher than Cases 3 and 4 in all stages. This is because Cases 1 and 2 do not consider the QoS. Besides, the waiting time and the queue length of four cases are increasing because of the increasing charging demand. At the early planning stages, the waiting time and the queue length of all cases are low because the penetration level of EVs is low. In Cases 1 and 2, the waiting time and the queue length increase dramatically under the EV usage growth. However, when considering the QoS in the planning strategy, this increasing trend is reduced. A similar pattern can also be found in the average leaving rate. Fewer EVs refuse to join the queue or leave the queue impatiently at the early stage because the queue length at the FCSs is short. It indicates less disutility is caused by queueing. However, with the increasing penetration level of EVs, more and more EVs choose to leave the queue in Cases 1 and 2, while the leaving rate of Cases 3 and 4 can be maintained. Therefore, it can be concluded that although Cases 1 and 2 provide the relatively same number of services, they cannot ensure a high-quality service under EV usage growth. In contrast, when conducting the QoS assessment in the FCS planning strategy, the QoS of the charging services can be ensured, which is essential to the popularization of EVs.

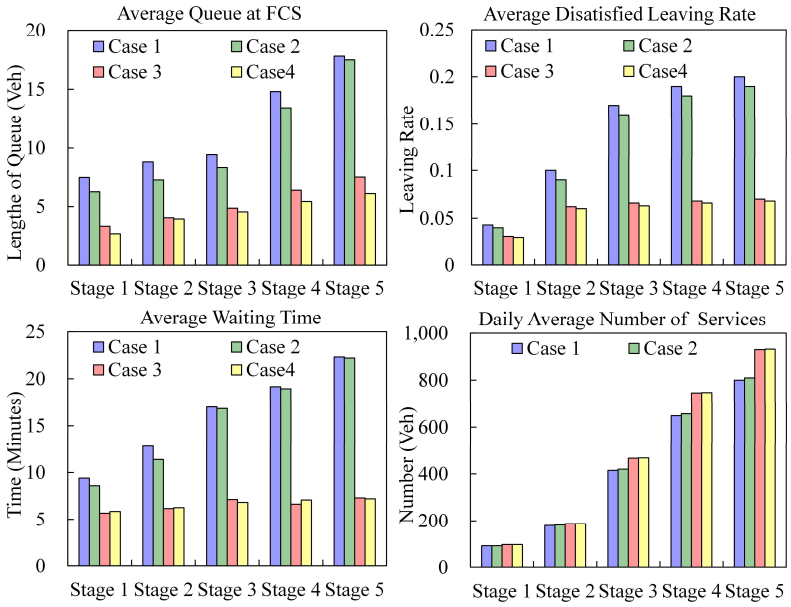

Fig. 6-7. The comparison between different cases in terms of the average queue, dissatisfied leaving rate, waiting time, and the number of services at FCSs.

Figs. 6-8 and 6-9 compare the probability distributions of the queue length and the number of EVs leaving the queue per day at the end of the planning stage. An interesting finding is that the tails of the distributions in Case 3 and Case 4 are close to the 80% confidence interval of the distributions in Case 1 and Case 2. It means that the QoS is significantly improved by applying the QoS assessment method.

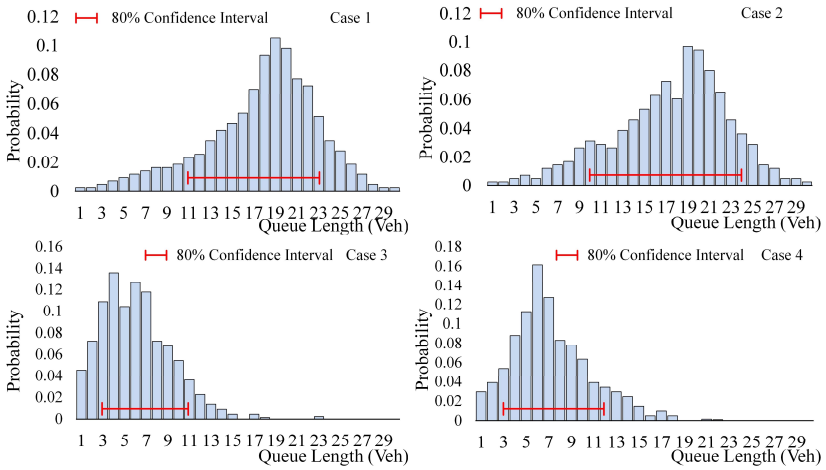

Fig. 6-8. The probability distribution of the queue lengths in four cases.

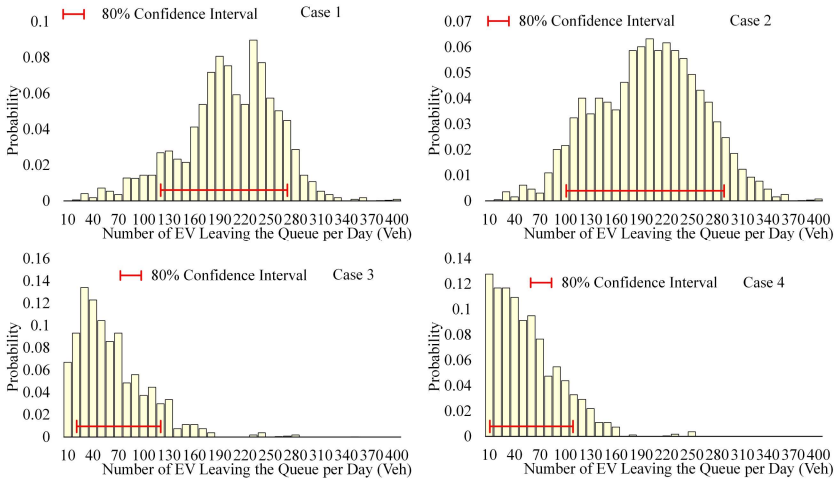

Fig. 6-9. The probability distribution of the number of EVs leaving the queue per day in four cases.

Then, the four cases are compared in terms of investment and operation cost in Tables 6-5 to 6-8. It can be concluded that Case 2 has the lowest total cost ($2.257 billion). That is because in Case 2, fewer FCSs are planned compared with Cases 3 and 4. However, combined with the previous simulation result, Case 2 shows poor performance in QoS, especially at the end of the planning stage. Case 3 has the highest total cost ($2.325 billion), but the QoS at all stages is ensured. Case 4 has the second-lowest total cost ($2.262 billion), and its QoS is also guaranteed under different penetration levels of EVs. Comparing Case 3 and Case 4, the main saving occurs in the adaptive cost in TEP. It indicates that in Case 4, more DGs and BESS are invested to satisfy the local loads, while in Case 3, more electricity is transmitted from the transmission level resulting in higher TEP cost. Besides, Case 4 has the lowest energy loss and load curtailment cost, which is $6.11 million and $31.12 million, respectively. That is because more FCSs are built so that the charging demand can be distributed to different nodes, and more DGs and BESS are planned to improve the electricity quality. Therefore, it indicates that the proposed planning strategy may encounter fewer voltage problems in active distribution systems.

TABLE 6-5. INVESTMENT AND OPERATION COST-CASE 1 (10^8 $)

Cost	Stage 1	Stage 2	Stage 3	Stage 4	Stage 5
Investment	1.8231	0.6962	0.7892	1.6321	0.5212
Energy	0. 9832	1.0923	1.2025	1.6203	1.8324
Maintenance	0.0646	0.0655	0.0676	0.0692	0.0721
Energy Loss	0.0131	0.0133	0.0137	0.0139	0.0140
Curtailed load	0.0672	0.0682	0.0692	0.0700	0.0702
Adaptive Cost	1.8924	2.0157	2.7821	3.0312	1.2315
Total: 22.914					

TABLE 6-6. INVESTMENT AND OPERATION COST-CASE 2 (10^8 $)

Cost	Stage 1	Stage 2	Stage 3	Stage 4	Stage 5
Investment	1.0623	2.0152	1.6602	2.9231	1.6721

Energy	0.8932	0.9001	0.9399	0.9721	1.1031
Maintenance	0.0378	0.0641	0.0702	0.0783	0.0800
Energy Loss	0.0125	0.0123	0.0129	0.0130	0.0130
Curtailed load	0.0653	0.0600	0.0612	0.0666	0.0652
Adaptive Cost	1.4023	1.6001	1.6203	1.5642	1.5315
Total: 22.5721					

TABLE 6-7. INVESTMENT AND OPERATION COST-CASE 3 (10^8 $)

Cost	Stage 1	Stage 2	Stage 3	Stage 4	Stage 5
Investment	2.7832	1.0932	1.8325	1.8881	2.1383
Energy	0.8301	0.8731	0.9213	0.9983	1.1345
Maintenance	0.0698	0.0699	0.0703	0.0713	0.0735
Energy Loss	0.012	0.0121	0.0126	0.0129	0.0132
Curtailed load	0.0641	0.0663	0.0666	0.0682	0.07
Adaptive Cost	1.5215	2.0213	1.5123	1.6213	1.3321
Total: 23.2539					

TABLE 6-8. INVESTMENT AND OPERATION COST-CASE 4 (10^8 $)

Cost	Stage 1	Stage 2	Stage 3	Stage 4	Stage 5
Investment	2.1627	0.8912	3.0123	1.8321	1.8672
Energy	0.8855	0.8983	0.9013	0.9512	1.1024
Maintenance	0.0678	0.0699	0.0711	0.0752	0.0785
Energy Loss	0.012	0.012	0.0121	0.0123	0.0127
Curtailed load	0.0623	0.0638	0.0592	0.0636	0.0623
Adaptive Cost	1.3121	1.7215	1.6523	1.5229	1.1724
Total: 22.6202					

6.7 Chapter Summary

In this chapter, we propose an adaptive integrated planning of electricity networks and FCSs under EV diffusion. First, based on the EV diffusion model and the proposed EV-integrated traffic assignment model, the spatial and temporal charging demands are simulated. Second, a multistage stochastic DEP model is presented, where the substations, feeders, DGs, BESS, and FCSs are jointly considered. Third, a QoS assessment is conducted to ensure that the planning solutions can provide high-quality charging services under EV diffusion. Finally, the integrated planning strategy of transmission and distribution systems is proposed. The cost of the TEP is considered as the adaptive cost arisen from the EV diffusion and the increase of the other normal loads. Based on the presented planning framework and methodologies, we aim to find an adaptive planning strategy that can adapt to a different penetration level of EVs. The proposed strategy is verified in IEEE 24-bus transmission systems encompassing 6 IEEE 33-bus distribution networks. Compared with the planning strategy in the state-of-art works, it can be concluded that the proposed method has a relatively lower total cost while ensuring the QoS. Besides, the proposed strategy has the lowest energy loss and

load curtailment cost, which indicates that the proposed planning strategy may encounter fewer electric issues in the active distribution systems.

CHAPTER 7

INTEGRATION OF FUEL CELL ELECTRIC VEHICLES IN MULTI-ENERGY NETWORK

Hydrogen is a promising energy carrier to mitigate environmental pollution and climate change. At the current stage, although hydrogen production is not commercialized due to high costs, governments are putting more emphasis on the application of hydrogen technologies. For instance, the Japanese government, the presidency of G20 in 2019, presented a report to the International Energy Agency (IEA) regarding the future of hydrogen. In this report, it is pointed out that "hydrogen holds long-term promise in many sectors beyond existing industrial applications, and the transport, buildings, and power sectors all have the potential to use hydrogen" [343]. The Australian government also formulates a series of development strategies for the hydrogen industry [344, 345]. It is believed that the development of hydrogen technologies can contribute to the achievement of an extra-low-carbon integration of power and transportation systems. Hydrogen serves as the fuel of modern fuel cell electric vehicles (FCEVs), which has the advantages of fast and convenient refueling and exhibit the potential of zero-carbon mobility. Although hydrogen FCEVs have a bright future, one of the main obstacles hindering the commercialization of FCEVs is the insufficient establishment of the hydrogen refueling system. In this chapter, we propose a multi-network coordinated planning strategy for hydrogen refueling stations (HRSs)and hydrogen production stations (HPSs).

7.1 Hydrogen Production and Refueling Station Modeling and Hydrogen Supply Chain

7.1.1 Multi-Network Hydrogen Refueling System

In this chapter, a multi-network planning framework for the hydrogen refueling system is proposed, as shown in Fig. 7-1. A hydrogen refueling system for FCEVs is mainly composed of HRSs, HPSs (P2G devices and liquefaction devices), hydrogen storage, and the hydrogen delivery network. Different from the on-site hydrogen generation setting in some references, the proposed system structure allows the HPSs and HRSs located at different places.

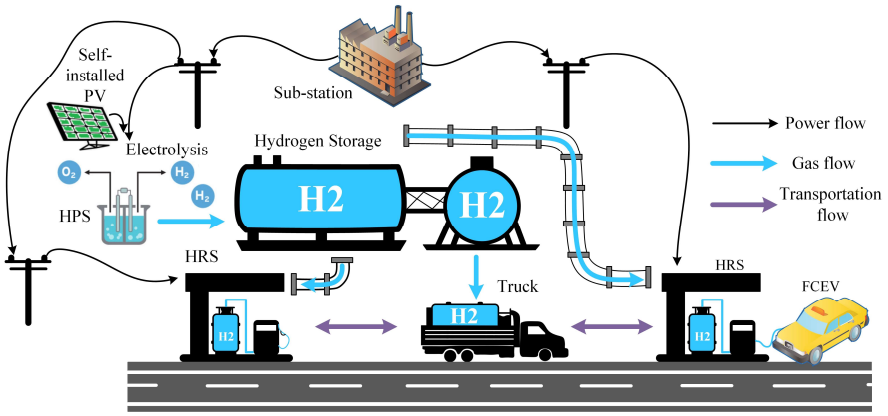

Fig. 7-1. Multi-network hydrogen refueling system.

Therefore, the HRSs can be built in prosperous places to capture more traffic flows, while the HPSs can be built in rural regions, thus causing less power congestion. The hydrogen delivery integrates the logistics system and the gas network. Therefore, the hydrogen can be delivered through gas pipelines and tank trucks. The trucks move between HPSs and HRSs to load and unload hydrogen and can serve as mobile energy storage. In the HPSs, hydrogen is produced through water electrolysis. The HPSs convert the electricity generated from the self-installed PVs and the electricity purchased from the utility grid to hydrogen. The produced hydrogen is stored in the hydrogen tanks and is liquefied to facilitate transportation. The electricity network also supplies energy to the HPSs and HRSs for normal operations. The proposed system structure coupled transportation network, electricity network, and gas network. Thus, the system flexibility is enhanced.

7.1.2 Hydrogen Logistics Modeling

In this part, the model of the temporal-spatial dynamic (TSD) model of the logistics system is presented [346]. The TSD model can be described as a multi-layer directed graph shown in Fig. 7-2. Each arc of the graph represents the possible routing action. Each layer represents a truck to deliver hydrogen. The trucks transit between transportation nodes. The arcs of the graph can be divided into transit arcs (solid lines) and parking arcs for hydrogen refueling (blue dash lines). The values of the directed arcs are binary variables indicating whether the truck is on the specific arc. Since the distance between some transportation nodes may be relatively long so that the truck cannot finish the trip within a time interval. In this case, a virtual node is created [250], shown as the red dots in Fig. 7-2. Therefore, a single long-distance trip is segmented into two separate trips.

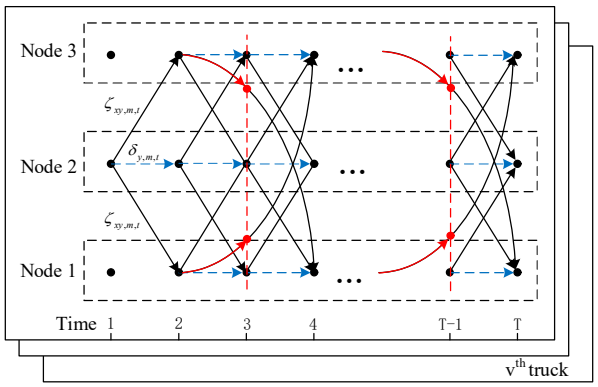

Fig. 7-2. Graph representation for the temporal-spatial dynamic model.

Based on the TSD graph, the logistics constraints can be described as:

$$\sum_{(m,n)\in\Omega^{TN,ARC}} \zeta_{yt\pi.mn,v} = 1, \quad \forall \pi \in \Pi, \forall y \in [1,Y], \forall t \in [1,T], \forall v \in \Upsilon \tag{7.1}$$

$$\sum_{(m,n)\in\Omega_n^{TN,ARC^-}} \zeta_{yt\pi.mn,v} = \sum_{(n,o)\in\Omega_n^{TN,ARC^+}} \zeta_{y(t+1)\pi.no,v}, \quad \forall \pi \in \Pi, \forall y \in [1,Y], \forall t \in [1,T], \forall v \in \Upsilon \tag{7.2}$$

$$S^{SK}_{yt\pi,mn,v} = S^{SK}_{y(t-1)\pi,mn,v} + \sum_{m\in\Omega^{HPS}} S^{LD}_{yt\pi,m,v} - \sum_{m\in\Omega^{HRS}} S^{UD}_{yt\pi,m,v}$$

$$, \quad \forall \pi \in \Pi, \forall y \in [1,Y], \forall t \in [1,T], \forall v \in \Upsilon, \forall m,n \in \Omega^{TN,ARC} \tag{7.3}$$

$$0 \le S^{SK}_{yt\pi,mn,v} \le C^{SK}, \quad \forall \pi \in \Pi, \forall y \in [1,Y], \forall t \in [1,T], \forall v \in \Upsilon, \forall m,n \in \Omega^{TN,ARC} \tag{7.4}$$

$$0 \le S^{LD}_{yt\pi,m,v} \le \zeta_{yt\pi.mm,v} S^{LD,\max}, 0 \le S^{UD}_{yt\pi,m,v} \le \zeta_{yt\pi.mm,v} S^{UD,\max}$$

$$, \quad \forall \pi \in \Pi, \forall y \in [1,Y], \forall t \in [1,T], \forall v \in \Upsilon, \forall m,n \in \Omega^{TN,ARC} \tag{7.5}$$

$$0 \le S^{LD}_{yt\pi,m,v} \le \delta^{HRS}_m \Phi, 0 \le S^{UD}_{yt\pi,m,v} \le \delta^{HRS}_m \Phi, \quad \forall \pi \in \Pi, \forall y \in [1,Y], \forall t \in [1,T], \forall v \in \Upsilon, \forall m \in \Omega^{TN,ARC} \tag{7.6}$$

Where $\Omega^{TN,ARC}$ is the set of arcs; Υ is the set of trucks; Π is the set of scenarios; Ω^{HPS} is the set of HPSs; $\zeta_{yt\pi,mn,v}$ is the binary variables indicating whether truck v is on the arc mn; $S^{SK}_{yt\pi,mn,v}$ is the hydrogen stock of the v^{th} truck; $S^{LD}_{yt\pi,m,v}$ is the amount of the hydrogen loaded at HPS m by the v^{th} truck; $S^{UD}_{yt\pi,m,v}$ is the amount of the hydrogen unloaded at HRS m by the v^{th} truck; C^{SK} is the maximum stock of the truck; $S^{LD,\max}$ and $S^{UD,\max}$ are the maximum amount of hydrogen that can be loaded and unloaded; Φ is a large number.

Equation (7.1) means that each truck can be on one arc at each time slot. Equation (7.2) indicates that for each truck, the ending point of the last time slot should be the starting point of the next time slot. Equation (7.3) describes the hydrogen stock balance in the trucks. Equation (7.4) is the maximum stock of the trucks. Equation (7.5) means that the trucks can only load and unload the hydrogen when they are at the parking arcs. Equation (7.6) means that the truck can only load the hydrogen at the built HPS and unload the hydrogen at the built HRS.

7.1.3 Hydrogen Production Station Modeling

The operation constraint of HPSs can be described as:

$$P^{ELE,\min}\delta_m^{HPS} \le P_{yt\pi,m}^{ELZ} \le P^{ELE,\max}\delta_m^{HPS}, \quad \forall \pi \in \Pi, \forall y \in [1,Y], \forall t \in [1,T], \quad \forall m \in \Omega^{HPS} \tag{7.7}$$

$$-P^{fluc} \le P_{yt\pi,m}^{ELZ} - P_{y(t-1)\pi,m}^{ELZ} \le P^{fluc}, \quad \forall \pi \in \Pi, \forall y \in [1,Y], \forall t \in [1,T], \quad \forall m \in \Omega^{HPS} \tag{7.8}$$

$$P_{yt\pi,m}^{ELZ} = P_{yt\pi,m}^{ELE,pur} + P_{yt\pi,m}^{RNW}, \quad P_{yt\pi}^{CP} = \gamma^{ELZ} P_{yt\pi,m}^{ELZ}, \quad \forall \pi \in \Pi, \forall y \in [1,Y], \forall t \in [1,T], \quad \forall m \in \Omega^{HPS} \tag{7.9}$$

$$\rho_{yt\pi,m}^{tank,HPS} = \rho_{y(t-1)\pi,m}^{tank,HPS} + \frac{R^A \cdot T^A}{\delta_m^{HPS} V^{CAP} \cdot Mol^H}\left(\frac{P_{yt\pi,m}^{CP}}{LHV^H}\Delta t Mol^H - S_{yt\pi,m}^{H,sell} - \sum_{v\in\Upsilon} S_{yt\pi,m,v}^{LD*}\right), P_{yt\pi}^{CP} = \gamma^{ELZ} P_{yt\pi,m}^{ELZ}$$

$$, \quad \forall \pi \in \Pi, \forall y \in [1,Y], \forall t \in [1,T], \quad \forall m \in \Omega^{HPS} \tag{7.10}$$

$$S_{yt\pi,m,v}^{LD} = S_{yt\pi,m,v}^{LD*}\eta^{LF}, \quad \forall \pi \in \Pi, \forall y \in [1,Y], \forall t \in [1,T], \forall v \in \Upsilon, \forall m \in \Omega^{HPS} \tag{7.11}$$

$$\rho^{tank,HPS,\min} \le \rho_{yt\pi,m}^{tank,HPS} \le \rho^{tank,HPS,\max}, \quad \forall \pi \in \Pi, \forall y \in [1,Y], \forall t \in [1,T], \forall m \in \Omega^{HPS} \tag{7.12}$$

$$0 \le S_{yt\pi,m}^{H,sell} \le \delta_m^{HPS}\Phi, \quad \forall \pi \in \Pi, \forall y \in [1,Y], \forall t \in [1,T], \forall m \in \Omega^{HPS} \tag{7.13}$$

where Ω^{HPS} is the set of HPSs; $P_{yt\pi,m}^{ELZ}$ is the input electrical power of the electrolyzer; δ_m^{HPS} is the utilization variables of HPS; $P_{yt\pi,m}^{ELE,pur}$ is the power purchased from the utility; $P_{yt\pi,m}^{RNW}$ is the self-generated renewable power of HPSs; $P^{ELE,\min}$ and $P^{ELE,\max}$ are the minimum and maximum power of the electrolyzer; P^{fluc} is the maximum power fluctuation; $P_{yt\pi}^{CP}$ is the input power of the compressor; γ^{ELZ} is the power loss coefficient of the compressor; $\rho_{yt\pi,m}^{tank,HPS}$ is the pressure of the hydrogen tank in HPS; R^A is the gas constant ($J \cdot mol^{-1} \cdot K^{-1}$); T^A is the mean temperature inside hydrogen tank; V^{CAP} is the capacity of hydrogen tank; Mol^H is the molar mass of hydrogen ($kg \cdot mol^{-1}$); LHV^H is the lower heating value; η^{LF} is the efficiency of the liquefaction; $\rho^{tank,HPS,\min}$ and $\rho^{tank,HPS,\max}$ are the minimum and maximum pressure; $S_{yt\pi,m,v}^{LD*}$ is the amount of hydrogen to be liquefied; $S_{yt\pi,m}^{H,sell}$ is the amount of hydrogen sold to the utility by HPS.

Equation (7.7) imposes the operating range of the electrolyzer. Equation (7.8) limits the maximum power fluctuation of the electrolyzer. Equation (7.9) calculates the input power of the compressor and compressor. Equation (7.10) is the pressure balance constraint of the hydrogen tank [261]. Equation (7.11) calculates the amount of hydrogen to be loaded into the truck through liquefaction. Equation (7.12) is the pressure limits of the hydrogen tank. Equation (7.13) means that if HPS is not built, no hydrogen can be sold.

7.1.4 Hydrogen Refueling Station Modeling

The operation constraint of HRSs can be described as:

$$\rho_{yt\pi,m}^{tank,HRS} = \rho_{y(t-1)\pi,m}^{tank,HRS} + \frac{R \cdot T^{A}}{\delta_{m}^{HRS} V^{CAP} \cdot Mol^{H}} \left(\sum_{v \in \Upsilon} S_{yt\pi,m,v}^{UD} - S_{yt\pi,m}^{RF} + S_{yt\pi,m}^{UE} + S_{yt\pi,m}^{H,pur} \right)$$

$$, \quad \forall \pi \in \Pi, \forall y \in [1,Y], \forall t \in [1,T], \quad \forall m \in \Omega^{HRS} \tag{7.14}$$

$$\rho^{tank,HRS,\min} \le \rho_{yt\pi,m}^{tank,HRS} \le \rho^{tank,HRS,\max}, \quad \forall \pi \in \Pi, \forall y \in [1,Y], \forall t \in [1,T], \quad \forall m \in \Omega^{HRS} \tag{7.15}$$

$$S_{yt\pi,m}^{DM} - S_{yt\pi,m}^{UE} = S_{yt\pi,m}^{RF}, \quad \forall \pi \in \Pi, \forall y \in [1,Y], \forall t \in [1,T], \quad \forall m \in \Omega^{HRS} \tag{7.16}$$

$$\sum_{t} \sum_{m \in \Omega^{HRS}} S_{yt\pi,m}^{RF} \ge \mathfrak{R} S^{TDM}, \quad \forall \pi \in \Pi, \forall y \in [1,Y], \tag{7.17}$$

$$0 \le S_{yt\pi,m}^{RF}, S_{yt\pi,m}^{UE}, S_{yt\pi,m}^{H,pur} \le \delta_{m}^{HRS} \Phi, \quad \forall \pi \in \Pi, \forall y \in [1,Y], \forall t \in [1,T], \quad \forall m \in \Omega^{HRS} \tag{7.18}$$

where Ω^{HRS} is the set of HRS; $\rho_{yt\pi,m}^{tank,HRS}$ is the pressure of the hydrogen tank in HRS; δ_{m}^{HRS} is the utilization variables of HRS; $S_{yt\pi,m,v}^{UD}$ is the amount of the hydrogen unloaded at HRS *m* by the v^{th} truck; $S_{yt\pi,m}^{UE}$ is the amount of the unserved energy to the FCEVs; $S_{yt\pi,m}^{H,pur}$ is the amount of hydrogen purchased by HRS; $S_{yt\pi,m}^{RF}$ is the amount of hydrogen delivered to FCEVs; $\mathfrak{R}$ is the demand satisfaction ratio; $S_{yt\pi,m}^{DM}$ is the refueling demand at HRS; S^{TDM} is the total refueling demand.

Equation (7.14) is the pressure balance constraints of the hydrogen tank. Equation (7.15) is the pressure limits of the hydrogen tank. Equation (7.16) means that the total hydrogen demand equals the sum of hydrogen refueled to the FCEVs and the unserved energy. Equation (7.17) constraints the total hydrogen refueling amount. Equation (7.18) means that if HRS is not built, there is no refueling, unserved, and purchased hydrogen.

7.2 Framework of Coordinated Planning of Multi-energy Networks and Hydrogen Production and Refueling Station based on Carbon Emission Flow

There are two stages in the proposed framework, as shown in Fig. 7-3. The first stage is feeder expansion and power source planning problems. This stage aims to build renewable power generation units and expand the feeders to cope with the increasing electricity demand and reduce the system emissions. After the first stage is completed, the nodal carbon intensity $e_{yt\pi,i}^{N}$ will be sent to the second stage. The nodal carbon intensity is calculated based on the CEF

model in section 4.1. The second stage is an optimization problem regarding hydrogen FCEVs considering the cost and the emissions in transportation networks. It will mainly solve two problems. The first problem is the site selection of the HRSs. The second problem is the penetration ratio of internal combustion vehicles, EVs, and FCEVs. It will find out which penetration ratio of different vehicles is the best choice to control emissions. The result can guide policymakers to adjust the transportation-related energy policy (e.g., subsidy and tax rebate for EVs) through macro-control and stimulation. The final electricity and hydrogen demand in the traffic network will be sent to the first stage. The iteration is processed to encourage the coordinated penetrations of renewable energy in electricity systems and EVs or FCEVs in transportation systems so that the energy consumed by the transportation system, such as EVs, is relatively green. Hence, two systems can corporate together to reduce the total emissions in the two energy subsectors.

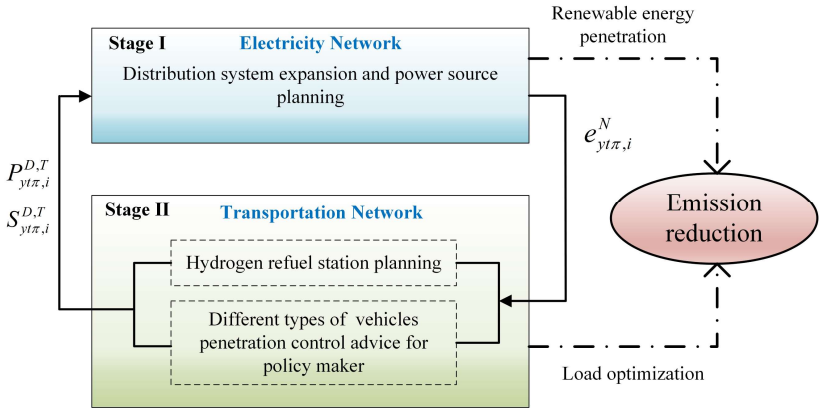

Fig. 7-3. Proposed framework of collaborative planning of electricity and transportation networks.

7.3 Stage I: Coordinated Planning of Multi-energy Network

Fig. 7-4 shows the methodology utilized in Stage I. Stage I is an electricity distribution network expansion planning problem mainly focusing on renewable energy source planning. The main input parameters include the network topology, per unit investment cost of different components, per unit cost of energy, electricity price, carbon price, as well as stochastic parameters, including wind speed, solar irradiation, and load profile. In the proposed model, there is an iteration process between Stage I and Stage II. The result from Stage II is also an important input for the model in Stage I. The result from stage II is the updated electricity and gas demand profile. The updated demand profile includes the consumption of EV charging facilities, HRSs, and HPSs. The objective function of Stage I is to minimize the total system cost, including investment cost, operation cost, and environmental cost. The decision variables include the binary decision variables indicating the construction state of the components in the network and the variables regarding the operation, such as the output of power generators, power flows, etc. The optimized value of these variables will be sent to Stage II as output.

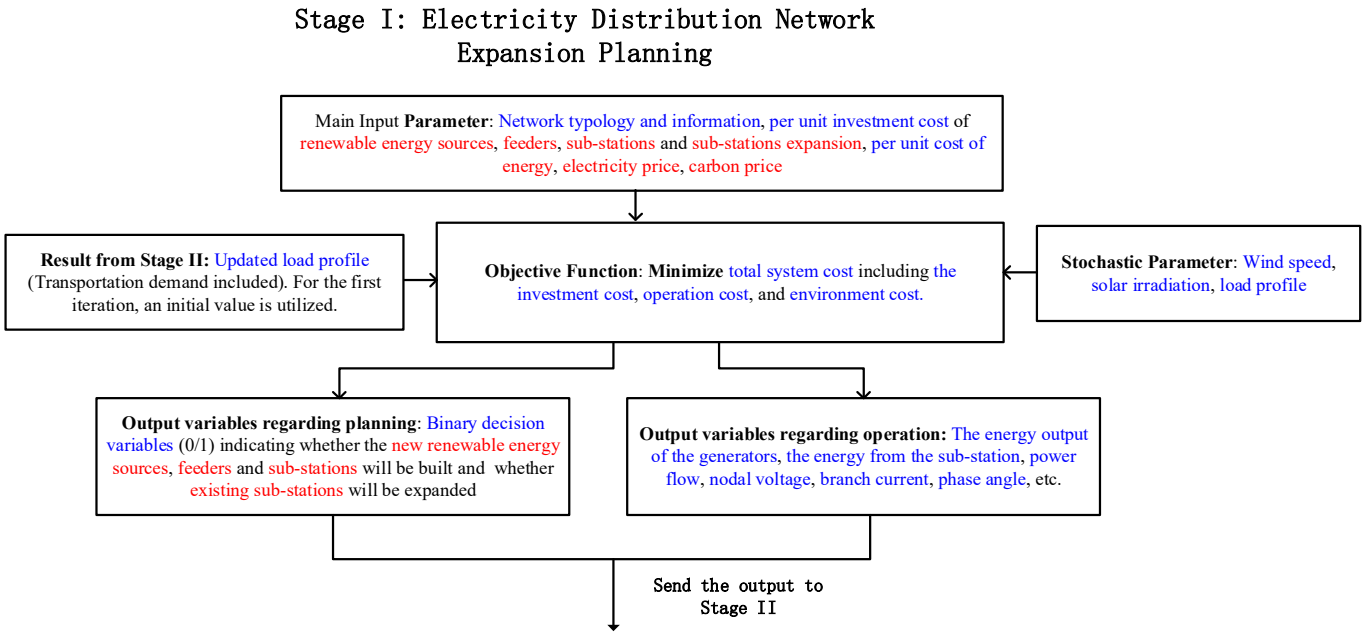

Fig. 7-4. The methodology of Stage I.

7.3.1 Objective Function

The objective function of stage I is to minimize the total cost of the system, including investment cost, operational cost, carbon environmental cost, and system loss cost.

$$Min\left\{\frac{1}{(1+\varepsilon)^{Y}}C^{IN}+\sum_{y=1}^{Y}\frac{1}{(1+\varepsilon)^{y}}\left(C_{y}^{OP}+C_{y}^{CAR}\right)\right\} \tag{7.19}$$

where Y is the total planning horizon; ε is the discount rate; C^{IN} is the investment cost; C_y^{OP} is the operational cost; C_y^{CAR} is the environmental cost.

The investment cost is divided into four parts shown as:

$$\begin{aligned} C^{IN} &= C^{IN,FD}+C^{IN,GP}+C^{IN,RNW}+C^{IN,ST} \\ &= \sum_{ij\in\Omega_{ij}^{FD}}\left(\delta_{ij}^{FD}\times\lambda_{ij}^{FD}\times l_{ij}^{FD}\right)+\sum_{pq\in\Omega_{ij}^{GP}}\left(\delta_{pq}^{GP}\times\lambda_{pq}^{GP}\times l_{pq}^{GP}\right)+\sum_{k\in\Omega^{RNW}}\sum_{i\in\Omega^{\gamma_k}}\left(\delta_{k,i}^{RNW}\times\lambda_{k}^{RNW}\times\overline{P_{k,i}^{RNW}}\right) \\ &+\sum_{i\in\Omega^{ST,NB}}\left(\delta_{i}^{ST,NB}\times\lambda^{ST,NB}\times\overline{P_{i}^{ST,NB}}\right)+\sum_{i\in\Omega^{ST,EP}}\left(\delta_{i}^{ST,EP}\times\lambda^{ST,EP}\times\overline{P_{i}^{ST,EP}}\right) \end{aligned} \tag{7.20}$$

where Ω^{FD}, Ω^{GP}, Ω^{RNW}, Ω^{γ_k}, $\Omega^{ST,NB}$, and $\Omega^{ST,EP}$ are the sets of candidate feeders, gas pipelines, renewable device types, k^{th} renewable devices located buses, new built sub-station buses, and existing sub-station buses for expansion; $C^{IN,FD}$, $C^{IN,GP}$, $C^{IN,RNW}$, and $C^{IN,ST}$ are the investment cost of feeders, pipelines; renewable devices, and sub-stations; δ_{ij}^{FD}, δ_{pq}^{GP}, $\delta_{k,i}^{RNW}$, $\delta_{i}^{ST,NB}$ and $\delta_{i}^{ST,EP}$ are binary decision variables; λ_{ij}^{FD}, λ_{pq}^{GP}, λ_{k}^{RNW}, $\lambda^{ST,NB}$ and $\lambda^{ST,EP}$ are the per-unit cost of building feeder between bus *i* and *j*, building gas pipeline between node *p* and *q*, building

k^{th} type of renewable energy devices, building new sub-stations and expanding existing sub-stations; $\overline{P_{k,i}^{RNW}}$, $\overline{P_i^{ST,NB}}$ and $\overline{P_i^{ST,EP}}$ are the maximum capacity of renewable energy devices, new built sub-stations and expanded sub-stations; l_{ij}^{FD} and l_{pq}^{GP} are the length of feeders and pipelines.

The operational cost of the system can be described as:

The operational cost contains the operation cost of the electricity network and hydrogen network, shown in (7.21).

$$C_y^{OP} = \sum_t \sum_{\pi \in \Pi} w_{yt\pi} \left(C_{yt\pi}^{OP,EN} + C_{yt\pi}^{OP,GN} \right), \quad \forall y \in [1, Y] \tag{7.21}$$

where Π is the set of the scenarios; $w_{yt\pi}$ is the weight of the scenarios.

The operational cost of the electricity network can be expressed as follows:

$$C_{yt\pi}^{OP,EN} = \sum_{i \in ST} \lambda_{yt\pi,i}^{ELE,UT} P_{yt\pi,i}^{ST} \Delta t + \sum_{i \in \Omega^{EN}} \vartheta^{LC} P_{yt\pi,i}^{LC} \Delta t + \sum_{(i,j) \in \Omega^{EN}} I_{yt\pi,ij} R_{ij} + \sum_{i \in G} \left[a_i \left(P_{yt\pi,i}^{G} \Delta t \right)^2 + b_i \left(P_{yt\pi,i}^{G} \Delta t \right) + c_i \right]$$

$$, \quad \forall \pi \in \Pi, \forall y \in [1, Y], \forall t \in [1, T] \tag{7.22}$$

where ST is the set of sub-stations; Ω^{EN} is the set of electricity buses; G is the set of thermal generators; $\lambda_{yt\pi}^{ELE,UT}$ is the nodal electricity price from the upper-level utility; $P_{yt\pi,i}^{ST}$ is the power delivered from sub-stations; $P_{yt\pi,i}^{LC}$ is the load curtailment; ϑ^{LC} is the penalty; $P_{yt\pi,i}^{G}$ is the power generation of the thermal generators in the distribution system; a_i, b_i, and c_i are the cost coefficients; $I_{yt\pi,ij}$ is the current magnitude; R_{ij} is the resistance.

The operational cost of the gas network can be expressed as follows:

$$C_{yt\pi}^{OP,GN} = \sum_{p \in GS} \lambda_{yt\pi,i}^{GS,UT} S_{yt\pi,p}^{GS}, \quad \forall \pi \in \Pi, \forall y \in [1, Y], \forall t \in [1, T] \tag{7.23}$$

where GS is the set of gas sources; $S_{yt\pi,p}^{GS}$ is the amount of hydrogen from upper-level utility; $\lambda_{yt\pi,i}^{GS,UT}$ is the nodal hydrogen price.

The carbon environmental cost is the penalty for exceeding the allocated carbon emission cap. It can be negative when the carbon emissions are below the cap.

$$C_y^{CAR} = \left\{ \begin{aligned} & \sum_{i \in \Omega^G} \left(\sum_t \sum_{\pi \in \Pi} \left(w_{yt\pi} P_{yt\pi,i}^{G} e_i^{G} \Delta t \right) - CAP_{i,y} \right) \\ & + \sum_{i \in \{\Omega_{ST,EP}, \Omega_{ST,NB}\}} \left(\sum_t \sum_{\pi \in \Pi} \left(w_{yt\pi} D_{yt} P_{yt\pi,i}^{ST} e_{yt\pi,i}^{ST} \Delta t \right) - CAP_{y,i} \right) \end{aligned} \right\} \times \lambda_y^{CAR}, \quad \forall y \in [1, Y] \tag{7.24}$$

where e_i^G is the unit carbon emission intensity; $e_{i,yt\pi}^{ST}$ is the nodal carbon emission intensity of sub-stations; $CAP_{i,y}$ is

the emission cap; λ_y^{CAR} is the carbon price.

7.3.1 Constraints

The constraints of the objective functions are shown as follows:

$$P_{yt\pi,i}^{L} + P_{yt\pi,i}^{L,T} - P_{yt\pi,i}^{LC} = P_{yt\pi,i}^{RNW} + P_{yt\pi,i}^{G} - \sum_{j\in J} P_{yt\pi,ij}^{B} + P_{yt\pi,i}^{ST}, \quad \forall i \in \Omega^{EN}, \forall \pi \in \Pi, \forall y \in [1,Y], \forall t \in [1,T] \tag{7.25}$$

$$Q_{yt\pi,i}^{L} - Q_{yt\pi,i}^{LC} = Q_{yt\pi,i}^{G} - \sum_{j\in J} Q_{yt\pi,ij}^{B}, \quad \forall i \in \Omega^{EN}, \forall \pi \in \Pi, \forall y \in [1,Y], \forall t \in [1,T] \tag{7.26}$$

$$0 \le P_{yt\pi,i}^{G} \le P_{i}^{G,\max}, 0 \le Q_{yt\pi,i}^{G} \le Q_{i}^{G,\max}, \quad \forall i \in \Omega^{EN}, \forall \pi \in \Pi, \forall y \in [1,Y], \forall t \in [1,T] \tag{7.27}$$

$$P_{yt\pi,k,i}^{RNW} = g_k(\overline{P_{k,i}^{RNW}}\delta_{k,i}^{RNW}), \quad \forall i \in \Omega^{EN}, \forall k \in \Omega^{\gamma_k}, \forall \pi \in \Pi, \forall y \in [1,Y], \forall t \in [1,T] \tag{7.28}$$

$$0 \le P_{yt\pi,i}^{ST} \le \delta_i^{ST,NB} \times \overline{P_i^{ST,NB}}, \quad \forall i \in \Omega^{EN}, \forall \pi \in \Pi, \forall y \in [1,Y], \forall t \in [1,T] \tag{7.29}$$

$$0 \le P_{yt\pi,i}^{ST} \le \delta_i^{ST,EP} \times \overline{P_i^{ST,EP}} + \overline{P_i^{ST}}, \quad \forall i \in \Omega^{EN}, \forall \pi \in \Pi, \forall y \in [1,Y], \forall t \in [1,T] \tag{7.30}$$

$$-\mathcal{S}_{ij}^{B,\max}\delta_{ij}^{FD} \le P_{yt\pi,ij}^{B} \le \mathcal{S}_{ij}^{B,\max}\delta_{ij}^{FD}, \quad \forall i,j \in \Omega^{EN}, \forall \pi \in \Pi, \forall y \in [1,Y], \forall t \in [1,T] \tag{7.31}$$

$$-\mathcal{S}_{ij}^{B,\max}\delta_{ij}^{FD} \le Q_{yt\pi,ij}^{B} \le \mathcal{S}_{ij}^{B,\max}\delta_{ij}^{FD}, \quad \forall i,j \in \Omega^{EN}, \forall \pi \in \Pi, \forall y \in [1,Y], \forall t \in [1,T] \tag{7.32}$$

$$-\sqrt{2}\mathcal{S}_{ij}^{B,\max}\delta_{ij}^{FD} \le P_{yt\pi,ij}^{B} + Q_{yt\pi,ij}^{B} \le \sqrt{2}\mathcal{S}_{ij}^{B,\max}\delta_{ij}^{FD}, \quad \forall i,j \in \Omega^{EN}, \forall \pi \in \Pi, \forall y \in [1,Y], \forall t \in [1,T] \tag{7.33}$$

$$U_{ty\pi,i} - U_{ty\pi,j} = \frac{R_{ij}P_{yt\pi,ij}^{B} + X_{ij}Q_{yt\pi,ij}^{B}}{U_0}, U_i^{\min} \le U_{ty\pi,i} \le U_i^{\max}, \quad \forall i,j \in \Omega^{EN}, \forall \pi \in \Pi, \forall y \in [1,Y], \forall t \in [1,T] \tag{7.34}$$

where J is the set of the buses connected to bus i; $P_{yt\pi,i}^{L}$ and $Q_{yt\pi,i}^{L}$ are the active and reactive normal electricity load; $P_{yt\pi,i}^{L,T}$ is the electricity load in transportation system obtained from stage II; $P_{yt\pi,i}^{LC}$ and $Q_{yt\pi,i}^{LC}$ are the active and reactive load curtailment; $P_{yt\pi,i}^{RNW}$ is the renewable energy generation; $P_{yt\pi,ij}^{B}$ and $Q_{yt\pi,ij}^{B}$ are the active and reactive power flow; $P_{yt\pi,i}^{G}$ and $Q_{yt\pi,i}^{G}$ are the active and reactive power generation of thermal generators; $P_i^{G,\max}$ and $Q_i^{G,\min}$ are the maximum and minimum generation of thermal generators; $\mathcal{S}_{ij}^{B,\max}$ is the maximum power flow; $U_{ty\pi,i}$ is the nodal voltage; $U_i^{\min}$ and $U_i^{\max}$ are the minimum and maximum nodal voltage.

Equations (7.25) and (7.26) are the active and reactive power flow equations. Equations (7.27)-(7.30) is the output limits of the power sources. Equations (7.31)-(7.33) are the limits of the power flows. Equation (7.34) limits the nodal voltage.

The gas network constraints can be described as:

$$S_{yt\pi,pq}^{PP}=\operatorname{sgn}\left(\rho_{yt\pi,p},\rho_{yt\pi,q}\right)\times\phi_{pq}\sqrt{\left|\left(\rho_{yt\pi,p}\right)^2-\left(\rho_{yt\pi,q}\right)^2\right|},\quad \forall p,q\in\Omega^{GN},\forall\pi\in\Pi,\forall y\in[1,Y],\forall t\in[1,T] \tag{7.35}$$

$$\operatorname{sgn}\left(\rho_{yt\pi,p},\rho_{yt\pi,q}\right)=\begin{cases}1 & \rho_{yt\pi,p}\geq\rho_{yt\pi,q}\\ -1 & \rho_{yt\pi,p}<\rho_{yt\pi,q}\end{cases},\quad \forall p,q\in\Omega^{GN},\forall\pi\in\Pi,\forall y\in[1,Y],\forall t\in[1,T] \tag{7.36}$$

$$S_{yt\pi,pq}^{comp}=\alpha_{pq}^{comp,3}+\alpha_{pq}^{comp,2}H_{yt\pi,pq}+\alpha_{pq}^{comp,1}\left(H_{yt\pi,pq}\right)^2,\quad \forall p,q\in\Omega^{GN},\forall\pi\in\Pi,\forall y\in[1,Y],\forall t\in[1,T] \tag{7.37}$$

$$H_{yt\pi,pq}=\kappa_{pq}S_{yt\pi,pq}^{PP}\times\left[\left(\rho_{yt\pi,p}/\rho_{yt\pi,q}\right)^{\phi_{pq}}-1\right],\quad \forall p,q\in\Omega^{GN},\forall\pi\in\Pi,\forall y\in[1,Y],\forall t\in[1,T] \tag{7.38}$$

$$S_{yt\pi,p}^{GS}-\sum_{p\in\Omega_q^{GN^+}}S_{yt\pi,pq}^{PP}-\sum_{q\in\Omega_q^{GN^+}}S_{yt\pi,pq}^{comp}\eta_{pq}^{comp}=S_{yt\pi,p}^{L}+S_{yt\pi,p}^{L,T},\quad \forall p,q\in\Omega^{GN},\forall\pi\in\Pi,\forall y\in[1,Y],\forall t\in[1,T] \tag{7.39}$$

$$\rho_p^{\min}\leq\rho_{yt\pi,p}\leq\rho_p^{\max},\quad \forall p\in\Omega^{GN},\forall\pi\in\Pi,\forall y\in[1,Y],\forall t\in[1,T] \tag{7.40}$$

$$-S_{pq}^{PP,\max}\delta_{pq}^{PP}\leq S_{yt\pi,pq}^{PP}\leq S_{pq}^{PP,\max}\delta_{pq}^{PP},\quad \forall p,q\in\Omega^{GN},\forall\pi\in\Pi,\forall y\in[1,Y],\forall t\in[1,T] \tag{7.41}$$

where $\Omega_q^{GN^+}$ is the set of the gas node connected to node q; $S_{yt\pi,pq}^{PP}$ is the gas flow; $\rho_{yt\pi,p}$ is the gas pressure at node p; ϕ_{pq} is the pipeline constant; $\operatorname{sgn}(\cdot)$ donates the flow direction; $S_{yt\pi,pq}^{comp}$ is the gas withdrawn by the station compressor; $H_{yt\pi,pq}$ is the horsepower consumption of the compressor station; α_{pq}^{comp} is the conversion factor; κ_{pq} is a constant associated with compressor suction temperature and efficiency; $S_{yt\pi,p}^{L}$ is the normal gas demand; $\rho_p^{\min}$ and $\rho_p^{\max}$ are the minimum and maximum nodal pressure; $S_{yt\pi,p}^{L,T}$ is the gas demand of transportation network obtained from stage II.

Equation (7.35) calculates the gas flow. Equation (7.36) defines the flow direction. Equation (7.37) calculates the withdrawn gas utilized to generate electricity by a micro-gas turbine to power the compressor. Equation (7.38) calculates the horsepower consumption of the compressor station. Equation (7.39) is the gas flow balance constraint. Equation (7.40) is the pressure limits at the gas node. Equation (7.41) limits the gas flow.

7.4 Stage II: Transportation System Planning and Optimal Penetration Ratio of Different Types of Vehicles

Fig. 7-5 shows the methodology proposed in section V. The problem in Stage II is a transportation system planning to solve the location of HPSs, HRSs, and the optimal penetration ratio of different types of vehicles. First, according to the result from Stage I, the nodal carbon intensity is calculated, and the carbon footprint is tracked by the CEF model. The CEF model in the gas network is similar. Second, according to the user equilibrium-based traffic assignment model (UETEAM) formulated in section 6.1, the traffic flow in the traffic network is simulated, and then the traffic captured

by the FCSs and HRSs can be evaluated. The other main input parameters include vehicle refueling demand, charging demand of EVs, rated charging power, travel ratio, etc. The objective function at this stage is to minimize the total cost and carbon emissions from the transportation system. The variables are the binary decision variables indicating whether the HRS is built and the penetration ratios of different types of vehicles. Based on the optimal value of these output variables, the electricity demand and hydrogen demand in the transportation system can be calculated and will be sent to Stage I for iteration.

The objective function focuses on carbon emissions. One of the technical difficulties in such an objective is carbon footprint tracking. For internal combustion vehicles, emissions occur when consuming gasoline (i.e., driving). Thus, carbon emission is relatively easy to be evaluated. However, for EVs, the indirect emissions occur when charging, and for FCEVs, the indirect emissions occur when electricity is converted to hydrogen. For both EVs and FCEVs, indirect emissions occur when electricity is consumed. Hence, a carbon flow model is utilized to calculate the nodal carbon intensity, and the carbon emissions can be further tracked.

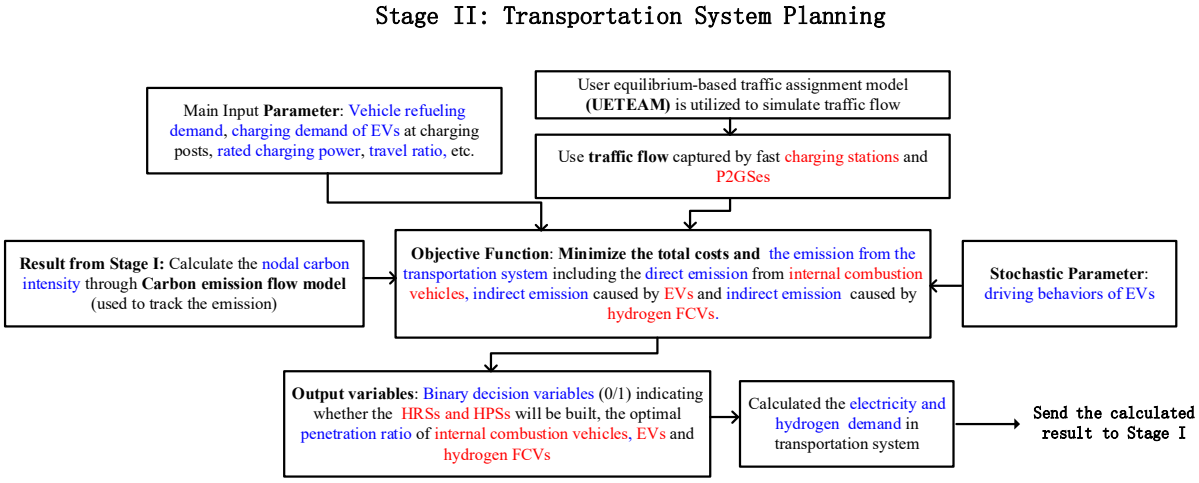

Fig. 7-5. The methodology of Stage II.

7.4.1 Objective Function

The objective function of stage II is to the total investment cost, operation cost, and environmental cost of the transportation system.

$$Min.C^{T} = \frac{1}{(1+\varepsilon)^{Y}} C^{IN,T} + \sum_{y=1}^{Y} \frac{1}{(1+\varepsilon)^{y}} \times \left(E_{y}^{TF,Gasoline} + E_{y}^{TF,EV} + E_{y}^{TF,FV} \right) \times \lambda_{y}^{CAR} + \sum_{y=1}^{Y} \frac{1}{(1+\varepsilon)^{y}} \times C_{y}^{OP,T} \quad (7.42)$$

where $C^{IN,T}$ is the investment cost in transportation network; $E_{yq}^{TF,Gasoline}$ is the emissions of internal combustion vehicles at the q^{th} quarter of the y^{th} year; $E_{yq}^{TF,EV}$ is the indirect emissions caused by EVs; $E_{yq}^{TF,FV}$ is the indirect

emissions caused by hydrogen FCEVs; $C_y^{OP,T}$ is the operation cost in the transportation network.

7.4.2 Investment Cost in Transportation Network

$$C^{IN,T} = \sum_{m\in\Omega^{HRS}}\left[\left(C^{HRS,E}+C_m^{HRS,G}\right)z_m^{HRS}+C^{HRS,F}\delta_m^{HRS}\right]+\sum_{m\in\Omega^{HPS}}\left[\left(C^{HPS,E}+C_m^{HPS,G}\right)z_m^{HPS}+C^{HPS,F}\delta_m^{HPS}\right] \quad (7.43)$$

where $C^{HRS,E}$ and $C^{HPS,E}$ are the equipment cost of the HRS and HPS, which is insensitive to the geographical location; $C_m^{HRS,G}$ and $C_m^{HPS,G}$ are the location-sensitive cost, such as land utilization cost; $C^{HRS,F}$ and $C^{HPS,F}$ are the fixed cost; z_m^{HRS} and z_m^{HPS} are the size of HRS and HPS to be invested; δ_m^{HRS} and δ_m^{HPS} are the binary variables indicating whether HRS and HPS are built.

7.4.3 Emissions of Different Types of Vehicles

The emissions of internal combustion vehicles are generated while driving. Emissions can be tracked by the driving behaviors of vehicles, which are calculated as:

$$E_y^{TF,Gasoline} = \left(e^{Gasoline}\times S_y^{Gasoline}\right)\times\xi^{Gasoline},\ \ \forall y\in[1,Y] \quad (7.44)$$

where $e^{Gasoline}$ is the emission factor of gasoline; $S_{yq}^{Gasoline}$ is vehicle fuel demand; $\xi^{Gasoline}$ is the penetration ratio of internal combustion vehicles.

The demand of vehicle fuels can be estimated as follows:

$$S_y^{Gasoline} = \sum_t\sum_{\pi\in\Pi}\sum_{v\in N^{Gs}}\left(w_{yt\pi}\times Dist_{v,yt\pi}\times\eta_{GS}\right),\ \ \forall y\in[1,Y],\forall v\in\Upsilon \quad (7.45)$$

where N^{Gs} is the total set of internal combustion vehicles; $Dist_{v,yt\pi}$ is the driving distance of the v^{th} vehicle; η_{GS} is the fuel consumption per km.

The indirect emissions caused by EVs happen when EVs are charging. Hence, emissions can be tracked by charging behaviors. There are two kinds of charging methods. The first one is charging at charging posts, while the second one is the FCSs. The total emissions of EVs can be calculated by:

$$E_y^{TF,EV} = E_y^{EV,CP}+E_y^{EV,FCS},\ \ \forall y\in[1,Y] \quad (7.46)$$

where $E_y^{EV,CP}$ is the emissions from the charging post; $E_y^{EV,FCS}$ is the emissions from the fast charging station.

The emissions from the charging post can be calculated by:

$$E_y^{EV,CP} = \sum_t\sum_{\pi\in\Pi}\sum_{i\in\Omega^{CP}}\left(w_{yt\pi}\times e_{yt\pi,i}^{N}\times S_{yt\pi,i}^{CP}\right)\times\xi^{EV},\ \ \forall y\in[1,Y] \quad (7.47)$$

where Ω^{CP} is the set of charging posts; $e_{i,yt\pi}^{N}$ is the nodal intensity of the located bus of the charging post; $S_{i,yt\pi}^{CP}$ is the

charging demand of the i^{th} charging post under π^{th} scenario; ξ^{EV} is the penetration ratio of EVs.

According to Ref. [101], the charging demand is estimated as follows:

$$S_{yt\pi,i}^{CP} = C_{y,i} h \frac{V_{yt\pi,i}}{\sum_{t}\sum_{\pi\in\Pi}\left(w_{yt\pi}V_{yt\pi,i}\right)} P^{CP}, \quad \forall y \in [1,Y] \tag{7.48}$$

where $C_{i,yq}$ is the charging demand of i^{th} charging post at the q^{th} quarter of y^{th} year; h is the average charging duration; $V_{i,yqb\pi}$ is the average number of EVs parked at i^{th} charging post; P^{CP} is the rated charging power of the charging posts.

The charging demand of i^{th} charging post is calculated by:

$$C_{y,i} = \frac{C_y \beta \sum_{t}\sum_{\pi\in\Pi}\left(w_{yt\pi}V_{yt\pi,i}\right)}{\sum_{i\in\Omega^{CP}}\sum_{t}\sum_{\pi\in\Pi}\left(w_{yt\pi}V_{yt\pi,i}\right)}, \quad \forall y \in [1,Y] \tag{7.49}$$

where C_y is the total charging demand at the y^{th} year; β is the choosing ratio of charging post.

The emissions from the FCSs can be calculated by:

$$E_y^{EV,FCS} = \sum_{t}\sum_{\pi\in\Pi}\sum_{i\in\Omega^{FCS}}\left(w_{yt\pi}\times e_{yt\pi,i}^{N}\times S_{yt\pi,i}^{FCS}\right)\times\xi^{EV}, \quad \forall y \in [1,Y] \tag{7.50}$$

where Ω^{FCS} is the set of the FCSs; $S_{yt\pi,i}^{FCS}$ is the charging demand of the i^{th} FCS.

$$S_{yt\pi,i}^{FCS} = C_y(1-\beta)\times\frac{f_{yt\pi,i}^{trip}}{\sum_{t}\sum_{\pi\in\Pi}f_{yt\pi,i}^{trip}}\times\frac{f_{yt\pi,i}}{\sum_{i\in\Omega^{FCS}}f_{yt\pi,i}}\times P^{FCS}, \forall y\in[1,Y], \forall t\in[1,T], \forall\pi\in\Pi, \forall i\in\Omega^{FCS} \tag{7.51}$$

where $f_{yt\pi,i}^{trip}$ is the travel ratio; $f_{yt\pi,i}$ is the traffic flow captured by the fast charging station; P^{FCS} is the rated charging power of the fast charging station.

In this chapter, the hydrogen for FCEVs is produced through the electrolysis of water. The P2GSes will take the role of HRSs.

The indirect emissions caused by FCEVs happen when P2GSes purchase electricity to generate hydrogen. Hence the emissions can be tracked by purchase behaviors, which can be calculated by:

$$E_y^{TF,FV} = \sum_{t}\sum_{\pi\in\Pi}\sum_{m\in\Omega^{HPS}}\left(\delta_m^{HPS}\times w_{yt\pi}\times e_{yt\pi,m}^{N}\times P_{yt\pi,m}^{ELE,pur}\right)\times\xi^{FV} + \sum_{t}\sum_{\pi\in\Pi}\sum_{m\in\Omega^{HRS}}\left(\delta_m^{HRS}\times w_{yt\pi}\times e_{yt\pi,m}^{N,G}\times S_{yt\pi,m}^{H,pur}\right)\times\xi^{FV}$$

$$, \forall y\in[1,Y] \tag{7.52}$$

where δ_i^{FV} is the binary variable indicating whether P2GS will be built; $P_{i,yqb\pi}^{P2G,pur}$ is the amount of electricity that the P2GSes purchase; ξ^{FV} is the penetration of FCEVs.

7.4.4 Operational Cost in Transportation Network

The operational cost contains three elements, including the operational cost of HRS, HPS, and transportation fees, shown in (7.21).

$$C_y^{OP} = \sum_t \sum_{\pi \in \Pi} w_{yt\pi} \left(C_{yt\pi}^{OP,HRS} + C_{yt\pi}^{OP,HPS} + C_{yt\pi}^{OP,TP} \right), \quad \forall y \in [1, Y] \tag{7.53}$$

where Π is the set of the scenarios; $w_{yt\pi}$ is the weight of the scenarios.

The operational cost in HRS can be expressed as (7.54). The operational cost includes the daily maintenance cost, the electricity purchase cost to maintain its normal operation, the hydrogen purchase cost, and the penalty cost for unserved energy to FCEVs.

$$C_{yt\pi}^{OP,HRS} = \sum_{m \in \Omega^{HRS}} \left(C^{HRS,MT} \delta_m^{HRS} + \lambda_{yt\pi}^{ELE} \left(P_m^{NOP} \delta_m^{HRS} \right) + \lambda_{yt\pi}^{GS} S_{yt\pi,m}^{H,pur} + \vartheta^{UE} S_{yt\pi,m}^{UE} \right), \quad \forall y \in [1, Y], \forall t \in [1, T], \forall \pi \in \Pi \tag{7.54}$$

where $C^{HRS,MT}$ is the maintenance cost of HRS; $\lambda_{yt\pi}^{ELE}$ is the electricity price; P_m^{NOP} is the per-unit power to support the normal operation in HRS; $\lambda_{yt\pi}^{GS}$ is the hydrogen price; $S_{yt\pi,m}^{H,pur}$ is the amount of hydrogen purchased by HRS; $S_{yt\pi,m}^{UE}$ is the amount of the unserved energy to the FCEVs; ϑ^{UE} is the penalty.

The operational cost in HPS can be expressed as (7.55). The operational cost includes the daily maintenance cost and the electricity purchase cost to maintain its normal operation, to support liquefaction and electrolysis devices, and to be converted to hydrogen. Besides, the HPS can sell hydrogen to the utility to earn additional revenues.

$$C_{yt\pi}^{OP,HPS} = \sum_{m \in \Omega^{HPS}} \left(C^{HPS,MT} \delta_m^{HRS} - \lambda_{yt\pi}^{GS} S_{yt\pi,m}^{H,sell} + \lambda_{yt\pi}^{ELE} \left(P_m^{NOP} \delta_m^{HPS} + S_{yt\pi,m,v}^{LD*} \varphi^{LF} + P_{yt\pi,m}^{ELZ} \varphi^{ELZ} \Delta t + P_{yt\pi,m}^{ELE,pur} \right) \right)$$

$$, \quad \forall y \in [1, Y], \forall t \in [1, T], \forall \pi \in \Pi \tag{7.55}$$

where $C^{HPS,MT}$ is the maintenance cost of HPS; $u_{y,m}^{HPS}$ is the utilization variables of HPS; $S_{yt\pi,m}^{H,sell}$ is the amount of hydrogen sold to the utility by HPS; $S_{yt\pi,m,v}^{LD*}$ is the amount of hydrogen to be liquefied; φ^{LF} is the per-unit power consumption of liquefaction; $P_{yt\pi,m}^{ELZ}$ is the input electrical power of electrolyzer; φ^{ELZ} is the per-unit power consumption of electrolyzation; $P_{yt\pi,m}^{ELE,pur}$ is the electricity purchased by HPS to be converted to hydrogen.

The transportation fee can be expressed as follows:

$$C_{yt\pi}^{OP,TP} = \sum_{v \in \Upsilon} \sum_{(m,n) \in \Omega^{TN}} C_{mn}^{TP} \zeta_{yt\pi,mn,v} + \sum_{v \in \Upsilon} \sum_{m \in \Omega^{HRS}} C^{LB} S_{yt\pi,m,v}^{UD} + \sum_{v \in \Upsilon} \sum_{m \in \Omega^{HPS}} C^{LB} S_{yt\pi,m,v}^{LD}$$

$$, \quad \forall y \in [1, Y], \forall t \in [1, T], \forall \pi \in \Pi \tag{7.56}$$

where Ω^{TN} is the set of transportation nodes; Υ is the set of tank trucks; C_{mn}^{TP} is the transportation cost on the arc

mn; $\zeta_{yt\pi,mn,v}$ is the binary variables indicating whether truck *v* is on the arc *mn*; C^{LB} is the labor cost; $S^{UD}_{yt\pi,m,v}$ is the amount of the hydrogen unloaded at HRS *m* by the v^{th} truck; $S^{LD}_{yt\pi,m,v}$ is the amount of the hydrogen loaded at HPS *m* by the v^{th} truck.

7.4.5 Decision Variables

The main decision variables in this problem can be listed as:

$$X = \left\{ \xi^{Gasoline}, \xi^{EV}, \xi^{FV}, \delta_m^{HRS}, \delta_m^{HPS}, z_m^{HRS}, z_m^{HPS}, P_{yt\pi,m}^{ELE,pur}, S_{yt\pi,m}^{H,pur} \right\} \tag{7.57}$$

The electricity demand in the transportation system can be calculated as equation (7.58), which will be sent to stage I.

$$P_{yt\pi,i}^{L,T} = \left(w_{yt\pi} \times S_{yt\pi,i}^{CP} \right) \times \xi^{EV} + \left(w_{yt\pi} \times S_{yt\pi,i}^{FCS} \right) \times \xi^{EV} + \left(\delta_i^{HPS} \times w_{yqb\pi} \times P_{yt\pi,i}^{ELE,pur} \right) \times \xi^{FCV}$$

$$, \quad \forall y \in [1,Y], \forall t \in [1,T], \forall \pi \in \Pi, \forall i \in \Omega^{EN} \tag{7.58}$$

$$S_{yt\pi,p}^{L,T} = \left(\delta_p^{HRS} \times w_{yt\pi} \times S_{yt\pi,p}^{H,pur} \right) \times \xi^{FCV} - \left(\delta_p^{HPS} \times w_{yt\pi} \times S_{yt\pi,p}^{H,sell} \right) \times \xi^{FCV}$$

$$, \quad \forall y \in [1,Y], \forall t \in [1,T], \forall \pi \in \Pi, \forall p \in \Omega^{GN} \tag{7.59}$$

7.4.6 Constraints

The operation constraints of transportation networks are modeled in (7.1)-(7.18).

The constraints that describe refueling demand is shown in (7.60).

$$S_{i,yt\pi}^{FV} = R_y \times \frac{f_{i,yt\pi}^{trip}}{\sum_{\pi \in \Pi} f_{i,yt\pi}^{trip}} \times \frac{f_{i,yt\pi}}{\sum_{i \in \Omega^{HRS}} f_{i,yt\pi}}, \quad \forall y \in [1,Y], \forall t \in [1,T], \forall \pi \in \Pi, i \in \Omega^{HRS} \tag{7.60}$$

where R_y is the refueling demand of the y^{th} year. The unit is converted to MW (1 mol H_2, under 273k, 101kpa, can provide 0.0786KWh).

Equation (7.61) means that the supply of hydrogen refueling should be larger than the demand.

$$\sum_{i \in \Omega^{HRS}} \sum_{t} \sum_{\pi \in \Pi} \left(\delta_i^{HRS} S_{i,yt\pi}^{FV} \right) \geq R_y \times \xi^{FV}, \quad \forall y \in [1,Y] \tag{7.61}$$

Equations (7.62) and (7.63) mean that the penetration ratio of different vehicles should be summed up to 1.

$$\xi^{Gasoline} + \xi^{EV} + \xi^{FV} = 1 \tag{7.62}$$

$$\xi^{Gasoline}, \xi^{EV}, \xi^{FV} \in (0,1) \tag{7.63}$$

7.5 Case Study

The proposed HRS and HPS planning framework and methodology are verified in an IEEE 33-bus electricity system coupled with a 41-node transportation system and a 19-node gas system, shown in Fig .7-6. In Fig. 7-6, the coupling relationships between the multi-networks are displayed.

To verify the advantages of the proposed planning model, four cases are established.

Case 1: The hydrogen is only delivered through the gas pipelines [347].

Case 2: The hydrogen is only delivered through the logistics system [348, 349].

Case 3: Both gas pipelines and logistics system are planned to deliver hydrogen. The QoS and reliability assessment is not conducted.

Case 4: Both gas pipelines and logistics system are planned to deliver hydrogen. The QoS and reliability assessment is conducted to ensure sufficient energy supplement infrastructures.

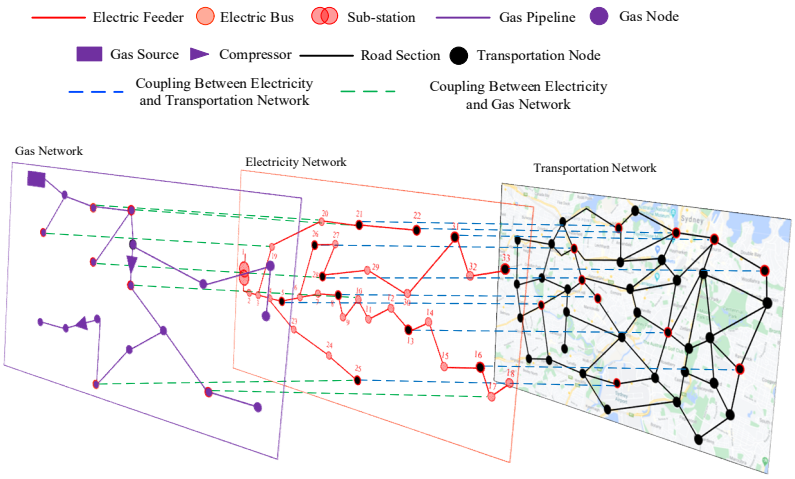

Fig. 7-6. Coupling of the electricity network, gas network, and transportation network.

The simulations were completed by a PC with an Intel Core (TM) i7-9750 CPU @ 2.60 GHz with 16.00 GB RAM.

7.5.1 Planning Results

Figs. 7-7 to 7-9 display the planning result in the transportation network, electricity network, and gas network. Fig. 7-7 shows the location of the planned and the candidate HRSs and HPSs. It can be found that there are five HRSs and five HPSs being built that are dispersed at different locations in the transportation network. Fig. 7-8 shows the expansion result in the electricity network. The new feeders are built to supply electricity to the HRSs and HPSs. Therefore, the HRSs and HPSs are connected to the electricity network and become the coupling points between the electricity network and the transportation network. Besides, to prevent congestion, some feeders are expanded. Fig. 7-9 shows the planning result in the gas network. The new pipelines are built so that the hydrogen can be transmitted between the HPSs and

HRSs through the gas network. Therefore, HRSs and HPSs become the coupling points in the multi-networks.

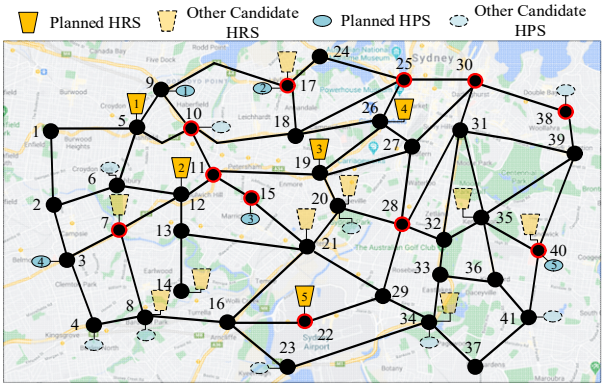

Fig. 7-7. Planning results in the transportation network.

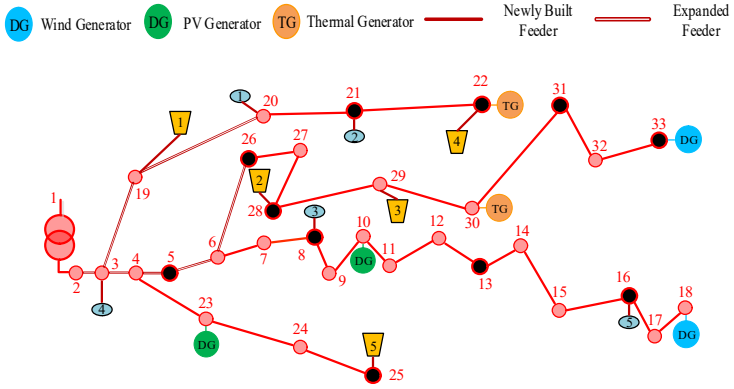

Fig. 7-8. Planning results in the electricity network.

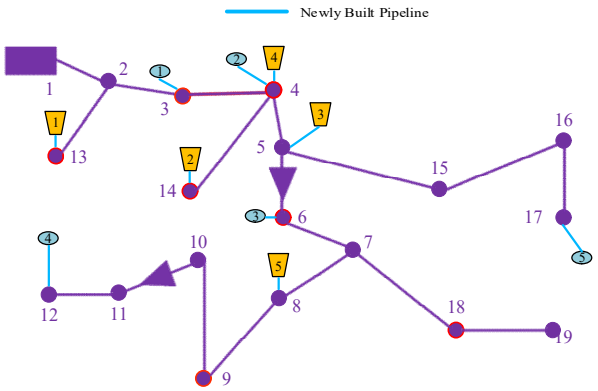

Fig. 7-9. Planning results in the gas network.

Fig. 7-10 shows the investment cost and the amount of unserved hydrogen under different demand satisfaction ratios in different cases. To pass the reliability assessment, the unserved amount of hydrogen should be kept within the threshold under the contingency. The increase in the demand satisfaction ratio can reduce the amount of unserved energy, and meanwhile, the investment cost will increase. When the demand satisfaction equals 1, which means the hydrogen supply can just meet the demand under normal operation, the unserved energy under contingency is relatively large in all cases. It indicates that more reserves should be retained through investing more assets to cope with the contingency. It is also found that Case 1 has the highest investment cost while Case 4 has the lowest investment cost. At the same

time, Case 1 has the highest unserved energy, whereas Case 4 has the lowest unserved energy.

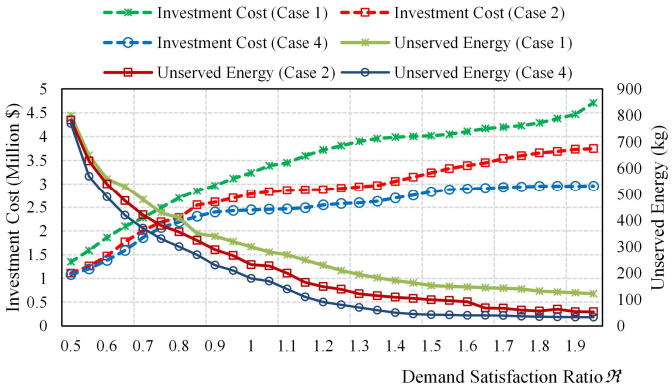

Fig. 7-10. Investment cost and unserved energy under different demand satisfaction ratios.

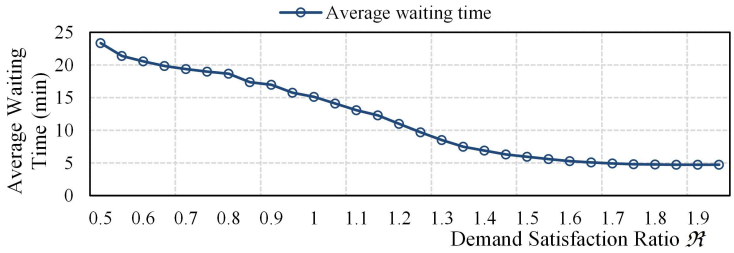

Fig. 7-11. Average waiting time under different demand satisfaction ratios.

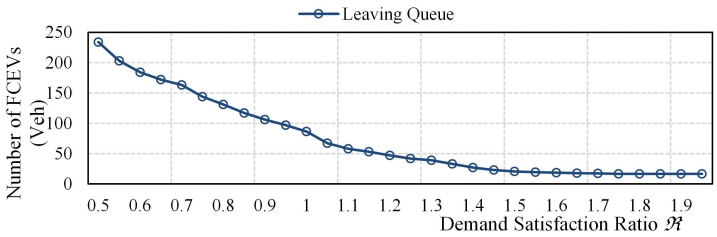

Fig. 7-12. Number of FCEVs leaving the queue under different demand satisfaction ratios.

Figs. 7-11 and 7-12 show the average waiting time in HRSs and the number of FCEVs leaving the queue due to dissatisfaction under different demand satisfaction ratios. To pass the QoS assessment, both the average waiting time and the number of FCEVs leaving the queue should be kept within the thresholds. Since different cases have little impact on the service quality at the HRSs, we choose to display the result of Case 4 only. It can be found that the increase in the demand satisfaction ratio can reduce the average waiting time and reduce the number of FCEVs leaving the queue. This is because more charging infrastructures are built to improve the QoS and users' satisfaction. Combining Figs. 7-10 to 7-12, the demand satisfaction ratio is finally selected as 1.55 to pass the reliability and QoS assessment in Case 4.

Table 7-1 provides the allocation of the cost in different cases. Case 1 has the highest total cost of 16.51 million dollars, and Case 4 has the lowest total cost of 11.46 million dollars. In Case 1, since the hydrogen transition only relies on the gas network, its investment cost on the gas network is the highest. In Case 2, the hydrogen is only delivered through the logistics system, so there is no investment cost on the gas network. In Case 3, the QoS and reliability

assessment is not conducted, so less charging infrastructure is invested, which leads to a lower investment cost. In Case 4, although its investment cost is higher than Case 3, its total cost is lower than Case 3. The main cost reduction lies in operation costs.

TABLE 7-1. TOTAL COST ALLOCATION IN DIFFERENT CASES

Cost (Million $)	Case 1	Case 2	Case 3	Case 4
Gas network investment	1.33	N/A	0.42	0.45
Electricity network investment	0.82	0.80	0.70	0.74
HRS investment	1.00	1.05	0.42	0.61
HPS investment	1.63	1.72	0.89	1.09
Operation cost	11.85	9.51	11.32	8.57
Total	16.63	13.08	13.75	11.46

7.5.2 Operation Results

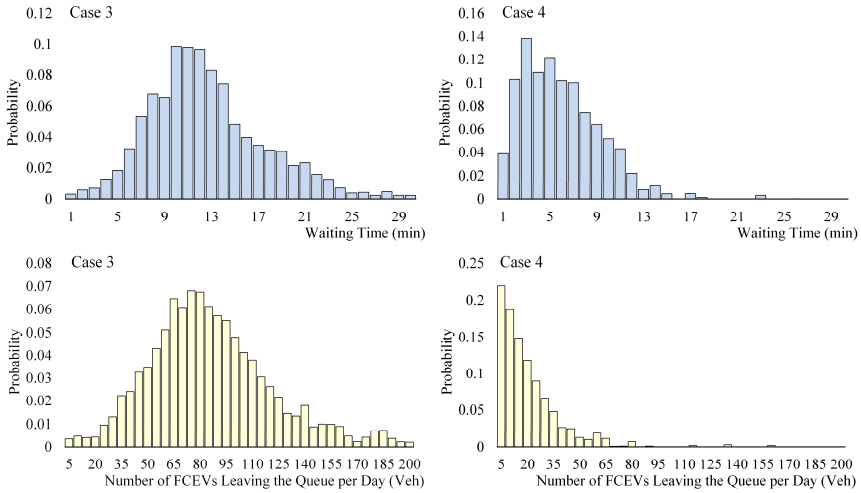

Fig. 7-13. Distribution of the waiting time and the number of FCEVs leaving the queue.

In this section, the operation simulation of the planned hydrogen refueling system is provided. Fig. 7-13 compares the probability distributions of the queue length and the number of EVs leaving the queue per day in Case 3 and Case 4. It can be found in Case 3, 80% confidence level of the waiting time falls into 6-19 minutes. In contrast, 80% confidence level of the waiting time falls into 2-10 minutes in Case 4. From the view of the number of FCEVs leaving the queue, 80% confidence level falls into 50-130 vehicles in Case 3, while in Case 4, 80% confidence level falls into 5-45 vehicles. It indicates that QoS is significantly enhanced through conducting the proposed assessment.

In Fig. 7-14, the hydrogen production at different time slots in Case 4 is provided. It is found that during 9:00-16:00, hydrogen production mainly relies on the conversion of self-generated renewable energy at the HPSs. During these periods, the hydrogen purchase from the utility is relatively low. During the periods that the solar irradiation is insufficient, the HPSs will purchase electricity from the utility to produce hydrogen, or the HRSs will directly purchase hydrogen from the utility.

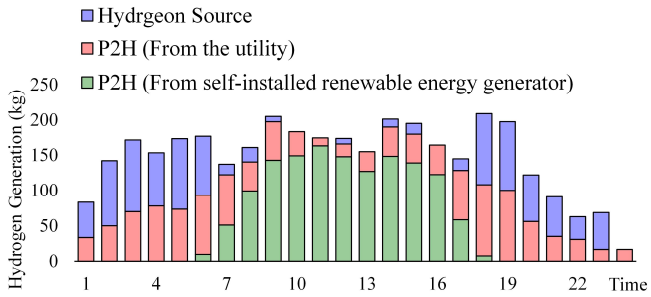

Fig. 7-14. Hydrogen production profile.

The hydrogen provision is provided in Fig. 7-15. The hydrogen provision at different HRSs and different time periods are different due to the spatial and temporal characteristics of the traffic capture. The total hydrogen demand also complies with the characteristics of the travel ratio, where 8:00 and 19:00 are two peaks.

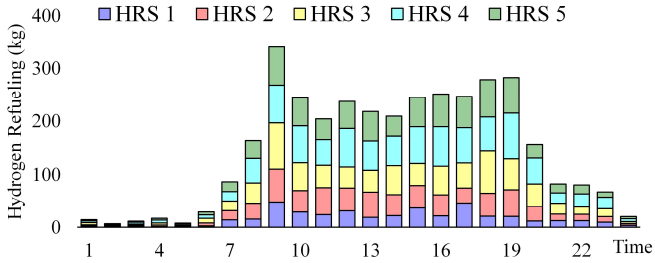

Fig. 7-15. Hydrogen refueling profile.

Fig. 7-16 shows hydrogen stock in the whole system. It can be found that the hydrogen stock begins to accumulate at an early time of the day. With the gradual increase of hydrogen demand, the total stock begins to reduce from 8:00. At the early of the day, the hydrogen stock is mainly at the HPSs, and the stock is gradually delivered to the HRSs through the trucks. Fig. 7-16 can display the stock transition process through the logistics system.

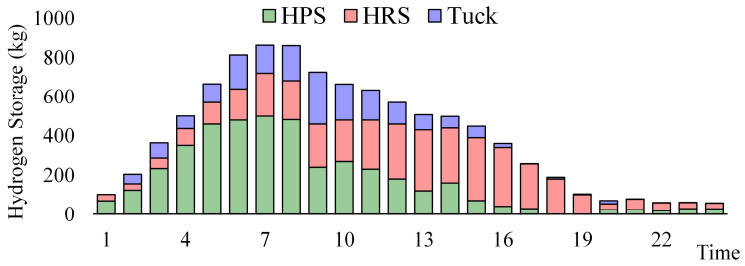

Fig. 7-16. Hydrogen storage profile.

Table 7-2 illustrates the cost allocation of the operation cost in different cases. In Case 1, the hydrogen delivery only relies on the gas network, so there is no transportation cost. However, due to the investment in the gas pipelines, the HPSs can earn extra revenue by selling hydrogen to the utility. In Case 2, the hydrogen is only delivered through the logistics system, so there is no hydrogen purchase cost for HRSs and no hydrogen export revenue for HPSs. Meanwhile, the electricity purchase cost of Case 2 is higher than Case 1. However, it can be found that the unserved hydrogen cost of Case 2 is less than Case 1, which means that hydrogen delivery through logistics is more reliable than through gas

pipelines. In Case 3, since fewer assets are invested, the electricity and hydrogen purchase costs are less than the other cases. However, its reliability cost is very high, which becomes the main reason that the total cost in Table 7-1 is the highest. In Case 4, the most obvious difference is that the reliability cost is the lowest. It means that the coordination of the gas network and logistics system, as well as the proposed assessment strategy, can benefit the system reliability and service quality.

TABLE 7-2. OPERATION COST ALLOCATION IN DIFFERENT CASES

Operation cost (Million $)	Case 1	Case 2	Case 3	Case 4
Electricity purchase	3.32	6.21	2.85	3.53
Hydrogen purchase	5.73	N/A	3.51	4.82
Hydrogen export	-1.25	N/A	-0.15	-1.66
Device maintenance	0.19	0.17	0.13	0.21
Traffic cost	N/A	1.85	0.73	1.31
Power loss	0.063	1.06	0.63	0.07
Load curtailment	0.16	0.35	0.14	0.12
Unserved hydrogen	3.44	1.04	3.21	0.10

7.5.3 Environmental Evaluation

The optimized penetration ratio of different vehicles in four cases is shown in Fig. 7-17. In case 1, there are no green vehicles, while in case 2, EVs take a dominant position. In case 3 and case 4, hydrogen FCEVs are put into use. The share of hydrogen FCEVs in case 4 (43.2%) is higher than that in case 3 (32.6%). Moreover, the energy supply for hydrogen FCEVs in case 4 mostly comes from renewable resources. This is because the iteration of stages I and II facilitates the electricity network to install renewable power generation units for the transportation network and helps two networks cooperate better.

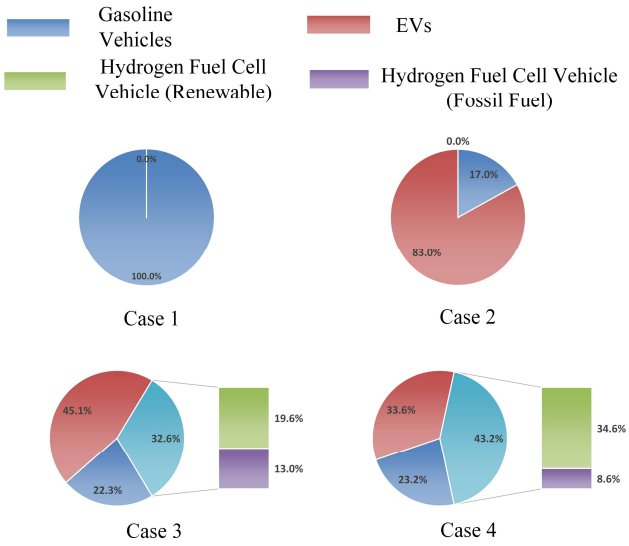

Fig. 7-17. Penetration ratio of different vehicles of different cases.

The emissions of the system of four cases on one specific day are shown in Fig. 7-18. The emissions of power generators and sub-station do not contain the energy supply to vehicles. Compared with case 1, case 2 has relatively higher total emissions, 1320 and 1430 tons/day, respectively. This is because the emissions of internal combustion vehicles are transferred to the electricity network. The massive penetration of EVs does not achieve emission reduction. In case 3, the emissions are reduced evidently, and the most emission reduction is realized in the transportation system (1170 tons/day). In case 4, the emissions of case 4 are reduced further, and the hydrogen FCEVs cause almost no emissions (920 tons/day).

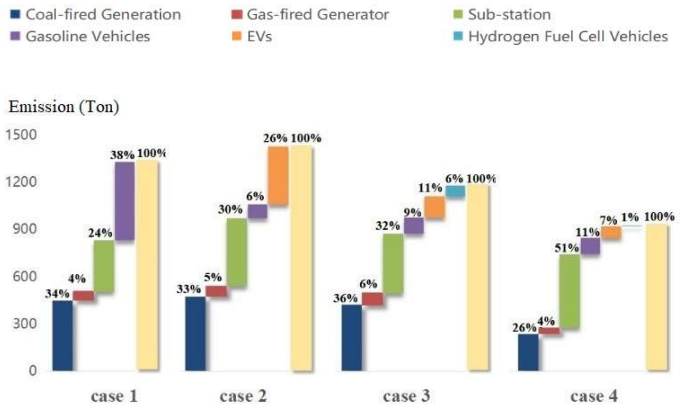

Fig. 7-18. The total emissions of the system of different cases.

The power usage of a P2GS located at bus 10 is shown in Fig. 7-19. The P2GS has its renewable power generation units. As a result, most of the energy supplied to hydrogen FCEVs is from renewable resources. The remaining demand is from other sources, such as thermal generators and substations. Moreover, the refueling stations tend to be built on buses where the travel ratio has the same characteristics as renewable output (peak at noon; valley at night). Hence, the consumption-ability of renewable energy is increased.

Fig. 7-20 shows the electricity purchasing behaviors and the SOC of the refueling station located at bus 10. The results show that the station tends to buy electricity when the nodal emission intensity is relatively low. This gives the renewable power generation units a promising prospect because the refueling station can help to smooth the output of renewable energy as an energy storage device. The proposed model can achieve the lowest emissions since the electricity and transportation systems can cooperate well. Collaborative planning enables the cooperation between the electricity network and the transportation system to reach lower system emissions.

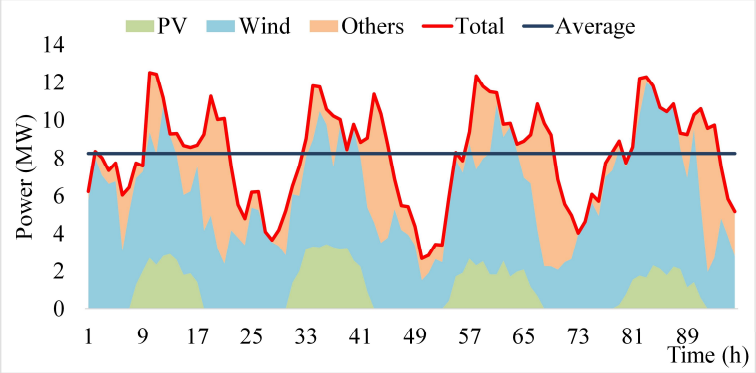

Fig 7-1.9. Power output of hydrogen refueling station.

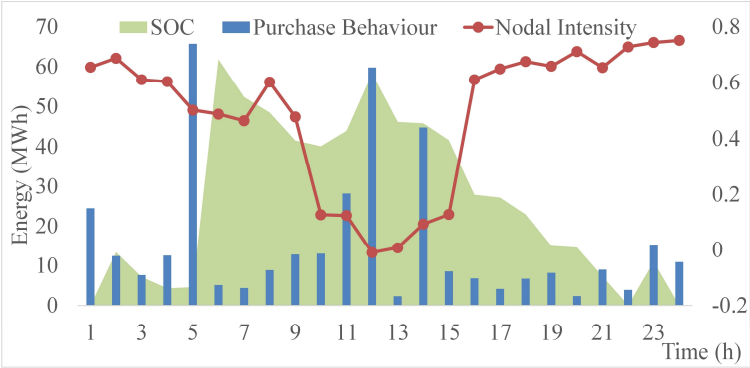

Fig. 7-20. Electricity purchase behaviors of hydrogen refueling stations.

7.6 Chapter Summary

A novel low-carbon oriented collaborative planning model for electricity and transportation systems is proposed in this chapter. Compared with the previous works regarding collaborative planning, the proposed model is from a new perspective looking at the mutual benefits between the environment and the carbon mitigation cost. Specifically, in the existing references, the cost-effective planning model aims to ensure the electricity supply of EV charging facilities through coupling electricity and transportation networks. By contrast, the proposed low-carbon oriented planning model focuses on not only the system cost but also the carbon emissions through tracking the carbon footprint of vehicles. The proposed collaboration planning model enables the electricity system and transportation system to cooperate with each other to reduce emissions at a minimum cost. Besides, the penetration of FCEVs and hydrogen refuel stations increase the multi-energy flexibility, thus helping decision-makers better implement energy sustainability strategies. According to the simulation results, the main findings can be listed as follows: first, the collaborative planning of power and transportation networks helps the whole system reach a lower emission rate (Case 4: 920 tons/day). The planning results for the power system can help to supply renewable resources to EV charging facilities and fuel cell refueling stations. Second, large-scale penetration of EVs may cause even higher emissions in the tested system (increased by 8%

compared with no EVs situation). Therefore, a proper ratio between different kinds of vehicles can realize complementarity. Moreover, the optimal penetration ratio between EVs and FCEVs is around 1:1.6. However, this value may be changed according to the topology and the traffic condition of different cities. Third, the proposed model can determine the location of the hydrogen refueling stations, which can act as storage facilities in the power system to smooth the output of renewable energy.

CHAPTER 8

EVALUATION OF THE COUPLED NETWORK TOWARDS EXTREME EVENTS

The power outage will significantly affect the normal operation of society and paralyze the functionality in the industrial, commercial, and residential sectors. Failure to recognize vulnerable points and critical assets of electricity grids may trigger a sequence of cascading events and eventually result in a large-area blackout when an outage does occur at these critical locations. To this end, a vulnerability assessment becomes an important task to mitigate the economic loss of contingencies [350]. In recent years, the fast development of the EV industry has brought new challenges and threats to the security and reliability of electricity networks since the charging demand of large-scale EVs has the potential to overburden electricity networks. On the other hand, following the emerging hydrogen industry, FCEVs powered by hydrogen and plug-in hybrid electric and hydrogen vehicles (PH2EVs) have come into public sight. Although the emergence of FCEVs and PH2EVs can enhance energy flexibility and provide transport alternatives [103], the synergistic effect of electricity, hydrogen, and transportation networks makes the whole coupled network more complicated. Due to the increasing coupling between transportation and multi-energy networks, a disruption in any network may directly affect the operation of the other networks as well as the energy supplement of EVs. To this end, a vulnerability assessment of the coupled transportation and multi-energy networks considering different types of EVs has become an emerging topic to be investigated. In this chapter, a vulnerability assessment methodology is proposed for the coupled transportation and multi-energy network.

8.1 Graph Presentation of the Coupled Transportation and Multi-Energy Network

8.1.1 Graph Formulation

The coupled transportation and multi-energy network can be represented by a graph $\Xi=(\mathcal{V},\mathcal{E})$, shown in Fig. 8-1 (a simple example). The electricity buses $\mathcal{V}^E$, gas nodes $\mathcal{V}^G$, and transportation nodes $\mathcal{V}^T$ form the vertex set $\mathcal{V}$, and the transmission lines $\mathcal{E}^{EE}$, gas pipelines $\mathcal{E}^{GG}$, road sections $\mathcal{E}^{TT}$, charging links $\mathcal{E}^{ET}$, and hydrogen refueling links $\mathcal{E}^{GT}$ make up the edge set $\mathcal{E}$. Every edge has an associated weight representing the asset rating. To be noted,

the traffic flow on each road can be bi-directional simultaneously (regardless of one-way roads). Hence, each physical road is separated into two road sections with pre-assigned directions. As for the transmission line and the gas pipelines, the power flow and gas flow on them can also be bi-directional, but they can be only in one direction at each time slot, and the weight is undirected. The direction of the charging links and hydrogen refueling links will be discussed in the latter section. Therefore, the transportation and multi-energy network can be represented by a hybrid directed and undirected graph.

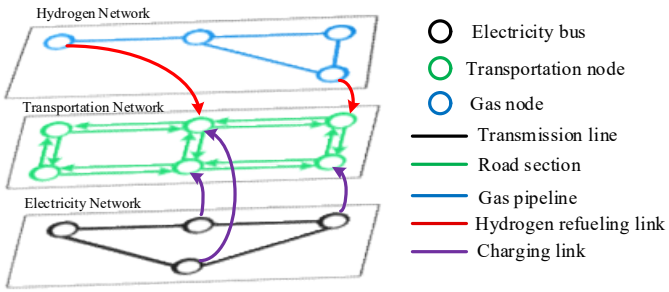

Fig. 8-1. Graph representation of the coupled network.

8.1.2 Coupling Relationship between Electricity and Transportation Networks

In this chapter, we utilize a graphic method to model the coupling relationship between electricity and transportation networks. To help the reader better understand the practical meaning of charging links, a toy example is provided to assist illustration, as shown in Fig. 8-2. It can be seen that the charging links connect the transportation network and the electricity network, and the corresponding transportation nodes will be the physical location of FCSs, i.e., transportation nodes 2, 5, and 6. The electricity load on transportation nodes represents charging demand. For example, transportation node 5 has a charging demand of 10 kWh currently (assuming that the time interval is 1 hour). The direction of the charging links is from the electric buses to the transportation nodes representing power delivery to FCSs.

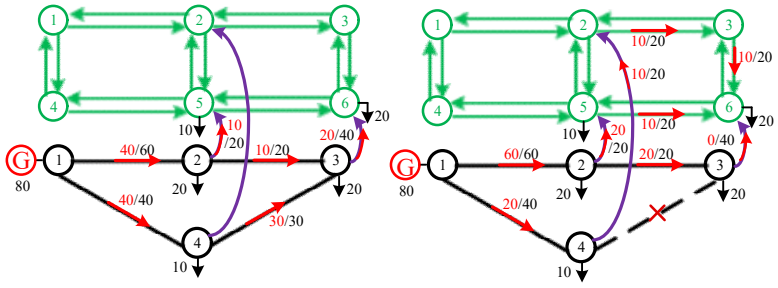

Fig. 8-2. Coupling relationship between electricity and transportation networks.

The left subplot of Fig. 8-2 shows a normal operation of the coupled network. The power flow and the line capacity are marked around transmission lines in red and black, respectively. The right subplot of Fig. 8-2 shows an operation of the coupled network under a contingency where line 3-4 is disconnected. Under this condition, the power flow on line

3-4 needs to be rerouted. However, the maximum capacity on line 1-2 is only 60 kW which fails to support the rerouting. It indicates that the FCS on transportation node 6 may encounter outages and fail to provide charging services. Therefore, the charging demand at this FCS will be spatially shifted to the other stations through road sections. In our proposed graph representation, the flow on the road sections is the virtual power flow representing the spatial shift of charging demand. For example, half of the 20 kWh charging demand at FCS 6 will be shifted to station 5 through road section 6-5, and the rest will be shifted to station 2 through road sections 6-3 and 3-2. It is found that the physical shift of the EV driving flow is in the opposite direction of the virtual power flow.

8.1.3 Coupling Relationship between Hydrogen and Transportation Networks

The graph representation of the coupling relationship between hydrogen and transportation networks is similar to that of the coupling relationship between electricity and transportation networks. In the toy example, the HRSs locate at transportation nodes 2 and 3, shown in Fig. 8-3. The left subplot of Fig. 8-3 shows a normal operation of the coupled network. For simplification, the energy unit of gas is converted to kWh. The right subplot of Fig. 8-3 shows the operation of the coupled network under a contingency where pipeline 3-4 is lost (neglect the slow dynamics of the gas network first). Then, the gas demand at HRS 3 is shifted to HRS 2 through road section 3-2.

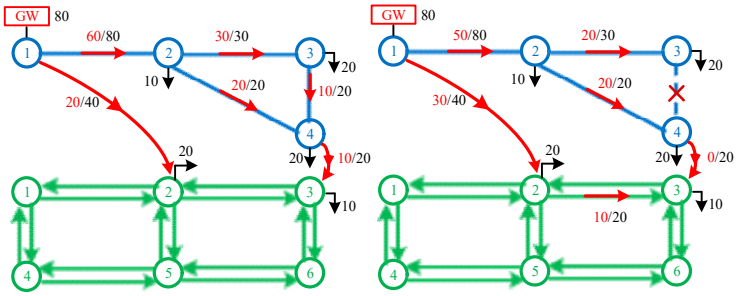

Fig. 8-3. Coupling relationship between hydrogen and transportation network.

8.1.4 Coupling Relationship between Hydrogen and Electricity Networks

Usually, the coupling point of the gas and electricity networks refers to the gas generators or P2G devices (hydrogen production through electrolytic water). In this chapter, we mainly focus on the energy supplement services of EVs and neglect these widely studied coupling relationships. With the emergence of PH2EVs and the integrated electricity-charging and hydrogen-refueling station (IEHS), a new coupling relationship is established based on the energy substitution effect of electricity and hydrogen. The IEHS, located at transportation node 2 in Figs. 8-2 and 8-3, becomes the coupling point.

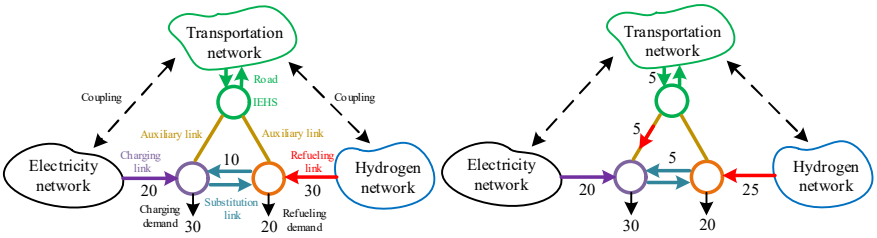

Fig. 8-4. Coupling relationship between hydrogen and electricity network.

To model the energy substitution effect through the graphic method, we further decompose the node of the IEHS into two sub-nodes, representing electricity charging services and hydrogen refueling services, respectively. Then, substitution links and auxiliary links are created, as shown in Fig. 8-4. The substitution link, of which the direction is pre-assigned according to the energy transition direction, connects two sub-nodes, representing the energy substitution effect between electricity and hydrogen. For example, shown in the left subplot of Fig. 8-4, when there is a contingency that happens in the electricity network, only 20 kWh can be delivered to the IEHS to satisfy the charging demand. Then, 10 kWh of the charging demand is shifted to the hydrogen refueling demand through the substitution link since the PH2EVs can either use electricity or hydrogen.

The auxiliary links are created in case the spatial demand shift happens in the IEHS. They connect the sub-nodes to the transportation node where IEHS is located. For example, as shown in the right subplot of Fig. 8-4, if only 5 kWh electricity demand can be shifted to the hydrogen demand, the rest of 5 kWh electricity demand will be shifted to the other stations through the auxiliary links. The auxiliary links are bi-directional and do not need to pre-assign the direction.

8.1.5 Wight Definition and Graph Decomposition

According to the formulated graph representation, the edges can be divided into several categories. The weight on each edge reflects the maximum power flow allowed to pass through the edge. Hence, the weight on each type of edge can be defined as:

$$W_{l^{EE}} = P_{l^{EE}}^{B,\max}, W_{l^{GG}} = S_{l^{GG}}^{B,\max}, \quad \forall l^{EE} \in \mathcal{E}^{EE}, \forall l^{GG} \in \mathcal{E}^{GG} \tag{8.1}$$

$$W_{l^{ET}} = P_{l^{ET}}^{Ch,\max}, W_{l^{GT}} = S_{l^{GT}}^{Rf,\max}, \quad \forall l^{ET} \in \mathcal{E}^{ET}, \forall l^{GT} \in \mathcal{E}^{GT} \tag{8.2}$$

$$W_{l^{TT}} = C_{l^{TT}}^{\max}, \quad \forall l^{TT} \in \mathcal{E}^{TT} \tag{8.3}$$

where $W_{(\cdot)}$ is the weight on each edge; l^{EE}, l^{GG}, l^{ET}, l^{GT}, and l^{TT} are the index of transmission lines, gas pipelines, charging links, hydrogen refueling links, and road sections, respectively; $P_{l^{EE}}^{B,\max}$ is the power capacity of transmission lines; $S_{l^{GG}}^{B,\max}$ is the maximum gas flow capacity of pipelines; $P_{l^{ET}}^{Ch,\max}$ is the maximum charging power

at the FCS (depending on the size of FCS); $S_{l^{GT}}^{Rf,\max}$ is the maximum hydrogen refueling power at the HRS (depending on the size of HRS); $C_{l^{TT}}^{\max}$ is the capacity of the virtual flow on the road sections.

The capacity of the gas pipeline $S_{l^{GG}}^{B,\max}$ is proportional to $\left(D_{l^{GG}}\right)^{\gamma}$, according to ref. [351], where $D_{l^{GG}}$ is the diameter of the corresponding pipeline, and γ is the constant conversion coefficient.

The capacity of the virtual flow on the road sections $C_{l^{TT}}^{\max}$ depends on transportation conditions. For example, if the traffic is crowded on a specific road, this road will have less capacity for virtual power flow to realize spatial demand shifts. Hence, $C_{l^{TT}}^{\max}$ is further defined as:

$$C_{l^{TT}}^{\max}=\left(\overline{\mathfrak{h}_{l^{TT}}}-\mathfrak{h}_{l^{TT}}\right)E^{EV/PH2EV},\ \ \forall l^{TT}\in\mathcal{E}^{TT} \tag{8.4}$$

where $\mathfrak{h}_{l^{TT}}$ is the traffic flow on the road sections; $\overline{\mathfrak{h}_{l^{TT}}}$ is the maximum vehicle capacity of the road sections; $E^{EV/PH2EV}$ is the average energy storage capacity of EVs and PH2EVs.

The traffic flow can be derived from the widely utilized User equilibrium (UE) model, which describes that each traveler wants to minimize his own travel time and the congestion effects:

As for the created substitution link, the weight is defined as:

$$W_{l^{SB}}=P_{l^{SB}}^{sub,\max},\ \ \forall l^{SB}\in\mathcal{E}^{SB} \tag{8.5}$$

where l^{SB} is the index of substitution link; $P_{l^{SB}}^{sub,\max}$ is the maximum capacity of the substitution link depending on the number of spare chargers/nozzles and the number of PH2EVs ready for energy substitution.

To further display the dynamic states of the coupled network, the network capacity graph $\Xi=(\mathcal{V},\mathcal{E})$ can be decomposed into two directed graphs: power flow graph $\mathcal{F}=(\mathcal{V},\mathcal{E})$ and spare capacity graph $\mathcal{S}=(\mathcal{V},\mathcal{E})$, which have the same topology as Ξ.

For the transmission lines and pipelines, when the power flow on edge *l* from vertex $\mathcal{V}^S$ toward $\mathcal{V}^D$ is f_l, the directed weight on the edge *l* will be assigned as $w^{SD}=f_l$ in the flow graph $\mathcal{F}$, and the directed weight on the edge *l* will be assigned as $w^{SD}=W_l-f_l$, $w^{DS}=W_l+f_l$ in the spare capacity graph $\mathcal{S}$.

For the road sections, charging link, and refueling link, the directed weight on the edge *l* will be assigned as $w^{SD}=f_l$ in $\mathcal{F}$, and the directed weight on the edge *l* will be assigned as $w^{SD}=W_l-f_l$, $w^{DS}=f_l$ in $\mathcal{S}$.

8.2 Critical Asset and Vulnerability Identification

8.2.1 Identification of Critical Asset

Let us define the edge *l* connecting vertices $\mathcal{V}^S$ and $\mathcal{V}^D$ as a direct path from $\mathcal{V}^S$ to $\mathcal{V}^D$. There could be other indirect paths to transfer power from $\mathcal{V}^S$ to $\mathcal{V}^D$. When the edge *l* is lost, the power flow f_l on *l* needs to be rerouted through indirect paths. Otherwise, overloads will occur. Therefore, a graph-theoretic approach is proposed to detect whether the indirect paths have enough capacity to reroute the original power flow on edge *l*.

In the previous sub-section, the coupled transportation and multi-energy network is formulated as a graph. When we use a contact surface to divide the graph Ξ into two parts, the original network becomes two interconnected sub-networks. A collection of branches passing through this contact surface is called *a cut-set* in graph theory [352]. As shown in Fig. 8-5, the whole network is divided into two sub-networks, and the collection of the connections between the two sub-networks is the *cut-set.*

Therefore, the energy exchanges between two sub-networks rely on the cut-set $\mathcal{C}$. The cut-set $\mathcal{C}$ is *saturated* if:

$$\sum_{l\in\mathcal{C}} f_l > \sum_{l\in\mathcal{C}} W_l \tag{8.6}$$

To be noted, equation (8.6) can be utilized as criteria to judge whether the $\mathcal{C}$ is saturated if all the edges in the cut-set are undirected. If parts of the edges in the cut-set are directed, such as the road sections, the judgment will be different. Let us first define a source sub-network and a sink sub-network, where the netload is positive and negative, respectively. As shown in Fig. 8-5, sub-network 1 is a source, while sub-network 2 is a sink. To this end, the judgment of saturation can be described as:

$$\sum_{l\in\mathcal{C}} f_l > \sum_{l\in\mathcal{C}_{UD}} W_l + \sum_{l\in\mathcal{C}_D^+} W_l \tag{8.7}$$

where $\mathcal{C}_{UD}$ is the collection of the undirected edges connecting the two sub-networks; $\mathcal{C}_{UD}^+$ is the collection of the directed edges connecting the two sub-network whose direction is from the source to sink.

Under normal operation, there is no saturated cut-set, and any saturated cut-set will result in overload.

Assume $P_{\mathcal{C}}$ unit of power needs to be transferred through cut-set $\mathcal{C}$ at a given time. If the loss of an edge $l \in \mathcal{C}$ saturates the cut-set $\mathcal{C}$, the edge *l* is called a *critical asset*. For example, as shown in Fig. 8-5, when the edge 5-6 is lost, 30 kWh of energy on the transmission lines needs to be rerouted. However, only 20 kWh of them can be routed through the remaining edges, and hence edge 5-6 is a *critical asset*. It indicates that the spare capacity of the cut-set

$R_{\mathcal{C}}$ is smaller than $P_{\mathcal{C}}$. The loss of the critical asset will result in that $\mathbb{M}=P_{\mathcal{C}}-R_{\mathcal{C}}$ unit of energy cannot be delivered, where $\mathbb{M}$ is called *transfer margin*.

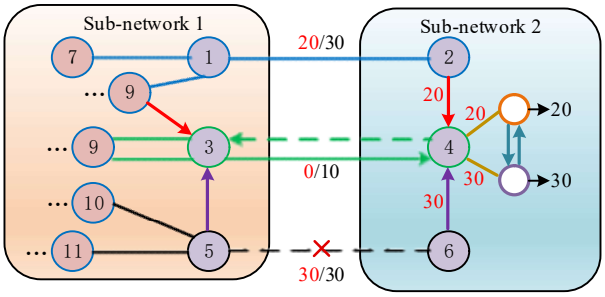

Fig. 8-5. Illustration of critical assets.

Based on the graph theory, the edge *l* can belong to more than one cut-set, and *N* of these cut-sets are saturated if edge *l* is lost. For each saturated cut-set, we have a different value of transfer margin, and we identify the largest transfer margin, i.e., $\mathbb{M}_l=\max\left(\mathbb{M}_{n,l}\right)$, n=1,2,3...N. The cut-set with the largest transfer margin is called *the limiting critical cut-set*. The identification of the critical asset and limiting critical cut-set is based on the graph searching algorithm with dynamic programming (DP) shown as the pseudocode in Algorithm I.

Algorithm I: Identification of the critical asset

main *void()*:

for *l* **in** $\mathcal{E}$ **do**

Initialize $\mathcal{S}'=\mathcal{S}=(\mathcal{V},\mathcal{E})$, $TC_l=0$ (*TC* is the counter of spare capacity).

Remove edge *l* with vertices $\mathcal{V}^S,\mathcal{V}^D$ from $\mathcal{S}'$.

while (no unsaturated path *P* between $\mathcal{V}^S$ and $\mathcal{V}^D$) **do**:

P=*DP*($\mathcal{S}'=(\mathcal{V},\mathcal{E})$, $\mathcal{V}^S$, $\mathcal{V}^D$). //select a path (*P* is an index)

Calculate the maximum spare capacity C_p that can reroute the flow on edge *l* through path *P*.

$TC_l=TC_l+C_p$. //add up spare capacity of indirect paths

Update the weight of the edges in $\mathcal{S}'=(\mathcal{V},\mathcal{E})$.

Mark path *P* as saturated.

end while

$\mathbb{M}_l = f_l - TC_l$. //calculate the transfer margin

if $\mathbb{M}_l > 0$ **then** mark edge *l* as a critical asset.

Cluster all vertices that can be reached from $\mathcal{V}^S$ without traversing a saturated edge as cluster 1.

Cluster the other vertices that cannot be reached from $\mathcal{V}^S$ without traversing a saturated edge as cluster 2.

Identify the limiting critical cut-set $\mathcal{C}$ as the edges starting from cluster 1, ending in cluster 2.

end for

function *DP*($\mathcal{S}' = (\mathcal{V}, \mathcal{E}), \mathcal{V}^S, \mathcal{V}^D$):

Traverse all the indirect paths *P* of the $\mathcal{S}'$ between $\mathcal{V}^S$ and $\mathcal{V}^D$ according to ref.[353].

Mark the spare capacity C_p of the indirect paths.

P= argmax(C_p).

return *P*

8.2.2 Proposed Vulnerability Criterion Under Cascade Contingencies

The identification of the critical asset and the limiting critical cut-set can reveal the vulnerability of the network. If the loss of an edge does not generate a critical asset, it indicates that the overload problem does not happen, and the transfer margin equals 0 at this moment. If the loss of an edge generates a critical asset, the transfer margin will be larger than 0, and $\mathbb{M}$ units of energy will be undelivered. Therefore, the transfer margin can be utilized as a criterion to assess the vulnerability of the network. A smaller $\mathbb{M}$ indicates a less vulnerable network.

The vulnerability assessment of the network can be a dynamic process during the cascade contingencies. When more contingencies happen sequentially, the network may become more vulnerable. First, a set of contingency scenarios are created based on the spatial and temporal distribution of extreme events. The loss of one edge under extreme events usually triggers a cascade. Therefore, in each scenario, a contingency list is established. A criterion called *transfer margin ratio* (TMR) that aims at assessing the vulnerability of the network under cascade contingency in different scenarios is proposed as:

$$TMR = \sum_s \sum_k \left(\left(\pi_s \mathbb{M}_{k,s} \Big/ \sum_{l \in \mathcal{C}_{k,s}} W_l \right) \times \exp(-\phi \cdot k) \Big/ \exp(-\phi) \right) \tag{8.8}$$

where s is the index of scenarios; k is the index of contingency events; π_s is the weight of the scenario; $\mathbb{M}_{k,s}$ is the transfer margin; ϕ is the positive decay factor.

The physical meaning of TMR is the ratio of undelivered power to the capacity (weights in Ξ) of the corresponding limiting critical cut-set, which represents the burden of the critical assets. The decay factor ϕ is designed to imply the level of risk aversion. If the operator is less risk-averse, ϕ will be set to a relatively large value, and the future cascade will be less focused.

8.3 Lower and Upper Bound of the Network Vulnerability

8.3.1 Hybrid Power Distribution Factor

The PTDF is widely utilized in power systems to indicate the sensitivity of the power flow on each line to power injection on each node. In ref. [14], the concept of hybrid power distribution factor (HPTDF) is proposed for the coupled power and EV networks. In this chapter, we borrow the similar concept and extend the HPTDF to the coupled transportation and multi-energy networks. The HPTDF can be expressed as the following matrix:

$$\mathcal{H} = \begin{bmatrix} \mathbf{P}^{SF}_{l^{EE},\mathcal{V}^E} & \mathbf{P}^{SF}_{l^{ET},\mathcal{V}^E} & \mathbf{P}^{SF}_{l^{IT},\mathcal{V}^E} & \mathbf{P}^{SF}_{l^{GT},\mathcal{V}^E} & \mathbf{P}^{SF}_{l^{GG},\mathcal{V}^E} \\ \mathbf{P}^{SF}_{l^{EE},\mathcal{V}^T} & \mathbf{P}^{SF}_{l^{ET},\mathcal{V}^T} & \mathbf{P}^{SF}_{l^{IT},\mathcal{V}^T} & \mathbf{P}^{SF}_{l^{GT},\mathcal{V}^T} & \mathbf{P}^{SF}_{l^{GG},\mathcal{V}^T} \\ \mathbf{P}^{SF}_{l^{EE},\mathcal{V}^G} & \mathbf{P}^{SF}_{l^{ET},\mathcal{V}^G} & \mathbf{P}^{SF}_{l^{IT},\mathcal{V}^G} & \mathbf{P}^{SF}_{l^{GT},\mathcal{V}^G} & \mathbf{P}^{SF}_{l^{GG},\mathcal{V}^G} \end{bmatrix}^T, \quad \forall l \in \mathcal{E}, \forall \mathcal{V} \tag{8.9}$$

where $P^{SF}_{l,\mathcal{V}}$ represents the power flow changes on edge l with a unit power injection/outflow at node $\mathcal{V}$, and $\mathbf{P}^{SF}_{l,\mathcal{V}}$ is its vector form.

The power flow variation on edge l with a unit power injection at the generation node g and a unit outflow at the demand node d can be calculated as (8.10) based on the element in the matrix $\mathcal{H}$.

$$P^{SF}_{l,gd} = P^{SF}_{l,g} - P^{SF}_{l,d}, \quad \forall l \in \mathcal{E}, \forall g,d \in \mathcal{V} \tag{8.10}$$

Then, the power flow on edge l associated with the power injection at g and the power outflow at d can be expressed as:

$$P^{B}_{l,gd,t} = P^{SF}_{l,gd} \cdot P^{B}_{l,t}, \quad \forall l \in \mathcal{E}, \forall g,d \in \mathcal{V}, \forall t \tag{8.11}$$

where $P^{B}_{l,t}$ is the power flow on edge l at time t.

8.3.2 Upper-level Problem

In this section, we derive the upper bound (optimistic case) and lower bound (pessimistic case) of the coupled network vulnerability envelope based on the bi-level MILP. The objective function of the upper-level problem is shown in

equation (8.12). It builds attacks to the coupled network to minimize or maximize the remaining network connectivity between the generation nodes and demand nodes after contingencies, representing the lower and upper vulnerability bound, respectively.

$$\text{min or max} \quad g_{N^{DR}}(\mathbf{x},\boldsymbol{\delta}) = \sum_{(g,d)\in\Omega^{GD}} \sum_{l\in\mathcal{E}} P^{B}_{l,gd,t} \cdot \delta_{gd,t} \cdot \Delta t \tag{8.12}$$

where $\delta_{gd,t}$ represents the connectivity between generation node *g* and demand node *d*; Ω^{GD} is the set of generation node and demand node pairs; $\sum_{l\in\mathcal{E}} P^{B}_{l,gd,t}$ calculates the power transition from the generation node *g* to the demand node *d*.

The constraints can be shown as:

$$\sum_{l} x_{l,t} \le N^{DR}, \quad \forall t \tag{8.13}$$

$$-\xi \cdot \left(1-\delta_{gd,t}\right) + \varepsilon \le Y_{gd,t} \le \xi \cdot \delta_{gd,t}, \quad \forall g,d \in \mathcal{V}, \forall t \tag{8.14}$$

$$x_{l,t} \in \{0,1\}, \delta_{gd} \in \{0,1\}, \quad \forall l \in \mathcal{E}, \forall g,d \in \mathcal{V}, \forall t \tag{8.15}$$

where $x_{l,t}$ indicates whether the edge l is disrupted; N^{DR} is the number of the disrupted edges; ξ is a large positive constant; ε is a small positive constant; $Y_{gd,t}$ is auxiliary flow.

Equation (8.13) constraints the maximum number of attacks that can be built. Equation (8.14), along with the lower-level problem, links the state variable $\delta_{gd,t}$ in the objective function to the decision variable $x_{l,t}$. The value of $Y_{gd,t}$ is obtained in the lower-level problem. Equation (8.15) indicates that $\delta_{gd,t}$ and $x_{l,t}$ are binary variables.

8.3.3 Lower-level Problem

The lower-level problem is modeled as (8.16)-(8.18).

$$\max_{y_{gd,t}} \quad Y_{gd,t} \tag{8.16}$$

$$\sum_{l\in\Theta_i^+} y_{l,t} - \sum_{d\in\Theta_i^-} y_{l,t} = \begin{cases} Y_{gd,t} & ,i=g \\ 0 & ,i\ne g,d \\ -Y_{gd,t} & ,i=d \end{cases}, \quad \forall t \tag{8.17}$$

$$y_{l,t} \le 1 - x_{l,t}, \quad \forall l \in \mathcal{E}, \forall t \tag{8.18}$$

where $y_{l,t}$ is a binary variable indicating whether the edge l is selected in the route sequence connection check; Θ_i^+ is the set of the edge emanating from node *g*; Θ_i^- is the set of the edge going to node *g*.

The objective function maximizes the auxiliary flow from node *g to* node *d*. Combined equations (8.14) and (8.16), it is found that if the auxiliary flow equals 0, the generation node *g* and demand node *g* are disconnected. Constraint (8.17) restricts the typology of the select transition from the generation node *g* to the demand node *g* is connected in sequence. Constraint (8.18) describes the relationship between $y_{l,t}$ and $x_{l,t}$. The bi-level optimization problem can be reformulated as a single-level problem by substituting the lower-level problem with its KKT conditions, according to ref. [354].

The upper and lower vulnerability bounds highlight the importance of systematically considering all possible simultaneous interruptions and the effectiveness of the proposed optimization method.

These vulnerability ranges can be used to assist in the development of possible system improvements in emergency plans. The interrupted link causing the maximum system loss should be protected as much as possible, and the interrupted link causing the minimum system loss can be ignored, especially when the resources of the emergency plan are limited.

8.4 Dynamic Vulnerability Assessment Framework

This section presents a dynamic vulnerability assessment framework before and during the contingencies.

Different from the outage of the transmission line, where the failure will lead to an immediate shutdown of the line, the gas pipeline can still operate with reduced service if the failure is a small leak rather than a complete rupture. In this case, the leaking pipeline will have a reduced capacity considering the leak load [351]:

$$S_{l^{GG}}^{B,\max} - \alpha\left(1+\beta\tau\right)^{-1/2}\sqrt{\pi_t}\,, \quad \forall l^{GG} \in \mathcal{E}^{GG}, \forall t \tag{8.19}$$

where α and β are given constant depend on the diameter of the leak and pipeline parameters; τ is the distance between the leaking point and its source node; π_t is the pressure of the source node.

The same as the gas pipeline, the road section can also provide reduced service if it is not fully blocked. The reduced capacity of the road section $C_{l^{TT}}^{\max,rd}$ is considered as a known parameter when contingencies occur. Furthermore, the spatial demand shift through the transportation network has a longer time delay than the energy transmission in hydrogen and electricity networks.

Considering the abovementioned fast and slow dynamic characteristics, a dynamic vulnerability assessment framework is proposed in Algorithm II to integrate the vulnerability assessment tools and the criteria presented in the previous sections.

Algorithm II: Dynamic Vulnerability Assessment

Initialize the network capacity graph Ξ of the coupled network.

Sample the load profile P_t^D and create the contingencies through Monte Carlo simulation.

Calculate the HPTDF.

for *t* **in** ***T*** **do**

  Calculate the power flow in the coupled network.

  if contingencies happen

    then remove the edge in Ξ or update the reduced weight in Ξ according to the type of contingencies.

    Create the power flow graph $\mathcal{F}$ and spare capacity graph $\mathcal{S}$.

    Calculate the HPTDF of the remaining network.

  end if

  Identify the critical asset according to Algorithm I.

  Calculate the TMR according to (8.8).

  Obtain the upper bound and lower bound of the coupled network vulnerability envelope according to (8.12)-(8.18).

  if there is flow on road section (spatial demand shift occurs)

    then calculate the spatial demand shift delay Δt acoordiing to the UE model.

    Update the future load profile by adding the spatial load shift at time *t* to the load profile of the corresponding node at $t+\Delta t$.

  end if

end for

8.5 Case Study

The proposed vulnerability assessment methodology is verified in the case studies. The test system is an IEEE 39-bus electricity network coupled with a 25-node transportation network and a 50-node hydrogen network, as shown in Fig. 8-6.

The following three cases are established for comparison.

Case 1: Only PEVs exist in the system, and all the charging relies on the electricity networks.

Case 2: Only PEVs and FCEVs exist in the system, and the energy supplement relies on both charging through the electricity network and refueling through the hydrogen network. However, the energy substitution effect does not exist.

Case 3: The penetration of PH2EVs is further considered, and the energy substitution effect can be formulated.

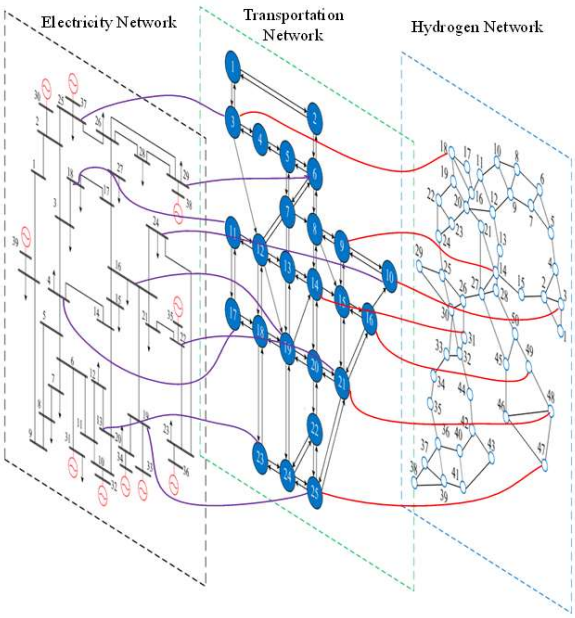

Fig. 8-6. Tested coupled transportation and multi-energy network.

8.5.1 Critical Asset and TMR

First, the vulnerability of the coupled transportation and multi-energy networks is assessed through critical asset identification and TMR. It is assumed that a cascade outage occurs at a certain time period, where edges 17-27, 16-18, 24^{*}-25^{*}, 26^{*}-27^{*}, and 14^{+}-20^{+} disrupted sequentially (the index with the asterisk mark "$*$" represents gas nodes; the index with the plus mark "$_{+}$" represents transportation nodes; the index without any mark represents electricity buses). Based on Fig. 8-6 and Table 8-1, the following information can be obtained:

Initial state: When there is no contingency, three critical assets are identified, namely edges 21-16, 23-25, 4^{*}-5^{*}, indicating any disruption occurring on these edges will result in an overload problem. The corresponding limiting critical cut-sets are {21-16, 21-22}, {21-22, 23-24}, {10^{*}-11^{*},9^{*}-12^{*},4^{*}-5^{*}}, with transfer margin 231.5, 165.2, 389.7 MW. The TMR of the initial state is 0.46.

Disruption 1: When the transmission line 17-27 is lost, a new critical asset occurs, i.e., transmission lines 25-26, and the TMR under this outage is 0.13.

Disruption 2: When the transmission line 16-17 is lost, a new critical asset occurs, i.e., transmission lines 17-18, and the TMR under this outage is 0.24. To be noted, this outage will result in potential risks to the charging services of EVs since the corresponding limiting critical cut-set contains several charging links.

Disruption 3: When pipeline 24*-25* is lost, two additional critical assets emerge, namely 26*-27* and 45*-46*, and the hydrogen refueling services will face risk since the refueling links are included in the limiting critical cut-set.

Disruption 4: When the pipeline 26*-27*, which is the critical asset in outage 3, is disrupted, the hydrogen refueling

services will be directly affected since refueling link 14*-9+ becomes a new critical asset.

Disruption 5: When the road 14*-20* is blocked, no new critical asset is created.

To summarize the abovementioned information, it is found that the contingency in the transportation system is less likely to cause an impact on the energy supplement of the EVs. Besides, the riskiest event is disruption 3, which has the highest TMR of 0.53. Additionally, the vulnerability of the coupled network during this period is relatively good since the charging and refueling services are not directly impacted until the fourth disruption.

TABLE 8-1. CRITICAL ASSET IDENTIFICATION AND TMR UNDER CASCADE CONTINGENCIES

Event	New critical asset	Limiting critical cut-set	Transfer margin (MW)	TMR
Initial	21-16	{21-16, 21-22}	231.5	0.46
	23-24	{21-22, 23-24}	165.2	
	4^{*}-5^{*}	{10^{*}-11^{*},9^{*}-12^{*},4^{*}-5^{*}}	389.7	
Disruption 1: Edge 17-27	25-26	{25-26,17-27,29-6^{+}}	85.2	0.13
Disruption 2: Edge 16-17	17-18	{26-25,17-18,16-17,25-3^{+},24-10^{+}, 18-11^{+},22-21^{+},16-19^{+},4-17^{+},13-23^{+}, 19-25^{+}}	126.2	0.24
Disruption 3: Edge 24^{*}-25^{*}	26^{*}-27^{*}	{26^{*}-27^{*},24^{*}-25^{*},27^{*}-45^{*} ,28^{*}-50^{*},3^{*}-10^{+},18^{*}-3^{+},14^{*}-9^{+}}	335.2	0.53
	45^{*}-46^{*}	{45^{*}-46^{*},48^{*}-49^{*},48^{*}-21^{+},47^{*}-25^{+}}	356.8	
Disruption 4: Edge 26^{*}-27^{*}	14^{*}-9^{+}	{26^{*}-27^{*},24^{*}-25^{*},27^{*}-45^{*}, 28^{*}-50^{*},3^{*}-10^{+},18^{*}-3^{+},14^{*}-9^{+}}	222.1	0.23
Outage 5: Edge 14^{+}-20^{+}	-	-	-	-

Apart from the presented contingencies above, we sample 500 different types of cascade contingencies through Monte Carlo simulation. The top 20 occurrence frequency of the edges that become a critical asset is shown in Figs. 8-7. It can be found that the first ten edges with the highest occurrence frequency are the transmission lines or gas pipelines. The charging link 16-19^{+} and 13-23^{+} ranked 15 and 20, respectively. The refueling link 14^{*}-9^{+} and 14^{*}-49^{+} ranked 11 and 18, respectively. Among the top 20, there is no transportation road.

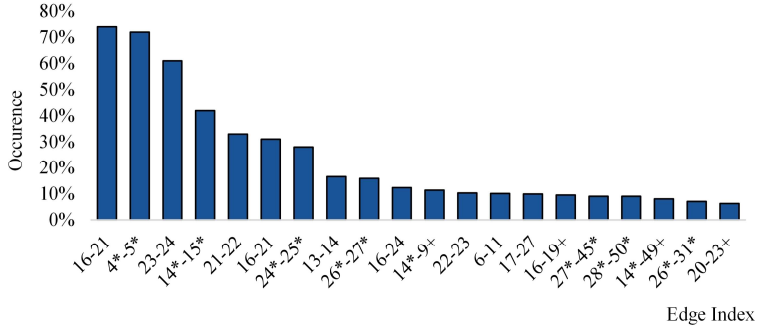

Fig. 8-7. Ranking of the critical assets with top 20 occurrence frequency.

Then, we further display the TMR at different time periods in three cases. Fig. 8-8 shows the scenario in that no contingency happens during the whole day. Generally, the shape of the TMR complies with the trend of the energy demand profile, and there are three peaks, a morning peak, a noon peak (especially in summer), and an evening peak. It is found that Case 1 has the highest TMR all the time. It means that although no contingency occurs, Case 1 has the highest energy transfer burden since all the energy supplement of EVs relies on the electricity network only. Compared with Case 1, Case 2 can help reduce the TMR level since part of the charging burden is transferred to hydrogen refueling. In Case 3, the TMR is further reduced, especially the peak values, since the energy substitution effect plays an important role during the peak hours.

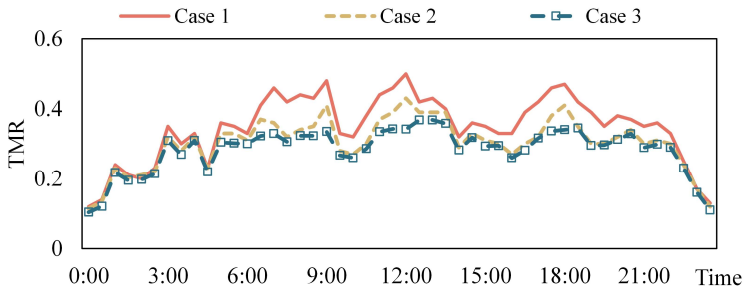

Fig. 8-8. TMR profile when no contingency happens.

Fig. 8-9 shows the TMR curve of the whole day under the situation that the contingencies only happen in the electricity network. Compared Fig. 8-8 with Fig. 8-9, it is not surprising that the TMR level is increased when contingencies occur. In Fig. 8-9, it is found that the penetration of FCEV and PH2EVs can help to reduce the energy transfer burden. When contingencies happen in electricity networks, the energy substitution effect of PH2EVs can significantly reduce the TMR during 8:00-10:00 and 17:00-18:00.

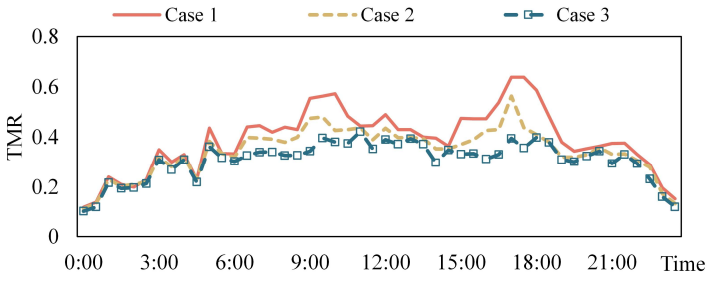

Fig. 8-9. TMR profile when contingencies happen only in the electricity network.

Fig. 8-10 shows the TMR curve of the whole day under the situation where the contingencies happen both in the electricity network and hydrogen network. In this scenario, although Case 2 and Case 3 can still reduce the TMR level, the effect is not obvious.

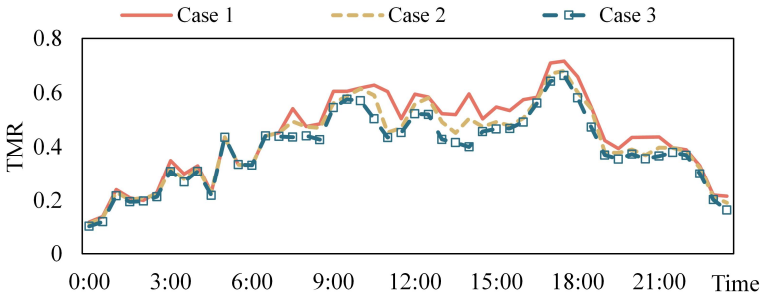

Fig. 8-10. TMR profile when contingencies happen in both electricity and hydrogen networks.

Figs. 8-11 to 8-13 show the average TMR at the different types of time periods of the whole coupled network, electricity network, and hydrogen network, respectively. The type of time period includes the traffic rush hour (7:00-9:00,17:00-19:00), morning electricity usage peak (8:00-10:00), noon peak (11:00-14:00), evening peak (18:00-21:00), and off-peak (the rest of the time). To be noted, there are overlapping between traffic rush hour and the electricity usage peaks (8:00-9:00,18:00-19:00).

From the view of the whole coupled system, the TMR during the rush hour and the electricity usage during peak hour is higher than that of off-peak, and the overlapping period has the highest value. During all the types of periods, Case 1 has the highest TMR, followed by Case 2. As for the electricity network, the TMR of Case 3 is higher than Cases 1 and 2 during the morning peak and evening peak. It may be because part of the hydrogen refueling burden is transferred to the electricity network through energy substitution to realize the overall reduction of TMR. From the view of the hydrogen network, the TMR at the overlapping period of Case 3 is higher than that of Cases 1 and 2. It means that hydrogen usage becomes intensive to ensure the overall energy supply of the system during this overlapping peak period, and the utilization of hydrogen helps enhance the flexibility and alternatives of energy during the energy usage peak.

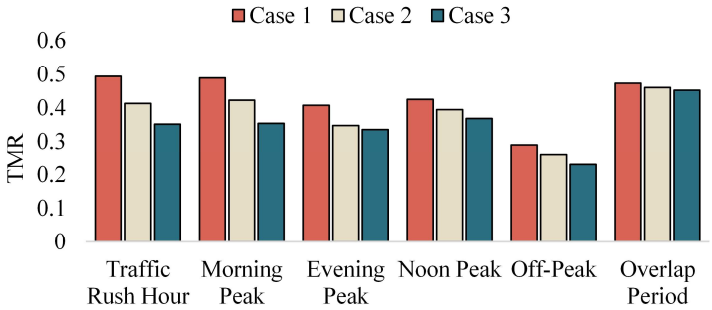

Fig. 8-11. TMR of the whole coupled network at different periods.

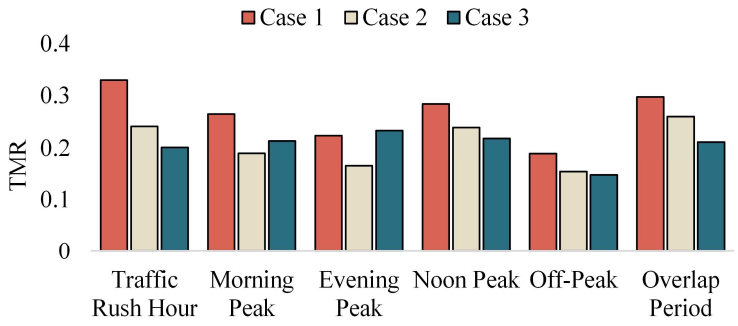

Fig. 8-12. TMR of the electricity network at different periods.

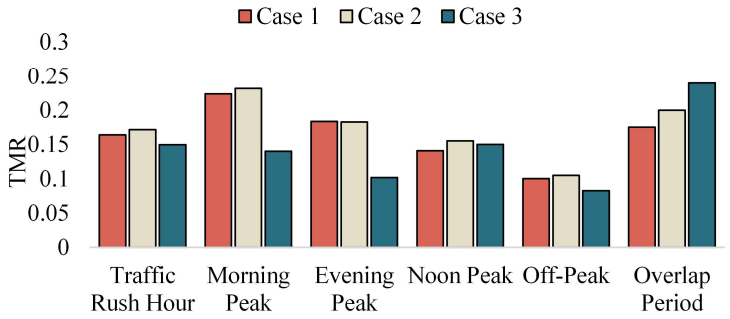

Fig. 8-13. TMR of the hydrogen network at different periods.

TABLE 8-2. TMR UNDER DIFFERENT RISK AVERSION

	TMR Under Different Risk Aversion, ϕ				
	0	0.1	0.2	0.3	0.4
Case 1	1.76	1.46	1.25	1.08	0.96
Case 2	1.69	1.39	1.18	1.02	0.91
Case 3	1.59	1.32	1.12	0.97	0.86

Table 8-2 provides the TMR of three cases under different risk aversion levels reflected by parameter ϕ. It can be concluded when a larger value of ϕ (less focused on the future cascade), a lower TMR value (less vulnerable) can be obtained. Compared ϕ =0.4 with ϕ =0, the TMR difference between the three cases is reduced. It indicates the future cascade will have a more severe impact on Case 1, while Case 3 shows a better vulnerability mitigation capability under cascade disruptions.

8.5.2 Upper and Lower Bound of Vulnerability

Second, the upper and lower bounds of vulnerability are assessed through the bi-level optimization problem. Figs. 8-14 to 8-16 show the relationship between the remaining network connectivity measured in the total energy transferred (the objective value of the upper-level problem) and the number of disrupted edges in different cases. Since the disruption in transportation roads has a relatively small impact on the vulnerability of the coupled network, we only consider the disruptions in electricity and hydrogen networks. The upper bound is a maximization problem representing the best case, while the lower bound is a minimum problem representing the worst case.

In Case 1, the best case starts to lose connectivity when there are 2 disrupted edges, and the largest slope occurs when there are 7 disrupted edges. The largest slope represents the riskiest disruption, whose failures could create a dramatic degradation of the vulnerability bound. In the worst case, the connectivity of the coupled network begins to reduce when there is 1 disrupted edge, and the largest slope occurs when there are 3 disrupted edges. The network is fully disconnected when there are 16 disrupted edges in the worst case, while the network still can support partial energy transfer when there are 20 disrupted edges in the best case. The largest range between upper bound and lower bound occurs when there are 6 disrupted edges. The largest range can inform how resilient the coupled network is against disruptions and the robustness under uncertainties.

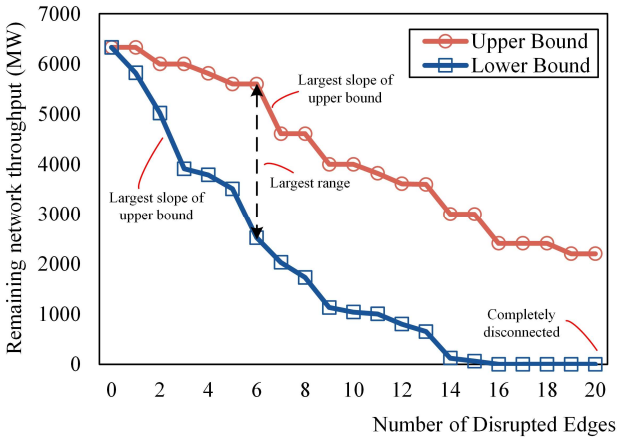

Fig. 8-14. Vulnerability envelope of the coupled network in Case 1.

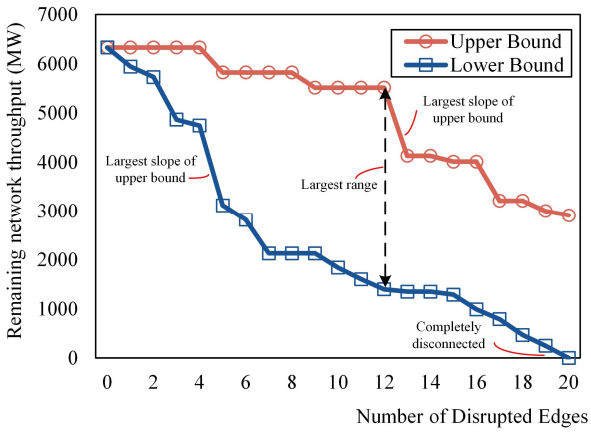

Fig. 8-15. Vulnerability envelope of the coupled network in Case 2.

Similar to Case 1, the best case of Case 2 starts to lose connectivity when there are 5 disrupted edges, and the largest slope occurs when there are 13 disrupted edges. In the worst case, the connectivity of the coupled network begins to reduce when there is 1 disrupted edge, and the largest slope occurs when there are 5 disrupted edges. The network is fully disconnected when there are 20 disrupted edges in the worst case. The largest range occurs when there are 12 disrupted edges.

Comparing Case 3 with Case 2, the largest difference is that the largest range occurs when there are 10 disrupted

edges in Case 3, and the largest slope occurs when there are 17 disrupted edges.

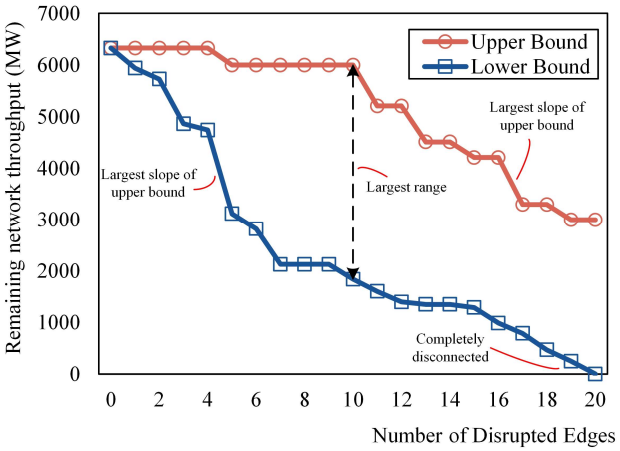

Fig. 8-16. Vulnerability envelope of the coupled network in Case 3.

In summary, both Case 2 and Case 3 show better performance for the following reasons: first, the network starts to lose connectivity earlier in Case 1 than in Cases 2 and 3 in the best case. Second, the largest slope occurs earlier in Case 1 than in Cases 2 and 3. Third, the earlier the completely disconnected point occurs in Case 1, the less survivable is the network to disruptions. Fourth, the overall remaining network connectively measured in power delivered of Cases 2 and 3 is obviously higher than in Case 1. To be noted, it is found that the value of the largest range of Case 1 is smaller than that of Cases 2 and 3. However, it does not mean that Case 1 overweighs Cases 2 and 3 in this aspect. The smaller largest range of Case 1 is caused by the fast reduction of the upper bound. Actually, it is expected that a smaller largest range can be obtained under the same level of upper bound. Hence, it can be concluded that the penetration of FCEVs and PH2EVs can help mitigate the vulnerability of the coupled network. However, the difference between Case 2 and Case 3 is very slight.

8.6 Chapter Summary

In this chapter, a vulnerability assessment methodology is proposed for the coupled transportation and multi-energy network, considering the integration of PEVs, FCEVs, and PH2EVs. First, a novel graph representation for the coupled transportation and multi-energy network is proposed, where the spatial charging/refueling demand shift between different charging/refueling stations and the energy substitution effect of electricity and hydrogen are reflected. Second, based on the graph theory, the critical assets are identified, and TMR is utilized to assess the vulnerability level. Finally, the lower bound and upper bound of vulnerability, representing the optimistic case and the pessimistic case, are found based on a bi-level optimization problem. The applicability of the proposed method is verified on the IEEE 39-bus power network coupled with a 25-node transportation network and a 50-node hydrogen network. The case studies

demonstrate the vulnerable point of the coupled network at the given cascade events, which will affect the charging/refueling services. Besides, based on TMR, the vulnerability level of the system at different time periods is displayed. Through vulnerability envelope assessment, the remaining network connectivity can be identified by considering all possible simultaneous disruptions. The simulation results also reveal that the penetration of FCEVs and PH2EVs can enhance energy flexibility through the energy substitution effect and thus mitigate the system vulnerability.

In future works, we will mainly focus on the methods to mitigate the vulnerability of the coupled network based on the proposed vulnerability assessment method. The development of possible system improvements in emergency plans will be focused on so that the reliability of the charging/refueling services for EVs can be ensured, especially during peak hours.

CHAPTER 9

CONCLUSION AND FUTURE WORKS

The energy transition and planning of future smart grids is a complex task that integrates various emerging network elements, including various ESS, DGs, etc., toward a low-carbon system. The planning of the smart grids refers to a comprehensive analysis to determine the time, location, and type of adding new facilities in multi-networks with multiple energy carriers to facilitate economic, secure and reliable operations of a complex artificial system. Apart from the network planning, the energy transition should further figure out the operation strategy and related trading mechanism to facilitate the stakeholders to adapt to the future transition.

To address the abovementioned problems, this thesis presents an energy transition roadmap and smart grid planning framework. The main contributions can be summarized as follow:

1) An electricity network transition roadmap is proposed. The early retirement of the CFPPs is optimized jointly with the system expansion and renewable energy investment. Therefore, the network can realize energy transition smoothly and reach a real low carbon level in the future. The concept of the average cost of emission reduction is presented to maximize the emission reduction efficiency. The P2GSes construction problem is modeled based on a carbon emission flow model. Hence, the energy consumed and re-produced by P2GSes is relatively clean.
2) An emission control strategy based on a chance-constrained carbon footprint management model is proposed to restrict the direct and indirect from both the generation side and demand side. On the generation side, the network will actively dispatch renewable energy as a priority, and on the demand side, the flexible load will actively respond to carbon-integrated electricity prices. The proposed model aims to address the carbon obligation allocation of the consumers from the perspective of consumption and provide a technical basis for demand-driven stimulation to reduce carbon emissions.
3) A novel CERs and RECs trading mechanism is formulated. A methodology is proposed to investigate the correlation between ETS and RECs, aiming at filling the gap between different mechanisms. The dominant buyers of RECs transfer from electricity consumers to thermal generators. The thermal generators can purchase RECs to increase the carbon emission quotas. The mature ETS drives the development of the RECs market and increases the purchase motivation of RECs. The pricing model of RECs is proposed for the first time. A bi-level optimization

model based on a cooperative game approach is proposed. In the optimization model, renewable plants can cooperate with P2GSes to compete with thermal generators aiming at earning more payoffs. Hence, the proposed model can investigate how P2GSes smooth the output of renewable energy.

4) Transportation electrification is integrated into smart grid planning to achieve a real low-carbon society. The FCS planning and the network expansion are solved jointly. To ensure that the FCSs can provide high-quality fast-charging services to EVs, a QoS assessment method is proposed to help the planned system better adapt to different EV penetration levels at all stages. The proposed planning strategy further considers the impact of the distribution system expansion on the transmission level. Hence, based on [13], an integrated transmission and distribution system planning strategy is further presented to help the planner select an adaptive planning strategy under the EV diffusion to maximize social welfare. The proposed integrated method further enhances the flexibility of the EV charging network and distribution network so that fewer changes are required in the transmission network under different future scenarios.

5) A multi-network planning framework for the hydrogen refueling system is proposed for FCEVs. The proposed framework couples the electricity network, transportation networks, and hydrogen network to enhance the system flexibility. Different from the on-site hydrogen generation, the proposed system structure allows the HPSs and HRSs to be located at different places, and a flexible hydrogen supply chain is presented. The penetration of different vehicles, including internal combustion vehicles, EVs, and FCEVs are discussed. An optimized penetration ratio is solved to realize the complementary role of different types of vehicles.

7) The vulnerability assessment of a multi-network system is proposed. The proposed graph representation can further reflect the spatial charging/refueling demand shift between different charging/refueling stations and the energy substitution effect of electricity and hydrogen. A critical asset identification tool is applied to find the vulnerability point of the coupled network. Based on critical asset identification, a new criterion called TMR is put forward to assess the dynamic vulnerability level under cascade contingencies. Based on the proposed bi-level optimization model, the lower bound and upper bound of vulnerability, which is the vulnerability envelope while circumventing the need to enumerate all possible disruption scenarios, is investigated. The identification of the vulnerability envelope can be used to assist in the development of possible system improvements in emergency plans.

In the future, the following works can be expected.

1) Following the deregulation of the electricity industry, power system planning encounters many challenges as a result of the advent of various market participants, such as market uncertainties and conflicting objectives. The

market competition and market-based planning and operation facilitating competition, alleviating congestion, improving social welfare, and minimizing risks, can be further analyzed.

2) The advanced uncertainties modeling technologies, which are expected to achieve a better trade-off between cost and reliability, can be further utilized
3) The evaluation of the planning solution can be further improved by considering more assessment criteria, frequency requirement modeling, and transient stability analysis.
4) The modeling considering different carbon policies can be further considered. The modeling of carbon emission control and carbon trading mechanism incorporated into the coordinated optimization for the multi-energy system still exists considerable room for further research in the future.
5) In recent years, big data technologies developed rapidly. The data-intensive simulations can be further integrated, e.g., price forecasting, load forecasting, and other tackling techniques of big data.
6) With the development of information and communication technologies, strategic planning in future energy transition roadmap and intelligent grid planning can be extended by considering the 5G technologies and beyond 5G applications.

REFERENCES

[1] M. L. Tuballa and M. L. Abundo, "A review of the development of smart grid technologies," *Renewable and Sustainable Energy Reviews,* vol. 59, pp. 710-725, 2016.

[2] R. Hemmati, R.-A. Hooshmand, and A. Khodabakhshian, "State-of-the-art of transmission expansion planning: Comprehensive review," *Renewable and Sustainable Energy Reviews,* vol. 23, pp. 312-319, 2013.

[3] S. K. Khator and L. C. Leung, "Power distribution planning: A review of models and issues," *IEEE Transactions on Power Systems,* vol. 12, no. 3, pp. 1151-1159, 1997.

[4] B. Singh and J. Sharma, "A review on distributed generation planning," *Renewable and Sustainable Energy Reviews,* vol. 76, pp. 529-544, 2017.

[5] A. Ehsan and Q. Yang, "State-of-the-art techniques for modelling of uncertainties in active distribution network planning: A review," *Applied Energy,* vol. 239, pp. 1509-1523, 2019.

[6] E. Guelpa, A. Bischi, V. Verda, M. Chertkov, and H. Lund, "Towards future infrastructures for sustainable multi-energy systems: A review," *Energy,* vol. 184, pp. 2-21, 2019.

[7] P. Mancarella, "MES (multi-energy systems): An overview of concepts and evaluation models," *Energy,* vol. 65, pp. 1-17, 2014.

[8] S. Micari, A. Polimeni, G. Napoli, L. Andaloro, and V. Antonucci, "Electric vehicle charging infrastructure planning in a road network," *Renewable and Sustainable Energy Reviews,* vol. 80, pp. 98-108, 2017.

[9] R. Allan, "Power system reliability assessment—A conceptual and historical review," *Reliability Engineering & System Safety,* vol. 46, no. 1, pp. 3-13, 1994.

[10] N. Council, "Reliability Concepts in Bulk Power Electric Systems," *Princeton, NJ: North American Electric Reliability Council,* 1985.

[11] N. Bhusal, M. Abdelmalak, M. Kamruzzaman, and M. Benidris, "Power system resilience: Current practices, challenges, and future directions," *IEEE Access,* vol. 8, pp. 18064-18086, 2020.

[12] A. Abedi, L. Gaudard, and F. Romerio, "Review of major approaches to analyze vulnerability in power system," *Reliability Engineering & System Safety,* vol. 183, pp. 153-172, 2019.

[13] G. Muñoz-Delgado, J. Contreras, J. M. Arroyo, A. S. de la Nieta, and M. Gibescu, "Integrated transmission and distribution system expansion planning under uncertainty," *IEEE Transactions on Smart Grid,* vol. 12, no. 5, pp. 4113 - 4125, 2021.

[14] N. Liu, X. Hu, L. Ma, and X. Yu, "Vulnerability assessment for coupled network consisting of power grid and EV traffic network," *IEEE Transactions on Smart Grid,* vol. 13, no. 1, pp. 589-598, 2021.

[15] D. Pozo, E. E. Sauma, and J. Contreras, "A three-level static MILP model for generation and transmission expansion planning," *IEEE Transactions on Power Systems,* vol. 28, no. 1, pp. 202-210, 2012.

[16] S. Jin and S. M. Ryan, "A tri-level model of centralized transmission and decentralized generation expansion planning for an electricity market—Part I," *IEEE Transactions on Power Systems,* vol. 29, no. 1, pp. 132-141, 2013.

[17] S. Teimourzadeh and F. Aminifar, "MILP formulation for transmission expansion planning with short-circuit level constraints," *IEEE Transactions on Power Systems,* vol. 31, no. 4, pp. 3109-3118, 2015.

[18] J. Choi, T. Tran, A. A. El-Keib, R. Thomas, H. Oh, and R. Billinton, "A method for transmission system expansion planning considering probabilistic reliability criteria," *IEEE Transactions on Power Systems,* vol. 20, no. 3, pp. 1606-1615, 2005.

[19] O. B. Tor, A. N. Guven, and M. Shahidehpour, "Congestion-driven transmission planning considering the impact of generator expansion," *IEEE Transactions on Power Systems,* vol. 23, no. 2, pp. 781-789, 2008.

[20] J. H. Zhao, Z. Y. Dong, P. Lindsay, and K. P. Wong, "Flexible transmission expansion planning with uncertainties in an electricity market," *IEEE Transactions on Power Systems,* vol. 24, no. 1, pp. 479-488, 2009.

[21] M. Shahidehpour, F. Tinney, and Y. Fu, "Impact of security on power systems operation," *Proceedings of the IEEE,* vol. 93, no. 11, pp. 2013-2025, 2005.

[22] S. Dehghan, N. Amjady, and A. Kazemi, "Two-stage robust generation expansion planning: a mixed integer linear programming model," *IEEE Transactions on Power Systems,* vol. 29, no. 2, pp. 584-597, 2013.

[23] J. H. Roh, M. Shahidehpour, and L. Wu, "Market-based generation and transmission planning with uncertainties," *IEEE Transactions on Power*

Systems, vol. 24, no. 3, pp. 1587-1598, 2009.

[24] H. Kim, S. Lee, S. Han, and W. Kim, "Integrated optimization of generation and transmission expansion planning using decomposition method," in *Proc. 2015 6th International Conference on Intelligent Systems, Modelling and Simulation*, 2015, pp. 158-163.

[25] S. K. Ng, J. Zhong, and C. W. Lee, "A game-theoretic study of the strategic interaction between generation and transmission expansion planning," in *Proc. 2009 IEEE/PES Power Systems Conference and Exposition*, 2009, pp. 1-10.

[26] S. K. Ng, C. Lee, and J. Zhong, "A game-theoretic approach to study strategic interaction between transmission and generation expansion planning," in *Proc. 2006 38th North American Power Symposium*, 2006, pp. 115-120.

[27] W. Shengyu, C. Lu, Y. Xiaoqing, and Y. Bo, "Long-term generation expansion planning under uncertainties and fluctuations of multi-type renewables," in *Proc. 2015 IEEE 5th International Conference on Power Engineering, Energy and Electrical Drives (POWERENG)*, 2015, pp. 612-616.

[28] J. Wen, X. Han, J. Li, Y. Chen, H. Yi, and C. Lu, "Transmission network expansion planning considering uncertainties in loads and renewable energy resources," *CSEE Journal of Power and Energy Systems,* vol. 1, no. 1, pp. 78-85, 2015.

[29] P. M. de Quevedo, G. Muñoz-Delgado, and J. Contreras, "Impact of electric vehicles on the expansion planning of distribution systems considering renewable energy, storage, and charging stations," *IEEE Transactions on Smart Grid,* vol. 10, no. 1, pp. 794-804, 2017.

[30] A. Moreira, D. Pozo, A. Street, and E. Sauma, "Reliable renewable generation and transmission expansion planning: co-optimizing system's resources for meeting renewable targets," *IEEE Transactions on Power Systems,* vol. 32, no. 4, pp. 3246-3257, 2016.

[31] M. Asensio, G. Munoz-Delgado, and J. Contreras, "Bi-level approach to distribution network and renewable energy expansion planning considering demand response," *IEEE Transactions on Power Systems,* vol. 32, no. 6, pp. 4298-4309, 2017.

[32] V. Asgharian and M. Abdelaziz, "A linear programing model for coordinated low-carbon generation and transmission expansion planning," in *Proc. 2017 IEEE Electrical Power and Energy Conference (EPEC)*, 2017, pp. 1-6.

[33] J. Wu, J. Qiu, X. Wang, Y. Ni, X. Han, J. Dai, Z. Du, and X. Xie, "Study on medium and long-term generation expansion planning method considering the requirements of green low-carbon development," in *Proc. 2018 IEEE PES Asia-Pacific Power and Energy Engineering Conference (APPEEC)*, 2018, pp. 689-694.

[34] L. C. da Costa Jr, F. S. Thomé, J. D. Garcia, and M. V. F. Pereira, "Reliability-constrained power system expansion planning: A stochastic risk-averse optimization approach," *IEEE Transactions on Power Systems,* vol. 36, no. 1, pp. 97-106, 2020.

[35] J. Qiu, Z. Y. Dong, J. Zhao, Y. Xu, F. Luo, and J. Yang, "A risk-based approach to multi-stage probabilistic transmission network planning," *IEEE Transactions on Power Systems,* vol. 31, no. 6, pp. 4867-4876, 2016.

[36] J. Qiu, H. Yang, Z. Y. Dong, J. Zhao, F. Luo, M. Lai, and K. P. Wong, "A probabilistic transmission planning framework for reducing network vulnerability to extreme events," *IEEE Transactions on Power Systems,* vol. 31, no. 5, pp. 3829-3839, 2015.

[37] J. A. López, K. Ponnambalam, and V. H. Quintana, "Generation and transmission expansion under risk using stochastic programming," *IEEE Transactions on Power Systems,* vol. 22, no. 3, pp. 1369-1378, 2007.

[38] R. Billinton, Y. Gao, and R. Karki, "Application of a joint deterministic-probabilistic criterion to wind integrated bulk power system planning," *IEEE Transactions on Power Systems,* vol. 25, no. 3, pp. 1384-1392, 2010.

[39] M. Petitet, "Effects of risk aversion on investment decisions in electricity generation: What consequences for market design?," in *Proc. 2016 13th International Conference on the European Energy Market (EEM)*, pp. 1-5.

[40] D. B. Richardson and L. D. D. Harvey, "Optimizing renewable energy, demand response and energy storage to replace conventional fuels in Ontario, Canada," *Energy,* vol. 93, pp. 1447-1455, 2015.

[41] H. Mavalizadeh, A. Ahmadi, F. H. Gandoman, P. Siano, and H. A. Shayanfar, "Multiobjective robust power system expansion planning considering generation units retirement," *IEEE Systems Journal,* vol. 12, no. 3, pp. 2664-2675, 2017.

[42] P. Suriya, S. Subramanian, S. Ganesan, and M. Hariprasath, "Multi-objective generation expansion and retirement planning using chaotic grasshopper optimisation algorithm," *Australian Journal of Electrical and Electronics Engineering,* vol. 16, no. 3, pp. 136-148, 2019.

[43] Y. Tohidi, F. Aminifar, and M. Fotuhi-Firuzabad, "Generation expansion and retirement planning based on the stochastic programming," *Electric Power Systems Research,* vol. 104, pp. 138-145, 2013.

[44] M. Farhoumandi, F. Aminifar, and M. Shahidehpour, "Generation expansion planning considering the rehabilitation of aging generating units," *IEEE Transactions on Smart Grid,* vol. 11, no. 4, pp. 3384-3393, 2020.

[45] W. Shen, J. Qiu, and Z. Dong, "Electricity network planning targeting low-carbon energy transition," *Global Energy Interconnection,* vol. 1, no. 4, pp. 487-499, 2018.

[46] A. Ehsan, Q. Yang, and M. Cheng, "A scenario-based robust investment planning model for multi-type distributed generation under uncertainties," *IET Generation, Transmission & Distribution,* vol. 12, no. 20, pp. 4426-4434, 2018.

[47] D. Q. Hung, N. Mithulananthan, and R. C. Bansal, "Analytical strategies for renewable distributed generation integration considering energy loss minimization," *Applied Energy,* vol. 105, pp. 75-85, 2013.

[48] A. Ehsan and Q. Yang, "Robust distribution system planning considering the uncertainties of renewable distributed generation and electricity demand," in *Proc*., pp. 1-6.

[49] N. Amjady, A. Attarha, S. Dehghan, and A. J. Conejo, "Adaptive robust expansion planning for a distribution network with DERs," *IEEE Transactions on Power Systems,* vol. 33, no. 2, pp. 1698-1715, 2017.

[50] V. F. Martins and C. L. T. Borges, "Active distribution network integrated planning incorporating distributed generation and load response uncertainties," *IEEE Transactions on Power Systems,* vol. 26, no. 4, pp. 2164-2172, 2011.

[51] F. A. Chacra, P. Bastard, G. Fleury, and R. Clavreul, "Impact of energy storage costs on economical performance in a distribution substation," *IEEE Transactions on Power Systems,* vol. 20, no. 2, pp. 684-691, 2005.

[52] Y. Yang, H. Li, A. Aichhorn, J. Zheng, and M. Greenleaf, "Sizing strategy of distributed battery storage system with high penetration of photovoltaic for voltage regulation and peak load shaving," *IEEE Transactions on Smart Grid,* vol. 5, no. 2, pp. 982-991, 2013.

[53] M. Sedghi, A. Ahmadian, and M. Aliakbar-Golkar, "Optimal storage planning in active distribution network considering uncertainty of wind power distributed generation," *IEEE Transactions on Power Systems,* vol. 31, no. 1, pp. 304-316, 2015.

[54] Y. J. A. Zhang, C. Zhao, W. Tang, and S. H. Low, "Profit-maximizing planning and control of battery energy storage systems for primary frequency control," *IEEE Transactions on Smart Grid,* vol. 9, no. 2, pp. 712-723, 2016.

[55] S. Mei, Y. Wang, F. Liu, X. Zhang, and Z. Sun, "Game approaches for hybrid power system planning," *IEEE Transactions on Sustainable Energy,* vol. 3, no. 3, pp. 506-517, 2012.

[56] H. Alharbi and K. Bhattacharya, "Stochastic optimal planning of battery energy storage systems for isolated microgrids," *IEEE Transactions on Sustainable Energy,* vol. 9, no. 1, pp. 211-227, 2017.

[57] H. Akhavan-Hejazi and H. Mohsenian-Rad, "Energy storage planning in active distribution grids: A chance-constrained optimization with non-parametric probability functions," *IEEE Transactions on Smart Grid,* vol. 9, no. 3, pp. 1972-1985, 2016.

[58] X. Shen, M. Shahidehpour, Y. Han, S. Zhu, and J. Zheng, "Expansion planning of active distribution networks with centralized and distributed energy storage systems," *IEEE Transactions on Sustainable Energy,* vol. 8, no. 1, pp. 126-134, 2016.

[59] A. S. A. Awad, T. H. M. El-Fouly, and M. M. A. Salama, "Optimal ESS allocation and load shedding for improving distribution system reliability," *IEEE Transactions on Smart Grid,* vol. 5, no. 5, pp. 2339-2349, 2014.

[60] Y. Zheng, Y. Song, A. Huang, and D. J. Hill, "Hierarchical optimal allocation of battery energy storage system for multiple services in distribution systems," *IEEE Transactions on Sustainable Energy,* vol. 11, no. 3, pp. 1911 - 1921, 2019.

[61] S. De La Torre, A. J. Conejo, and J. Contreras, "Transmission expansion planning in electricity markets," *IEEE Transactions on Power Systems,* vol. 23, no. 1, pp. 238-248, 2008.

[62] L. P. Garcés, A. J. Conejo, R. García-Bertrand, and R. Romero, "A bilevel approach to transmission expansion planning within a market environment," *IEEE Transactions on Power Systems,* vol. 24, no. 3, pp. 1513-1522, 2009.

[63] P. Maghouli, S. H. Hosseini, M. O. Buygi, and M. Shahidehpour, "A multi-objective framework for transmission expansion planning in deregulated environments," *IEEE Transactions on power systems,* vol. 24, no. 2, pp. 1051-1061, 2009.

[64] R. Hemmati, R.-A. Hooshmand, and A. Khodabakhshian, "Market based transmission expansion and reactive power planning with consideration of wind and load uncertainties," *Renewable and Sustainable Energy Reviews,* vol. 29, pp. 1-10, 2014.

[65] N. E. Koltsaklis, A. S. Dagoumas, M. C. Georgiadis, G. Papaioannou, and C. Dikaiakos, "A mid-term, market-based power systems planning model," *Applied Energy,* vol. 179, pp. 17-35, 2016.

[66] J. H. Roh, M. Shahidehpour, and Y. Fu, "Market-based coordination of transmission and generation capacity planning," *IEEE Transactions on Power Systems,* vol. 22, no. 4, pp. 1406-1419, 2007.

[67] A. Mirakyan and R. De Guio, "Modelling and uncertainties in integrated energy planning," *Renewable and Sustainable Energy Reviews,* vol. 46,

pp. 62-69, 2015.

[68] T. Sowa, A. Stroband, W. Cramer, S. Koopmann, and A. Schnettler, "An AC power flow linearization for power system optimization using linear programming," in *Proc. 2016 IEEE Electrical Power and Energy Conference (EPEC)*, pp. 1-5.

[69] J. Qiu, H. Yang, Z. Y. Dong, J. H. Zhao, K. Meng, F. J. Luo, and K. P. Wong, "A linear programming approach to expansion co-planning in gas and electricity markets," *IEEE Transactions on Power Systems,* vol. 31, no. 5, pp. 3594-3606, 2015.

[70] S. Rehman, L. M. Al-Hadhrami, and M. M. Alam, "Pumped hydro energy storage system: A technological review," *Renewable and Sustainable Energy Reviews,* vol. 44, pp. 586-598, 2015.

[71] H. Blanco and A. Faaij, "A review at the role of storage in energy systems with a focus on Power to Gas and long-term storage," *Renewable and Sustainable Energy Reviews,* vol. 81, pp. 1049-1086, 2018.

[72] G. Guandalini, S. Campanari, and M. C. Romano, "Power-to-gas plants and gas turbines for improved wind energy dispatchability: Energy and economic assessment," *Applied Energy,* vol. 147, pp. 117-130, 2015.

[73] Y. Yang, H. Long, K. Wu, X. Yan, and S. Xia, "Integrated electricity and heating load control based on smart grid technology," in *Proc. 2012 China International Conference on Electricity Distribution*, pp. 1-5.

[74] R. Li, W. Wei, S. Mei, Q. Hu, and Q. Wu, "Participation of an energy hub in electricity and heat distribution markets: An MPEC approach," *IEEE Transactions on Smart Grid,* vol. 10, no. 4, pp. 3641-3653, 2018.

[75] K. Orehounig, R. Evins, and V. Dorer, "Integration of decentralized energy systems in neighbourhoods using the energy hub approach," *Applied Energy,* vol. 154, pp. 277-289, 2015.

[76] A. Bostan, M. S. Nazar, M. Shafie-Khah, and J. P. S. Catalão, "Optimal scheduling of distribution systems considering multiple downward energy hubs and demand response programs," *Energy,* vol. 190, p. 116349, 2020.

[77] I. Ersoz and U. Colak, "Combined cooling, heat and power planning under uncertainty," *Energy,* vol. 109, pp. 1016-1025, 2016.

[78] C. Wang, N. Gao, J. Wang, N. Jia, T. Bi, and K. Martin, "Robust operation of a water-energy nexus: A multi-energy perspective," *IEEE Transactions on Sustainable Energy,* vol. 11, no. 4, pp. 2698-2712, 2020.

[79] S. Schiebahn, T. Grube, M. Robinius, V. Tietze, B. Kumar, and D. Stolten, "Power to gas: Technological overview, systems analysis and economic assessment for a case study in Germany," *International journal of hydrogen energy,* vol. 40, no. 12, pp. 4285-4294, 2015.

[80] N. Liu, J. Wang, and L. Wang, "Hybrid energy sharing for multiple microgrids in an integrated heat–electricity energy system," *IEEE Transactions on Sustainable Energy,* vol. 10, no. 3, pp. 1139-1151, 2018.

[81] S. Wang, Y. Ding, C. Ye, C. Wan, and Y. Mo, "Reliability evaluation of integrated electricity–gas system utilizing network equivalent and integrated optimal power flow techniques," *Journal of Modern Power Systems and Clean Energy,* vol. 7, no. 6, pp. 1523-1535, 2019.

[82] X. Zhang, M. Shahidehpour, A. Alabdulwahab, and A. Abusorrah, "Optimal expansion planning of energy hub with multiple energy infrastructures," *IEEE Transactions on Smart Grid,* vol. 6, no. 5, pp. 2302-2311, 2015.

[83] M. A. Mirzaei, M. Z. Oskouei, B. Mohammadi-Ivatloo, A. Loni, K. Zare, M. Marzband, and M. Shafiee, "Integrated energy hub system based on power-to-gas and compressed air energy storage technologies in the presence of multiple shiftable loads," *IET Generation, Transmission & Distribution,* vol. 14, no. 13, pp. 2510-2519, 2020.

[84] L. Ma, N. Liu, J. Zhang, and L. Wang, "Real-time rolling horizon energy management for the energy-hub-coordinated prosumer community from a cooperative perspective," *IEEE Transactions on Power Systems,* vol. 34, no. 2, pp. 1227-1242, 2018.

[85] W. Zhong, C. Yang, K. Xie, S. Xie, and Y. Zhang, "ADMM-based distributed auction mechanism for energy hub scheduling in smart buildings," *IEEE Access,* vol. 6, pp. 45635-45645, 2018.

[86] A. Sheikhi, M. Rayati, S. Bahrami, and A. M. Ranjbar, "Integrated demand side management game in smart energy hubs," *IEEE Transactions on Smart Grid,* vol. 6, no. 2, pp. 675-683, 2015.

[87] S. Bahrami, M. Toulabi, S. Ranjbar, M. Moeini-Aghtaie, and A. M. Ranjbar, "A decentralized energy management framework for energy hubs in dynamic pricing markets," *IEEE Transactions on Smart Grid,* vol. 9, no. 6, pp. 6780-6792, 2017.

[88] Y. Liang, W. Wei, and C. Wang, "A generalized Nash equilibrium approach for autonomous energy management of residential energy hubs," *IEEE Transactions on Industrial Informatics,* vol. 15, no. 11, pp. 5892-5905, 2019.

[89] S. Fan, Z. Li, J. Wang, L. Piao, and Q. Ai, "Cooperative economic scheduling for multiple energy hubs: a bargaining game theoretic perspective," *IEEE Access,* vol. 6, pp. 27777-27789, 2018.

[90] F. Ueckerdt, R. Brecha, and G. Luderer, "Analyzing major challenges of wind and solar variability in power systems," *Renewable energy,* vol. 81, pp. 1-10, 2015.

[91] X. Deng and T. Lv, "Power system planning with increasing variable renewable energy: A review of optimization models," *Journal of Cleaner Production,* vol. 246, p. 118962, 2020.

[92] J. Aghaei, M. A. Akbari, A. Roosta, and A. Baharvandi, "Multiobjective generation expansion planning considering power system adequacy," *Electric Power Systems Research,* vol. 102, pp. 8-19, 2013.

[93] T. Luz, P. Moura, and A. de Almeida, "Multi-objective power generation expansion planning with high penetration of renewables," *Renewable and Sustainable Energy Reviews,* vol. 81, pp. 2637-2643, 2018.

[94] P. S. Moura and A. T. de Almeida, "Multi-objective optimization of a mixed renewable system with demand-side management," *Renewable and Sustainable Energy Reviews,* vol. 14, no. 5, pp. 1461-1468, 2010.

[95] P. Tafarte, S. Das, M. Eichhorn, and D. Thrän, "Small adaptations, big impacts: Options for an optimized mix of variable renewable energy sources," *Energy,* vol. 72, pp. 80-92, 2014.

[96] J. Hui, W. Cai, C. Wang, and M. Ye, "Analyzing the penetration barriers of clean generation technologies in China's power sector using a multi-region optimization model," *Applied Energy,* vol. 185, pp. 1809-1820, 2017.

[97] N. E. Koltsaklis and M. C. Georgiadis, "A multi-period, multi-regional generation expansion planning model incorporating unit commitment constraints," *Applied Energy,* vol. 158, pp. 310-331, 2015.

[98] S.-G. Kim, J.-Y. Jung, and M. K. Sim, "A two-step approach to solar power generation prediction based on weather data using machine learning," *Sustainability,* vol. 11, no. 5, p. 1501, 2019.

[99] J. Lin, J. Ma, and J. Zhu, "A privacy-preserving federated learning method for probabilistic community-level behind-the-meter solar generation disaggregation," *IEEE Transactions on Smart Grid,* vol. 13, no. 1, pp. 268-279, 2021.

[100] W. Sun, M. Zamani, M. R. Hesamzadeh, and H.-T. Zhang, "Data-driven probabilistic optimal power flow with nonparametric Bayesian modeling and inference," *IEEE Transactions on Smart Grid,* vol. 11, no. 2, pp. 1077-1090, 2019.

[101] W. Yao, J. Zhao, F. Wen, Z. Dong, Y. Xue, Y. Xu, and K. Meng, "A multi-objective collaborative planning strategy for integrated power distribution and electric vehicle charging systems," *IEEE Transactions on Power Systems,* vol. 29, no. 4, pp. 1811-1821, 2014.

[102] A. Shukla, K. Verma, and R. Kumar, "Multi-objective synergistic planning of EV fast-charging stations in the distribution system coupled with the transportation network," *IET Generation, Transmission & Distribution,* vol. 13, no. 15, pp. 3421-3432, 2019.

[103] Y. Tao, J. Qiu, S. Lai, X. Zhang, and G. Wang, "Collaborative planning for electricity distribution network and transportation system considering hydrogen fuel cell vehicles," *IEEE Transactions on Transportation Electrification,* vol. 6, no. 3, pp. 1211 - 1225, 2020.

[104] X. Zhang, P. Li, J. Hu, M. Liu, G. Wang, J. Qiu, and K. W. Chan, "Yen's algorithm based charging facility planning considering congestion in coupled transportation and power systems," *IEEE Transactions on Transportation Electrification,* vol. 5, no. 4, pp. 1134 - 1144, 2019.

[105] W. Gan, M. Shahidehpour, M. Yan, J. Guo, W. Yao, A. Paaso, L. Zhang, and J. Wen, "Coordinated planning of transportation and electric power networks with the proliferation of electric vehicles," *IEEE Transactions on Smart Grid,* vol. 11, no. 5, pp. 4005-4016, 2020.

[106] F. He, D. Wu, Y. Yin, and Y. Guan, "Optimal deployment of public charging stations for plug-in hybrid electric vehicles," *Transportation Research Part B: Methodological,* vol. 47, pp. 87-101, 2013.

[107] X. Dong, Y. Mu, H. Jia, X. Yu, and P. Zeng, "Heuristic planning method of EV fast charging station on a freeway considering the power flow constraints of the distribution network," *Energy Procedia,* vol. 105, pp. 2422-2428, 2017.

[108] X. Dong, Y. Mu, H. Jia, J. Wu, and X. Yu, "Planning of fast EV charging stations on a round freeway," *IEEE Transactions on Sustainable Energy,* vol. 7, no. 4, pp. 1452-1461, 2016.

[109] Z. Liu, F. Wen, and G. Ledwich, "Optimal planning of electric-vehicle charging stations in distribution systems," *IEEE Transactions on Power Delivery,* vol. 28, no. 1, pp. 102-110, 2012.

[110] C. Wu, C. Li, L. Du, and Y. Cao, "A method for electric vehicle charging infrastructure planning," *Automation of Electric Power Systems,* vol. 34, no. 24, pp. 36-39, 2010.

[111] A. Ip, S. Fong, and E. Liu, "Optimization for allocating BEV recharging stations in urban areas by using hierarchical clustering," in *Proc. 2010 6th International Conference on Advanced Information Management and Service (IMS)*, pp. 460-465.

[112] A. Amer, A. Azab, M. A. Azzouz, and A. S. A. Awad, "A stochastic program for siting and sizing fast charging stations and small wind turbines

in urban areas," *IEEE Transactions on Sustainable Energy,* vol. 12, no. 2, pp. 1217-1228, 2021.

[113] A. Hajebrahimi, I. Kamwa, E. Delage, and M. M. A. Abdelaziz, "Adaptive distributionally robust optimization for electricity and electrified transportation planning," *IEEE Transactions on Smart Grid,* vol. 11, no. 5, pp. 4278-4289, 2020.

[114] C. Li, Z. Dong, G. Chen, B. Zhou, J. Zhang, and X. Yu, "Data-driven planning of electric vehicle charging infrastructure: a case study of Sydney, Australia," *IEEE Transactions on Smart Grid,* vol. 12, no. 4, pp. 3289-3304, 2021.

[115] W. Yao, C. Y. Chung, F. Wen, M. Qin, and Y. Xue, "Scenario-based comprehensive expansion planning for distribution systems considering integration of plug-in electric vehicles," *IEEE Transactions on Power Systems,* vol. 31, no. 1, pp. 317-328, 2015.

[116] W. Yang, W. Liu, C. Y. Chung, and F. Wen, "Joint planning of EV fast charging stations and power distribution systems with balanced traffic flow assignment," *IEEE Transactions on Industrial Informatics,* vol. 17, no. 3, pp. 1795-1809, 2020.

[117] C. Zhang, Y. Liu, F. Wu, B. Tang, and W. Fan, "Effective charging planning based on deep reinforcement learning for electric vehicles," *IEEE Transactions on Intelligent Transportation Systems,* vol. 22, no. 1, pp. 542-554, 2020.

[118] L. Luo, W. Gu, Z. Wu, and S. Zhou, "Joint planning of distributed generation and electric vehicle charging stations considering real-time charging navigation," *Applied Energy,* vol. 242, pp. 1274-1284, 2019.

[119] M. Asna, H. Shareef, P. Achikkulath, H. Mokhlis, R. Errouissi, and A. Wahyudie, "Analysis of an optimal planning model for electric vehicle fast-charging stations in Al Ain City, United Arab Emirates," *IEEE Access,* vol. 9, pp. 73678-73694, 2021.

[120] D. Ding, J. Li, P. Tu, H. Wang, T. Cao, and F. Zhang, "Electric vehicle charging warning and path planning method based on spark," *IEEE Access,* vol. 8, pp. 8543-8553, 2020.

[121] N. Wang, C. Wang, Y. Niu, M. Yang, and Y. Yu, "A two-stage charging facilities planning method for electric vehicle sharing systems," *IEEE Transactions on Industry Applications,* vol. 57, no. 1, pp. 149-157, 2020.

[122] Q. Yang, S. Sun, S. Deng, Q. Zhao, and M. Zhou, "Optimal sizing of PEV fast charging stations with Markovian demand characterization," *IEEE Transactions on Smart Grid,* vol. 10, no. 4, pp. 4457-4466, 2018.

[123] S. Wang, Z. Y. Dong, C. Chen, H. Fan, and F. Luo, "Expansion planning of active distribution networks with multiple distributed energy resources and EV sharing system," *IEEE Transactions on Smart Grid,* vol. 11, no. 1, pp. 602-611, 2019.

[124] S. S. K. Madahi, H. Nafisi, H. A. Abyaneh, and M. Marzband, "Co-optimization of energy losses and transformer operating costs based on smart charging algorithm for plug-in electric vehicle parking lots," *IEEE Transactions on Transportation Electrification,* vol. 7, no. 2, pp. 527-541, 2020.

[125] T. Long, Q.-S. Jia, G. Wang, and Y. Yang, "Efficient real-time EV charging scheduling via ordinal optimization," *IEEE Transactions on Smart Grid,* vol. 12, no. 5, pp. 4029 - 4038, 2021.

[126] I. Aravena, S. J. Chapin, and C. Ponce, "Decentralized failure-tolerant optimization of electric vehicle charging," *IEEE Transactions on Smart Grid,* vol. 12, no. 5, pp. 4068 - 4078, 2021.

[127] K. Schwenk, S. Meisenbacher, B. Briegel, T. Harr, V. Hagenmeyer, and R. Mikut, "Integrating battery aging in the optimization for bidirectional charging of electric vehicles," *IEEE Transactions on Smart Grid,* vol. 12, no. 6, pp. 5135 - 5145, 2021.

[128] L. Yan, X. Chen, J. Zhou, Y. Chen, and J. Wen, "Deep reinforcement learning for continuous electric vehicles charging control with dynamic user behaviors," *IEEE Transactions on Smart Grid,* vol. 12, no. 6, pp. 5124 - 5134, 2021.

[129] J. Jin and Y. Xu, "Optimal policy characterization enhanced actor-critic approach for electric vehicle charging scheduling in a power distribution network," *IEEE Transactions on Smart Grid,* vol. 12, no. 2, pp. 1416-1428, 2020.

[130] E. L. Karfopoulos, K. A. Panourgias, and N. D. Hatziargyriou, "Distributed coordination of electric vehicles providing V2G regulation services," *IEEE Transactions on Power Systems,* vol. 31, no. 4, pp. 2834-2846, 2015.

[131] Y. Tao, J. Qiu, and S. Lai, "A data-driven management strategy of electric vehicles and thermostatically controlled loads based on modified generative adversarial network," *IEEE Transactions on Transportation Electrification,* vol. 8, no. 1, pp. 1430 - 1444, 2021.

[132] R. Abousleiman and R. Scholer, "Smart charging: System design and implementation for interaction between plug-in electric vehicles and the power grid," *IEEE Transactions on Transportation Electrification,* vol. 1, no. 1, pp. 18-25, 2015.

[133] E. Sortomme and M. A. El-Sharkawi, "Optimal scheduling of vehicle-to-grid energy and ancillary services," *IEEE Transactions on Smart Grid,* vol. 3, no. 1, pp. 351-359, 2011.

[134] X. Wang, F. Li, J. Dong, M. M. Olama, Q. Zhang, Q. Shi, B. Park, and T. Kuruganti, "Tri-level scheduling model considering residential demand

flexibility of aggregated HVACs and EVs under distribution LMP," *IEEE Transactions on Smart Grid,* vol. 12, no. 5, pp. 3990 - 4002, 2021.

[135] L. Cheng, Y. Chang, and R. Huang, "Mitigating voltage problem in distribution system with distributed solar generation using electric vehicles," *IEEE Transactions on Sustainable Energy,* vol. 6, no. 4, pp. 1475-1484, 2015.

[136] M. Wang, Y. Mu, F. Li, H. Jia, X. Li, Q. Shi, and T. Jiang, "State space model of aggregated electric vehicles for frequency regulation," *IEEE Transactions on Smart Grid,* vol. 11, no. 2, pp. 981-994, 2019.

[137] H. Liu, Z. Hu, Y. Song, and J. Lin, "Decentralized vehicle-to-grid control for primary frequency regulation considering charging demands," *IEEE Transactions on Power Systems,* vol. 28, no. 3, pp. 3480-3489, 2013.

[138] W. Liu, S. Chen, Y. Hou, and Z. Yang, "Optimal reserve management of electric vehicle aggregator: discrete bilevel optimization model and exact algorithm," *IEEE Transactions on Smart Grid,* vol. 12, no. 5, pp. 4003 - 4015, 2021.

[139] X. Sun and J. Qiu, "Hierarchical voltage control strategy in distribution networks considering customized charging navigation of electric vehicles," *IEEE Transactions on Smart Grid,* vol. 12, no. 6, pp. 4752 - 4764, 2021.

[140] L. Zeng, C. Li, Z. Li, M. Shahidehpour, B. Zhou, and Q. Zhou, "Hierarchical bipartite graph matching method for transactive V2V power exchange in distribution power system," *IEEE Transactions on Smart Grid,* vol. 12, no. 1, pp. 301 - 311, 2020.

[141] S. Gao, Z. Zhang, and L. I. U. Chunhua, "Vehicle-to-home, vehicle-to-vehicle, and vehicle-to-grid energy systems," in *Energy Systems for Electric and Hybrid Vehicles*, Ed.: IET, 2016, pp. 431-460.

[142] D. Wu, K. T. Chau, and S. Gao, "Multilayer framework for vehicle-to-grid operation," in *Proc. 2010 IEEE Vehicle Power and Propulsion Conference*, pp. 1-6.

[143] C. Liu, K. T. Chau, D. Wu, and S. Gao, "Opportunities and challenges of vehicle-to-home, vehicle-to-vehicle, and vehicle-to-grid technologies," *Proceedings of the IEEE,* vol. 101, no. 11, pp. 2409-2427, 2013.

[144] E. Bulut and M. C. Kisacikoglu, "Mitigating range anxiety via vehicle-to-vehicle social charging system," in *Proc. 2017 IEEE 85th Vehicular Technology Conference (VTC Spring)*, pp. 1-5.

[145] R. Zhang, X. Cheng, and L. Yang, "Flexible energy management protocol for cooperative EV-to-EV charging," *IEEE Transactions on Intelligent Transportation Systems,* vol. 20, no. 1, pp. 172-184, 2018.

[146] M. Wang, M. Ismail, R. Zhang, X. Shen, E. Serpedin, and K. Qaraqe, "Spatio-temporal coordinated V2V energy swapping strategy for mobile PEVs," *IEEE Transactions on Smart Grid,* vol. 9, no. 3, pp. 1566-1579, 2016.

[147] G. Muñoz-Delgado, J. Contreras, J. M. Arroyo, A. S. de la Nieta, and M. Gibescu, "Transmission and distribution system expansion planning considering network and generation investments under uncertainty," in *Proc. 2020 International Conference on Smart Energy Systems and Technologies (SEST)*, pp. 1-6.

[148] J. Liu, H. Cheng, P. Zeng, L. Yao, C. Shang, and Y. Tian, "Decentralized stochastic optimization based planning of integrated transmission and distribution networks with distributed generation penetration," *Applied Energy,* vol. 220, pp. 800-813, 2018.

[149] M. L. Baughman, "Incorporating transmission and distribution into integrated resource planning," in *Proc. Proceedings of IEEE International Conference on Systems, Man and Cybernetics*, pp. 2361-2366.

[150] A. Z. Dhunny, Z. Allam, D. Lobine, and M. R. Lollchund, "Sustainable renewable energy planning and wind farming optimization from a biodiversity perspective," *Energy,* vol. 185, pp. 1282-1297, 2019.

[151] Y. P. Li and G. H. Huang, "Electric-power systems planning and greenhouse-gas emission management under uncertainty," *Energy Conversion and Management,* vol. 57, pp. 173-182, 2012.

[152] W. Shen, J. Qiu, K. Meng, X. Chen, and Z. Y. Dong, "Low-Carbon Electricity Network Transition Considering Retirement of Aging Coal Generators," *IEEE Transactions on Power Systems,* vol. 35, no. 6, pp. 4193-4205, 2020.

[153] Y. Tao, J. Qiu, S. Lai, J. Zhao, and Y. Xue, "Carbon-oriented electricity network planning and transformation," *IEEE Transactions on Power Systems,* vol. 36, no. 2, pp. 1034-1048, 2020.

[154] Z. Ji, C. Kang, Q. Chen, Q. Xia, C. Jiang, Z. Chen, and J. Xin, "Low-carbon power system dispatch incorporating carbon capture power plants," *IEEE Transactions on Power Systems,* vol. 28, no. 4, pp. 4615-4623, 2013.

[155] E. Denny and M. O'Malley, "Wind generation, power system operation, and emissions reduction," *IEEE Transactions on power systems,* vol. 21, no. 1, pp. 341-347, 2006.

[156] S. Lu, S. Lou, Y. Wu, and X. Yin, "Power system economic dispatch under low-carbon economy with carbon capture plants considered," *IET*

Generation, Transmission & Distribution, vol. 7, no. 9, pp. 991-1001, 2013.

[157] X. Zhou, G. James, A. Liebman, Z. Y. Dong, and C. Ziser, "Partial carbon permits allocation of potential emission trading scheme in Australian electricity market," *IEEE Transactions on Power Systems,* vol. 25, no. 1, pp. 543-553, 2009.

[158] Y. Zhu, Y. P. Li, and G. H. Huang, "Planning carbon emission trading for Beijing's electric power systems under dual uncertainties," *Renewable and Sustainable Energy Reviews,* vol. 23, pp. 113-128, 2013.

[159] X. Wang, Y. Gong, and C. Jiang, "Regional carbon emission management based on probabilistic power flow with correlated stochastic variables," *IEEE Transactions on Power Systems,* vol. 30, no. 2, pp. 1094-1103, 2014.

[160] P. Rajendhar and B. E. Jeyaraj, "Application of DR and co-simulation approach for renewable integrated HEMS: a review," *IET Generation, Transmission & Distribution,* vol. 13, no. 16, pp. 3501-3512, 2019.

[161] N. G. Paterakis, O. Erdinc, A. G. Bakirtzis, and J. P. S. Catalão, "Optimal household appliances scheduling under day-ahead pricing and load-shaping demand response strategies," *IEEE Transactions on Industrial Informatics,* vol. 11, no. 6, pp. 1509-1519, 2015.

[162] Y. Zhang, M. H. Hajiesmaili, S. Cai, M. Chen, and Q. Zhu, "Peak-aware online economic dispatching for microgrids," *IEEE Transactions on Smart Grid,* vol. 9, no. 1, pp. 323-335, 2016.

[163] K. M. Tsui and S.-C. Chan, "Demand response optimization for smart home scheduling under real-time pricing," *IEEE Transactions on Smart Grid,* vol. 3, no. 4, pp. 1812-1821, 2012.

[164] J. H. Yoon, R. Baldick, and A. Novoselac, "Dynamic demand response controller based on real-time retail price for residential buildings," *IEEE Transactions on Smart Grid,* vol. 5, no. 1, pp. 121-129, 2014.

[165] B. Wang, C. Zhang, and Z. Dong, "Interval optimization based coordination of demand response and battery energy storage system considering SoC management in a microgrid," *IEEE Transactions on Sustainable Energy,* vol. 11, no. 4, pp. 2922 - 2931, 2020.

[166] H. Shareef, M. S. Ahmed, A. Mohamed, and E. Al Hassan, "Review on home energy management system considering demand responses, smart technologies, and intelligent controllers," *IEEE Access,* vol. 6, pp. 24498-24509, 2018.

[167] A. Taşcıkaraoğlu, N. G. Paterakis, O. Erdinç, and J. P. S. Catalao, "Combining the flexibility from shared energy storage systems and DLC-based demand response of HVAC units for distribution system operation enhancement," *IEEE Transactions on Sustainable Energy,* vol. 10, no. 1, pp. 137-148, 2018.

[168] S. Zheng, Y. Sun, B. Li, B. Qi, K. Shi, Y. Li, and X. Tu, "Incentive-based integrated demand response for multiple energy carriers considering behavioral coupling effect of consumers," *IEEE Transactions on Smart Grid,* vol. 11, no. 4, pp. 3231 - 3245, 2020.

[169] B. Qela and H. T. Mouftah, "Peak load curtailment in a smart grid via fuzzy system approach," *IEEE Transactions on Smart Grid,* vol. 5, no. 2, pp. 761-768, 2014.

[170] P. Tarasak, C. C. Chai, Y. S. Kwok, and S. W. Oh, "Demand bidding program and its application in hotel energy management," *IEEE Transactions on Smart Grid,* vol. 5, no. 2, pp. 821-828, 2014.

[171] L. Yao and W. H. Lim, "Optimal purchase strategy for demand bidding," *IEEE Transactions on Power Systems,* vol. 33, no. 3, pp. 2754-2762, 2017.

[172] A. S. Algarni, S. Suryanarayanan, H. J. Siegel, and A. A. Maciejewski, "Combined impact of demand response aggregators and carbon taxation on emissions reduction in electric power systems," *IEEE Transactions on Smart Grid,* vol. 12, no. 2, pp. 1825-1827, 2020.

[173] Y. Wang, J. Qiu, Y. Tao, and J. Zhao, "Carbon-oriented operational planning in coupled electricity and emission trading markets," *IEEE Transactions on Power Systems,* vol. 35, no. 4, pp. 3145-3157, 2020.

[174] Y. Wang, J. Qiu, Y. Tao, X. Zhang, and G. Wang, "Low-carbon oriented optimal energy dispatch in coupled natural gas and electricity systems," *Applied Energy,* vol. 280, p. 115948, 2020.

[175] B. Li, Y. Song, and Z. Hu, "Carbon flow tracing method for assessment of demand side carbon emissions obligation," *IEEE Transactions on Sustainable Energy,* vol. 4, no. 4, pp. 1100-1107, 2013.

[176] H. A. Gil and G. Joos, "Generalized estimation of average displaced emissions by wind generation," *iEEE Transactions on Power Systems,* vol. 22, no. 3, pp. 1035-1043, 2007.

[177] C. Kang, T. Zhou, Q. Chen, Q. Xu, Q. Xia, and Z. Ji, "Carbon emission flow in networks," *Scientific reports,* vol. 2, p. 479, 2012.

[178] Y. Cheng, N. Zhang, Y. Wang, J. Yang, C. Kang, and Q. Xia, "Modeling carbon emission flow in multiple energy systems," *IEEE Transactions on Smart Grid,* vol. 10, no. 4, pp. 3562-3574, 2018.

[179] M. Shao and W. T. Jewell, "CO 2 emission-incorporated ac optimal power flow and its primary impacts on power system dispatch and operations," in *Proc. IEEE PES General Meeting*, pp. 1-8.

[180] N. Zhang, Z. Hu, D. Dai, S. Dang, M. Yao, and Y. Zhou, "Unit commitment model in smart grid environment considering carbon emissions trading," *IEEE Transactions on Smart Grid,* vol. 7, no. 1, pp. 420-427, 2015.

[181] A. Shabanpour-Haghighi and A. R. Seifi, "Multi-objective operation management of a multi-carrier energy system," *Energy,* vol. 88, pp. 430-442, 2015.

[182] A. K. Xenophon and D. J. Hill, "Emissions reduction and wholesale electricity price targeting using an output-based mechanism," *Applied Energy,* vol. 242, pp. 1050-1063, 2019.

[183] Z. Lu, C. Lu, T. Feng, and H. Zhao, "Carbon dioxide capture and storage planning considering emission trading system for a generation corporation under the emission reduction policy in China," *IET Generation, Transmission & Distribution,* vol. 9, no. 1, pp. 43-52, 2014.

[184] J. Huang, Y. Xue, C. Jiang, F. Wen, F. Xue, K. Meng, and Z. Y. Dong, "An experimental study on emission trading behaviors of generation companies," *IEEE Transactions on Power Systems,* vol. 30, no. 2, pp. 1076-1083, 2014.

[185] X. R. Li, C. W. Yu, Z. Xu, F. J. Luo, Z. Y. Dong, and K. P. Wong, "A multimarket decision-making framework for GENCO considering emission trading scheme," *IEEE Transactions on Power Systems,* vol. 28, no. 4, pp. 4099-4108, 2013.

[186] S. Lu, Y. Wu, S. Lou, and X. Yin, "A model for optimizing spinning reserve requirement of power system under low-carbon economy," *IEEE Transactions on Sustainable Energy,* vol. 5, no. 4, pp. 1048-1055, 2014.

[187] J. Wang, V. Koritarov, and J.-H. Kim, "An agent-based approach to modeling interactions between emission market and electricity market," in *Proc. IEEE Power & Energy Society General Meeting* pp. 1-8.

[188] D. J. Olsen, Y. Dvorkin, R. Fernandez-Blanco, and M. A. Ortega-Vazquez, "Optimal carbon taxes for emissions targets in the electricity sector," *IEEE Transactions on Power Systems,* vol. 33, no. 6, pp. 5892-5901, 2018.

[189] D. Yang, S. He, Q. Chen, D. Li, and H. Pandžić, "Bidding strategy of a virtual power plant considering carbon-electricity trading," *CSEE Journal of Power and Energy Systems,* vol. 5, no. 3, pp. 306-314, 2019.

[190] Y. Cheng, N. Zhang, Z. Lu, and C. Kang, "Planning multiple energy systems toward low-carbon society: A decentralized approach," *IEEE Transactions on Smart Grid,* vol. 10, no. 5, pp. 4859-4869, 2018.

[191] Y. Cheng, N. Zhang, and C. Kang, "Bi-level expansion planning of multiple energy systems under carbon emission constraints," in *Proc. 2018 IEEE Power & Energy Society General Meeting (PESGM)*, pp. 1-5.

[192] Y. Cheng, N. Zhang, B. Zhang, C. Kang, W. Xi, and M. Feng, "Low-carbon operation of multiple energy systems based on energy-carbon integrated prices," *IEEE Transactions on Smart Grid,* vol. 11, no. 2, pp. 1307-1318, 2019.

[193] M. Pourakbari-Kasmaei, M. Lehtonen, J. Contreras, and J. R. S. Mantovani, "Carbon footprint management: A pathway toward smart emission abatement," *IEEE Transactions on Industrial Informatics,* vol. 16, no. 2, pp. 935-948, 2019.

[194] N. Aparicio, I. MacGill, J. R. Abbad, and H. Beltran, "Comparison of wind energy support policy and electricity market design in Europe, the United States, and Australia," *IEEE Transactions on Sustainable Energy,* vol. 3, no. 4, pp. 809-818, 2012.

[195] P. K. C. Wong, A. Kalam, and R. Barr, "Modelling and analysis of practical options to improve the hosting capacity of low voltage networks for embedded photo-voltaic generation," *IET Renewable Power Generation,* vol. 11, no. 5, pp. 625-632, 2017.

[196] R. Nicoloiu, I. Ionel, and I. Voda, "The evolution of green certificate support scheme for promoting renewable energy in Romania," in *Proc. 2017 International Conference on ENERGY and ENVIRONMENT (CIEM)*, pp. 359-362.

[197] Q. Zhang, G. Wang, Y. Li, H. Li, B. McLellan, and S. Chen, "Substitution effect of renewable portfolio standards and renewable energy certificate trading for feed-in tariff," *Applied Energy,* vol. 227, pp. 426-435, 2018.

[198] M. Hustveit, J. S. Frogner, and S.-E. Fleten, "Tradable green certificates for renewable support: The role of expectations and uncertainty," *Energy,* vol. 141, pp. 1717-1727, 2017.

[199] X. Li, W. Wang, H. Wang, J. Wu, X. Fan, and Q. Xu, "Dynamic environmental economic dispatch of hybrid renewable energy systems based on tradable green certificates," *Energy,* vol. 193, p. 116699, 2020.

[200] Y. Tao, J. Qiu, S. Lai, and J. Zhao, "Renewable energy certificates and electricity trading models: Bi-level game approach," *International Journal of Electrical Power & Energy Systems,* vol. 130, p. 106940, 2021.

[201] CO2 emissions in worldwide shipping in 2020 [Online]. Available: www.statista.com/statistics/216048/worldwide-co2-emissions-by-ship-type/

[202] C. Shang, D. Srinivasan, and T. Reindl, "Economic and environmental generation and voyage scheduling of all-electric ships," *IEEE Transactions on Power Systems,* vol. 31, no. 5, pp. 4087-4096, 2015.

[203] J. Hou, J. Sun, and H. Hofmann, "Adaptive model predictive control with propulsion load estimation and prediction for all-electric ship energy management," *Energy,* vol. 150, pp. 877-889, 2018.

[204] K. Hein, Y. Xu, G. Wilson, and A. K. Gupta, "Coordinated optimal voyage planning and energy management of all-electric ship with hybrid energy storage system," *IEEE Transactions on Power Systems,* vol. 36, no. 3, pp. 2355-2365, 2020.

[205] H. Lan, S. Wen, Y.-Y. Hong, C. Y. David, and L. Zhang, "Optimal sizing of hybrid PV/diesel/battery in ship power system," *Applied Energy,* vol. 158, pp. 26-34, 2015.

[206] Z. Li, Y. Xu, L. Wu, and X. Zheng, "A risk-averse adaptively stochastic optimization method for multi-energy ship operation under diverse uncertainties," *IEEE Transactions on Power Systems,* vol. 36, no. 3, pp. 2149-2161, 2021.

[207] S. Fang, Y. Xu, S. Wen, T. Zhao, H. Wang, and L. Liu, "Data-driven robust coordination of generation and demand-side in photovoltaic integrated all-electric ship microgrids," *IEEE Transactions on Power Systems,* vol. 35, no. 3, pp. 1783-1795, 2019.

[208] E. A. Sciberras, B. Zahawi, D. J. Atkinson, A. Breijs, and J. H. van Vugt, "Managing shipboard energy: A stochastic approach special issue on marine systems electrification," *IEEE Transactions on Transportation Electrification,* vol. 2, no. 4, pp. 538-546, 2016.

[209] R. Tang, X. Li, and J. Lai, "A novel optimal energy-management strategy for a maritime hybrid energy system based on large-scale global optimization," *Applied Energy,* vol. 228, pp. 254-264, 2018.

[210] G. Parise, L. Parise, L. Martirano, P. B. Chavdarian, C.-L. Su, and A. Ferrante, "Wise port and business energy management: Port facilities, electrical power distribution," *IEEE Transactions on Industry Applications,* vol. 52, no. 1, pp. 18-24, 2015.

[211] M. Acciaro, H. Ghiara, and M. I. Cusano, "Energy management in seaports: A new role for port authorities," *Energy Policy,* vol. 71, pp. 4-12, 2014.

[212] D. Paul, K. Peterson, and P. R. Chavdarian, "Designing cold ironing power systems: electrical safety during ship berthing," *IEEE Industry Applications Magazine,* vol. 20, no. 3, pp. 24-32, 2014.

[213] P. Wang, C. Jin, D. Zhu, Y. Tang, P. C. Loh, and F. H. Choo, "Distributed control for autonomous operation of a three-port AC/DC/DS hybrid microgrid," *IEEE Transactions on Industrial Electronics,* vol. 62, no. 2, pp. 1279-1290, 2014.

[214] S. Fang, Y. Wang, B. Gou, and Y. Xu, "Toward future green maritime transportation: An overview of seaport microgrids and all-electric ships," *IEEE Transactions on Vehicular Technology,* vol. 69, no. 1, pp. 207-219, 2019.

[215] Ç. Iris, D. Pacino, and S. Ropke, "Improved formulations and an adaptive large neighborhood search heuristic for the integrated berth allocation and quay crane assignment problem," *Transportation Research Part E: Logistics and Transportation Review,* vol. 105, pp. 123-147, 2017.

[216] S. Wen, H. Lan, Y.-Y. Hong, C. Y. David, L. Zhang, and P. Cheng, "Allocation of ESS by interval optimization method considering impact of ship swinging on hybrid PV/diesel ship power system," *Applied Energy,* vol. 175, pp. 158-167, 2016.

[217] R. Tang, Z. Wu, and X. Li, "Optimal operation of photovoltaic/battery/diesel/cold-ironing hybrid energy system for maritime application," *Energy,* vol. 162, pp. 697-714, 2018.

[218] F. D. Kanellos, E.-S. M. Volanis, and N. D. Hatziargyriou, "Power management method for large ports with multi-agent systems," *IEEE Transactions on Smart Grid,* vol. 10, no. 2, pp. 1259-1268, 2017.

[219] A. Rolán, P. Manteca, R. Oktar, and P. Siano, "Integration of cold ironing and renewable sources in the barcelona smart port," *IEEE Transactions on Industry Applications,* vol. 55, no. 6, pp. 7198-7206, 2019.

[220] T. P. V. Zis, "Prospects of cold ironing as an emissions reduction option," *Transportation Research Part A: Policy and Practice,* vol. 119, pp. 82-95, 2019.

[221] T. Zis, R. J. North, P. Angeloudis, W. Y. Ochieng, and M. G. H. Bell, "Evaluation of cold ironing and speed reduction policies to reduce ship emissions near and at ports," *Maritime Economics & Logistics,* vol. 16, no. 4, pp. 371-398, 2014.

[222] E. A. Sciberras, B. Zahawi, and D. J. Atkinson, "Electrical characteristics of cold ironing energy supply for berthed ships," *Transportation Research Part D: Transport and Environment,* vol. 39, pp. 31-43, 2015.

[223] R. Danilak, "Why energy is a big and rapidly growing problem for data centers," *Forbes,* vol. 15, pp. 12-17, 2017.

[224] X. Zhang, D. Biagioni, M. Cai, P. Graf, and S. Rahman, "An edge-cloud integrated solution for buildings demand response using reinforcement learning," *IEEE Transactions on Smart Grid,* vol. 12, no. 1, pp. 420 - 431, 2020.

[225] L. Wei, C. H. Foh, B. He, and J. Cai, "Towards efficient resource allocation for heterogeneous workloads in IaaS clouds," *IEEE Transactions on Cloud Computing,* vol. 6, no. 1, pp. 264-275, 2015.

[226] X. Zhang, H. Cheng, Z. Yu, and N. Xiong, "Design and analysis of an efficient multi-resource allocation system for cooperative computing in Internet of Things," *IEEE Internet of Things Journal,* 2021.

[227] H. Zhang, Y. Xiao, S. Bu, F. R. Yu, D. Niyato, and Z. Han, "Distributed resource allocation for data center networks: A hierarchical game approach," *IEEE Transactions on Cloud Computing,* vol. 8, no. 3, pp. 778-789, 2018.

[228] T. Abergel, C. Delmastro, and K. Lane. (2020). Tracking Buildings 2020. [Online]. Available: https://www.iea.org/reports/tracking-buildings-2020

[229] M. Ghamkhari, A. Wierman, and H. Mohsenian-Rad, "Energy portfolio optimization of data centers," *IEEE Transactions on Smart Grid,* vol. 8, no. 4, pp. 1898-1910, 2016.

[230] M. Chen, C. Gao, M. Song, S. Chen, D. Li, and Q. Liu, "Internet data centers participating in demand response: A comprehensive review," *Renewable and Sustainable Energy Reviews,* vol. 117, p. 109466, 2020.

[231] N. H. Tran, D. H. Tran, S. Ren, Z. Han, E.-N. Huh, and C. S. Hong, "How geo-distributed data centers do demand response: A game-theoretic approach," *IEEE Transactions on Smart Grid,* vol. 7, no. 2, pp. 937-947, 2015.

[232] J. Li, Z. Bao, and Z. Li, "Modeling demand response capability by internet data centers processing batch computing jobs," *IEEE Transactions on Smart Grid,* vol. 6, no. 2, pp. 737-747, 2014.

[233] Z. Song, X. Zhang, and C. Eriksson, "Data center energy and cost saving evaluation," *Energy Procedia,* vol. 75, pp. 1255-1260, 2015.

[234] A. N. Toosi, C. Qu, M. D. de Assunção, and R. Buyya, "Renewable-aware geographical load balancing of web applications for sustainable data centers," *Journal of Network and Computer Applications,* vol. 83, pp. 155-168, 2017.

[235] Y. Zhan, M. Ghamkhari, D. Xu, S. Ren, and H. Mohsenian-Rad, "Extending demand response to tenants in cloud data centers via non-intrusive workload flexibility pricing," *IEEE Transactions on Smart Grid,* vol. 9, no. 4, pp. 3235-3246, 2016.

[236] Y. Wang, X. Wang, and Y. Zhang, "Leveraging thermal storage to cut the electricity bill for datacenter cooling," in *Proc. Proceedings of the 4th Workshop on Power-Aware Computing and Systems*, pp. 1-5.

[237] M. Chen, C. Gao, M. Shahidehpour, Z. Li, S. Chen, and D. Li, "Internet data center load modeling for demand response considering the coupling of multiple regulation methods," *IEEE Transactions on Smart Grid,* vol. 12, no. 3, pp. 2060 - 2076, 2021.

[238] M. Chen, C. Gao, M. Shahidehpour, and Z. Li, "Incentive-compatible demand response for spatially-coupled Internet data centers in electricity markets," *IEEE Transactions on Smart Grid,* vol. 12, no. 4, pp. 3056 - 3069, 2021.

[239] M. Chen, C. Gao, Z. Li, M. Shahidehpour, Q. Zhou, S. Chen, and J. Yang, "Aggregated model of data network for the provision of demand response in generation and transmission expansion planning," *IEEE Transactions on Smart Grid,* vol. 12, no. 1, pp. 512-523, 2020.

[240] A. Vafamehr, M. E. Khodayar, S. D. Manshadi, I. Ahmad, and J. Lin, "A framework for expansion planning of data centers in electricity and data networks under uncertainty," *IEEE Transactions on Smart Grid,* vol. 10, no. 1, pp. 305-316, 2017.

[241] N. Z. Xu, K. W. Chan, C. Y. Chung, and M. Niu, "Enhancing adequacy of isolated systems with electric vehicle-based emergency strategy," *IEEE Transactions on Intelligent Transportation Systems,* vol. 21, no. 8, pp. 3469 - 3475, 2019.

[242] H. Ko, S. Pack, and V. C. M. Leung, "Mobility-aware vehicle-to-grid control algorithm in microgrids," *IEEE Transactions on Intelligent Transportation Systems,* vol. 19, no. 7, pp. 2165-2174, 2018.

[243] H. H. Abdeltawab and Y. A.-R. I. Mohamed, "Mobile energy storage scheduling and operation in active distribution systems," *IEEE Transactions on Industrial Electronics,* vol. 64, no. 9, pp. 6828-6840, 2017.

[244] G. He, J. Michalek, S. Kar, Q. Chen, D. Zhang, and J. F. Whitacre, "Utility-scale portable energy storage systems," *Joule,* vol. 5, no. 2, pp. 379-392, 2021.

[245] X. Liu, C. B. Soh, T. Zhao, and P. Wang, "Stochastic scheduling of mobile energy storage in coupled distribution and transportation networks for conversion capacity enhancement," *IEEE Transactions on Smart Grid,* vol. 12, no. 1, pp. 117 - 130, 2020.

[246] Y. Sun, Z. Li, M. Shahidehpour, and B. Ai, "Battery-based energy storage transportation for enhancing power system economics and security," *IEEE Transactions on Smart Grid,* vol. 6, no. 5, pp. 2395-2402, 2015.

[247] Y. Song, Y. Liu, R. Wang, and M. Ming, "Multi-objective configuration optimization for isolated microgrid with shiftable loads and mobile energy storage," *IEEE Access,* vol. 7, pp. 95248-95263, 2019.

[248] P. Prabawa and D.-H. Choi, “Multi-agent framework for service restoration in distribution systems with distributed generators and static/mobile energy storage systems,” *IEEE Access,* vol. 8, pp. 51736-51752, 2020.

[249] J. Kim and Y. Dvorkin, “Enhancing distribution system resilience with mobile energy storage and microgrids,” *IEEE Transactions on Smart Grid,* vol. 10, no. 5, pp. 4996-5006, 2018.

[250] S. Yao, P. Wang, and T. Zhao, “Transportable energy storage for more resilient distribution systems with multiple microgrids,” *IEEE Transactions on Smart Grid,* vol. 10, no. 3, pp. 3331-3341, 2018.

[251] S. Yao, P. Wang, X. Liu, H. Zhang, and T. Zhao, “Rolling optimization of mobile energy storage fleets for resilient service restoration,” *IEEE Transactions on Smart Grid,* vol. 11, no. 2, pp. 1030-1043, 2019.

[252] S. Lei, C. Chen, H. Zhou, and Y. Hou, “Routing and scheduling of mobile power sources for distribution system resilience enhancement,” *IEEE Transactions on Smart Grid,* vol. 10, no. 5, pp. 5650-5662, 2018.

[253] H. Yang, S. Zhang, J. Qiu, D. Qiu, M. Lai, and Z. Dong, “CVaR-constrained optimal bidding of electric vehicle aggregators in day-ahead and real-time markets,” *IEEE Transactions on Industrial Informatics,* vol. 13, no. 5, pp. 2555-2565, 2017.

[254] H. Wu, M. Shahidehpour, A. Alabdulwahab, and A. Abusorrah, “A game theoretic approach to risk-based optimal bidding strategies for electric vehicle aggregators in electricity markets with variable wind energy resources,” *IEEE Transactions on Sustainable Energy,* vol. 7, no. 1, pp. 374-385, 2015.

[255] A. Hajebrahimi, I. Kamwa, M. Abdelaziz, and A. Moeini, “Scenario-wise distributionally robust optimization for collaborative intermittent resources and electric vehicle aggregator bidding strategy,” *IEEE Transactions on Power Systems,* vol. 35, no. 5, pp. 3706 - 3718, 2020.

[256] B. Li, X. Wang, M. Shahidehpour, C. Jiang, and Z. Li, “Robust bidding strategy and profit allocation for cooperative DSR aggregators with correlated wind power generation,” *IEEE Transactions on Sustainable Energy,* vol. 10, no. 4, pp. 1904-1915, 2018.

[257] J. Donadee and M. D. Ilić, “Stochastic optimization of grid to vehicle frequency regulation capacity bids,” *IEEE Transactions on Smart Grid,* vol. 5, no. 2, pp. 1061-1069, 2014.

[258] M. Ansari, A. T. Al-Awami, E. Sortomme, and M. A. Abido, “Coordinated bidding of ancillary services for vehicle-to-grid using fuzzy optimization,” *IEEE Transactions on Smart Grid,* vol. 6, no. 1, pp. 261-270, 2014.

[259] S. I. Vagropoulos and A. G. Bakirtzis, “Optimal bidding strategy for electric vehicle aggregators in electricity markets,” *IEEE Transactions on Power Systems,* vol. 28, no. 4, pp. 4031-4041, 2013.

[260] L. Bird and B. Swezey, "Green power marketing in the United States: A status report," National Renewable Energy Lab.(NREL), Golden, CO (United States)2005.

[261] Y. Xiao, X. Wang, P. Pinson, and X. Wang, “A local energy market for electricity and hydrogen,” *IEEE Transactions on Power Systems,* vol. 33, no. 4, pp. 3898-3908, 2017.

[262] R. Ghorani, M. Fotuhi-Firuzabad, and M. Moeini-Aghtaie, “Optimal bidding strategy of transactive agents in local energy markets,” *IEEE Transactions on Smart Grid,* vol. 10, no. 5, pp. 5152-5162, 2018.

[263] A. Yu, C. Zhang, and Y.-J. A. Zhang, “Optimal bidding strategy of prosumers in distribution-level energy markets,” *IEEE Transactions on Power Systems,* vol. 35, no. 3, pp. 1695-1706, 2019.

[264] W. Tushar, T. K. Saha, C. Yuen, D. Smith, and H. V. Poor, “Peer-to-peer trading in electricity networks: an overview,” *IEEE Transactions on Smart Grid,* vol. 11, no. 4, pp. 3185 - 3200, 2020.

[265] Y. Tao, J. Qiu, S. Lai, and J. Zhao, “Integrated electricity and hydrogen energy sharing in coupled energy systems,” *IEEE Transactions on Smart Grid,* vol. 12, no. 2, pp. 1149-1162, 2020.

[266] P. Baez-Gonzalez, E. Rodriguez-Diaz, J. C. Vasquez, and J. M. Guerrero, “Peer-to-peer energy market for community microgrids [technology leaders],” *IEEE Electrification Magazine,* vol. 6, no. 4, pp. 102-107, 2018.

[267] F. Moret and P. Pinson, “Energy collectives: A community and fairness based approach to future electricity markets,” *IEEE Transactions on Power Systems,* vol. 34, no. 5, pp. 3994-4004, 2018.

[268] N. Liu, X. Yu, W. Fan, C. Hu, T. Rui, Q. Chen, and J. Zhang, “Online energy sharing for nanogrid clusters: A Lyapunov optimization approach,” *IEEE Transactions on Smart Grid,* vol. 9, no. 5, pp. 4624-4636, 2017.

[269] B. A. Bhatti and R. Broadwater, “Energy trading in the distribution system using a non-model based game theoretic approach,” *Applied Energy,* vol. 253, p. 113532, 2019.

[270] S. Cui, Y.-W. Wang, and J.-W. Xiao, "Peer-to-peer energy sharing among smart energy buildings by distributed transaction," *IEEE Transactions on Smart Grid,* vol. 10, no. 6, pp. 6491-6501, 2019.

[271] S. Cui, Y.-W. Wang, Y. Shi, and J.-W. Xiao, "A new and fair peer-to-peer energy sharing framework for energy buildings," *IEEE Transactions on Smart Grid,* vol. 11, no. 5, pp. 3817-3826, 2020.

[272] S. Lai, J. Qiu, and Y. Tao, "Credit-based pricing and planning strategies for hydrogen and electricity energy storage sharing," *IEEE Transactions on Sustainable Energy,* vol. 13, no. 1, pp. 67 - 80, 2022.

[273] T. Chen and W. Su, "Indirect customer-to-customer energy trading with reinforcement learning," *IEEE Transactions on Smart Grid,* vol. 10, no. 4, pp. 4338-4348, 2018.

[274] J. Wang, H. Zhong, C. Wu, E. Du, Q. Xia, and C. Kang, "Incentivizing distributed energy resource aggregation in energy and capacity markets: An energy sharing scheme and mechanism design," *Applied Energy,* vol. 252, p. 113471, 2019.

[275] G. van Leeuwen, T. AlSkaif, M. Gibescu, and W. van Sark, "An integrated blockchain-based energy management platform with bilateral trading for microgrid communities," *Applied Energy,* vol. 263, p. 114613, 2020.

[276] A. Esmat, M. de Vos, Y. Ghiassi-Farrokhfal, P. Palensky, and D. Epema, "A novel decentralized platform for peer-to-peer energy trading market with blockchain technology," *Applied Energy,* vol. 282, p. 116123, 2020.

[277] H. Almasalma, S. Claeys, and G. Deconinck, "Peer-to-peer-based integrated grid voltage support function for smart photovoltaic inverters," *Applied Energy,* vol. 239, pp. 1037-1048, 2019.

[278] A. I. Nikolaidis, C. A. Charalambous, and P. Mancarella, "A graph-based loss allocation framework for transactive energy markets in unbalanced radial distribution networks," *IEEE Transactions on Power Systems,* vol. 34, no. 5, pp. 4109-4118, 2018.

[279] L. Wang, F. Bai, R. Yan, and T. K. Saha, "Real-time coordinated voltage control of PV inverters and energy storage for weak networks with high PV penetration," *IEEE Transactions on Power Systems,* vol. 33, no. 3, pp. 3383-3395, 2018.

[280] W. Tushar, T. K. Saha, C. Yuen, T. Morstyn, H. V. Poor, and R. Bean, "Grid influenced peer-to-peer energy trading," *IEEE Transactions on Smart Grid,* vol. 11, no. 2, pp. 1407-1418, 2019.

[281] S. Cui, Y.-W. Wang, Y. Shi, and J.-W. Xiao, "Community energy cooperation with the presence of cheating behaviors," *IEEE Transactions on Smart Grid,* vol. 12, no. 1, pp. 561-573, 2020.

[282] L. Han, T. Morstyn, and M. D. McCulloch, "Scaling up cooperative game theory based energy management using prosumer clustering," *IEEE Transactions on Smart Grid,* vol. 12, no. 1, pp. 289-300, 2020.

[283] J. Lin, M. Pipattanasomporn, and S. Rahman, "Comparative analysis of auction mechanisms and bidding strategies for P2P solar transactive energy markets," *Applied Energy,* vol. 255, p. 113687, 2019.

[284] W. Zhong, K. Xie, Y. Liu, C. Yang, and S. Xie, "Multi-resource allocation of shared energy storage: A distributed combinatorial auction approach," *IEEE Transactions on Smart Grid,* vol. 12, no. 1, pp. 561-573, 2020.

[285] K. Chen, J. Lin, and Y. Song, "Trading strategy optimization for a prosumer in continuous double auction-based peer-to-peer market: A prediction-integration model," *Applied Energy,* vol. 242, pp. 1121-1133, 2019.

[286] J. Guerrero, A. C. Chapman, and G. Verbič, "Decentralized P2P energy trading under network constraints in a low-voltage network," *IEEE Transactions on Smart Grid,* vol. 10, no. 5, pp. 5163-5173, 2018.

[287] M. Song, W. Sun, Y. Wang, M. Shahidehpour, Z. Li, and C. Gao, "Hierarchical scheduling of aggregated TCL flexibility for transactive energy in power systems," *IEEE Transactions on Smart Grid,* vol. 11, no. 3, pp. 2452-2463, 2019.

[288] A. Nedic and A. Ozdaglar, "Distributed subgradient methods for multi-agent optimization," *IEEE Transactions on Automatic Control,* vol. 54, no. 1, pp. 48-61, 2009.

[289] Z. Guo, P. Pinson, S. Chen, Q. Yang, and Z. Yang, "Chance-constrained peer-to-peer joint energy and reserve market considering renewable generation uncertainty," *IEEE Transactions on Smart Grid,* vol. 12, no. 1, pp. 798-890, 2020.

[290] Q. Wu, M. Shahidehpour, C. Li, S. Huang, and W. Wei, "Transactive real-time electric vehicle charging management for commercial buildings with PV on-site generation," *IEEE Transactions on Smart Grid,* vol. 10, no. 5, pp. 4939-4950, 2018.

[291] H. Hao, C. D. Corbin, K. Kalsi, and R. G. Pratt, "Transactive control of commercial buildings for demand response," *IEEE Transactions on Power Systems,* vol. 32, no. 1, pp. 774-783, 2016.

[292] D. H. Nguyen, "Optimal solution analysis and decentralized mechanisms for peer-to-peer energy markets," *IEEE Transactions on Power*

Systems, vol. 36, no. 2, pp. 1470-1481, 2020.

[293] M. Khorasany, Y. Mishra, and G. Ledwich, "A decentralized bilateral energy trading system for peer-to-peer electricity markets," *IEEE Transactions on Industrial Electronics,* vol. 67, no. 6, pp. 4646-4657, 2019.

[294] Y. Li, W. Yang, P. He, C. Chen, and X. Wang, "Design and management of a distributed hybrid energy system through smart contract and blockchain," *Applied Energy,* vol. 248, pp. 390-405, 2019.

[295] Y. Wang, W. Saad, Z. Han, H. V. Poor, and T. Başar, "A game-theoretic approach to energy trading in the smart grid," *IEEE Transactions on Smart Grid,* vol. 5, no. 3, pp. 1439-1450, 2014.

[296] L. He and J. Zhang, "A community sharing market with PV and energy storage: An adaptive bidding-based double-side auction mechanism," *IEEE Transactions on Smart Grid,* vol. 12, no. 3, pp. 2450-2461, 2020.

[297] W. Tushar, B. Chai, C. Yuen, S. Huang, D. B. Smith, H. V. Poor, and Z. Yang, "Energy storage sharing in smart grid: A modified auction-based approach," *IEEE Transactions on Smart Grid,* vol. 7, no. 3, pp. 1462-1475, 2016.

[298] J. Liu, Y. Xu, Z. Y. Dong, and K. P. Wong, "Retirement-driven dynamic VAR planning for voltage stability enhancement of power systems with high-level wind power," *IEEE Transactions on Power Systems,* vol. 33, no. 2, pp. 2282-2291, 2017.

[299] W. R. Scott and P. C. O'Brien, *Financial accounting theory* vol. 3: Prentice Hall Toronto, 2003.

[300] W. Li, in *Risk Assessment of Power Systems: Models, Methods, and Applications*, Ed.: Wiley-IEEE Press, 2014.

[301] V. Khaligh and A. Anvari-Moghaddam, "Stochastic expansion planning of gas and electricity networks: A decentralized-based approach," *Energy,* vol. 186, p. 115889, 2019.

[302] E. Comission, "A European strategic long-term vision for a prosperous, modern, competitive and climate neutral economy," 28.11.2018 2018.

[303] ENA and CSIRO, "Electricity Network Transformation Roadmap," Energy Networks, Australia2017.

[304] J. Zhao, F. Wen, Z. Y. Dong, Y. Xue, and K. P. Wong, "Optimal dispatch of electric vehicles and wind power using enhanced particle swarm optimization," *IEEE Transactions on Industrial Informatics,* vol. 8, no. 4, pp. 889-899, 2012.

[305] AEMO. National Electricity Market: Data-dashboard [Online]. Available: https://www.aemo.com.au/Electricity/National-Electricity-Market-NEM/Data-dashboard

[306] AEMO. Wholesale Gas Market: Data-dashboard [Online]. Available: https://www.aemo.com.au/Gas/Declared-Wholesale-Gas-Market-DWGM/Data-dashboard

[307] BOM. Australian Climate Data [Online]. Available: http://www.bom.gov.au/climate/data/

[308] CommTrade. Carbon Price [Online]. Available: https://www.commtrade.co.nz/

[309] AEMO. 2019 Planning and Forecasting Consultation [Online]. Available: https://www.aemo.com.au/Stakeholder-Consultation/Consultations/2019-Planning-and-Forecasting-Consultation

[310] J. Qiu, Z. Y. Dong, J. H. Zhao, Y. Xu, Y. Zheng, C. Li, and K. P. Wong, "Multi-stage flexible expansion co-planning under uncertainties in a combined electricity and gas market," *IEEE Transactions on Power Systems,* vol. 30, no. 4, pp. 2119-2129, 2014.

[311] X. Zhang, K. Chan, H. Wang, J. Hu, B. Zhou, Y. Zhang, and J. Qiu, "Game-theoretic planning for integrated energy system with independent participants considering ancillary services of power-to-gas stations," *Energy,* vol. 176, pp. 249-264, 2019.

[312] C. Kang, T. Zhou, Q. Chen, Q. Xu, Q. Xia, and Z. Ji, "Carbon emission flow in networks," *Sci Rep,* vol. 2, p. 479, 2012.

[313] C. Kang, T. Zhou, Q. Chen, J. Wang, Y. Sun, Q. Xia, and H. Yan, "Carbon emission flow from generation to demand: A network-based model," *IEEE Transactions on Smart Grid,* vol. 6, no. 5, pp. 2386-2394, 2015.

[314] C. Thrampoulidis, S. Bose, and B. Hassibi, "Optimal placement of distributed energy storage in power networks," *IEEE Transactions on Automatic Control,* vol. 61, no. 2, pp. 416-429, 2015.

[315] X. Xi, R. Sioshansi, and V. Marano, "A stochastic dynamic programming model for co-optimization of distributed energy storage," *Energy Systems,* vol. 5, no. 3, pp. 475-505, 2014.

[316] G. J. Offer, D. Howey, M. Contestabile, R. Clague, and N. P. Brandon, "Comparative analysis of battery electric, hydrogen fuel cell and hybrid vehicles in a future sustainable road transport system," *Energy Policy,* vol. 38, no. 1, pp. 24-29, 2010.

[317] A. F. Burke, "Batteries and ultracapacitors for electric, hybrid, and fuel cell vehicles," *Proceedings of the IEEE,* vol. 95, no. 4, pp. 806-820, 2007.

[318] R. de Sá Ferreira, L. A. Barroso, P. R. Lino, M. M. Carvalho, and P. Valenzuela, "Time-of-use tariff design under uncertainty in price-elasticities

of electricity demand: A stochastic optimization approach," *IEEE Transactions on Smart Grid,* vol. 4, no. 4, pp. 2285-2295, 2013.

[319] H. Yang, J. Zhang, J. Qiu, S. Zhang, M. Lai, and Z. Y. Dong, "A Practical Pricing Approach to Smart Grid Demand Response Based on Load Classification," *IEEE Transactions on Smart Grid,* vol. 9, no. 1, pp. 179-190, 2018.

[320] Y. Liu, L. Zhong, J. Qiu, J. Lu, and W. Wang, "Unsupervised domain adaptation for non-Intrusive load monitoring via adversarial and joint adaptation network," *IEEE Transactions on Industrial Informatics,* pp. 1-1, 2021.

[321] D. Görür and C. Edward Rasmussen, "Dirichlet process Gaussian mixture models: Choice of the base distribution," *Journal of Computer Science and Technology,* vol. 25, no. 4, pp. 653-664, 2010.

[322] J. Wang, C. Wang, Y. Liang, T. Bi, M. Shafie-khah, and J. P. S. Catalão, "Data-driven chance-constrained optimal gas-power flow calculation: A Bayesian nonparametric approach," *IEEE Transactions on Power Systems,* vol. 36, no. 5, pp. 4683-4698, 2021.

[323] Time series [Online]. Available: https://data.open-power-system-data.org/time_series/2020-10-06

[324] L. Nielson, *The European Emissions Trading System: Lessons for Australia*: Department of Parliamentary Services, Parliamentary Library, 2008.

[325] D. Fudenberg and J. Tirole, *Game theory*: MIT press, 1991.

[326] M. J. Osborne and A. Rubinstein, *A course in game theory*: MIT press, 1994.

[327] N. G. Mankiw, *Principles of economics*: Cengage Learning, 2020.

[328] A. Sinha, P. Malo, and K. Deb, "A review on bilevel optimization: from classical to evolutionary approaches and applications," *IEEE Transactions on Evolutionary Computation,* vol. 22, no. 2, pp. 276-295, 2017.

[329] J. B. Rosen, "Existence and uniqueness of equilibrium points for concave n-person games," *Econometrica: Journal of the Econometric Society,* pp. 520-534, 1965.

[330] AEMO. (2019). National Electricity Market: Data-dashboard. [Online]. Available: https://www.aemo.com.au/Electricity/National-Electricity-Market-NEM/Data-dashboard

[331] AEMO. (2019). Wholesale Gas Market: Data-dashboard. [Online]. Available: https://www.aemo.com.au/Gas/Declared-Wholesale-Gas-Market-DWGM/Data-dashboard

[332] CommTrade. (2019). Carbon Price. [Online]. Available: https://www.commtrade.co.nz/

[333] Y. Deng, Y. Zhang, F. Luo, and Y. Mu, "Operational planning of centralized charging stations utilizing second-life battery energy storage systems," *IEEE Transactions on Sustainable Energy,* vol. 12, no. 1, pp. 387-399, 2020.

[334] N. He, N. Liu, and S.-c. Zhao, "A study of road traffic impedance based on BPR function " *Journal of Nanjing Institute of Technology: Natural Science Edition,* vol. 11, no. 1, pp. 6-11, 2013.

[335] M. J. Smith and D. P. Watling, "A route-swapping dynamical system and Lyapunov function for stochastic user equilibrium," *Transportation Research Part B: Methodological,* vol. 85, pp. 132-141, 2016.

[336] C. Fisk, "Some developments in equilibrium traffic assignment," *Transportation Research Part B: Methodological,* vol. 14, no. 3, pp. 243-255, 1980.

[337] L. Sun and D. Lubkeman, "Agent-based modeling of feeder-level electric vehicle diffusion for distribution planning," *IEEE Transactions on Smart Grid,* vol. 12, no. 1, pp. 751-760, 2020.

[338] M. Lavorato, J. F. Franco, M. J. Rider, and R. Romero, "Imposing radiality constraints in distribution system optimization problems," *IEEE Transactions on Power Systems,* vol. 27, no. 1, pp. 172-180, 2011.

[339] M. Cui, J. Zhang, Q. Wang, V. Krishnan, and B.-M. Hodge, "A data-driven methodology for probabilistic wind power ramp forecasting," *IEEE Transactions on Smart Grid,* vol. 10, no. 2, pp. 1326-1338, 2017.

[340] O. Hafez and K. Bhattacharya, "Queuing analysis based PEV load modeling considering battery charging behavior and their impact on distribution system operation," *IEEE Transactions on Smart Grid,* vol. 9, no. 1, pp. 261-273, 2016.

[341] L. Han, T. Morstyn, and M. D. McCulloch, "Scaling up cooperative game theory-based energy management using prosumer clustering," *IEEE Transactions on Smart Grid,* vol. 12, no. 1, pp. 289-300, 2020.

[342] A. Garcia-Cerezo, R. Garcia-Bertrand, and L. Baringo, "Enhanced representative time periods for transmission expansion planning problems," *IEEE Transactions on Power Systems,* vol. 36, no. 4, pp. 3802 - 3805, 2021.

[343] F. Birol, "The Future of Hydrogen, Seizing today's opportunities," IEA, Japan2019.

[344] S. Bruce, M. Temminghoff, J. Hayward, E. Schmidt, C. Munnings, D. Palfreyman, and P. Hartley, "National hydrogen roadmap," CSIRO, Australia2018.

[345] "Australia's National Hydrogen Strategy," COAG Energy Council, Australia2019.

[346] X. Liu, T. Zhao, S. Yao, C. B. Soh, and P. Wang, "Distributed operation management of battery swapping-charging systems," *IEEE Transactions on Smart Grid,* vol. 10, no. 5, pp. 5320-5333, 2018.

[347] M. E. Demir and I. Dincer, "Cost assessment and evaluation of various hydrogen delivery scenarios," *International Journal of Hydrogen Energy,* vol. 43, no. 22, pp. 10420-10430, 2018.

[348] M. Ban, W. Bai, L. Zhu, W. Song, S. Xia, Z. Zhu, and T. Wu, "Optimal scheduling for integrated energy-mobility systems based on a renewable-to-hydrogen station and tank truck fleets," *IEEE Transactions on Industry Applications,* 2021.

[349] M. Shahidehpour, X. Wang, C. Shao, X. Wang, Q. Zhou, and C. Jia Feng, "Optimal stochastic operation of integrated electric power and renewable energy with vehicle-based hydrogen energy system," *IEEE Transactions on Power Systems,* 2021.

[350] A. Wang, Y. Luo, G. Tu, and P. Liu, "Vulnerability assessment scheme for power system transmission networks based on the fault chain theory," *IEEE Transactions on Power Systems,* vol. 26, no. 1, pp. 442-450, 2010.

[351] O. A. Ansari, C. Y. Chung, and E. Zio, "A novel framework for the operational reliability evaluation of integrated electric power–gas networks," *IEEE Transactions on Smart Grid,* vol. 12, no. 5, pp. 3901-3913, 2021.

[352] J. Fang, C. Su, Z. Chen, H. Sun, and P. Lund, "Power system structural vulnerability assessment based on an improved maximum flow approach," *IEEE Transactions on Smart Grid,* vol. 9, no. 2, pp. 777-785, 2016.

[353] R. S. Biswas, A. Pal, T. Werho, and V. Vittal, "A graph theoretic approach to power system vulnerability identification," *IEEE Transactions on Power Systems,* vol. 36, no. 2, pp. 923 - 935, 2020.

[354] X. Xu, A. Chen, and C. Yang, "An optimization approach for deriving upper and lower bounds of transportation network vulnerability under simultaneous disruptions of multiple links," *Transportation Research Procedia,* vol. 23, pp. 645-663, 2017.